University of Glasgow

Cobalt Rhenium Catalysts for Ammonia Synthesis

A thesis submitted in fulfilment
of the requirements for the degree
of Doctor of Philosophy

Kate McAulay

September 2017

"Promise me you'll
always remember:

You're braver than you believe,
and stronger than you seem,
and smarter than you think."

– Christopher Robin
to Winnie the Pooh

For a G

Declaration of Authorship

I declare that, except where explicit reference is made to the contribution of others, that this thesis is the result of my own work and has not been submitted for any other degree at the University of Glasgow or any other institution.

Signed:

____

Date:

____

Abstract

Cobalt rhenium ammonia synthesis catalysts which are highly active at ambient pressure and 400°C under N_2/H_2 (1:3) have been prepared without an ammonolysis step. For all highly active cobalt rhenium materials the post-reaction powder XRD patterns reveal there is a shift of their Re reflections to a slightly higher 2θ angle. This shift is due to mixing of cobalt and rhenium within the material and this interaction was confirmed *via* XAS analysis. The XRD patterns of cobalt rhenium materials with minimum ammonia synthesis activity resemble the reference pattern for metallic rhenium and show no signs of bimetallic mixing. Cobalt rhenium materials have been benchmarked against $CsNO_3$ doped Ru/Al_2O_3 materials.

Pre-treatments under N_2/H_2 (1:3), Ar/H_2 (1:3), N_2 and Ar gas mixtures have been shown to influence catalytic performance, with the first resulting in an instantly active material, whereas, the others lead to a 20 minute induction period prior to the development of activity upon switching to an ammonia synthesis feedstream. Also, pre-treatment in N_2/H_2 (1:3) resulted in a material with higher catalytic activity.

$CoRe_4$ was studied *via in situ* XAS/XRD to elucidate the reducibility and local environment of the two metals during reaction conditions. The phases present in the $CoRe_4$ catalyst during ammonia production are largely bimetallic Co-Re and also monometallic Co and Re species formed during both pre-treatments. It was found the presence of nitrogen during the pre-treatment strongly promotes the mixing of the both Co and Re.

Preliminary tests were also conducted on cobalt rhenium catalysts for ammonia decomposition and the materials were found to have high activity. To the author's knowledge this is the first report of low surface area materials being particularly active for this reaction.

Acknowledgements

Most importantly I would like to say a massively huge thank you to my supervisor, Dr Justin Hargreaves. I could not have wished to work for a more kind or supportive person and I am so thankful for all the help and guidance he has given me over the years. It has been an incredible honour and pleasure working for you. You are a constant source of support, inspiration and thanks for putting up with me!

Cory you are my office rock, knowing exactly when a soup and toastie is required for a pick me up, thank for all the fun and laughter! To Andrew for showing me the ropes and sharing the love of cari bo curries! Kathleen and Nicola you are both amazing and little rays of sunshine! Thank you to my girls Angela and Yalinu you made the time in the lab super happy and full of fun and to all the members of the Hargreaves and Jackson groups.

Within the School of Chemistry a huge thanks to Jim Gallagher for all the help at the SEM but more importantly the laughs and great chat! Also, to Andy Monaghan for help with the TGA measurements and excellent stories recounting the weekend antics and Kim Wilson for performing the elemental analysis.

Further afield thanks to Karina Mathisen and Karsten Kirste for all their help at the ESRF and analysing the XAS results. Also, to Nicolas Bion and his team at Poitiers for performing the isotopic exchange experiments.

A massive thank you goes to Tugba and Servaas at Huntsman for giving me the inspiration and confidence to pursue a PhD in the first place.

Thanks so much to my parents for all their help and support over the years and also the pick me up shopping trips and holidays!

Finally, I need to thank Graeme for the constant pep talks, laughter, and support. Always there for me, listening to me practice presentations and for designing me beautiful slides and constantly reminding me how horrible justified text is! – Couldn’t have done it without you.

Table of Contents

Table of Figures

Table of Tables

Table of Equations

Chapter 1

Introduction

1.1 Ammonia and World Population

During the 20th Century there was a massive increase in the global population, it grew from 1.6 billion in the early 1900s to close to the current 7 billion. Many factors have contributed to this population boom; however, this expansion would not have been possible without the production of ammonia. Ammonia is mainly used to produce ammonium nitrate; an essential component in synthetic fertilisers, which are crucial for crop production. The increasing industrial production of ammonia after World War II has resulted in a huge surge in the global population. The global production of ammonia has been ever increasing over this period and from 2001 to 2010 it rose from 129 to 158 million tonnes[1].

Nitrogen is crucial for our bodies. Amino acids contain nitrogen and they are required to make proteins in muscles, hair, skin and other important tissues[2,3]. Humans cannot survive without nitrogen in their diet which is acquired from proteins in food. Nitrogen fixation is required for every life form as nitrogen is essential for the biosynthesis of molecules. In nature nitrogenases are enzymes which catalyse N_2 into NH_3. Diatomic nitrogen constitutes over 78% of the atmosphere[2]. However, due to the strong nitrogen-nitrogen triple bond it is in a generally biologically and chemically unusable form which does not allow plants to uptake it with ease. It is estimated that around 175 million tonnes of nitrogen are incorporated into farming croplands around the world annually; roughly 50% of this is absorbed by plants. Synthetic fertiliser enables *ca*. 40% of this total nitrogen uptake in plants[2]. Between 1908 and 2008 it is believed the number of humans supported per hectare of arable land increased from 1.9 to 4.3 people[2].

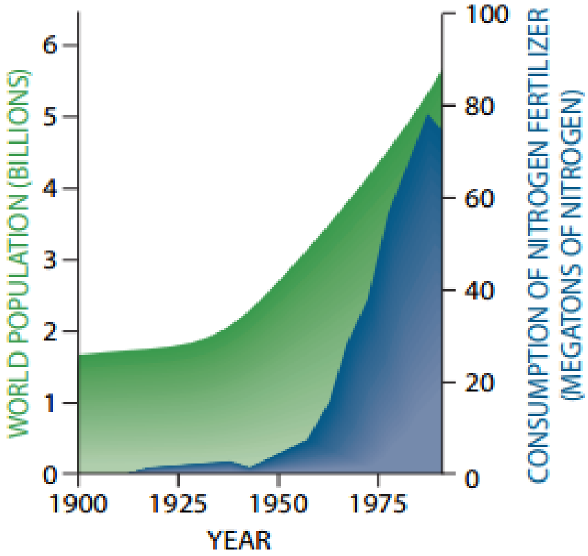

Figure 1: Correlation between population growth and global consumption of nitrogen fertilizer during the 20th Century[2].

From Figure 1 no drastic increase is observed in global population and ammonia production before the 1940's[2]. This is attributed to economic difficulties between the World Wars and annual ammonia production remained below five million tonnes until the late 1940s. During the 1950's ammonia production gradually rose to over 10 million tonnes per year[2]. A giant increase in ammonia production was achieved in the 1960's by technological advances which decreased the electricity consumption of the process by 90%. Following the 1960s there is a clear exponential growth in global production of ammonia which correlates with the surge in global population[2]. In 1999 40% of the world's population was sustained through the Haber-Bosch synthesis of ammonia which clearly demonstrates that humanity's dependence on ammonia increases with increasing population size[4].

1.2 Industrial Synthesis of Ammonia

1.2.1 Haber-Bosch Process

The industrial production of ammonia is achieved *via* the Haber-Bosch Process. The development of the Haber-Bosch Process enabled nitrogen based synthetic fertilisers to be synthesised on an industrial scale[2]. Ammonia is also a key component in the production of polymers and explosives[1]. The development of this process has facilitated an increase in agricultural productivity in most regions throughout the world[5]. The commercial production of ammonia has a projected growth of 1-2 % every year to account for the increasing food demands required for the growing population[6, 7]. Also, 3 – 5% of the world's natural gas supply is consumed to produce ammonia[7, 8]. The incorporation of ammonia in synthetic fertiliser sustains 40% of the world's population though food production.

The reaction is exothermic ($\Delta H = 46.1$ kJ mol^{-1}) and performed at moderate temperature and high pressure (Equation 1) and with respect to Le Chatelier's Principle the reaction is thermodynamically more favourable at lower temperatures. However, industrially, a higher temperature is used to obtain acceptable reaction kinetics. Due to required high temperatures/pressures and the purification of reactant feed streams, the Haber-Bosch Process is believed to consume 1-2 % of the world's total annual energy supply[9,7]. The source of dihydrogen is from natural gas. It is estimated the Haber-Bosch Process accounts for 3% of the world's carbon emissions[10] and each plant produces over 500 tonnes of ammonia per day[11].

Equation 1: Haber-Bosch Ammonia Reaction[9].

$$N_2 + 3\,H_2 \xrightarrow[\text{200-500 atm, 350-600°C}]{\text{cat. } Fe_3O_4/K_2O/Al_2O_3} 2\,NH_3$$

In the early 1900's Fritz Haber developed a successful method of combining hydrogen and nitrogen to produce ammonia[12]. In 1908 Haber approached BASF and by the end of the year was awarded the first BASF patent for ammonia synthesis[6]. The Haber-Bosch Process started in 1913 and is one of the most important industrial processes today[1]. The promoted iron catalyst is considered an ideal catalyst as it shows no deactivation over 10+ years on stream[1]. The physical form of the catalyst is reduced magnetite which forms iron particles with large pores[13]. Promotion with potassium increases the rate by over two orders of magnitude this is due to a combination of facilitating desorption of ammonia from the surface of the catalyst and an electron donating effect which weakens the dinitrogen bond enhancing dissociation[14]. α-Al_2O_3 acts as a structural promoter which prevents the sintering of Fe particles and does not directly impact the rate[15]. Rayment and co-workers[15] used XRD measurements to investigate the promoted iron catalyst and found inclusion of the promoters under the same conditions the only product is α-iron and that the active material contains regions of non-crystalline phase.

Initial work on ammonia synthesis by reaction of N_2 with H_2 discounted iron based catalysts due to low activity and deactivation on stream over time[16]. Work by Mittasch looked at a wide variety of metals for example; Fe, Co, Ni, Os, Mn, W, U and Mo. The initial focus was on osmium and uranium because in this context they showed promising results and had higher activity and a prolonged lifetime compared to iron. There were limitations working with these heavy metals including their high cost and low crustal abundance. Due to the limited reserves of osmium, BASF bought almost the entire world's supply in 1910. Considering all the disadvantages including cost, abundance and health and safety Mittasch revisited iron based catalysts.

The original work by Mittasch involved over 6,500 experiments using over 2,500 different catalyst compositions before a final material of magnetite (iron oxide) promoted with alumina and potassium was obtained. The promoted material had enhanced lifetime and stability. Moreover, the promoted iron catalyst had comparable activity to the original uranium and osmium catalysts. Over the last 100 years many improvements have been made to the catalyst and ammonia process. However, many modern ammonia plants still use iron catalysts based on the original formula presented in the original patents. Also, a new Ru based catalyst has been introduced in the KBR Advanced Ammonia Process (KAAP) which is in operation in 7 plants worldwide.

Any modification to this process to yield a lower energy consuming pathway potentially could have very attractive environmental and economic benefits with a particular focus being placed on the development of more sustainable and localised NH_3 production. The identification of a new catalytic material for ammonia synthesis could lead to desirable lower reaction temperatures and pressures and improved poison resistance. This would enable operation under a more favourable equilibrium regime. Also, lower temperatures and pressures would require less capital input into the process. Another consideration to be made is that iron is highly abundant and inexpensive.

1.2.2 KBR Advanced Ammonia Process

As discussed in Section 1.2.1, the Haber-Bosch Process is one of the most important developments of the 20th Century. For approximately 80 years the Haber-Bosch Process had no active competitor although improvements in activity were a popular research focus[11]. The initial study of ruthenium based ammonia synthesis catalysts dates back to the early work of Mittasch in 1913[17]. Aika and Ozaki initiated systematic studies in ruthenium ammonia synthesis catalysts which triggered interest in field which began growing in the 1970's[18]. In the 1970's BP started to develop a new ammonia synthesis catalyst. This new material is a doubly promoted ruthenium catalyst supported on graphitised carbon[1].

BP developed high surface area graphite (HSAG) supports using heat treatments up to approximately 2200°C. Heat treatments were used to remove surface sites which could compete with the active metal for alkali metals[1]. The HSAG support has many advantages over other activated carbons. It is resistant to methanation at high hydrogen pressures. Also, importantly it has the ability to support nanometre Ru particles at relatively high loadings (approximately 8 wt%) and importantly it does not interact with the promoter enabling the promoter to interact with the metal effectively[1].

Work by Ozaki *et al*[19] demonstrated the potential of alkali promotion on Ru based catalysts. Testing showed a combination of both Cs^+ and Ba^{2+} gave the optimum ammonia synthesis activity. LEED studies on a Ru (0001) crystallographic face revealed there was no reorientation when promoted with alkali metals[1].

Table 1 shows the difference in gas feeds between the two processes. Part of the development of the KAAP process was changing the nitrogen to hydrogen gas feed ratio. For the Haber-Bosch Process the reactor operates with a 3:1 N_2/H_2 ratio, whereas the Ru based catalyst uses a 1.5:1 ratio. This difference arises from the differences in kinetic characteristics of the iron and ruthenium catalysts. The Ru catalyst shows a continuous increase in activity with increasing nitrogen partial pressure.

Table 1: Relative yields of ammonia (arbitrary units) from Brown *et al* [1].

	Haber Catalyst	**Promoted Ru/HSAG**
Conditions	3:1 H/N Ratio	1.5:1 H/N Ratio
Yield at 86 bar and 380°C	1	26
Yield at 138 bar and 400°C	3	55

By 1991, BP were able to manufacture Ru/Ba/Cs/HSAG catalysts in industrial quantities[1]. This Ru/Ba/Cs/HSAG catalyst was successfully implemented on a plant in 1994 for the KBR Advanced Ammonia Process (KAAP)[11]. This was the first new type of catalyst to be commercialised for synthesising ammonia occurring approximately 80 years after the promoted iron Haber-Bosch catalyst was introduced[1]. Generally, to replace a current process, industry will seek a 10-20% reduction in overall costs[11]. The co-promoted ruthenium catalyst allows the KAAP to be performed at lower pressures than the Haber-Bosch Process which results in a reduction of plant operating costs. The catalyst is claimed to have 20 times the activity of the iron catalyst and maintains this activity at relatively low pressure and temperature[20]. Currently, worldwide there are 7 KAAP plants in operation in

Trinidad, Egypt and Venezuela each generating approximately 2000 tonnes of ammonia per day[11].

1.3 Metal Nitride Catalysts

Regarding ammonia synthesis and decomposition, it is well documented that transition metal nitrides exhibit catalytic properties for these reactions, some of which are listed in Table 2. Some transition metals have the ability to form interstitial nitrides. Interstitial nitrides are compounds which can be described in terms of the occupancy of interstitial sites in close packed metallic structures by nitrogen atoms[21].

Table 2: Nitride Based Materials for Ammonia Synthesis and Decomposition.

Reaction	Catalyst
Ammonia Synthesis	Co_3Mo_3N[22,23] , Cs-Co_3Mo_3N[22], Ni_2Mo_3N, Re_3N[24,25], VN[26], Fe_3Mo_3N[27], U_xN_x[28,29], CeN[30]
Ammonia Decomposition	VN[31], Mo_2N, Co_3Mo_3N, Ni_2Mo_3N, and Fe_3Mo_3N[32]

In 2001 Jacobsen *et al*[33] published a paper that argued up until this point the discovery of active ammonia synthesis catalysts was entirely random and by chance. The example they present is in the early work by Mittasch[34], where over 2500 catalysts were synthesised and tested in over 6500 experiments[13]. Jacobsen *et al*[33] rationalised the performance of materials based on N_2 binding energies. Figure 2 compares the calculated turnover frequencies for different metals, as a function of N_2 binding energy. The high activity of Ru, Os and Fe can be clearly seen and it is interesting to draw attention to the corresponding d-block pattern in the periodic table, in which these elements are all within the same group.

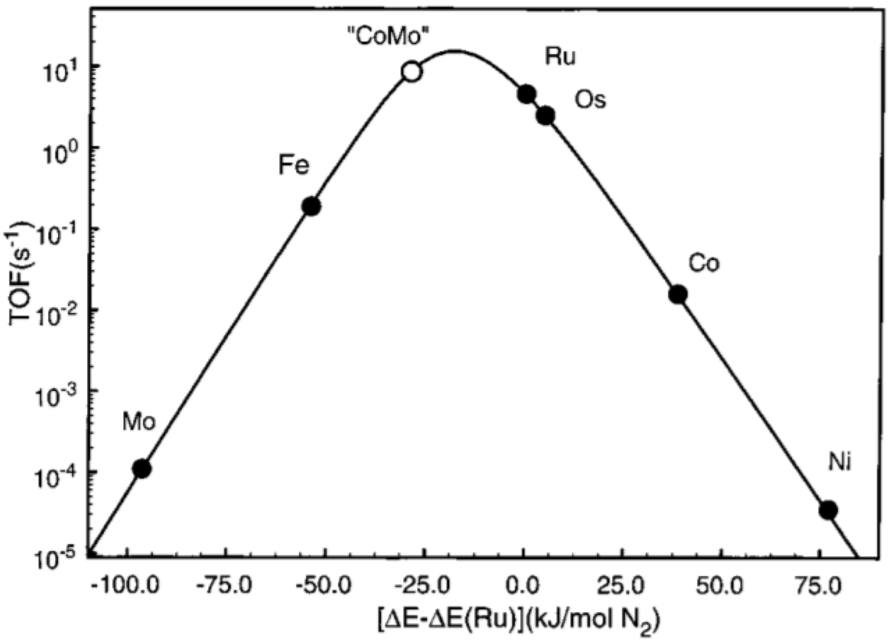

Figure 2: Relationship between the TOF of different metals for the NH_3 synthesis reaction at 400°C with respect to their nitrogen adsorption energy. Reprinted with permission from Jacobsen *et al*[33] Copyright 2017 American Chemical Society. [ΔE-ΔE(Ru)](kJ/mol N_2) Corresponds to the Binding Energy of the Metal minus the Binding Energy of Ru.

In the literature, attention has mainly focused on molybdenum containing interstitial nitrides (binary and ternary)[35]. One of the key factors which influences the ammonia synthesis reaction has been identified as the structure sensitivity of molecular nitrogen adsorption on the catalyst[36]. This has been shown for iron and rhenium; with indirect evidence of it occurring on ruthenium, nickel, cobalt, iridium and certain nitrides such as Mo_2N. One of the predominant interests for nitrides lies in hydrogen activation, dehydrogenation and base catalysis. Hillis *et al*[37] reduced molybdenum dioxide between 450 – 550°C to give Mo powder and found this powder could be easily reacted with nitrogen to give γ-Mo_2N.

Co_3Mo_3N was synthesised by the nitridation of cobalt using a high temperature ammonolysis treatment and was found to be particularly active for ammonia synthesis at 400°C and ambient pressure under 1:3 N_2/H_2[38, 39]. Jacobsen *et al*[33] rationalised the activity of Co_3Mo_3N using the volcano plot presented in Figure 2. They argue the Co-Mo alloy has the combination of strongly binding Co and weakly binding Mo resulting in a material with near optimum adsorption energy. Also, they note the incorporation of interstitial nitrogen enables the correct ordering of a Co and Mo containing (111) surface, which is consistent with microkinetic work performed on the Co_3Mo_3N system[39]. Zeinalipour-Yazdi *et al*[38] examined nitrogen surface vacancies in Co_3Mo_3N using vacancy formation energy calculations (VFE) and adsorption energies. They reveal two types of nitrogen vacancies are present: 3f and 5f. The catalytic active site was proposed to be a 3f-hollow-N which is comparable to the structure of a bifunctional catalyst. The nitrogen atoms which are bound to the molybdenum framework were found to coexist with a hexagonal array of embedded nanoclusters of Co_8. This work indicates a potential more direct involvement of interstitial nitrogen in the process.

Industrial scale ammonia synthesis is of pivotal importance to society. Under industrial conditions the Haber-Bosch iron catalyst bulk phase is nitrided which gives a distorted structure which invokes catalytic activity[40]. Molybdenum metal has a high ability to dissociate dinitrogen to form a metal nitride. Under ammonia synthesis conditions molybdenum forms a stable nitride[41]. Mittasch *et al*[34] reported the ammonia synthesis activity of molybdenum metal increases on alloying with cobalt, nickel or iron. Mixed metal nitrides were prepared by calcination of the corresponding metal nitrate and ammonium molybdate mixture, followed by reduction under N_2/H_2 gas mixture. Using a 50% Mo content the activities were Co-Mo > Fe-Mo > Ni-Mo. However, after prolonged time on stream deactivation occurred.

There are many nitride based systems with comparable or enhanced activity compared to the current commercial catalytic systems; for example Cs^+ promoted Co_3Mo_3N has been found to be more active for ammonia synthesis than the conventional Haber-Bosch based iron catalyst[22]. The activity of Co_3Mo_3N is greatly enhanced by alkali promotion; Cs^+ was found to be a more effective promoter than K^+[22]. Under N_2 and H_2 pre-treatments the activity of Co_3Mo_3N was found to decrease. This was attributed to the formation of Co and Mo_2N phases; therefore, the active phase was concluded to be Co_3Mo_3N. The equivalent molybdenum bimetallic nitrides were prepared with iron and nickel; however, they were less active than Co_3Mo_3N, their activities 143 μmol g^{-1} h^{-1}, 275 μmol g^{-1} h^{-1} and 652 μmol g^{-1} h^{-1} respectively under ammonia synthesis conditions: 400°C under N_2/H_2 (1:3) at ambient pressure[22].

Lesser known rhenium nitride has received attention within the literature for ammonia synthesis[24,42,43,44]. It was claimed that the direct synthesis of rhenium nitride from the elements is not possible at high temperature. Kawamura *et al*[45] report the synthesis of Re_2N *via* a high pressure metathesis reaction between $ReCl_5$ and Li_3N. Plate-like crystals were obtained with a diameter on the millimetre scale. Analysis with XRD revealed the Re_2N structure was similar to that of ReB_2 and MoS_2. Soto and co-workers[46] synthesised

ReN_3 using DC sputtering. Originally, it was thought ReN_2 was forming however using DFT calculations it was concluded ReN_3 was more likely. They found incorporation of nitrogen expands the rhenium lattice. Rhenium nitride (Re_3N), can also be prepared by ammonolysis of NH_4ReO_4 at 350°C and reportedly decomposes to the metal above *ca.* 370°C[44]. Rhenium nitride (Re_3N) has been investigated for its ammonia synthesis activity and partial decomposition at 350°C, it was found to yield a mixture of Re metal and Re_3N[44]. It was found rhenium nitride lost close to 90 % of its nitrogen at 350°C under Ar/H_2[44]. Since it is known potassium promotion greatly increases the activity of the industrial iron catalyst, Somorjai *et al*[47] studied the effect of doping single and polycrystalline rhenium with potassium. They found potassium adsorbed on the rhenium surface did not affect the ammonia synthesis rate.

This initial high activity of the Re_3N system led studies into cobalt rhenium based materials. Kojima and Aika[24, 43, 48] used bulk modified rhenium with cobalt and claimed the cobalt helped stabilise the active Re_3N phase. The most active composition was found to be in the atomic ratio 1:4 ($Co\text{-}Re_4$). The materials were prepared *via* high temperature ammonolysis of their precursors following reduction in N_2/H_2. These materials were shown to be particularly active for ammonia synthesis at ambient pressure[44, 48]. The high activity has been attributed to the formation and stabilisation of a rhenium nitride phase[48].

1.4 Alternative Ammonia Synthesis Routes

1.4.1 Electrochemical Synthesis of Ammonia

In the search for more cost effective and efficient processes electrochemical ammonia synthesis has been explored[49,50]. It is suggested electrochemical routes can reduce the energy output by 20%. Traditional electrochemical synthesis of ammonia is achieved *via* Equation 2. Nitrogen gas is supplied to the cathode and hydrogen atoms are generated[51].

Equation 2: Electrochemical Ammonia Synthesis[50].

$$\frac{1}{2}N_2 + 3H^+ + 3e^- \rightarrow NH_3$$

Due to the high bond strength of the nitrogen triple bond there is a high probability of the H^+ recombining with electrons to form H_2 gas, as this reaction is more favourable. This causes low current efficiency for systems operating under Equation 2. To counteract this problem a new method has been investigated; molten salts and nitride ions are utilized to form ammonia (Equation 4)[50]. Nitride ions are formed at the cathode *via* Equation 3. At the cathode nitrogen is continually reduced enabling it to supply nitride ions to the system. Ammonia is formed at the anode from the reaction between hydrogen gas and nitride ions. The anode is a porous material or a hydrogen permeable membrane. Molten salts are used as the electrolyte and are generally alkali metal halides which contain nitride ions. Some examples of molten salts are LiCl-KCl-CsCl-Li_3N and LiCl-KCl-Li_3N[50].

Equation 3: Electrochemical Nitride Formation[50].

$$\frac{1}{2}N_2 + 3e^- \rightarrow N^{3-}$$

Equation 4: Anodic Electrochemical Ammonia Synthesis[50].

$$N^{3-} + \frac{3}{2}H_2 \rightarrow NH_3 + 3e^-$$

In 2002 Murakami *et al*[50] confirmed it was feasible to synthesise ammonia *via* this method at ambient pressure. The authors obtained a current efficiency of 72% and proposed that this should increase with advancements in gas electrodes and optimizing synthesis conditions. Ammonia can be produced from N_2 and H_2O gases using aqueous electrochemical cells at ambient pressure and low temperatures (< 400°C)[49, 50,51]. Murakami[50] reported ammonia synthesis is achieved through reaction of nitride ions with water vapour.

1.4.2 Synthetic Nitrogen Fixation

Two historic methods for synthetic nitrogen fixation were: the Birkeland–Eyde Process and the Cyanamide Process. The Birkeland–Eyde Process (also known as the Norwegian Arc Process) was one of the earliest to use a thermal plasma to perform nitrogen fixation. The Birkeland–Eyde Process was first developed in 1903 for the manufacture of nitric acid from dioxygen and dinitrogen. It is based on work by Cavendish dating back to the 18th Century but only became a realistic commercial venture with the introduction of cheap hydroelectric power[52]. Birkeland was an academic who had developed an electric cannon which used an electric current to rapidly heat an enclosed quantity of air, with the idea the compressed air would fire the projectile. Eyde was a structural engineer and company director who attended a lecture by Birkeland and realised the temperatures generated by this system were comparable to those required for nitrogen oxidation and the current produced had the ability to heat up large quantities of gas[11, 53]. From this, both Birkeland and Eyde founded a company and developed an industrial sized furnace with the ability to oxidise dinitrogen. This process was established in 1903 and was first successful electrical arc plant in Norway[53]. Controlling the energy of the arc and velocity of the air stream yields of $\leq 4\%$ nitric oxide were obtained[54].

An electrical arc is formed when a current is flowed between an anode and a cathode, separated by a gas. Temperatures of over 3000°C are utilised in the plasma discs. Air is introduced to the arc and oxygen reacts with nitrogen producing nitric acid. The Equations involved are shown in Equation 5. The arc was approximately 20 cm in diameter and comprised of spaced out sparks produced by an alternating current using 5000 V[53].

Equation 5: Reactions Involved in the Birkeland–Eyde Process.

$$N_2 + O_2 \rightarrow 2NO$$

$$2NO + O_2 \rightarrow 2NO_2$$

$$3NO_2 + H_2O \rightarrow 2HNO_3 + NO$$

The Birkeland–Eyde Process produced very small amounts of NO and was relatively energy inefficient[55] and therefore was gradually replaced by a combination of the Haber-Bosch and the Oswald Processes in the 1910 – 1920's.

An ammonia producing process which relied upon cheap electrical energy was the Frank-Caro Process (also, known as the Cyanamide Process). It involved the fixation of nitrogen with calcium carbide in an electrical furnace at temperatures of up to 2700°C[55, 56]. The overall energy requirement was lower than that of the Birkeland–Eyde Process[55].

In 1900, Caro discovered when heated in steam $CaCN_2$ produced ammonia and calcium carbonate (Equation 6). The following year Frank and Freudenberg reported $CaCN_2$ released ammonia when added to soil which is then converted to ammonium nitrate and absorbed by plants. By 1914, the annual production of calcium cyanamide reached over 220,000 tones[57].

Equation 6: Cyanamide Reaction[58].

$$CaCN_2 + 3H_2O \rightarrow CaCO_3 + 2NH_3$$

1.4.3 Biological Synthesis of Ammonia

Enzymes are nature's catalysts and as such are essential for life. Certain plants can synthesise ammonia and ammonia derivatives directly from air and water at ambient temperature[59]. There are two separate routes for biologically producing ammonia: nitrogenase and the nitrate/nitrite reductase[60]. Nitrate/nitrite reductase uses an already oxidised or fixed form of NO_2^- and NO_3^- to produce NH_4^+. It is postulated reduction of nitrogen *via* nitrogenases occurs with the reduction of hydrogen as shown in Equation 3. During this reaction eight protons and eight electrons are involved in the generation two moles of ammonia and one mole of hydrogen.

Equation 7: Biological Nitrogen Reduction[61,62].

$$N_2 + 8H^+ + 8e^- + 16ATP \rightarrow 2NH_3 + H_2 + 16ADP + 16P_i$$

Nitrogen fixation is crucial for living organisms, within nature diazotrophic microorganisms that contain the enzyme nitrogenase have the ability to convert water and air to ammonia[61]. Nitrogenases are enzymes which convert nitrogen to ammonia. They are essential for nitrogen fixation and are produced by specific bacteria (for example cyanobacteria).

The nitrogenase has multiple reduction centres (Mo- and Fe- containing). The breaking of the nitrogen triple bond may not be as relevant in the biological system and a stepwise associative route for ammonia synthesis may be more relevant. Nitrogenase acts as a catalyst for the MgATP dependent reduction of nitrogen to ammonia. The nitrogenase enzyme consists of two sets of metalloproteins: Fe and FeMo proteins. Generally, the catalytic protein is Mo containing however FeFe- and VFe-dependent proteins have also been investigated[63,64]. The structure of nitrogenase presented by Hinnemann and Nørskov[65] is given in Figure 3.

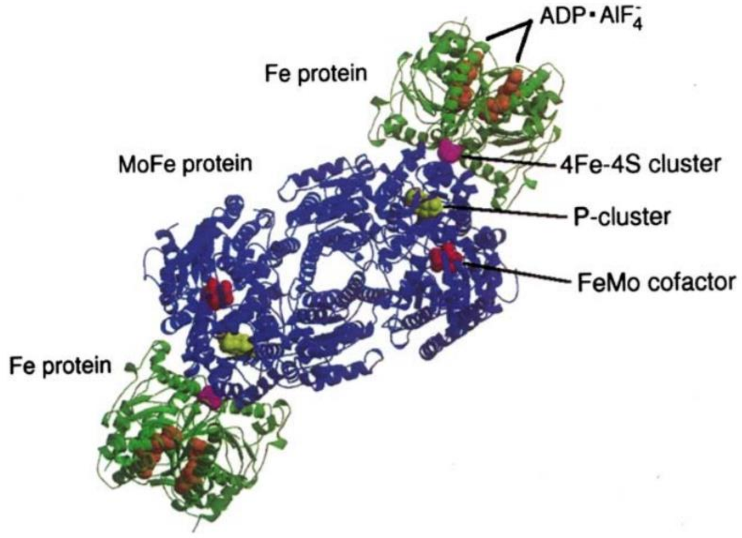

Figure 3: Nitrogenase Enzyme from Hinnemann *et al*[65].

The homodimeric Fe protein constitutes dinitrogenase reductase (DiN) which as two 60-64 kDa $[Fe_4S_4]^{2+/1+}$ α_2 dimers[61]. It has a high reducing capacity and is responsible for providing electrons from a reducing agent (for example flavodoxin or ferredoxin) to the MoFe protein. The heterotetrameric FeMo protein is the dinitrogenase (DiNR) enzyme which consumes the electrons produced by the Fe protein to reduce N_2 to NH_3. It is s cluster of $[Fe_8S_7]$P with a 230 - 250 kDa $[Mo{:}Fe_7S_9]$ homocitrate $\alpha_2\beta_2$ tetramer[61,66,67,68,69].

Along with producing ammonia, nitrogenases also produce hydrogen which provides a new research area into hydrogen fuel, for example a recent publication by Milton *et al*[70] discusses the potential of using nitrogenase enzymes in bioelectrochemical fuel cell applications. Methyl viologen was used to supply electrons to the nitrogenase, which facilitates N_2 reduction to NH_3 at an electrode. Subsequential coupling to a nitrogenase cathode with a bio-anode with the ability to oxidise H_2 results in an enzymatic fuel cell (EFC). When a current is supplied the resulting EFC has the potential to produce ammonia from hydrogen and nitrogen.

Another potential use of nitrogenases is in the development of new solar technology. Biological synthesis of ammonia is not a light dependent process however this technology has been investigated by Banerjee and co-workers[71]. Chalcogels composed of $[Mo_2Fe_6S_8(SPh)_3]^{3+}$ and clusters of $[Sn_2S_6]^{4-}$ were found to have good optical properties in solution along with high surface area and good stability. They conclude using MoFe sulfides, ammonia production using light is a new potential process.

1.5 Aim

Cobalt rhenium catalysts have been found to be particularly active for ammonia synthesis. They possess unprecedented high activity despite having an exceptionally low surface area. However, in previous literature[24, 42, 44, 43, 48] there is a lack of characterisation data and incomplete understanding of the origin of the performance of the cobalt rhenium system. Therefore, the main focus of this thesis is to further investigate the high ammonia synthesis activity and corresponding structure of cobalt rhenium catalysts. The effect of doping Ru/C materials with caesium has been studied in order to benchmark against the new cobalt rhenium materials. Finally, there is no current literature on the ammonia decomposition ability of these cobalt rhenium materials. Therefore, a preliminary study has been conducted to assess the potential of these materials as ammonia decomposition catalysts.

Chapter 2

Experimental

The experimental techniques employed in this work are presented in three sections; catalyst preparation, catalytic testing and catalyst characterisation.

2.1 Catalyst Preparation

2.1.1 Preparation of Cobalt Rhenium Catalysts

Cobalt rhenium catalysts were prepared by mixing varying amounts of ammonium perrhenate (NH_4ReO_4, Sigma Aldrich, >99%) in deionized water with cobalt nitrate ($Co(NO_3)_2.6H_2O$, Sigma Aldrich, >98%). The solutions were stirred for 1 hour then dried in an oven at 125°C for 12 hours. After drying, the materials were ground by hand and calcined in air at 700°C (using a 10°C min^{-1} ramp rate) for 3 hours. The materials were labelled according to the original synthesis molar ratio between the cobalt and rhenium and the compositions were as follows: Co_8Re, Co_4Re, Co_2Re, CoRe, $CoRe_2$, $CoRe_4$, $CoRe_8$ and $CoRe_{16}$.

To investigate the effect on activity on changing the rhenium precursor; $CoRe_4$ was prepared by the above method using ammonium perrhenate (NH_4ReO_4, Sigma Aldrich, >99%), rhenium oxide (Re_2O_7, Sigma Aldrich, 99.995%), potassium perrhenate ($KReO_4$, Sigma Aldrich, 99%), and rhenium (V) chloride ($ReCl_5$, Sigma Aldrich) as the Re precursor.

2.1.2 Preparation of Mixed Metal Catalysts

Mixed metal materials were prepared by the method outlined in Section 2.1.1.

A $CoZn_4$ cobalt zinc catalyst was prepared using zinc oxide (ZnO, Sigma Aldrich, >99%) and cobalt nitrate ($Co(NO_3)_2.6H_2O$, Sigma Aldrich, >98%).

A $NiRe_4$ nickel rhenium catalyst was prepared using nickel nitrate ($Ni(NO_3)_2.6H_2O$, Sigma Aldrich, >98.5%) and ammonium perrhenate (NH_4ReO_4, Sigma Aldrich, >99%).

An $FeRe_4$ iron rhenium catalyst was prepared using cobalt nitrate ($Co(NO_3)_2.6H_2O$, Sigma Aldrich, >98%) and ammonium perrhenate (NH_4ReO_4, Sigma Aldrich, >99%).

A $CoMn_4$ cobalt manganese catalyst was prepared using cobalt nitrate ($Co(NO_3)_2.6H_2O$, Sigma Aldrich, >98%) and manganese nitrate ($Mn(NO_3)_2$, Sigma Aldrich, 99.99%) or manganese oxide (MnO_3, Sigma Aldrich, >99.99%).

2.1.3 Ammonolysis Reactor Set Up

The diagram in Figure 4 shows the experimental set up applied for nitriding materials by ammonolysis. The gases were delivered to a vertical quartz reactor tube (10.5 mm internal diameter) fitted with a sinter, *via* 1/4 inch stainless steel tubing. The temperature was regulated using a Carbolite furnace. The gas flow was monitored using Brooks 5850 TR mass flow controllers and controlled using a Brooks microprocessor control and readout unit. Due to the hazards of working with ammonia the reactor was situated in a ventilated fume cupboard and a check valve and a one-way valve (Swagelok) were fitted to the line to prevent any possible back flow of gases and or liquids through the mass flow controllers[21].

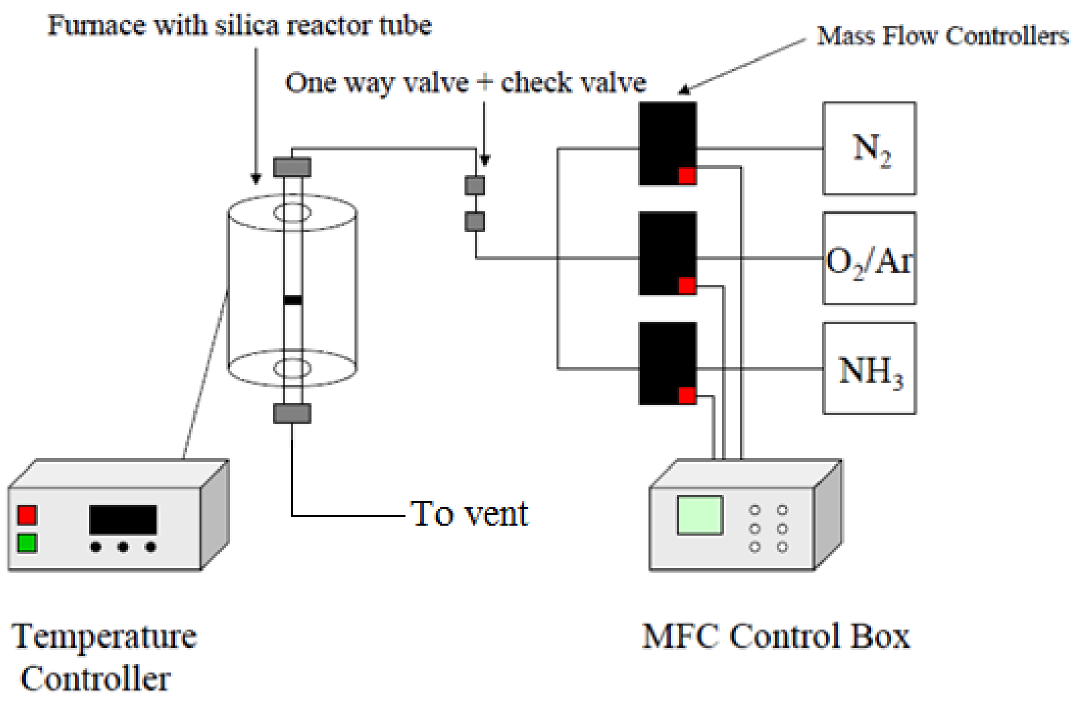

Figure 4: Ammonolysis Reactor Set Up[21].

2.1.4 Ammonolysis Procedure

In some cases, prior to ammonia synthesis, the catalyst was subjected to ammonolysis. Approximately 0.5 g of material was nitrided in a vertical quartz reactor tube (10.5 mm internal diameter). Ammonia (NH_3, BOC, 99.98%) was passed over the material using a flow rate of 94 ml min^{-1}. The furnace was programmed to heat the material to 700°C using a ramp rate of 5°C min^{-1} with a dwell of 3 hours. The material was then cooled to room temperature under flowing ammonia. When reaching room temperature nitrogen was flushed through the reactor (100 ml min^{-1}) for 3 hours to remove residual NH_3. In order to prevent bulk re-oxidation on exposure to air, the material was passivated for 4 hours with a mixture of 2% O_2/Ar (BOC) (using a flow rate of 5 ml min^{-1}) and N_2 (BOC, 99.998%) passed through an oxygen trap (95 ml min^{-1}), which gave a gas mixture with <0.1% O_2. The material was passivated in order to provide a protective oxide layer over the material, which allows air sensitive and pyrophoric materials to be safely discharged from the reactor.

2.1.5 Preparation of Cobalt Rhenium Supported Catalysts

10 wt% and 20 wt% silica supported rhenium cobalt catalysts were prepared with a 1:4 cobalt to rhenium ratio (ie 20 wt % = 16% Re and 4% Co). The materials were named according to the original synthesis ratio between $CoRe_4$ and silica. The materials were synthesised using two separate methods:

1. Silica (Sigma Aldrich, 99.8%) was impregnated simultaneously with an aqueous solution of ammonium perrhenate (NH_4ReO_4, Sigma Aldrich, >99%) and cobalt nitrate ($Co(NO_3)_2.6H_2O$, Sigma Aldrich, >98%). The material was then dried at 125°C for 12 hours then ground by hand.

2. Silica (Sigma Aldrich) was impregnated with an aqueous solution of ammonium perrhenate (NH_4ReO_4, Sigma Aldrich, >99%). The material was then dried at 125°C for 12 hours then ground by hand. Next the material was impregnated by cobalt nitrate ($Co(NO_3)_2.6H_2O$, Sigma Aldrich, >98%) in aqueous solution and further dried for 12 hours at 125°C. Prior to ammonia synthesis the supported catalyst was ground by hand.

2.1.6 Preparation of $CoRe_4$ Pellets

In order to assess any effects on the ammonia synthesis activity between powder and pelleted $CoRe_4$, $CoRe_4$ pre- and post-reaction samples were pressed into self-supporting discs using an Atlas Series Laboratory Hydraulic Press. To form a pellet 0.3 g of material was pressed with 10 tonnes of pressure for 5 minutes, forming a disc with a 1 cm dimeter which was then split into two semi circles which were both placed inside the quartz reactor tube, plugged with quartz wool and tested.

2.1.7 Preparation of Doped $CoRe_4$ Materials

In order to assess whether the addition of Cs^+ to $CoRe_4$ enhances the ammonia synthesis rate, doped $CoRe_4$ materials were prepared *via* two distinct methods:

1. Cs^+ was introduced during the initial synthesis stage: 0.02 g of $CsNO_3$ (99.99%, Sigma Aldrich), 4.00 g ammonium perrhenate (NH_4ReO_4, Sigma Aldrich, >99%) and 1.0850 g cobalt nitrate ($Co(NO_3)_2.6H_2O$, Sigma Aldrich, >98%) were added to 5 ml deionised water with stirring for 2 hours and then dried in an oven at 125°C overnight. Then the material was placed in a quartz reactor tube and tested for ammonia synthesis activity.
2. Cs^+ was introduced after the initial synthesis and 700°C calcination of $CoRe_4$: 0.03 g of $CsNO_3$ (99.99%, Sigma Aldrich) was dissolved in 1 ml of deionised water and added dropwise to 0.30 g to $CoRe_4$ in a quartz reactor tube and then tested for ammonia synthesis activity.

2.1.8 Preparation of Ruthenium Catalysts

5 wt% Ru/Al_2O_3 (reduced, dry, Sigma Aldrich) was impregnated with various amounts of $CsNO_3$ (99.99%, Sigma Aldrich). $CsNO_3$ was dissolved in deionized water and added to 1 g of 5 wt% Ru/Al_2O_3 and stirred for 1 hour prior to drying in an oven at 125°C overnight.

From previous literature it was hard to determine the amount of dopant precursor added to the Ru material due to ambiguity in the way in which it is recorded. Therefore, in this study materials will be referred to by the amount of $CsNO_3$ added to 1 g of 5 wt% Ru/Al_2O_3. The amounts of $CsNO_3$ added is as follows: 0 g, 0.0038 g, 0.0174 g, 0.1253 g, 0.2621 g and 0.3528 g.

2.2 Catalyst Testing

2.2.1 Ammonia Synthesis Reactor Set Up

The activities of the ammonia synthesis catalysts were investigated using a procedure related to that used by Kojima *et al*[43].

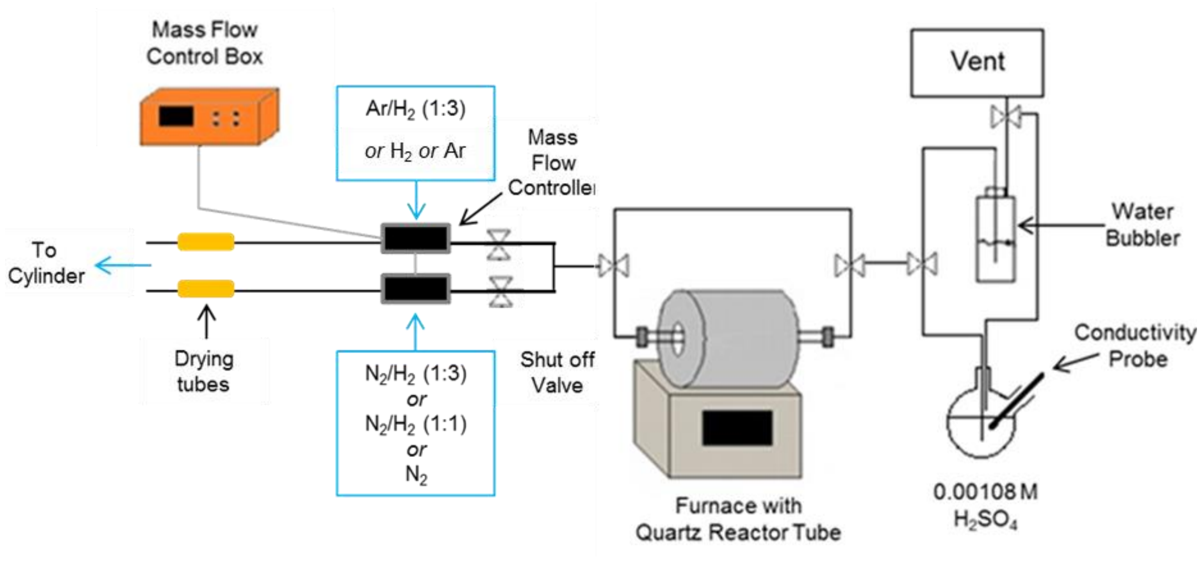

Figure 5: Ammonia Synthesis Reactor Set Up.

The reactor consisted of shut off valves (Swagelok) and Brooks 5850TR mass flow controllers. The temperature was regulated using a Carbolite furnace and ¼ inch stainless steel tubing was used to deliver the gas to the silica reactor (10.5 mm internal diameter). The vent gas from the reactor was bubbled through a dilute sulfuric acid solution (H_2SO_4, 0.00108 M) and the decrease in conductivity, corresponding to the consumption of H^+ by NH_3 was collected using either a manual EDT BA380 Meter or an automated HACH HQ14d Portable Conductivity Meter. It was verified both conductivity meters gave the same change in conductivity by using both meters simultaneously for multiple reactions.

2.2.2 Ammonia Synthesis Procedure

0.3 g of material was loaded into a horizontal quartz reactor tube and held in place with quartz wool. The catalyst was held in the centre of the furnace. The material was pre-treated for 2 hours at 600 °C, using a ramp rate of 10°C min^{-1} and flow rate of 60 ml min^{-1}. A variety of different pre-treatment gas mixtures were used; N_2/H_2 (BOC, N_2 99.995%, H_2 99.998%, 1:3), Ar/H_2 (BOC, Ar min. 99.99%, H_2 99.998%, 1:3), Ar (BOC, 99.998%) and N_2 (BOC, 99.998%). After pre-treatment the reaction was cooled to 400°C. The ammonia synthesis reaction was performed in a microreactor (Figure 5) at 400°C (unless stated otherwise) using a flow rate of 60 ml min^{-1}, N_2/H_2 = 1:3 at ambient pressure. The formation of ammonia was detected by monitoring the decrease in conductivity over time of a dilute sulfuric acid solution (H_2SO_4, 0.00108 M). Steady state reactions present as continuous linear decrease in conductivity over extended periods of time.

2.2.3 Variation in Reaction Temperature

The effect of changing the reaction temperature on the rate of ammonia synthesis was investigated. 0.3 g of $CoRe_4$ was pre-treated with N_2/H_2 (BOC, N_2 99.995%, H_2 99.998%, 1:3) at 600°C (ramp rate and flow rate 10°C min^{-1} of 60 ml min^{-1} respectively) for 2 hours. The pre-treatment conditions were kept consistent for each reaction in order to ensure the same material was present at the start of the ammonia synthesis reaction. After pre-treatment the material was cooled to the reaction temperature which was varied between 300-500°C under N_2/H_2 (BOC, N_2 99.995%, H_2 99.998%, 1:3).

2.2.4 Kinetic Study: Ammonia Synthesis

0.3g of $CoRe_4$ was pre-treated under N_2/H_2 (1:3) for 2 hours at 600 °C (using a ramp rate of 10°C min^{-1} and flow rate of 60 ml min^{-1}). After pre-treatment the reactor was cooled to 400°C and reacted under a variety of different N_2/H_2 gas mixtures. To achieve the desired gas compositions pure N_2 (BOC, 99.998%) and pure H_2 (BOC, 99.99%) were mixed in the reactor lines prior to reaching the catalyst. The ratios of N_2 to H_2 were as follows: 1:3, 1:6, 1:12, 3:1, 6:1 and 12:1. The overall gas flow was kept constant at 60 ml min^{-1}. The rate of ammonia production was monitored by measuring the decrease in conductivity over time of a dilute sulfuric acid solution (H_2SO_4, 0.00108 M).

2.2.5 Nessler's Reagent Test

To verify the formation of ammonia, Nessler's reagent was employed. Nessler's reagent is a solution of potassium tetraiodomercurate (II) with a sensitivity of 0.3 µg NH_3 in 2 µL. On reaction with ammonia a colour change from pale yellow to orange is observed and a brown precipitate forms. The formula of the precipitate is given as $3HgO.Hg(NH_3)_2I_2$ and as $NH_2.Hg_2I_3$[73]. To verify the presence of ammonia, vent gas was bubbled through 5 ml of deionised H_2O for 10 minutes. Then 2 ml of Nessler's Reagent (Sigma Aldrich) was added to the ammonia/H_2O solution. Addition of Nessler's reagent was not directly exposed to the vent from the reactor to avoid contamination. A blank reaction was conducted and no colour change was observed.

2.2.6 Temperature Programmed Homomolecular $^{15}N_2/^{14}N_2$ Isotopic Exchange

Isotopic exchange was performed at the University of Poitiers by Drs Nicolas Bion, Fabien Can and Melissandre Richard. Measurements were performed using apparatus developed for oxygen exchange previously[74, 75]. A U-form reactor was placed in a closed recycle system which was connected to a mass spectrometer (Pfeiffer Vacuum, QMS 200) for monitoring the gas phase composition and a vacuum pump. The recycling pump placed in the system removes limitations due to gas-phase diffusion. $^{15}N_2/^{14}N_2$ homomolecular exchange is described in Equation 8.

Equation 8: $^{15}N_2/^{14}N_2$ Homomolecular Exchange.

$$^{15}N_{2(g)} + {}^{14}N_{2(g)} \rightarrow 2\,{}^{14}N^{15}N_{(g)}$$

Experiments were undertaken using 0.1 g of $CoRe_4$. Samples were subjected to either a N_2/H_2 (1:3) or Ar/H_2 (1:3) 1 hour pre-treatment at 600°C using a ramp rate of 10°C min^{-1} and flow rate of 80 ml min^{-1}. Next the sample was cooled to 200°C under the same gas mixture. Then, the system was purged using a secondary vacuum at 200°C for 1 hour. Next 50 mbar of a $^{14}N_2$ and $^{15}N_2$ mixture (>98% purity, supplied by Cambridge Isotope Laboratories, Inc.) was charged into the recycle system at 200 °C and the temperature was increased to 600°C with a ramp rate of 2°C min^{-1}.

Another homomolecular exchange experiment was performed with the addition of an activation step: After the N_2/H_2 (1:3) pre-treatment, the catalyst was purged using N_2 (20 ml min^{-1}) at 600°C for 30 minutes prior to cooling down to 200°C under N_2. The masses 28, 29, 30 m/z were monitored as a function of time to follow the exchange and converted into $^{14}N_2$, $^{14}N^{15}N$ and $^{15}N_2$ partial pressures respectively. The m/z values of 2, 17 and 18 were also recorded to determine if H atoms remained at the surface of the material, thus yielding NH_3 or H_2 in the gas phase after decomposition. The absence NO_x and O_2 was confirmed by monitoring the corresponding m/z values. The quantity of H_2 (mbar) was also estimated after calibration step.

2.2.7 Ammonia Decomposition Procedure

Ammonia decomposition was performed in conjunction with Dr Laura Torrente-Murciano and Ms Tamsin Bell at the University of Bath. The experimental set up is described elsewhere[76].

25.0 mg of cobalt rhenium catalyst was dispersed in a packed bed along with 450 mg of inert silicon carbide acting as a diluent inside a quartz U-shape ¼ inch O.D reactor. The temperature was controlled by a Carbolite furnace and a K type thermocouple was situated at the exit of the catalyst bed. A blank reaction was conducted in a reactor with only SiC which showed no ammonia decomposition activity within the experimental temperature range. Prior to the ammonia decomposition reaction the materials were first pre-treated for 1 hour in pure hydrogen (H_2, BOC, 99.99%) at 600°C using a ramp and flow rate of 100°C min^{-1} and 25 ml min^{-1} respectively. Next samples were cooled to 100°C and ammonia decomposition performed. A gas flow consisting of 6 ml min^{-1} helium (He, BOC, 99.99%) and 2.4 ml min^{-1} ammonia (NH_3 BOC, 99.98%) was introduced to the reactor. The temperature was ramped in two separate stages: 100°C-300°C (5°C min^{-1}) and then 300-500°C (2.5°C min^{-1}). The vent gas was fed into on-line gas chromatography (GC) equipped with a HayeSep Q column and thermal conductivity detector and the mass balance was closed to within a 10% error.

2.3 Catalyst Characterisation

2.3.1 *Ex Situ* Powder X-Ray Diffraction

Powder X-ray diffraction (XRD) was performed on all pre- and post-reaction materials to identify the phases present. XRD patterns were obtained using a Siemens D5000 X-ray diffractometer or a PANalytical X'PERT Pro Ray diffractometer fitted with a reflection/transmission spinning flat plate and both operating at 40 kV and 40 mA with a Cu Kα source. Scans were run from 5-85° 2θ with a counting time of 1 s per step and a step size of 0.01°. Sample powders were prepared by compaction into a round sample holder *ca.* 0.3 g of material was used.

Many of the samples contain cobalt and the presence of cobalt can result in fluorescence with the CuKα radiation. This results in a high background, which may obscure peaks with lower intensity.

2.3.2 Surface Area Determination

The surface areas of the materials were determined by the application of the Brunauer Emmett and Teller (BET) method to nitrogen physisorption isotherms which were determined on an accurately known mass of sample at liquid nitrogen temperature on a Micromeritics ASAP 2020 surface area and porosity analyser. Prior to analysis the samples were degassed in N_2 at 110°C overnight to remove any adsorbed moisture prior to analysis.

2.3.3 Scanning Electron Microscopy with Energy Dispersive X-Ray Spectroscopy

Scanning electron microscopy (SEM) images were obtained using an XL30 ESEM Phillips tungsten filament electron microscope with a secondary electron detector operating at 20 kV. Energy dispersive X-ray (EDX) analysis was performed using a connected Oxford Instruments Inca Energy 250 system with X-act 10 mm^2. All samples were mounted on carbon tabs attached to the surface. To decrease sample charging, prior to analysis all samples were sputtered with Au using a Polaron SC7640 sputter coater. SEM-EDX analysis was performed with the kind help of Mr Jim Gallagher at the University of Glasgow.

2.3.4 Transmission Electron Microscopy

Transmission electron microscopy (TEM) images were attained using a JEOL JEM-2011 electron microscope operating at an accelerating voltage of 200 kV. The TEM and high-resolution TEM (HRTEM) images were recorded using a Gatan 794 CCD camera. TEM was performed at the University of St. Andrews with the kind help of Professor Wuzong Zhou and Dr Heather Greer.

2.3.5 Thermal Gravimetric Analysis

Thermogravimetric analysis (TGA) was performed using a TA Instruments Q600 combined TGA/DTA coupled to an ESS evolution mass spectrometer. Samples were run in air from room temperature to 700°C using a ramp rate of 10°C min^{-1}. Materials were also tested by a method designed to mimic reaction conditions. The temperature was ramped from room temperature to 600°C using a ramp rate of 10°C min^{-1} under Ar/H_2 or N_2/H_2 using a flow rate of 60 ml min^{-1} and held at 600°C for 2 h. Then the temperature was dropped to 400°C under Ar or N_2/H_2 then held at 400°C under N_2/H_2 for 2 hours. TGA/DTA measurements were performed at the University of Glasgow with the kind help of Mr Andrew Monaghan.

2.3.6 Elemental Analysis

The total weight percentage of nitrogen and hydrogen was determined for pre- and post-reaction materials. Elemental analysis was performed *via* combustion analysis using an Exeter analytical CE-440 analyser. This technique was very kindly performed by Mrs Kim Wilson at the University of Glasgow.

2.3.7 Temperature Programmed Reduction

To investigate the reduction temperatures of cobalt rhenium materials, temperature programmed reduction (TPR) was performed on a Micromeritics Autochem II equipment equipped with a thermal conductivity detector (TCD). Catalysts were pre-treated at 500°C under flowing argon for 20 minutes prior to temperature programmed reduction using 30 ml min^{-1} of 5% H_2/Ar from 60 to 100°C with a ramp rate of 10°C min^{-1}. TPR was performed at the University of Bath with the kind assistance of Ms Tamsin Bell and Dr Laura Torrente-Murciano.

2.3.8 Inductively Coupled Plasma Mass Spectrometry

Inductively Coupled Plasma Mass Spectroscopy (ICP-MS) was performed by Mr Karsten Kirste from the Norwegian University of Science and Technology. Elemental analysis was conducted using a High Resolution Inductively Coupled Plasma MS Element 2 (Thermo Scientific). In a Teflon tube (25 ml) 10 - 20 mg of sample was decomposed by adding 1.5 ml concentrated nitric acid (HNO_3) and 0.6 g hydrofluoric acid (HF, 40 wt%). The resulting solution was transferred to a Teflon canister and diluted with deionized water until a total weight of 216.6 g was reached. A Teflon tube (16 ml) was then washed and filled with the sample solution. In order to eliminate contaminants three blanks were tested prior to sample analysis.

2.3.9 X-Ray Absorbance Spectroscopy

X-ray absorbance spectroscopy (XAS) data collection was performed in collaboration with Dr Karina Mathisen and Mr Karsten Kirste from the Norwegian University of Science and Technology. Data collection and analysis was performed at the ESRF with the kind help of Dr Karina Mathisen, Mr Karsten Kirste (NTNU), Dr Wouter van Beek (ESRF), Drs Justin Hargreaves, Nicholas Spencer, Andrew McFarlane and Said Laassri (University of Glasgow).

Due to the high energy of X-rays they have the ability to ionise and excite core electrons in atoms[77]. EXAFS concerns the oscillating behaviour of X-ray absorption as a function of photon energy beyond an absorption edge[78]. Absorption is generally is expressed as the absorption coefficient (μ) which is determined by measuring the attenuation of X-rays as they pass through a material. When measuring the absorption coefficient over a range of energies; from slightly below to slightly above the binding energy, a sharp increase in absorption is observed when the X-ray energy is tuned to the binding energy. This in known as the 'absorption edge' and these absorption edges are element specific[77]. The absorption coefficient decreases monotonically for isolated atoms as a function of energy after the edge. This is in contrast to atoms in molecules, frameworks or condensed phases which give oscillations above and below the edge. Therefore, X-ray absorption spectroscopy (XAS) is able to give structural information about the absorber environment and can be used to elucidate the structure of non-crystalline samples[77]. XAS can be used to explore the local structure in disordered materials or local environment of an impurity in a matrix of different atomic species. It can be also used to investigate: the coordination environment of active material site, alloys, amorphous glasses and follow structural changes during processes such as diffusion and corrosion. EXAFS is a bulk averaging technique.

The fraction of bimetallic phase has been calculated based on the method of Shibata and co-workers[79] which is based on the average coordination number (N) of Re-Co and Co-Re shells and the total coordination number ($N_{Re\text{-}Re}$+ $N_{Re\text{-}Co}$, $N_{Co\text{-}Co}$ + $N_{Co\text{-}Re}$) to follow the amount of bimetallic phase. For the EXAFS analysis, attention was directed towards analysis of the structure of the Co-Re phase, more precisely the mixing and bimetallic nature during pre-treatment and ammonia synthesis reaction conditions. The degree of bimetallic mixing is obtained by comparing the obtained average coordination of the first absorption shell which for the cobalt edge will constitute of Co-Co and/or Co-Re, and similarly Re-Re and/or Re-Co at the rhenium edge. As EXAFS sees sums of contributions, both absorption pairs will be present on the respective edges if the material consists of a mixture of mono- and bimetallic species. However, as these shells exhibit different bond distances the contributions should be resolved in EXAFS refinements. In a bimetallic system the degree of mixing is often best obtained from the minority element[31], in the case of the cobalt rhenium system this is Co. This can be exemplified by the following relationship C_{Re} x $N_{Re\text{-}Co}$ = C_{Co} x $N_{Co\text{-}Re}$, where C_{Re} and C_{Co} are the concentrations of each metal, which means that heteroatomic bonds will be better visualized at the element of low concentration in bimetallic phases[30]. Due to rhenium being a heavy absorber optimising the dilution for XAS, data collection was challenging, which in turn led to the *in situ* cobalt data being of rough quality. Another challenge in this study is obtaining reliable information about rhenium as a backscatterer due to the fact that a large part of the EXAFS signal lies in the high k-region, and the data in this study utilises a k-window of 3.5 - 9.5 $Å^{-1}$ as the resolution is limited by the *in situ* conditions beyond this value[80].

2.3.9.1 Preparation of Standards

Nitrided cobalt, rhenium and cobalt-rhenium were prepared and analysed to compare the $CoRe_4$ material against.

Nitrided cobalt (denoted CoN_x) was prepared by reaction of ammonia with Co_3O_4 at 700°C for 2 hours. The temperature was increased from room temperature to 300°C over 30 minutes, after which it was increased to 450°C at a rate of 0.7 C min^{-1} and then up to 700 °C at a rate of 1.67°C min^{-1}.

Nitrided rhenium (denoted ReN_x) was prepared *via* ammonolysis of NH_4ReO_4 (Sigma Aldrich, 99.5 %) at 350°C for 2 hours (ramp rate of 5°C min^{-1}).

Nitrided cobalt rhenium (denoted $CoRe_yN_x$) was prepared *via* ammonolysis of a cobalt rhenium oxide precursor, prepared as described above, at 700 °C for 3 hours. A temperature ramp rate of 5 °C min^{-1} was applied.

2.3.9.2 XAS Data Collection

Rhenium L_3 edge and Co K edge XAS data was collected at the Swiss-Norwegian Beamline (SNBL, BM1B) at the European Synchrotron Radiation Facility (ESRF) in transmission mode. The data was collected in the 16-bunch filling mode, providing a maximum current of 90 mA. A bending magnet supplies the white beam from the storage ring to the beamline. SNBL is equipped with a Si (111) double crystal monochromator for EXAFS data collection. The incident and transmitted intensities (I_0 and I_t + I_2) were detected with ion chambers filled with, I_0 (17 cm) 50 % N_2 + 50 % He, and I_t and I_2 (31 cm) with 85 % N_2 + 15 % Ar at the cobalt edge. Post ammonolysis samples (CoN_x, ReN_x and $CoRe_yN_x$), cobalt references (CoO, Co_3O_4) and rhenium references (ReO_3, $KReO_4$ and NH_4ReO_4) were also collected *ex situ* mixed with boron nitride for optimum absorption placed in aluminium sample holders. The cobalt XAS data were measured in continuous step scan from 7600 eV to 8300 eV with a step size of 0.5 eV and counting time 300 ms. The rhenium L_3 edge data was collected in transmission mode , using ion chamber fillings 100 % N_2 (I_0, 17 cm) and 50 % N_2 + 50 % Ar (I_t, 30 cm). Step scans were collected between 10350 eV to 11800 eV, with a step size of 0.5 eV and counting time 200 ms.

For all *in situ* measurements, great care was taken to ensure similar conditions and setup were applied on both edges, hence sample weight, cell thickness and gas flow were kept constant. The $CoRe_4$ catalyst was mixed with boron nitride, pressed to wafers and sieved fractions (above 375 microns) were then placed inside 0.9 mm quartz capillaries with quartz wool on either side. The capillary was heated by a blower placed directly under the sample.

2.3.9.3 ***In situ* Ammonia Synthesis Experiments**

The first set of beam time experiments involved using 2% H_2 gas mixtures: samples were pre-treated under 2% H_2/Ar or 2% H_2/N_2 at 600°C for two hours using a ramp rate of 5°C min^{-1} and flow rate of 10 ml min^{-1}, before cooling to 400°C and switching to the reaction gas 2% H_2/N_2. EXAFS step scans were collected continuously through the entire reactions with XRD patterns being collected at the end points.

The second set of experiments involved 75% H_2 gas mixtures: samples were pre-treated with 75% Ar/H_2 (1:3) or N_2/H_2 (1:3) at 600°C for two hours using a ramp rate of 5°C min^{-1} and flow rate of 10 ml min^{-1}. EXAFS step scans were collected continuously following the protocol shown in Figure 6 with XRD patterns being collected at the end points. After pre-treatment the samples were cooled to 400°C and switched to the reaction gas or 75% N_2/H_2. EXAFS step scans were collected continuously with XRD patterns being taken at the end points. A setup with pneumatic switching valves and a secondary by-pass line was employed to prevent gas build-up during switching between gases.

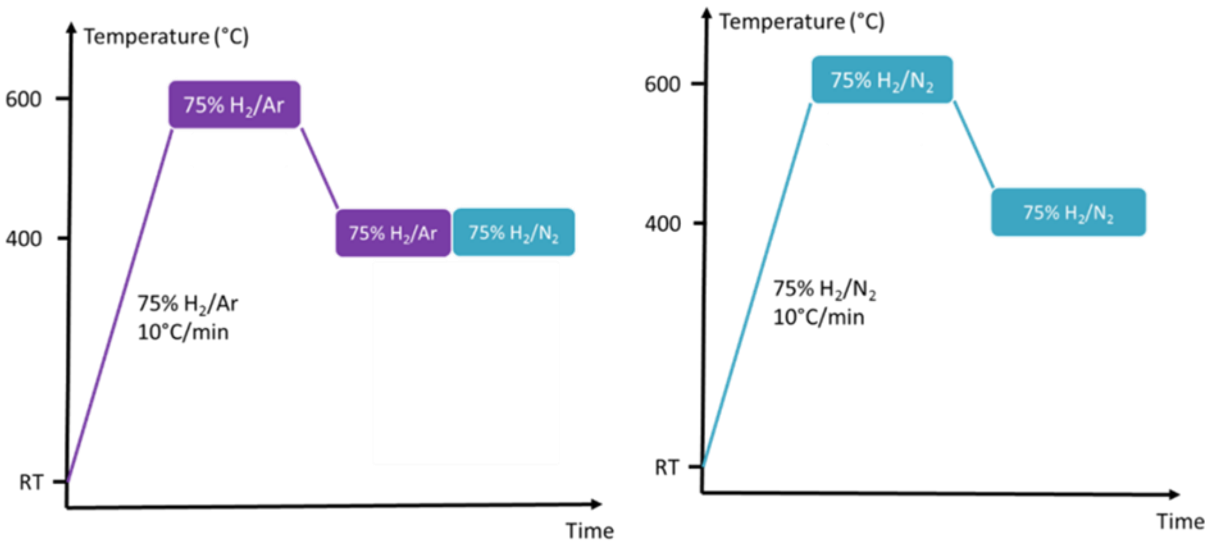

Figure 6: The Two Protocols Used for the *In situ* XAS/XRD Study of $CoRe_4$ for Ammonia Synthesis.

2.3.9.4 XAS Data Refinement

The XAS data was binned (Edge region -30 eV to 50 eV; pre-edge grid 10 eV; XANES grid 0.5 eV; EXAFS grid 0.05 $Å^{-1}$) and background subtracted, and the EXAFS part of the spectrum extracted to yield the $\chi_i^{exp}(k)$ using Athena software from the IFFEFITT package. The XANES spectra were normalised from 30 to 150 eV above the edge, while the EXAFS spectra were normalised from 150 eV to the end point[81]. When required, the data was deglitched and truncated at the end of the EXAFS spectra. The smooth background $\mu_0(E)$ was checked and corrected for to achieve the maximum overlap with total absorption $\mu(E)$. Athena uses the Autobk algorithm to determine the background and normalise $\mu(E)$ data. Edge step normalisation is used, meaning that the difference between $\mu(E)$ and $\mu_0(E)$ is divided by an estimation of $\mu_0(E_0)$. A line is regressed to the data in the region below the edge and subtracted from the data. Next a quadratic polynomial regressed to the data above the edge and extrapolated back to E_0[20]. For cobalt the threshold energy (E_0) was set to be at the mid-point (0.5) of the normalised absorption edge step ensuring it was chosen after any pre-edge or shoulder features. For rhenium samples E_0 was determined to be the first infliction point in the first derivative spectra, as there are no pre-edges or shoulder features. All XANES spectra are energy corrected against the corresponding reference foil (Co = 7709 eV, Re = 10535 eV).

XANES is used for distinguishing between valence states of transition metals and is highly sensitive towards changes in the electronic states and or the local environment. At any stage of the process the experimental spectra were attempted fitted to reference compounds, including corresponding foils, using the linear combination feature in the Athena package. The normalised data were fitted from -20 eV below the edge and 60 eV above the edge, allowing also the E_0 value to be fitted, due to the ambiguity in selecting this value due to pre-edge features. At various stages of the process attempts were made to fit reference compounds, including corresponding foils to the experimental spectra using the linear combination feature in the Athena package[81]. The normalised data were fitted from -20 eV below the edge and 60 eV above the edge, allowing also the E_0 value to be fitted, due to the ambiguity in selecting this value due to pre-edge features. All fits with unreasonable ΔE_0 values (+/- 2.5 eV) were excluded. The maximum number of standards was set to three and the most relevant were chosen on the basis of the statistical goodness of fit.

EXAFS least-squares refinements were carried out using DL-EXCURV[21], which conducts the curve fitting of the theoretical $\chi^{th}(k)$ to the experimental $\chi^{exp}(k)$ using the curved wave theory. The fit parameter reported for each refinement procedure is given by the statistical R-factor, defined as:

$$R = \sum_{i}^{N} [\frac{1}{\sigma_i} (|\chi_i^{exp}(k) - \chi_i^{th}(k)|] \cdot 100\%$$

Ab initio phase shifts were also calculated within DL-EXCURV and verified using reference compounds. The least-squares refinements were carried out in typical wave number k range 2 - 8.5 Å^{-1} for cobalt and k range 3.5 - 9.5 Å^{-1} for rhenium using a k^3 weighting scheme.

Chapter 3

Cobalt Rhenium Ammonia Synthesis Catalysts

3.1 Introduction to Rhenium

Rhenium was finally isolated in May 1925 when Tacke and Noddack successfully extracted rhenium (as an impurity) from gadolinite[82]. It is amongst one of the rarest elements on earth with a crustal abundance of 0.001 parts per million. In 1928 the first gram of rhenium was isolated and in 1933 rhenium was being produced commercially[83]. Due to the scarcity of rhenium it is extremely expensive, in 2015 rhenium metal averaged at $2,900 per kilogram[84]. Rhenium is found with molybdenum in porphyry copper deposits and is produced by extraction from dust from molybdenum and copper smelters[82, 83, 84, 85]. Rhenium is element 75 in the periodic table and is in Group 7 with the electron configuration [Xe] $4f^{14}$ $5d^5$ $6s^2$. Rhenium is a third row transition metal and is in the same group as manganese and technetium. There is limited literature on technetium catalysts due to their radioactive nature. However, there are two Russian reports by Spetsyn *et al*[86, 87] which claim technetium catalysts are active for ammonia synthesis. Bearing in mind the general group trends within the periodic table, rhenium chemistry differs from the chemistry of manganese. For example, metallic Mn is reactive and has the ability to react with dilute acids and slowly decompose water, whereas in comparison Re metal is fairly inert as it does not react with water or non-oxidizing acids[88]. Davenport *et al*[88] argue rhenium holds an and intermediate position between tungsten and the platinum group metals (Pt, Os, Ir, Ru, Rh and Pd)[88]. With regard to catalysis, rhenium has great selectivity, especially in hydrogenation reactions[88]. Also, it shows a greater tolerance to common catalysts poisons such as; sulfur, nitrogen and phosphorus[88]. Due to this property, despite the high cost and low crustal abundance of rhenium, it is still used in commercial applications.

Ni-based superalloys dominate the market place for high temperature gas turbines. However, the Ni-based alloys are temperature limited to 1300 – 1400°C[89]. Co- based alloys are also used for static parts of gas turbines[89]. There is a need to increase the melting point of these alloys and due to the high melting point and mechanical strength rhenium is often incorporated into metals to produce superalloys[89, 90, 91, 92]. In the 1980's rhenium was introduced *via* alloying to Ni based superalloys and it is widely documented rhenium improves the high temperature properties of Ni-based alloys[84, 89, 90] and the creep and fatigue properties of alloys[93, 94]. For example, the formation of brittle phases are observed on addition of high rhenium percentages in the Ni based alloys[94]. Rhenium superalloys are mainly used in components for high temperature turbine engines, this use accounted for 70% of overall rhenium usage within the US in 2015[84]. Regarding alloys, important properties include friction, adhesion, strength at elevated temperatures and wear. Hexagonal close packed (hcp) structures are preferred with respect to these properties. US Patent 6039920A describes a process for forming high rhenium containing alloys (30 % – 70 % Re) by melting together Re with Co, Fe or Ni then casting and allowing the molten mixture to solidify[95].

Metals with close to ideal stacking ratios and hcp structures give enhanced friction properties due to the basel slip mechanism[96]. Cobalt and rhenium have near ideal stacking ratios (1.633) and a hcp structure at ambient temperature. Above 400°C cobalt transforms from hexagonal close packed to face centred cubic (fcc). Various studies have looked at preventing this transformation and/or increasing the transformation temperature[97]. Co-Re phase diagrams suggest the addition of Re to Co will increase the hpc to fcc transformation temperature[89, 98]. Brainard[98] and Mukherji[89] found this was the case, the addition of Re causes an almost linear increase in transformation temperature with amount of rhenium added. Rösler and co-workers[90] compared phase diagrams and found both Ni-Re and Co-Re alloys rhenium was found to increase the melting point. In the Ni-Re alloy Re was found to have limited solubility, whereas, complete miscibility is achieved in the Co-Re alloy[99]. Mukherji and Rösler[89] suggest there is an urgent need for materials that have an operating temperature that exceeds that of Ni-based superalloys and Re-Co alloys have high potential to meet this need. Cobalt-rhenium alloys have been investigated for military and space flight applications[92,98].

Rhenium alloys also find use in: electromagnets, metallic coatings, heating elements, thermocouples, electrical contacts and other applications[84]. Kablov *et al*[100] investigated the structure and properties of nickel alloys with the introduction of up to 12 wt% Re. With the inclusion of Re the self-diffusion coefficient of Ni decreases and the diffusion process at operating temperatures is hindered and an elevation in melting point was observed. The authors claim rhenium is a more effective component at increasing the overall and long term strength at 1000°C compared to other refractory metals (Hf, Mo, Nb, Ta or W). A Fe-Re-S alloy was synthesised *via* heating between 900 – 1200°C. Re was found to predominately reside in ReS_2 and Fe-Re and not in pyrrhotite or the sulfide melts[101, 102].

Rhenium catalysts are also used for olefin metathesis[103] and dehydrogenation of light alkanes[104].

Chevron first introduced a bimetallic Pt-Re based catalyst in 1967 for the reforming of low octane naphtha to high octane petrol[105, 106, 107]. Pt-Re reforming catalysts were found to have bimetallic interactions where the platinum and rhenium form alloyed metal particles[108,109]. Interestingly, it has been reported the metal characteristics are highly dependent on the pre-treatment used. High temperature (> 400°C) pre-treatment under N_2 results in a lower degree of Pt-Re interaction and sintering. Air pre-treatments do not affect the platinum dispersion and reduction in H_2 increased sintering[109, 110] A Re promoted Co_3O_4/Al_2O_3 catalyst was investigated *via in situ* XAFS[111]. Reduction under different hydrogen concentrations (100% H_2 and 5% H_2/He) resulted in differences in the materials. Reduction under 5% H_2/He creates 'bulk-like' Co metal particles with the face centred cubic (fcc) or hexagonal close packed (hcp) structure. whereas, reduction using 100% H_2 resulted in a material with an increased dispersion and smaller Co particles (< 40Å). The structure of these Co particles could not be determined however the authors postulate the particle may have the metastable non close-packed body centred cubic structure.

Regarding the Fischer-Tropsch Process, Co is often used as an active catalyst component[112]. Generally, Co is supported on a high surface area material. In certain cases Co can interact too strongly with the support and the metal-support interaction prevents the Co from fully reducing, which leaves part of the Co inactive[113]. In order to improve the Co reduction Re promotion has been widely studied[114, 115]. Rhenium is believed to facilitate the reduction of Co *via* a hydrogen spillover effect, which improves the Co dispersions and no direct contact between Co and Re is required for this enhancement[116, 117, 118]. Cobalt reduction is a two stage process: $Co_3O_4 \rightarrow CoO \rightarrow Co$[119]. Promotion *via* rhenium has little effect on the first step of the reduction of cobalt oxide, this is because it occurs at roughly the same temperature as Re reduction. However, the temperature of the second stage of cobalt oxide reduction is lowered by the presence of Re[118].

Rhenium promotion on Co/Al_2O_3 Fischer-Tropsch catalysts was found to enhance the overall activity. These materials were studied *via in situ* EXAFS on the Re L_3 (10535 eV) and K (71676 eV) edges[115]. Analysis of both edges indicated Re was atomically distributed inside the bulk Co particles. On the Re L_3 edge an increased Re-Co interatomic distance was found (in comparison to a model based on DTF calculations by Bakken *et al*[120]) and this was attributed to a distortion of the local Co environment for the Co particles which were in direct contact with Re particles. This distortion was only evident on the Re L_3 edge and was not found on the Co K edge or *via* XRD analysis[121]. This distortion was attributed to the increase in activity for the Re promoted catalysts compared to the un-promoted Co catalyst. Analysis also revealed approximately 15 % of Re remained unreduced in the material. Bimetallic Re-Co interactions were confirmed by Rønning *et al*[122] *via* EXAFS analysis. Reduction of Co-Re/Al_2O_3 (2 wt% Co and 4.6 wt% Re) at 450°C results in materials with bimetallic Re-Co bonds. However, the difference in initial elemental loading disappeared after being reduced for 6 hours as the resulting material contained roughly equal amounts of both Re and Co. the Re-Co bond distance was found to be approximately 2.53 Å.

Fung *et al*[123] used NH_4ReO_4 to synthesize a 1 wt% Re/γ-Al_2O_3 catalyst. After reduction at 400°C the material was non-homogeneous comprising of rhenium oxides and metallic rhenium. Yao *et al*[124] investigated surface interactions of Re/γ-Al_2O_3 *via* ESR, TPR and chemisorption. It was revealed on the surface two rhenium phases are present: an easily reducible rhenium phase that forms strong interactions with the support and metallic Re. Due to this strong interaction reduction to Re^0 at temperatures < 500°C was possible.

Zhao *et al*[125] investigated rhenium nitrides *via* DFT calculations. Re_3N, Re_2N and Re_3N_2 were found to have high mechanical strength and N content was concluded as the main factor in controlling the hardness and metallicity of the rhenium nitrides. The authors claim the rhenium nitride phases are stabilised by a combination of 3D polyhedral stacking and strong covalent N≡N and Re-N bonding.

Clark *et al*[126] prepared rhenium nitride for use in hydrodenitrogenation reactions. Ammonium perrhenate (NH_4ReO_4) was heated under pure NH_3 to 350°C using a flow rate of 267 µmol s^{-1} and ramp rate of 0.0833°C s^{-1} and held at 350°C for 2 hours. They report a characteristic XRD pattern of Re_3N which is presented in Figure 7.

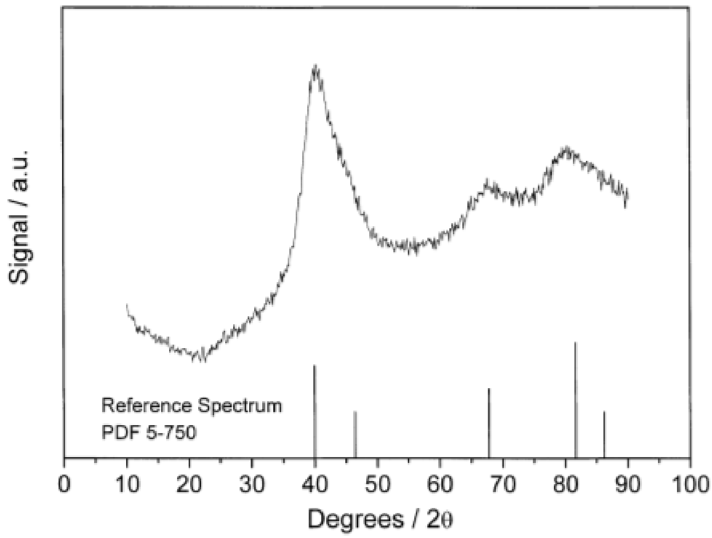

Figure 7: X-ray Diffraction Pattern of Rhenium Nitride as reported by Clark *et al* [126].

Re_3N has been investigated for ammonia synthesis[24, 42-44]. Kojima and Aika[24] synthesized Re_3N. Ammonium perrhenate (NH_4ReO_4) was heated to 350°C (using a ramp rate of 5°C min^{-1}) under ammonia gas (flow rate of 160 ml min^{-1}) and held at 350°C for 2 hours then cooled to room temperature. Re_3N showed initial high activity but deactivated over time and decomposed to a mixture of Re metal and Re_3N[24, 43]. Clark *et al*[126] also report up to 350°C rhenium nitride was found to be stable in H_2, He and NH_3. However, it was found to decompose to metallic rhenium at temperatures over 375°C or upon prolonged exposure to H_2 at 350°C. These results are in agreement with Alexander *et al*[44] who investigated the partial decomposition of Re_3N. At temperatures over 350°C rhenium nitride was found to give a mixture of Re metal and Re_3N.

Kojima *et al*[43] prepared Re/γ-Al_2O_3 catalysts. An aqueous solution of NH_4ReO_4 was used to impregnate γ-Al_2O_3 and the loadings were varied between 2 – 80 %. The materials were dried in air at 100°C for 12 hours then reduced in pure H_2 at 600°C for 2 hours. The 20 wt% Re/γ-Al_2O_3 was characterized *via ex situ* XRD (Figure 8). For the as prepared catalyst only Re metal and Al_2O_3 were reflections were observed (Figure 8 (a)). Compared to the as prepared material, further activation with H_2 at 600°C created no apparent changes in the XRD pattern (Figure 8 (c)). However, when compared to activation with reaction gas, N_2/H_2 (1:3) (Figure 8 (b)) the peaks appear to change with the formation of an amorphous section under the three main Re peaks; this is attributed to a rhenium nitride phase. Pure rhenium nitride is presented in (Figure 8 (d)). The background of the N_2/H_2 pre-treated material shows a broad feature which the authors attribute to rhenium nitride.

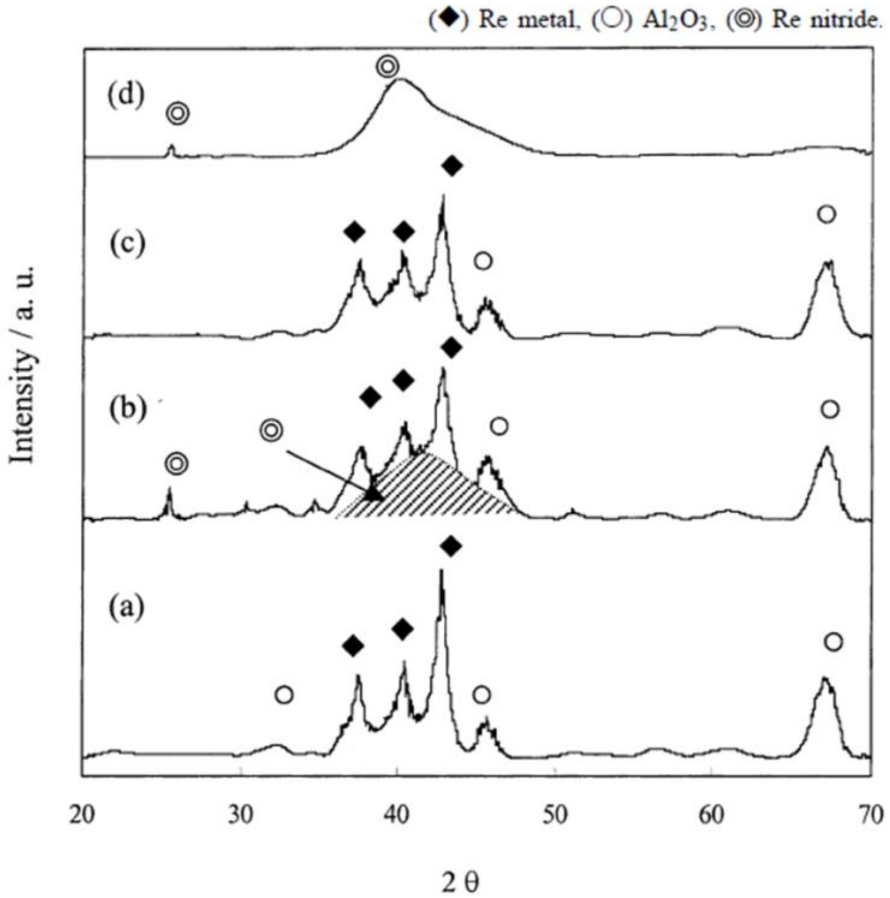

Figure 8: XRD patterns of the 20 wt% Re/Al_2O_3 catalysts (a) as prepared, (b) after activation in N_2/H_2 (1:3), (c) activation in H_2 and (d) Re nitride. Re metal (diamond), Al_2O_3 (circle) and Re Nitride (double circle)[43].

This initial high activity of the Re_3N system led to studies into cobalt rhenium based materials as it was claimed the cobalt helped stabilise the active Re_3N phase. There is a limited amount of literature on these materials and most published work on cobalt rhenium catalysts for ammonia synthesis originates from Kojima and Aika[24,48,43]. These cobalt rhenium catalysts consisted of bulk rhenium modified with cobalt and the most active composition was found to be in the atomic ratio 1:4 (Co-Re_4). The materials were prepared *via* high temperature ammonolysis of their precursors following reduction. These materials were shown to be particularly active for ammonia synthesis at ambient pressure[44,48]. The high activity has been attributed to the formation and stabilization of a rhenium nitride phase[48]. A Co-Re_4 powder XRD pattern is shown in Figure 9 as presented by Kojima and Aika[24]. Three rhenium metal reflections are present with a high amorphous background and a Co metal reflection is also present. This pattern is consistent with results presented by Alexander and co-workers[44].

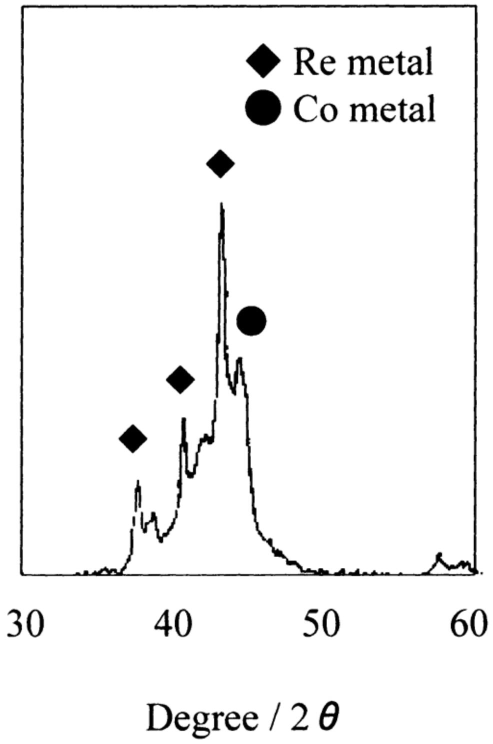

Figure 9: XRD Pattern of Co-Re_4 adapted from Kojima and Aika[24].

Kojima *et al*[43] performed ammonia synthesis reactions using 0.4 g of catalyst at 350°C under N_2/H_2 (1:3) using a flow rate of 60 ml min^{-1} at ambient pressure. To quantify the amount of product, the conductivity of a 0.00108 M H_2SO_4 solution was monitored. It was found Re nitride had higher activity (108 µmol g^{-1} h^{-1}) in comparison to other higher surface area metallic nitrides under the same conditions despite its very low surface area of < 0.5 m^2 g^{-1}. For example, Mo_2N has a surface area of 286 m^2g^{-1} but a lower rate of 20 µmol g^{-1} h^{-1}. Re_3N had an initially high rate for ammonia synthesis, however, deactivated after 2 hours on stream. This deactivation was attributed to hydrogen poisoning[24]. It is suggested there is an equilibrium between the Re and Re_3N, resulting in a rate higher than that of Re metal alone. Kojima *et al*[43] examined the possible cause of this deactivation *via* XRD measurements. Pure Re_3N leads to a single broad reflection. After a 5 hour ammonia synthesis run it was found rhenium nitride decomposes to a mixture of the nitride and Re metal. The deactivation is also suggested to be connected with the decomposition of the Re_3N and it is suggested this is the active state[43].

Alexander *et al*[44] prepared a cobalt rhenium nitride *via* ammonolysis of the precursors at 700°C. Ambient pressure reaction at 400°C under Ar/H_2 (1:3) yielded low levels of NH_3 (approximately 75 µmol g^{-1}) whereas, reaction under N_2/H_2 (1:3) gave a steady state ammonia synthesis rate of 472 µmol g^{-1} h^{-1}. This steady state rate can be compared to results presented by Kojima and Aika; 492 µmol g^{-1} h^{-1} and 600 µmol g^{-1} h^{-1} at 350°C[24, 48].

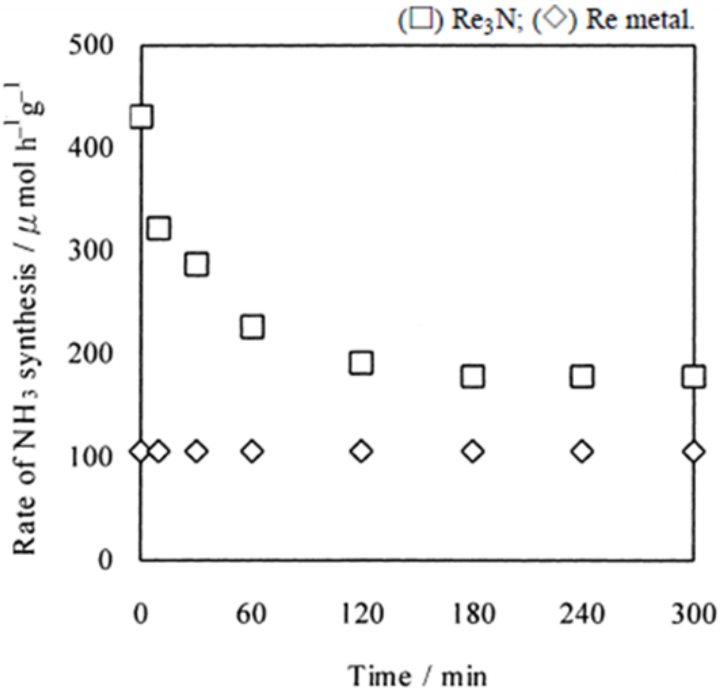

Figure 10: Ammonia Synthesis Rates 350°C under 0.1 MPa using 0.4 g of Re_3N (squares) and Re metal (diamonds) catalyst[24].

Caesium promoted Re/γ-Al_2O_3 catalysts were prepared and tested by Kojima *et al*[43]. Caesium nitrate was used as the Cs^+ precursor and it was introduced to Re/γ-Al_2O_3 by incipient wet impregnation. The material was then dried in air at 100°C for 12 hours. Prior to ammonia synthesis the materials were activated at with N_2/H_2 (1:3) for 2 hours between 350°C – 600°C. It was found in the case of non-promoted samples the activation temperature had little effect on their activity. This was in contrast to the Cs^+ promoted catalyst, as the activation temperature increased the rate of ammonia production also increased. At 350°C non-promoted Re/γ-Al_2O_3 showed higher activity compared to Cs^+ doped Re/γ-Al_2O_3. However, at higher temperatures the promoted catalyst had higher activity with maximum activity obtained at 550°C. It was noted at temperatures above 550°C there was the possibility of vaporization of the caesium promoter. A drawback of the addition of caesium is rhenium nitride was not formed; which is believed to be more active than Re metal[43] and complete formation of Re metal was not possible. Caesium is believed to be present on the surface as caesium hydroxide.

H_2 chemisorption was performed on the Cs^+ promoted and non-promoted 20 wt% Re/Al_2O_3 (Table 3). H_2 uptake on the non-promoted material was 39.4 µmol g^{-1} with 4% of Re atoms at the surface of the catalyst; with an estimated particle diameter of 33 nm. The results for the Cs^+ promoted catalyst were significantly different; the dispersion decreases to from 4% to 1.3%, with the estimated particle size increasing to 110 nm. The H_2 uptake is notably lower at 6.8 µmol g^{-1}. A difference could be expected with the addition of promoters due to: the promoter partially covering the active sites or Cs^+ electronically modifying the surface causing it to become less reactive to H_2. However, the decrease is larger than would be expected. It was concluded Cs^+ is a very efficient promoter for these materials giving enhanced activity.

Table 3: H_2 Chemisorption for Supported Re Catalysts[43].

Catalyst	H_2 uptake (μmol g^{-1})	Dispersion (%)
20 wt % Re/Al_2O_3	39.4	4.0
1Cs-20 wt % Re/Al_2O_3	6.8	1.3

Cobalt rhenium catalysts with bulk rhenium modified with cobalt in the atomic ratio 1:4 ($Co\text{-}Re_4$) have been shown to be particularly active for ammonia synthesis[44,48,127]. The high activity has been attributed to the formation and stabilization of a rhenium nitride phase[48]. Work by Kojima and Aika[24, 48] studied the effect of different metals and metal ratios on rhenium containing materials. The ratio of rhenium to cobalt, iron and nickel was investigated[48]. With respect to cobalt, the highest ammonia synthesis activity was achieved with an 80% Re content corresponding to a composition of $Co\text{-}Re_4$. The activity of the nickel-rhenium system remained fairly consistent with varying Ni to Re ratios. The maximum activity of the iron-rhenium system was also obtained at 80% ($Fe\text{-}Re_4$).

Rates for different transition metal containing rhenium catalysts are tabulated in Table 4. The highest activity was observed for $Co\text{-}Re_4$. The presence of both Re and Co are required for enhanced activity; the activities over pure Re and Co were 108 μmol g^{-1} h^{-1} and 3 μmol g^{-1} h^{-1} respectively[24]. Fe was found to slightly elevate the rate, this could be due to a synergy between the two metals or that Fe has intrinsic ammonia synthesis activity. The rate drastically decreases on addition of Cu and the rate is lower than that of pure Re metal, this is attributed to Cu acting as a diluent. Cr and Ni did not appear to significantly alter the ammonia synthesis activity.

Table 4: Ammonia Synthesis Rates for Different Rhenium Catalysts at 350°C under N_2/H_2 (1:3) at ambient pressure[24].

Catalyst	Rate ($\mu mol\ g^{-1}\ h^{-1}$)
Re	108
$Co-Re_4$	492
$Fe-Re_4$	275
$Ni-Re_4$	143
$Cr-Re_4$	119
$Cu-Re_4$	60

Due to the low surface area of $Co-Re_4$ Kojima and Aika dispersed the material on an $\gamma-Al_2O_3$ support[43]. In contrast to initial expectation, the higher surface area supported $Re/\gamma-Al_2O_3$ materials showed lower activity opposed to the unsupported Re metal. It was proposed rhenium interacts too strongly with the support forming rhenium oxides which cannot be easily reduced. Another possible explanation considers structural sensitivity. This is precedented in the case of supported NH_3 synthesis catalysts for example: for an Fe/MgO catalyst, it was found as the dispersion was increased the turnover frequency (TOF) decreased. The authors claim by decreasing the dispersion the active Fe (111) face becomes less exposed, therefore decreasing the TOF[128]. This is in contrast to Ru-based catalysts where by increasing the surface area increases the ammonia synthesis rate and studies have involved supporting Ru on high surface area materials[129-131].

Kojima and Aika[48] preformed a kinetic analysis on rhenium containing ammonia synthesis catalysts at 350°C and 3.1 MPa. In the case of Re, $Co-Re_4$ and $Ni-Re_4$ the results tabulated in Table 5. The authors suggest the rate limiting step is N_2 activation because the N_2 orders are close to 1, however, this is not always the case. Additionally, NH_3 and H_2 have negative reaction orders suggesting they saturate the surface of the catalyst. In comparison to Re metal the addition of cobalt simultaneously increases the degree of H_2 poisoning and decreases the strength of NH_3 poisoning. With the introduction of nickel both H_2 and NH_3 poisoning apparently strengthened. Kojima and Aika report the activity of $Co-Re_4$ increases with increasing reaction pressure[24].

Table 5: Reaction order for ammonia synthesis on Re catalysts at 350°C at 3.1 MPa. Adapted from[48].

Catalyst	NH_3 Order	H_2 Order	N_2 Order
Re	-0.82	-0.23	0.92
Co-Re_4	-0.54	-0.70	0.91

The work by Kojima and Aika[24, 43, 48] shows promising results for cobalt rhenium ammonia synthesis catalysts. However, after the early 2000's there has been limited published work on cobalt rhenium ammonia synthesis catalysts[25, 44, 127]. This shows there is huge scope to develop, understand and exploit these materials. The results and discussion in this chapter will be split into two distinct sections. The first will focus on cobalt rhenium catalysts and their precursors prepared and pre-treated at 600°C under N_2/H_2 (1:3). The second section will focus on the effect of different pre-treatment gas mixtures have on the structure and activity of $CoRe_4$. The main aim of this section is to characterise highly active, low surface area cobalt rhenium materials in greater detail than is currently available in the literature.

3.2 Ammonia Synthesis Activity of Cobalt Rhenium Catalysts and Corresponding Precursors

3.2.1 Precursor Activity: NH_4ReO_4 and $Co(NO_3)_2.6H_2O$

In order to establish whether the activity for ammonia production was due to one particular metal or if both rhenium and cobalt components are required; the individual precursors were reacted and compared to the $CoRe_4$ catalyst. The materials were pre-treated at 600°C for 2 hours under N_2/H_2 (1:3) then reacted at 400°C under the same gas composition. The vent gas was bubbled through a solution of 0.00108 M H_2SO_4 and the conductivity monitored. Steady state reactions present as linear decrease in conductivity over time. Figure 11 presents a plot of conductivity versus time for NH_4ReO_4, $Co(NO_3)_2.6H_2O$ and $CoRe_4$ catalyst. A distinction can be observed between the performance of the Re and Co precursors and the $CoRe_4$ catalyst.

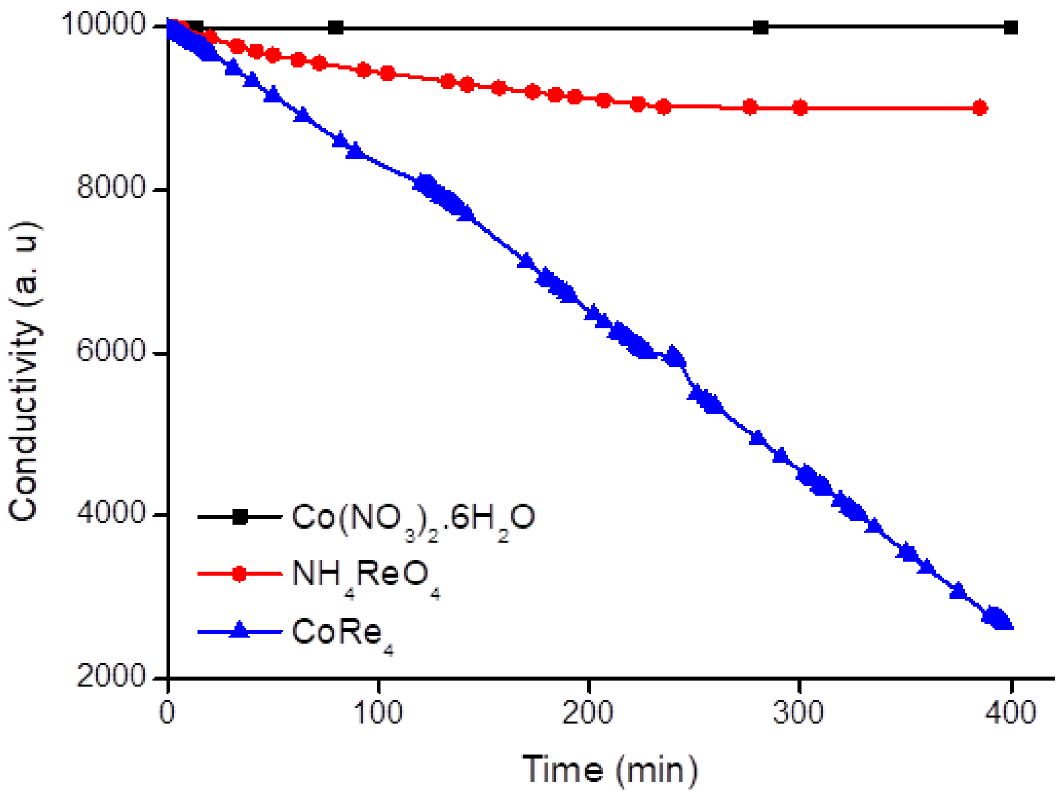

Figure 11: Reaction conductivity profiles for Re and Co Precursors compared with $CoRe_4$, pre-treated for 2 hours at 600°C with N_2/H_2 (1:3) then reacted at 400°C with N_2/H_2 (1:3) at ambient pressure.

It was found $Co(NO_3)_2.6H_2O$ is completely inactive towards ammonia synthesis under these reaction conditions. The NH_4ReO_4 shows some apparent initial activity which presents as a deactivation over time resulting in an eventual deactivation after approximately 3 hours. The post reaction sample of NH_4ReO_4 gives a metallic material which was found to be rhenium metal. A marked difference in activity can be observed for the $CoRe_4$. This material gives a highly active material with an activity of 943 ± 44 µmol g^{-1} h^{-1} and presents as a continuous linear decrease in conductivity over time which would be expected for ammonia being catalytically produced. The plot in Figure 11 is truncated to 400 minutes however, $CoRe_4$ was tested for more than 48 hours and retained steady state behaviour during the entire testing period (Figure 12).

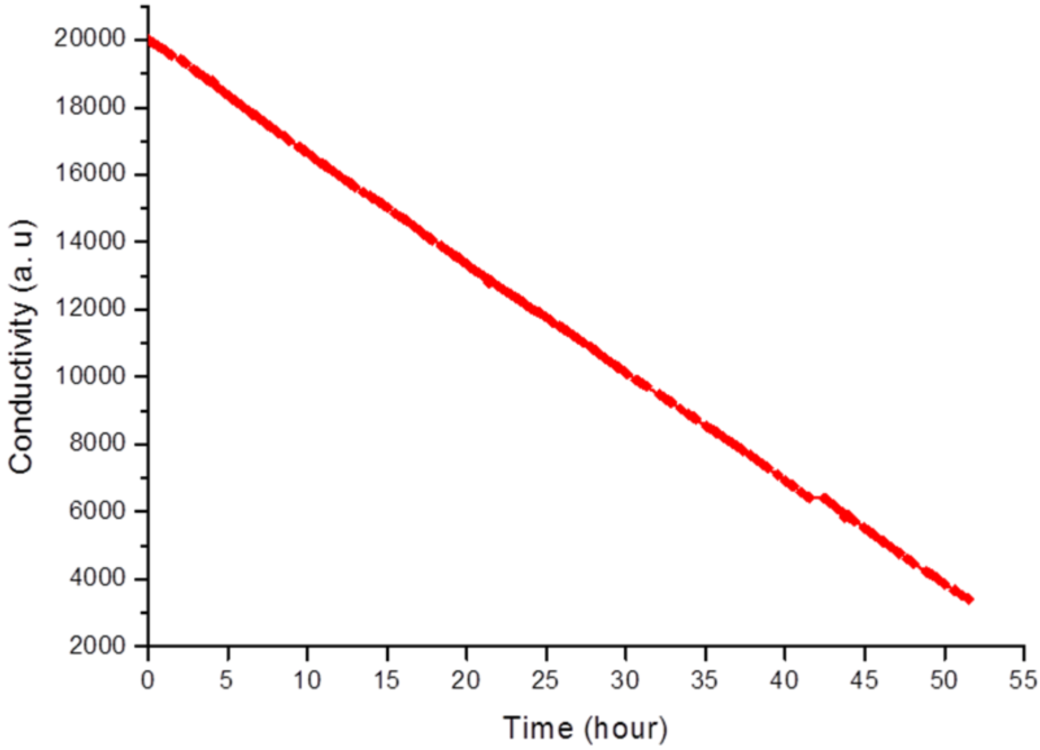

Figure 12: Extended reaction conductivity profile for $CoRe_4$, pre-treated for 2 hours at 600°C with N_2/H_2 (1:3) then reacted at 400°C with N_2/H_2 (1:3) at ambient pressure.

The steady state activity for the extended $CoRe_4$ reaction was found to be 915 µmol g^{-1} h^{-1} (which occurs within the reported ammonia synthesis rate of 943 ± 44 µmol g^{-1} h^{-1})[127]. To further verify the production of ammonia the vent gas was flowed into 5 ml of deionized H_2O for 10 minutes then Nessler's reagent was added to the sample, which gave a positive result for the presence of ammonia. It was concluded a combination of both rhenium and cobalt are required for the enhanced ammonia synthesis activity and the high activity could not be achieved through the individual metal precursors.

3.2.2 Effect of Employing an Ammonolysis Stage

Previously in the literature, active $CoRe_4$ catalysts were prepared by pre-treatment of their precursors with NH_3[24, 43, 44, 48]. However, Wise and Markel argue in relation to the binary molybdenum nitride system, ammonolysis is not practical on a large scale for the preparation of nitrides from oxide precursors due to a number of issues such as heat transfer and it is suggested nitridation from N_2/H_2 mixtures would be preferable[132]. It is important to note prior to the current study[127] there was no mention within the literature of producing cobalt rhenium materials without employing an ammonolysis stage.

In this study we have compared $CoRe_4$ catalysts prepared with and without ammonolysis of the precursors. For both resultant materials, pre-treatment has been undertaken using N_2/H_2 (1:3) at 600°C and the ambient pressure steady state ammonia synthesis activities at 400°C are reported in Table 6.

Table 6: Ammonia Synthesis Rates of $CoRe_4$ Prepared with and without Ammonolysis, pre-treated for 2 hours at 600°C with N_2/H_2 (1:3) then reacted at 400°C with N_2/H_2 (1:3) at ambient pressure.

Preparation Route	**Steady State Ammonia Synthesis Rate (μmol g^{-1} h^{-1})**
Ammonolysis Step	655 ± 129
No Ammonolysis Step	943 ± 44

In this work employing an ammonolysis stage gives a steady state rate of 665 ± 129 μmol g^{-1} h^{-1} which is relatively similar to values reported by Kojima and Aika[24]. However, from Table 6 it can be clearly seen ammonolysis is not a necessary step in the preparation of active cobalt rhenium catalysts. Hypothetically if thermodynamic equilibrium was attained under the same reaction conditions it would correspond to a 0.4 % yield and hence a limiting mass normalised rate of approximately 2140 μmol g^{-1} h^{-1} under the flowrate applied. Therefore, the higher activity catalyst appears to be operating at approximately 44% of the equilibrium value. Drawing comparisons from other systems verifies the high activity of this material, rates of 437 μmol g^{-1} h^{-1} Re/MCM-41[133], 652 μmol g^{-1} h^{-1} for Co_3Mo_3N[22] and *ca.* 400 μmol g^{-1} h^{-1} for Ni_2Mo_3N[134] are reported for systems with comparable conditions applied to those in this study. The highest activities reported in the literature to date are those reported on Ru dispersed on electride, a rate of 3550 μmol g^{-1} h^{-1} has been reported at atmospheric pressure and 340°C[135].

In this work conductivity measurements were used to monitor ammonia production. Absolute ammonia synthesis rates are not presented due to high noise in the measurements (Figure 27) and incomplete dissolution of ammonia in the acid solution. However, the rates presented in this work can be used comparatively as Kojima and Aika use the same conductivity method of ammonia analysis.

To investigate any changes in phase, XRD was performed and the results are presented in Figure 13. Reference patterns were taken from Re PDF: 00-005-0702 and Co PDF: 01-089-4307.

Regarding the material prepared by the ammonolysis method, this pattern is in accordance with XRD patterns presented by Kojima and Aika who synthesised Co-Re_4 using the same process (Figure 9)[24]. The Re reflections are broad and there is a Co (111) shoulder present. Also, in the NH_3 treated material the Re (102) reflection is present which is not as evident in the un-treated material. For the un-treated $CoRe_4$ catalyst it can be argued there is a shift of rhenium reflections to a higher angle. The ratios of intensity of the standard Re (100), (002) and (101) reflections match the trend in intensities of the three main reflections in the un-treated $CoRe_4$. Also, the position of the reflections are shifted approximately 2° higher for each of the main reflections in the un-treated XRD pattern. The Co (111) shoulder is not obviously present in un-treated $CoRe_4$ this could possibly be due to the overlap of the Co (111) and shifted Re (101) reflection. Soto *et al*[46] prepared rhenium nitride films by reactive DC sputtering. The films were deposited at ambient temperature using various nitrogen concentrations and the authors discuss the shifting of rhenium XRD reflections with varying nitrogen content. They find with increasing nitrogen content this causes a downward shift of peaks. This is attributed to incorporation of nitrogen causing an expansion in the unit cell.

For the $CoRe_4$ material used in this study, when an ammonolysis stage is performed this material gives Re (101), (002) and (011) reflections. The shifting of the Re reflections to a higher 2θ angle could indicative of a bimetallic interaction with Co (metallic radius 152 pm) substituting for Re (metallic radius 188 pm)[136].

The differences between these two XRD patterns shows the effect of using an ammonolysis stage during synthesis and implies two different catalysts are forming which is reflected in the higher activity of the un-treated $CoRe_4$ catalyst.

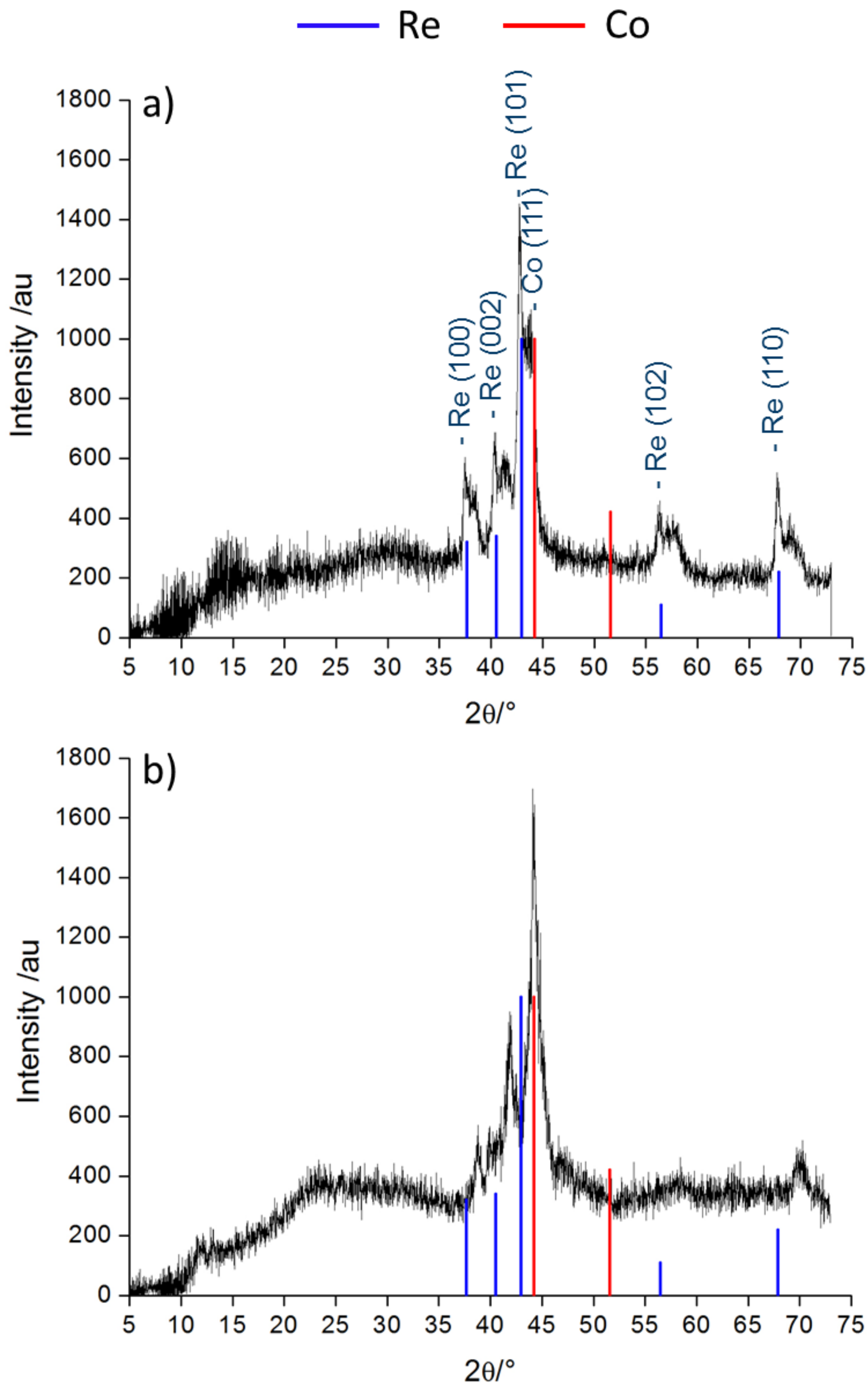

Figure 13: Powder X-ray diffraction patterns of post reaction $CoRe_4$ prepared a) with ammonolysis b) without ammonolysis, pre-treated for 2 hours at 600°C with N_2/H_2 (1:3) then reacted at 400°C with N_2/H_2 (1:3) at ambient pressure.

The effect of ammonolysis on the morphology of $CoRe_4$ was investigated *via* SEM and the results are presented in Figure 14. Although 2 micrographs are shown on the 50µm scale from each material, multiple SEM images (> 25) were taken for each sample and the images presented are representative of the material and no other features were observed.

When treatment with NH_3 is used the post reaction $CoRe_4$ has a more plate-like shape. However, around the platelets there are crystals that resemble the morphology observed in the un-treated $CoRe_4$. On closer inspection the platelets have irregular orientation and a wide distribution of sizes which are generally smaller compared to $CoRe_4$ that has not been subjected to ammonolysis. The un-treated $CoRe_4$ material has an irregular structure with rough and smooth regions and analysis *via* EDX can detect no difference in the concentrations of both Re and Co within the different areas.

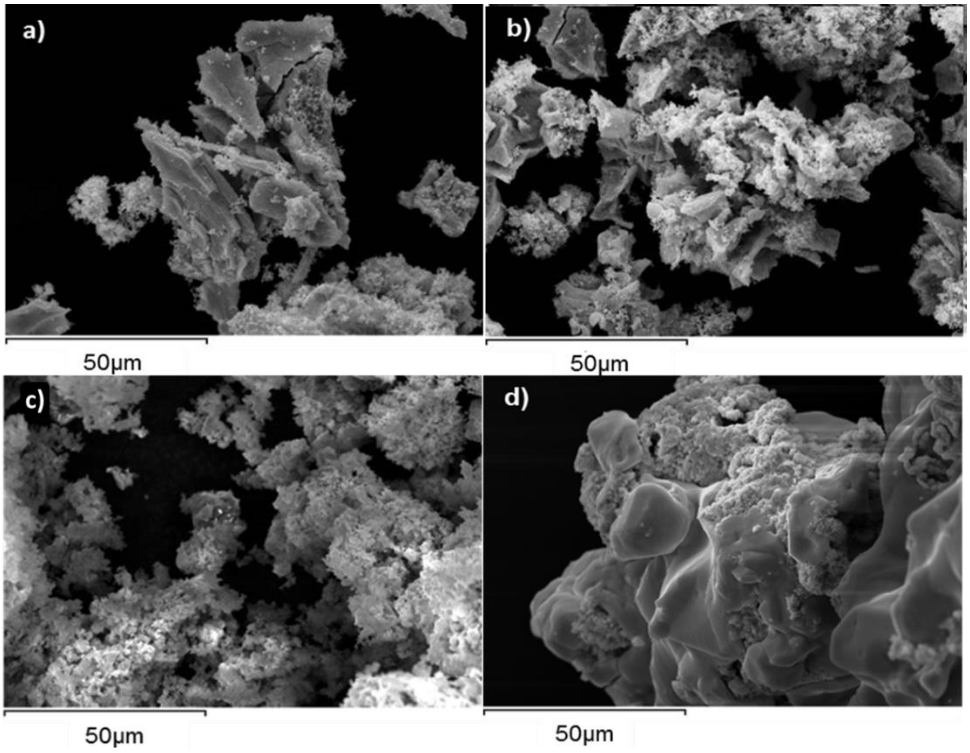

Figure 14: Post reaction SEM images for $CoRe_4$. $CoRe_4$ pre-treated with N_2/H_2 (1:3) for 2 h at 600°C N_2/H_2 reaction at 400°C a-b) ammonolysis step used and c-d) no ammonolysis step.

It was concluded ammonolysis is not a necessary step in the preparation of highly active ammonia synthesis catalysts and indeed the mass normalised rates determined exceed that of the material prepared by ammonolysis. Therefore, to achieve a higher activity with a simplified synthesis route, in this work from here on in an ammonolysis step was not used.

3.2.3 Effect of Changing Cobalt and Rhenium Precursors

In all previous literature, cobalt rhenium materials were prepared with NH_4ReO_4 as the Re precursor[24, 25, 43, 48]. Therefore, different rhenium precursors were used to investigate the effect of rhenium precursor on the ammonia synthesis activity of $CoRe_4$. The resulting ammonia synthesis rates are displayed in Figure 15.

The difference in precursor structure may help to understand if the precursor phase is an important factor or if the presence of Re is the only requirement. NH_4ReO_4 possesses a tetragonal crystal system with the Re species tetrahedrally coordinated to four oxygen ions forming ReO_4^-, with the NH_4^+ acting as a charge balancing counter ion. Re is in the +7 oxidation state. The Re_2O_7 structure consists of a double layer chain structure of Re_4O and Re_6O units covalently bound together with oxygen bridges[137,138]. The terminal Re-O bonds are shorter than the bridging Re-O bonds. The crystal structure of $ReCl_5$ was studied by Mucker *et al*[139]. They report $ReCl_5$ consists of monoclinic crystals with eight $ReCl_5$ units contained within the cell. The structure is based on a double-hexagonal close packing of Cl species where Re atoms occupy one fifth of the octahedral holes. $KReO_4$ consists of ReO_4^- units which form a tristetrahedron around the potassium.

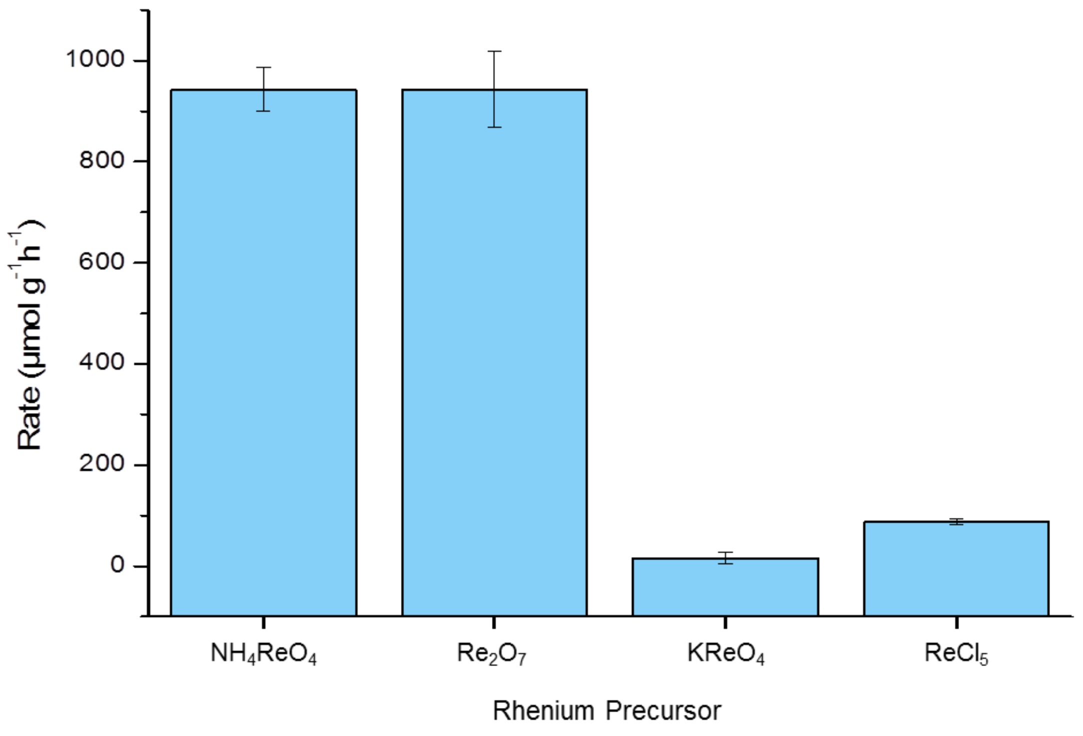

Figure 15: Steady State Ammonia Synthesis Rates for $CoRe_4$ Prepared from Different Rhenium Precursors, pre-treated for 2 hours at 600°C with N_2/H_2 (1:3) then reacted at 400°C with N_2/H_2 (1:3) at ambient pressure.

From the ammonia synthesis rates presented in Figure 15, no marked contrast in activity can be observed between $CoRe_4$ catalysts prepared with NH_4ReO_4 (943 ± 44 µmol g^{-1} h^{-1}) or Re_2O_7 (943 ± 75 µmol g^{-1} h^{-1}). However, it is evident the inclusion of potassium or chloride in the precursor has a drastic negative effect on the catalytic ability of the material; $KReO_4$ (16 ± 11 µmol g^{-1} h^{-1}) or $ReCl_5$ (88 ± 5 µmol g^{-1} h^{-1}). It can be postulated the presence of these elements disrupts the formation of the active catalyst, possibly by a detrimental electronic modification of the material. With regard to the Haber-Bosch Process it is well established the introduction of K^+ greatly increases the ammonia synthesis rate of the iron catalyst *via* an electronic promotion effect[1,6]. However, in the case of $CoRe_4$ the presence of potassium appears to have the opposite effect and causes almost complete deactivation of the material.

Pre-reaction XRD patterns for $CoRe_4$ prepared from different Re precursors are presented in Figure 16. Reference patterns were taken from NH_4ReO_4 PDF: 00-010-0252, Re_2O_7 PDF: 00-039-0934, $KReO_4$ PDF: 00-008-0044 and $ReCl_5$ PDF: 00-037-1291. The pre-reaction materials the XRD patterns are representative of the calcined material that is initially placed in the reactor after which further transformation occurs *in situ*. These materials have been synthesised then calcined at 700°C in air for 3 hours. In all cases the pre-reaction XRD patterns resemble the specific Re precursor used along with additional unidentifiable reflections.

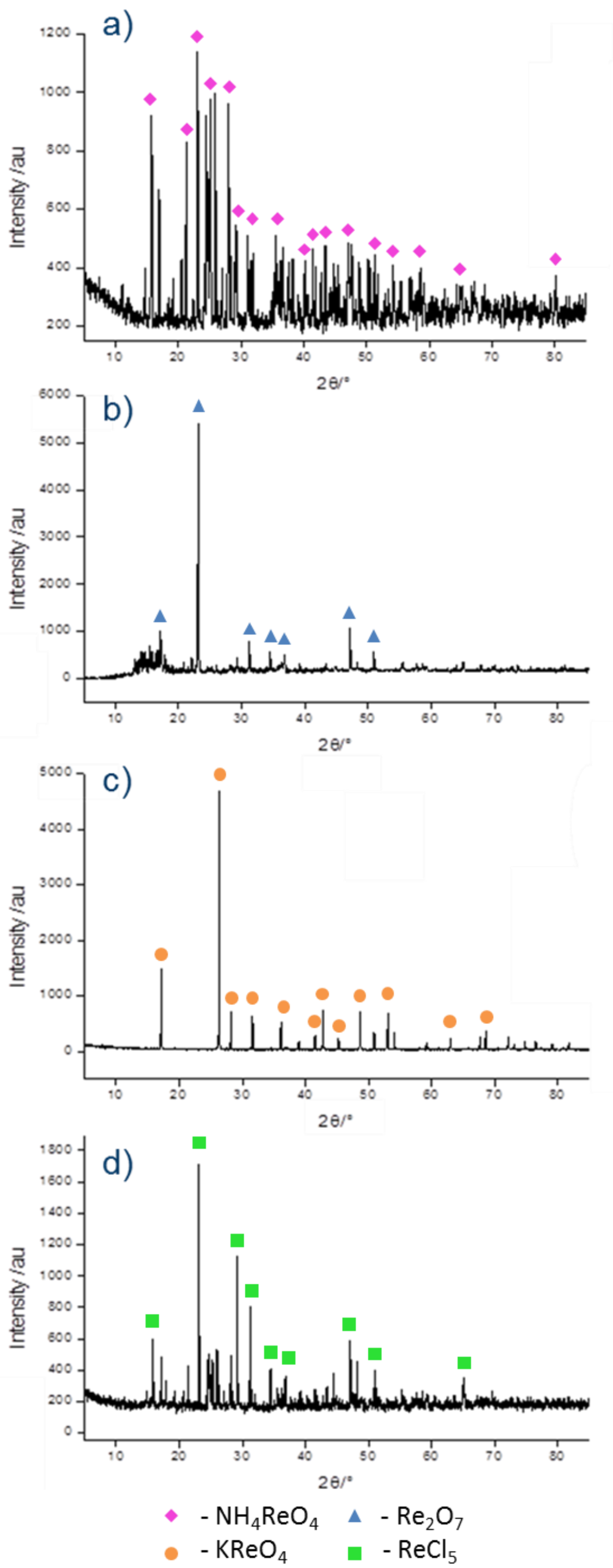

Figure 16: Pre-reaction XRD Patterns for $CoRe_4$ Prepared from Different Re Precursors a) NH_4ReO_4, b) Re_2O_7, c) $KReO_4$ and d) $ReCl_5$.

Figures 17-20 present the post-reaction patterns for $CoRe_4$ from the different starting materials. All catalysts were pre-treated for 2 hours at 600°C under N_2/H_2 (1:3) then cooled to 400°C and reacted under N_2/H_2 (1:3).

The patterns from materials prepared from NH_4ReO_4 and Re_2O_7 are very similar. Again as mentioned in Section 3.2.2 the XRD patterns appear to have the Re (100), (002) and (101) reflections shifted to a higher 2θ angle and for this reason the Re and Co reflections are not labelled. The have a broad amorphous section under the peaks, which could be attributed to rhenium nitride. It can be postulated due to the similarity of the XRD patterns the materials synthesised from these two precursors results in the same active material.

$CoRe_4$ synthesised from $KReO_4$ has sharp narrow crystalline peaks which exactly correspond to Re metal. The reflections above 50° are more prominent in comparison to $CoRe_4$ from other precursors. There is evidence of ReO_3 (reference PDF: 00-045-1039) however, it is postulated this most likely forms on discharge from the reactor. Also, the amorphous rhenium nitride feature is not present as the background under the Re (100), (002) and (101) reflections is flat.

The post-reaction XRD pattern from $ReCl_5$ has a high background which may obscure features. The exact Re (100), (002) and (101) reflections are present but of a lower intensity. The Re (002) reflection is very weak and the Co (200) reflection is present. Also, the emergence of the ReO_3 (012) reflection is consistent with the other low activity material derived from $KReO_4$.

Interestingly the two materials which have very low ammonia synthesis activity (synthesised from $KReO_4$ and $ReCl_5$) have patterns which exactly match the Re (100), (002) and (101) reference pattern. Also, the catalyst synthesised from $KReO_4$ has the lowest activity and the XRD pattern the most similar to pure Re metal. In contrast the catalysts synthesised from NH_4ReO4 and Re_2O_7 show high ammonia synthesis activity and both the XRD patterns show a shift of the Re reflections to a higher 2θ.

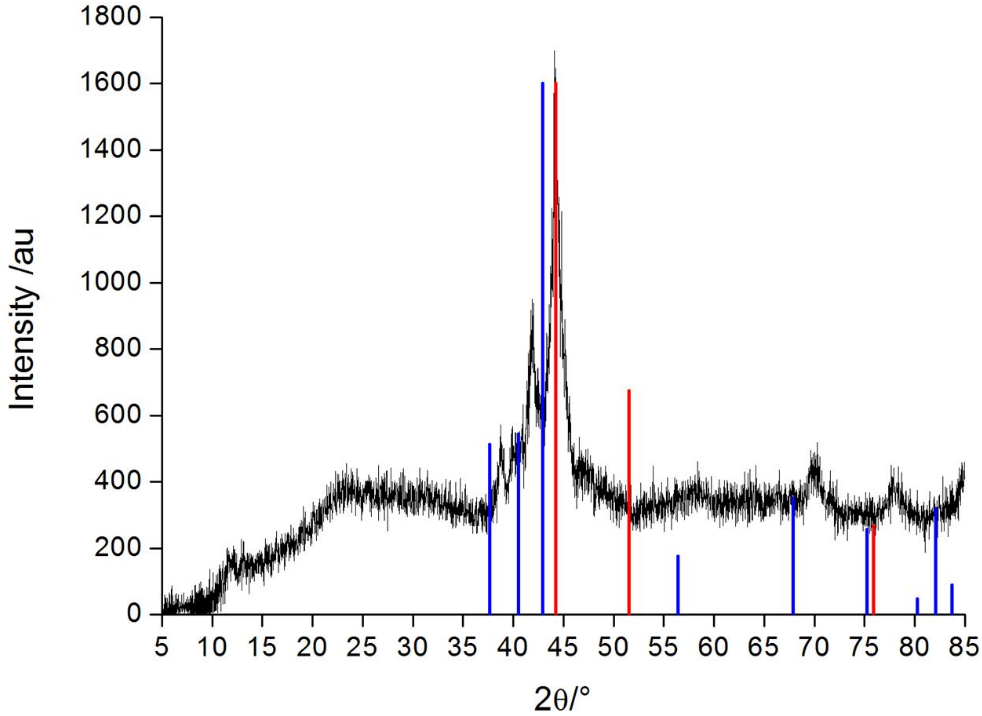

Figure 17: XRD Patterns for Post-reaction $CoRe_4$ Prepared from NH_4ReO_4. Blue) Re PDF 00-005-0702 and Red) Co PDF 01-089-4307.

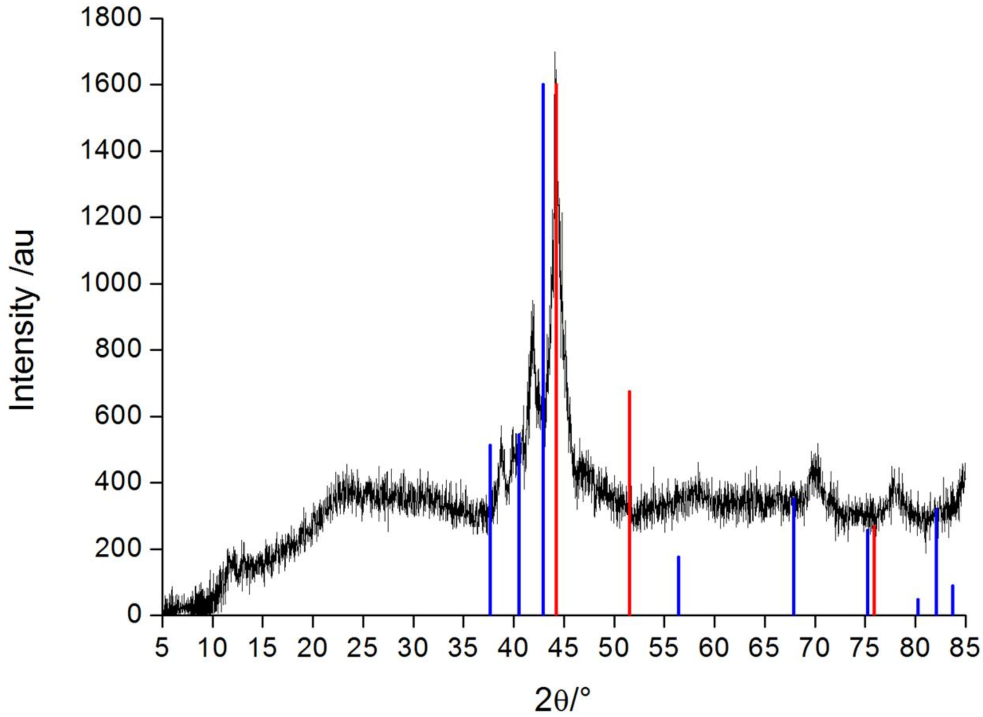

Figure 18: XRD Patterns for Post-reaction $CoRe_4$ Prepared from Re_2O_7. Blue) Re PDF 00-005-0702 and Red) Co PDF 01-089-4307.

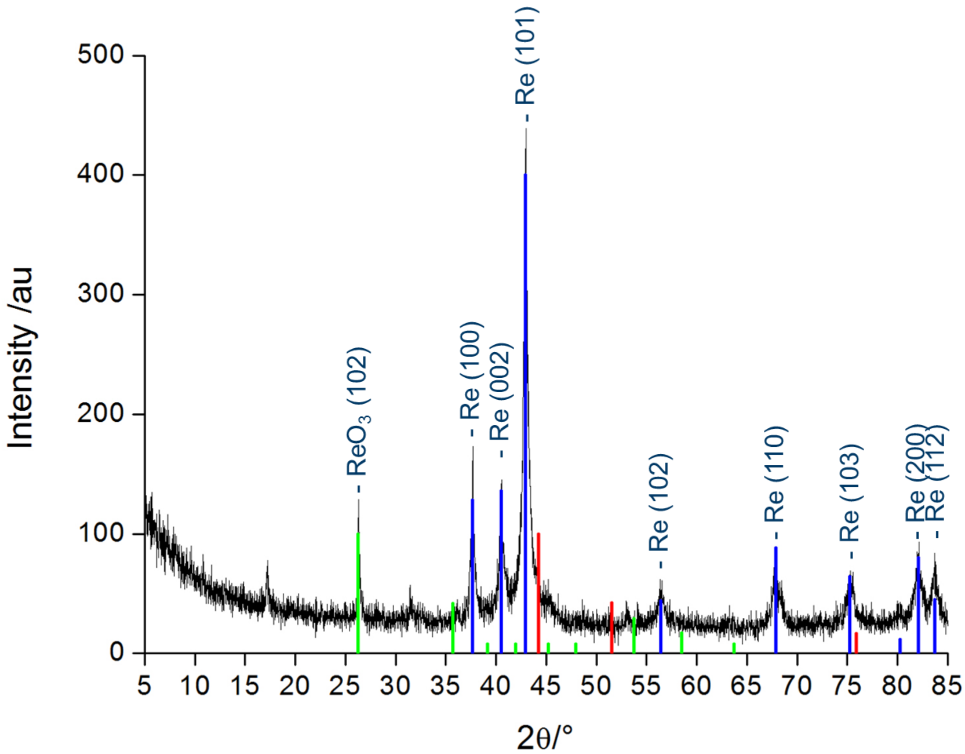

Figure 19: XRD Patterns for Post-reaction $CoRe_4$ Prepared from $KReO_4$. Blue) Re PDF 00-005-0702, Red) Co PDF 01-089-4307 and Green) ReO_3 PDF 00-045-1039.

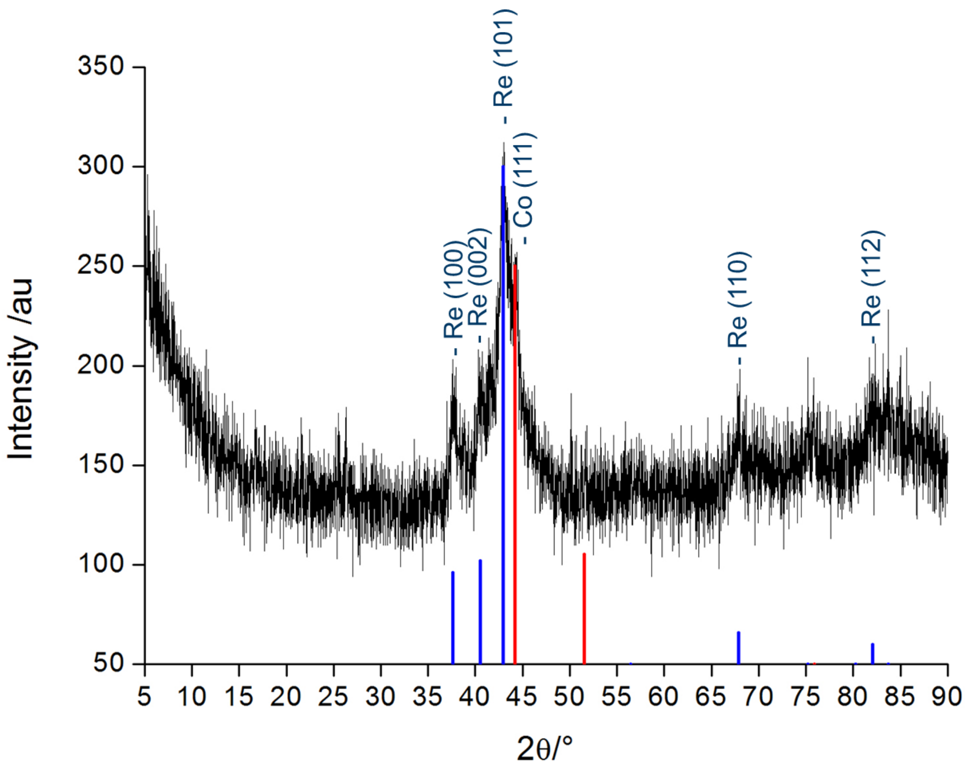

Figure 20: XRD Patterns for Post-reaction $CoRe_4$ Prepared from $ReCl_5$ Blue) Re PDF 00-005-0702 and Red) Co PDF 01-089-4307.

Surface morphology and particle size/shape were investigated *via* SEM. Figure 21 presents SEM images for post-reaction $CoRe_4$ prepared from NH_4ReO_4, Re_2O_7, $KReO_4$ and $ReCl_5$.

When the NH_4ReO_4 precursor is used the resulting $CoRe_4$ catalyst has a very high ammonia synthesis rate despite having an irregular morphology and no distinct shape. $CoRe_4$ synthesised from Re_2O_7 has the same high activity but results in cubic particles ranging from approximately 10 µm to 100 µm. However, on close inspection it can be argued both catalysts have smooth features with agglomerated smaller particles on the surface. This suggests the activity is not dependent on the gross shape of the particles but more the texture of the surface. Analysis by EDX detects no difference in the smooth and rough regions and therefore, cannot specifically assign a Re or Co species to either. $CoRe_4$ synthesised from $KReO_4$ gives small (< 50 µm) agglomerated particles with a smooth surface and the attached agglomerates also have a smooth texture. Round nodules of 2 – 5 µm in diameter appear on the surface of post reaction $CoRe_4$ synthesized from $ReCl_5$, these are not present when other precursors are used. The formation of these nodules may be the reason the material has extremely low ammonia synthesis activity. The particle size is smaller in the case of the lower activity materials prepared from $KReO_4$ and $ReCl_5$ (< 50 µm) compared to (> 50 µm) more active NH_4ReO_4 and Re_2O_7 synthesised $CoRe_4$ materials.

To further investigate the surface compositions of the materials elemental mapping was performed in order to elucidate whether the different textured regions on the surface can be attributed to different species. The results are presented for NH_4ReO_4 (Figure 22), Re_2O_7 (Figure 23), $KReO_4$ (Figure 24), and $ReCl_5$ (Figure 25).

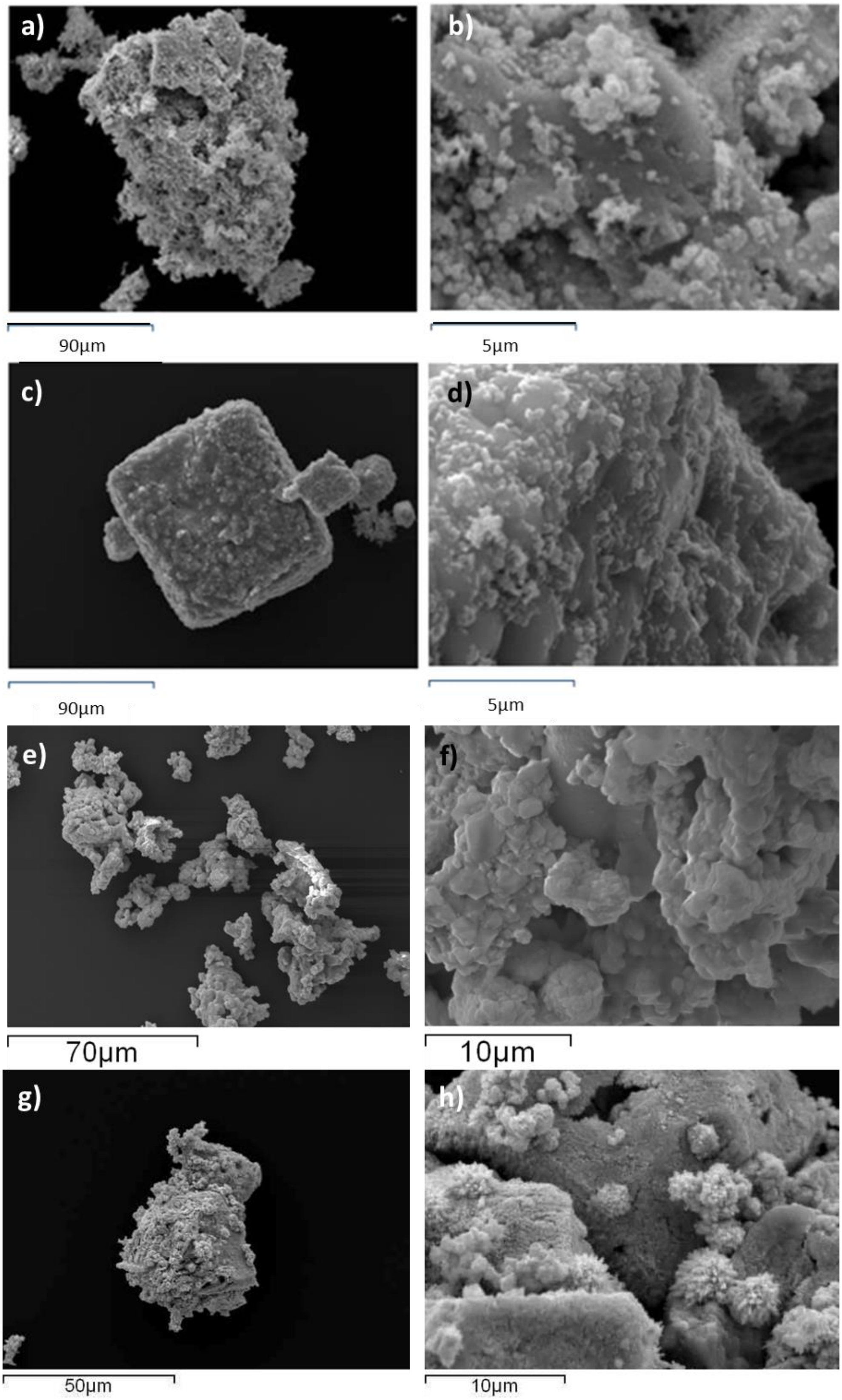

Figure 21: SEM Images for Post Reaction $CoRe_4$ Prepared with Different Rhenium Precursors: a-b) NH_4ReO_4, c-d) Re_2O_7, e-f) $KReO_4$ and g-h) $ReCl_5$.

Figures 22 and 23 present element maps for $CoRe_4$ prepared from NH_4ReO_4 and Re_2O_7 respectively. It can be seen in both cases there is a fairly homogeneous mix of both Re and Co. For $CoRe_4$ prepared from NH_4ReO_4 it could be argued the smooth areas contain a slightly higher amount of Re and the small agglomerated particles on the surface have a slightly higher concentration of Co. However, both materials do have a moderately homogeneous mix of both Re and Co.

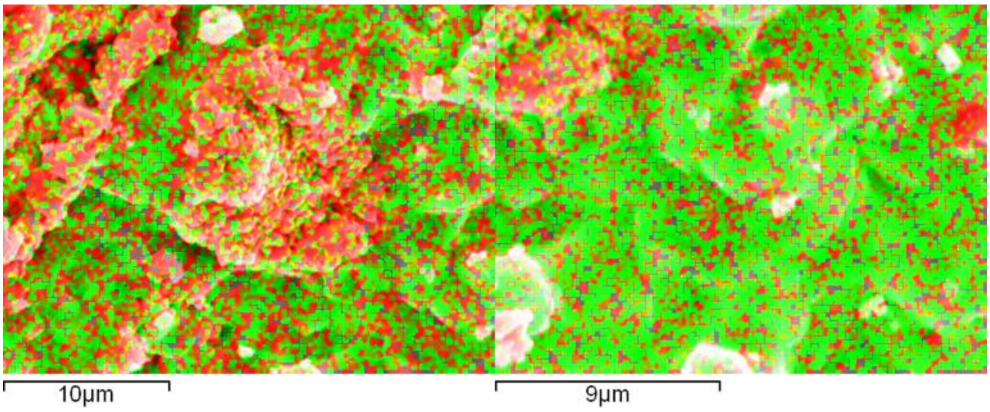

Figure 22: Element Maps for Post Reaction $CoRe_4$ Prepared from NH_4ReO_4. Elements: Re (green), Co (red).

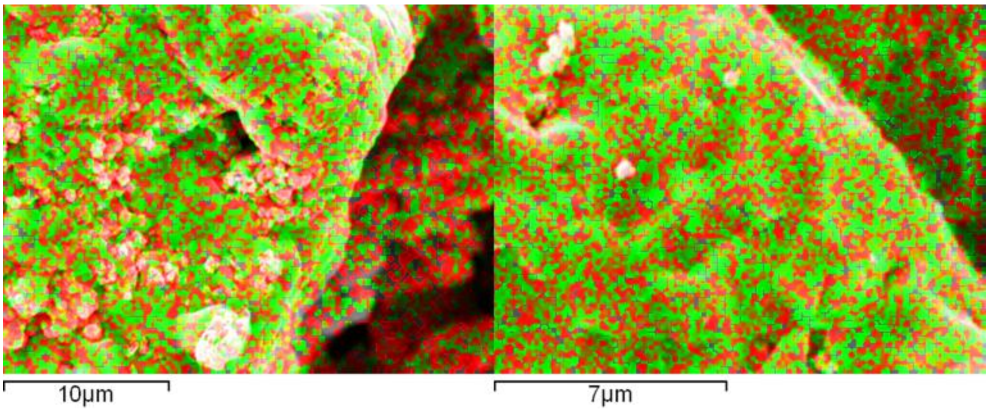

Figure 23: Element Maps for Post Reaction $CoRe_4$ Prepared from Re_2O_7. Elements: Re (green), Co (red).

Considering the surface of $CoRe_4$ prepared from $KReO_4$, from the element maps shown in Figure 24 it can be seen the potassium (represented in blue) appears to accumulate in specific areas and is not homogeneously dispersed throughout the material. It is postulated the potassium is likely to be highly mobile under reaction conditions and the decrease in activity could possibly be attributed to electronic modification by K^+ as potassium often acts as a promoter. Also, comparing these element maps to those of the other precursors it can be seen the overall surface concentrations of Re and Co are much lower.

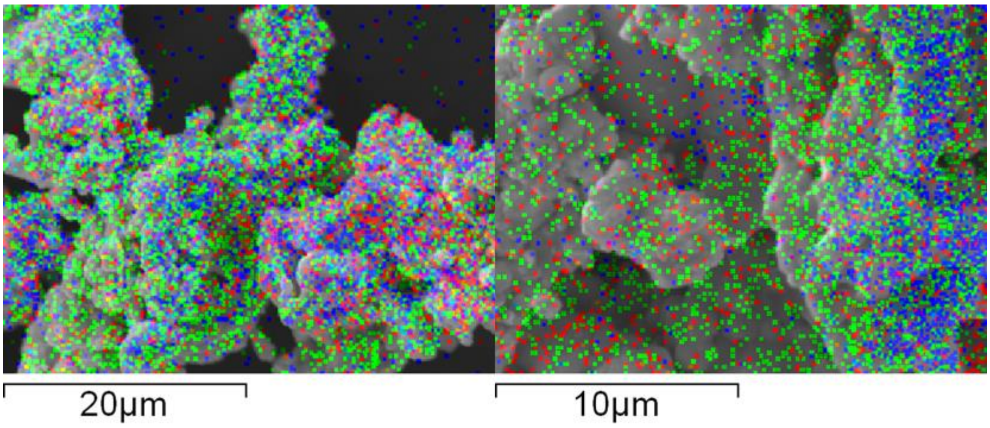

Figure 24: Element Maps for Post Reaction $CoRe_4$ Prepared from $KReO_4$. Elements: Re (green), Co (red) and K (blue).

Element mapping of $CoRe_4$ prepared from $ReCl_5$ (Figure 25) reveals an inhomogeneous material. Round nodules are present on the surface, which are clearly seen in Figure 21 (image h). Element mapping of the surface reveals these growths mainly comprise of Re. Clusters of Co are also seen on the surface. There is a high O surface content in comparison to the other $CoRe_4$ materials. The distinct areas of Co and Re suggests lack of mixing of the metals during synthesis which may contribute to the inactivity of the material.

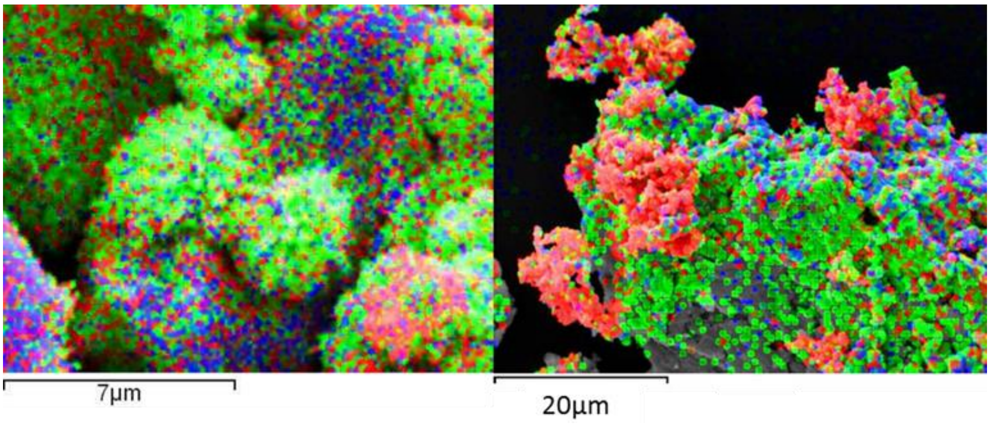

Figure 25: Element Maps for Post Reaction $CoRe_4$ Prepared from $ReCl_5$. Elements: Re (green), Co (red) and O (blue).

To conclude, potassium is a known promoter for the Haber-Bosch iron catalyst but appears to cause significant deactivation when introduced at the initial synthesis stage of $CoRe_4$. $CoRe_4$ materials prepared from NH_4ReO_4 and Re_2O_7 have the same high ammonia synthesis activity despite having a different particle shape (ill-defined versus cubic). Also, for these two active materials the XRD patterns are very similar with a slight shift of Re reflections. Whereas, for the materials prepared from $ReCl_5$ and $KReO_4$ the ammonia synthesis activity is low and features in the XRD patterns exactly match Re metal. In order to advance this work it would be desirable to vary the Co precursor to see if an enhanced rate can be achieved.

3.2.4 Probing $CoRe_4$ for Surface or Lattice Nitrogen

To assess for potential lattice or surface stored nitrogen $CoRe_4$ was pre-treated with N_2/H_2 at 600°C for two hours under N_2/H_2 (1:3). Then the temperature reduced to 400°C and reacted under Ar/H_2 (1:3) and the conductivity of 0.00108 M H_2SO_4 solution monitored. The conductivity profile is presented in Figure 26.

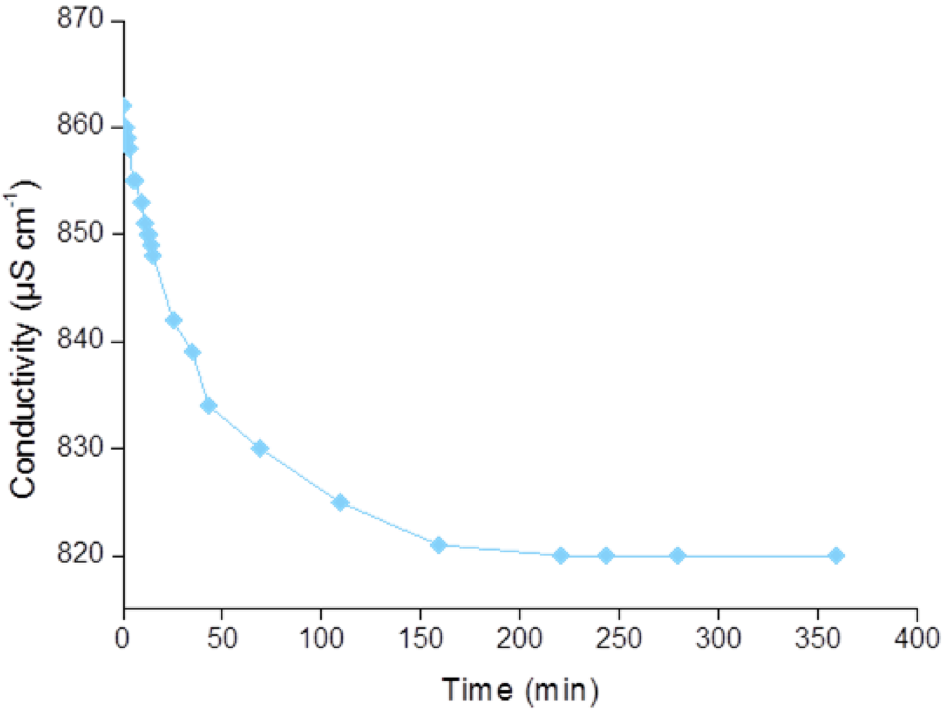

Figure 26: Conductivity Profile for $CoRe_4$ pre-treated with N_2/H_2 (1:3) at 600°C for 2 hours then reacted under Ar/H_2 (1:3) at 400°C.

Figure 26 presents an overall drop in conductivity of 42 µS cm^{-1} which corresponds to a total ammonia production of approximately 35 µmoles of ammonia over 200 minutes, after which no further ammonia production is observed. In comparison the $CoRe_4$ gives steady state behaviour for over 48 hours and in 200 minutes gives a drop in conductivity of over 1000 µS cm^{-1} corresponding to the production of over 880 µmoles of ammonia. Due to the low ammonia production is it postulated the residual nitrogen is stored on the surface and/or in the near surface region after pre-treatment and not in the bulk. However, due to the low surface area (< 0.2 m^2 g^{-1}) it is not possible to store substantial quantities of nitrogen on the surface.

In order to confirm the drop in conductivity is due to NH_3 production and not thermal effects in the 0.00108 M H_2SO_4 solution a blank reaction was carried out (Figure 27). It can be seen the blank reaction does show a variation in conductivity over the testing period. However, the fluctuations are sporadic unlike the smooth exponential decrease observed in Figure 26. Also, the reaction probing the surface nitrogen for $CoRe_4$ was repeated and in both cases the result presented as a smooth decrease over time.

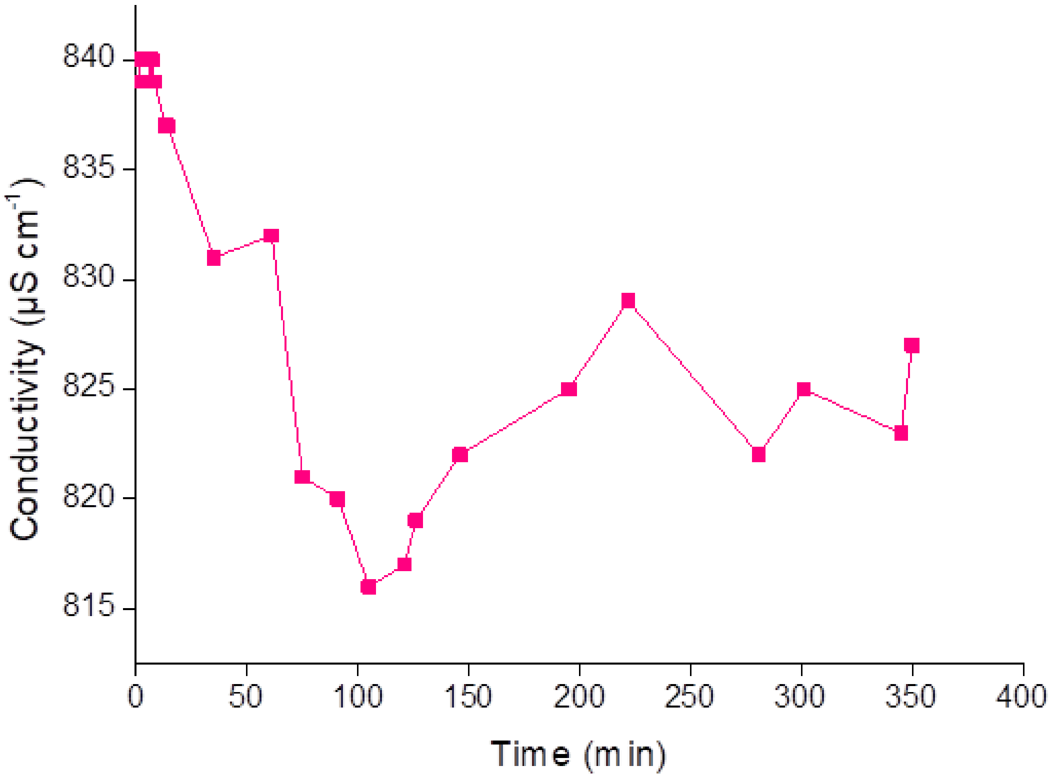

Figure 27: Blank Reaction.

3.2.5 Re-usability Tests for $CoRe_4$

The current Haber-Bosch promoted iron catalyst has a lifetime of over 10 years[1]. Therefore, stability and longevity of a catalyst is highly important. An initial study has been performed to test the durability of $CoRe_4$. In order to test the reusability of $CoRe_4$ the same sample was reacted multiple times over approximately 100 days. $CoRe_4$, was prepared from NH_4ReO_4 and $Co(NO_3)_2.6H_2O$. For these tests, the same 0.3 g sample of $CoRe_4$ was reacted four times. After each reaction the sample was removed (in the quartz reactor tube) from the reactor and stored in air. A 600°C N_2/H_2 (1:3) pre-treatment was only performed on the initial run and subsequent runs involved ramping to 400°C at 10°C min^{-1} under N_2/H_2 (1:3) and reaction at 400°C under the same gas mixture. Regarding the reaction time frames: Run 1 (initial reaction), Run 2 (11 days after initial reaction), Run 3 (20 days after initial reaction) and Run 4 (103 days after initial reaction) the steady state ammonia synthesis reaction rates for each run are presented in Figure 28.

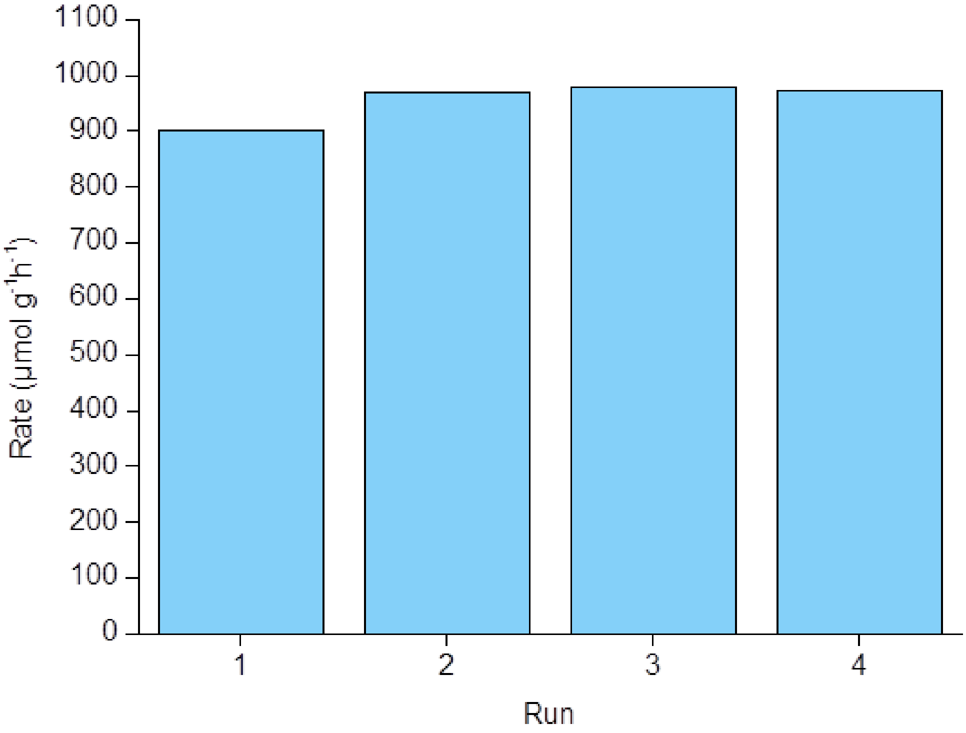

Figure 28: Reaction Rates for Repeated Reactions of the Same $CoRe_4$, Run 1 pre-treated for 2 hours at 600°C with N_2/H_2 (1:3) then reacted at 400°C with N_2/H_2 (1:3) at ambient pressure. Runs 2 - 4 reacted at 400°C with N_2/H_2 (1:3) at ambient pressure.

From Figure 28 it may be argued a slight increase in rate is observed from Run 1 to Run 2 (902 to 971 µmol g^{-1} h^{-1}). Then no change is observed between Runs 2, 3 and 4 (971, 980 and 973 µmol g^{-1} h^{-1}). However, all these values fall within the experimental steady state ammonia synthesis rate of 943 ± 44 µmol g^{-1} h^{-1} previously reported in Table 6. This is a promising result as it shows $CoRe_4$ does not simply deactivate after one reaction run and exposure to air and ambient moisture does not seem to affect the catalytic ability of the material. To further test the behaviour and longevity of $CoRe_4$ it would be beneficial to preform aging cycles on the material.

3.2.6 Effect of Changing the Cobalt to Rhenium Synthesis Ratio

Concerning cobalt rhenium catalysts for ammonia synthesis; within the literature the main focus has been on the synthesis ratio Co to Re of 1:4[24, 43, 44, 48, 127]. Therefore, the main focus in this study has been on $CoRe_4$ materials in order to draw suitable comparisons from previous work. A brief study by Kojima and Aika[24] investigated $CoRe_3$, $CoRe_4$, $CoRe_6$ and $CoRe_9$ at 350°C and ambient pressure. For the cobalt rhenium system they claim the maximum activity was obtained using the $CoRe_4$ catalyst. However, regarding the activity data the authors present no proof of repeated measurements as no error bars are given. Thus the question as to whether is this 1:4 (Co:Re) synthesis ratio is optimal or is it possible to maintain a high ammonia synthesis rate with a lower rhenium content can be raised. Lowering the rhenium content is obviously highly desirable due to the expense and scarcity of the metal. In this work the cobalt to rhenium synthesis ratios were altered between: Co_8Re, Co_4Re, Co_2Re, CoRe, $CoRe_2$, $CoRe_4$ and $CoRe_8$.The ammonia synthesis rates are displayed in Figure 29 and are tabulated in Table 7.

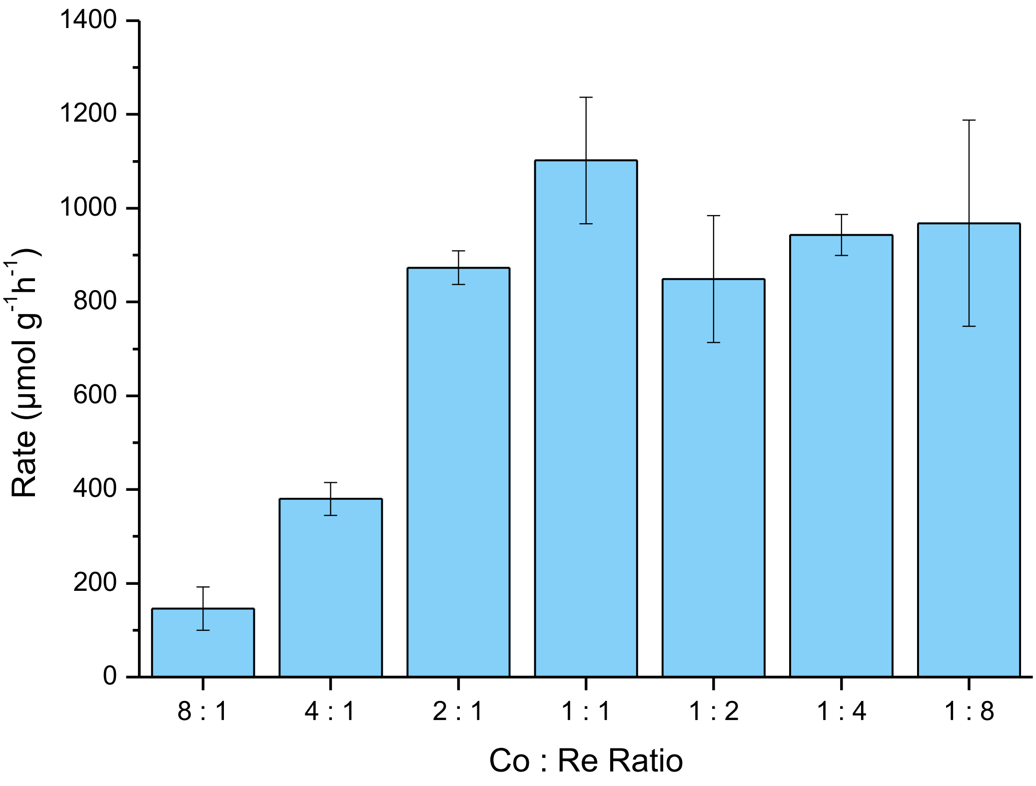

Figure 29: Reaction rates for different cobalt rhenium catalysts, pre-treated for 2 hours at 600°C with N_2/H_2 (1:3) then reacted at 400°C with N_2/H_2 (1:3) at ambient pressure.

Table 7: Reaction rates for different cobalt rhenium catalysts, pre-treated for 2 hours at 600°C with N_2/H_2 (1:3) then reacted at 400°C with N_2/H_2 (1:3) at ambient pressure.

Catalyst	Ratio Co:Re		Rate (μmol g^{-1} h^{-1})
Co_8Re	8	1	146 ± 46
Co_4Re	4	1	380 ± 35
Co_2Re	2	1	873 ± 36
CoRe	1	1	1102 ± 135
$CoRe_2$	1	2	848 ± 135
$CoRe_4$	1	4	943 ± 44
$CoRe_8$	1	8	986 ± 220
$CoRe_{16}$	1	16	Deactivates

From Figure 29 within experimental error no clear difference in activity is observed from Co_2Re to $CoRe_8$. The activity begins to drop in the case of the higher Co containing materials Co_4Re (380 ± 35 μmol g^{-1} h^{-1}) and Co_8Re (146 ± 46 μmol g^{-1} h^{-1}) and deactivation is observed in the high Re containing $CoRe_{16}$ material.

To assess potential catalyst deactivation extended reaction testing of 48 hours was conducted for $CoRe_4$ and CoRe the results of which are presented in Figures 12 and 30 respectively. They were found to maintain high activity and steady state behaviour over the entire testing period. The steady state ammonia synthesis rates for the extended CoRe material was found to be 1236 μmol g^{-1} h^{-1} and 915 μmol g^{-1} h^{-1} for $CoRe_4$.

This is in contrast to the behaviour of $CoRe_{16}$ a marked deactivation is observed during time on steam. To investigate the deactivation, ammonia synthesis rates were calculated at different time frames throughout the reaction and the results are presented in Figure 31. Initially, $CoRe_{16}$ has a high rate but as the reaction progresses this rate gradually decreases over time. This is attributed to the lack of cobalt with in the sample which results in a material that closely resembles rhenium metal. This corresponds to Section 3.2.3 where it was shown the single Re and Co precursors do not have enhanced activity and a combination is required for prolonged high activity. Within the literature it has been previously reported Re metal shows initial high activity then deactivates after 2 hours on stream[43]. It has also been suggested Co helps stabilise the Re[43, 48]. Therefore, in the case of

$CoRe_{16}$ the lack of Co may cause degradation of the catalyst during reaction. This was observed in the integrity of the post-reaction catalyst on discharge from the reactor.

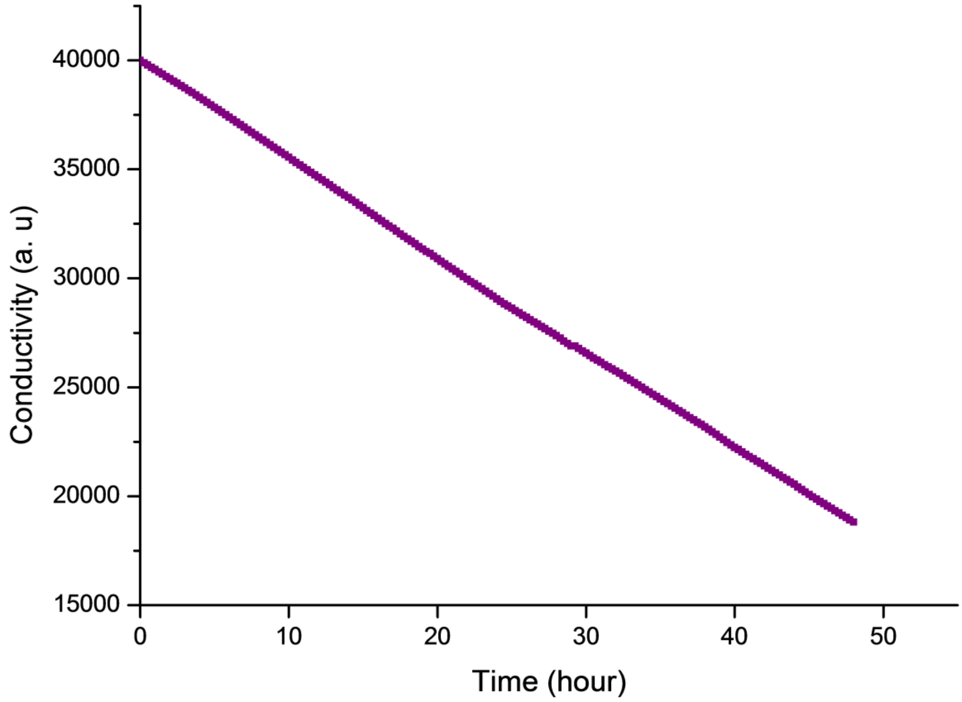

Figure 30: Extended reaction conductivity profile for CoRe, pre-treated for 2 hours at 600°C with N_2/H_2 (1:3) then reacted at 400°C with N_2/H_2 (1:3) at ambient pressure.

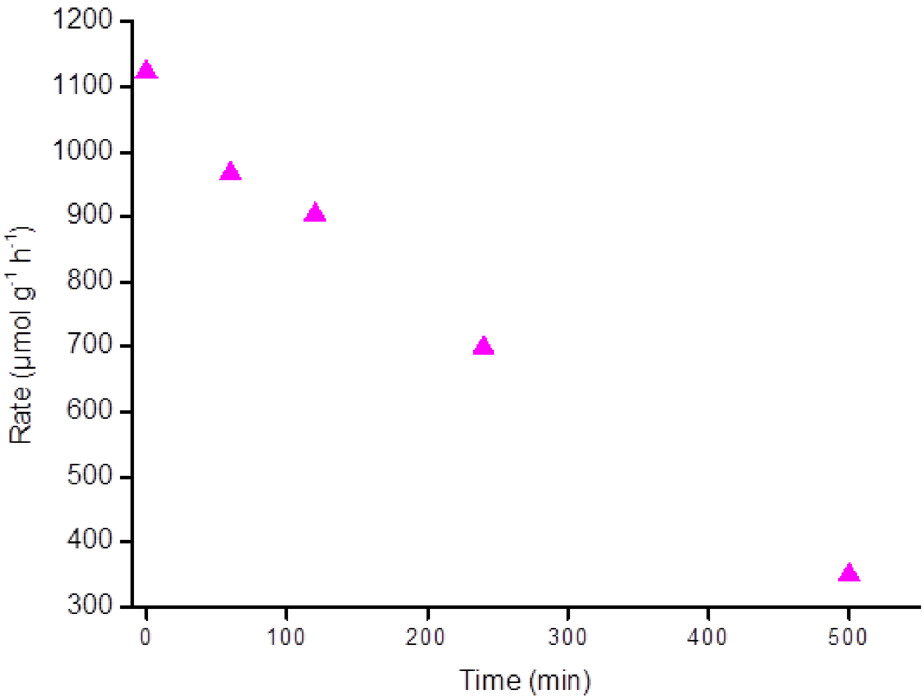

Figure 31: Plot Representing the Decrease in Ammonia Synthesis Rate over Time for $CoRe_{16}$.

A similar trend is observed in the temperature programed reduction (TPR) profiles presented in Figure 32, which were performed by Ms Tamsin Bell at the University of Bath.

The $Co(NO_3)_2.6H_2O$ precursor begins to reduce in pure H_2 at lower temperatures compared to the NH_4ReO_4 precursor. The broad shape of the TPR profiles for CoRe to $CoRe_8$ are analogous. The start of reduction occurs at higher temperatures with increasing rhenium content. This trend is clearly seen spanning Co_2Re to $CoRe_4$. When $CoRe_8$ is reached the reduction profile occurs at a lower temperature compared to $CoRe_4$. There is a marked difference in the reduction profile for $CoRe_{16}$. There is a single sharp peak over a narrow temperature range of approximately 300 – 400°C. This profile is attributed to the reduction of Re metal as the features of the reduction do not match the other cobalt rhenium materials or the NH_4ReO_4 precursor.

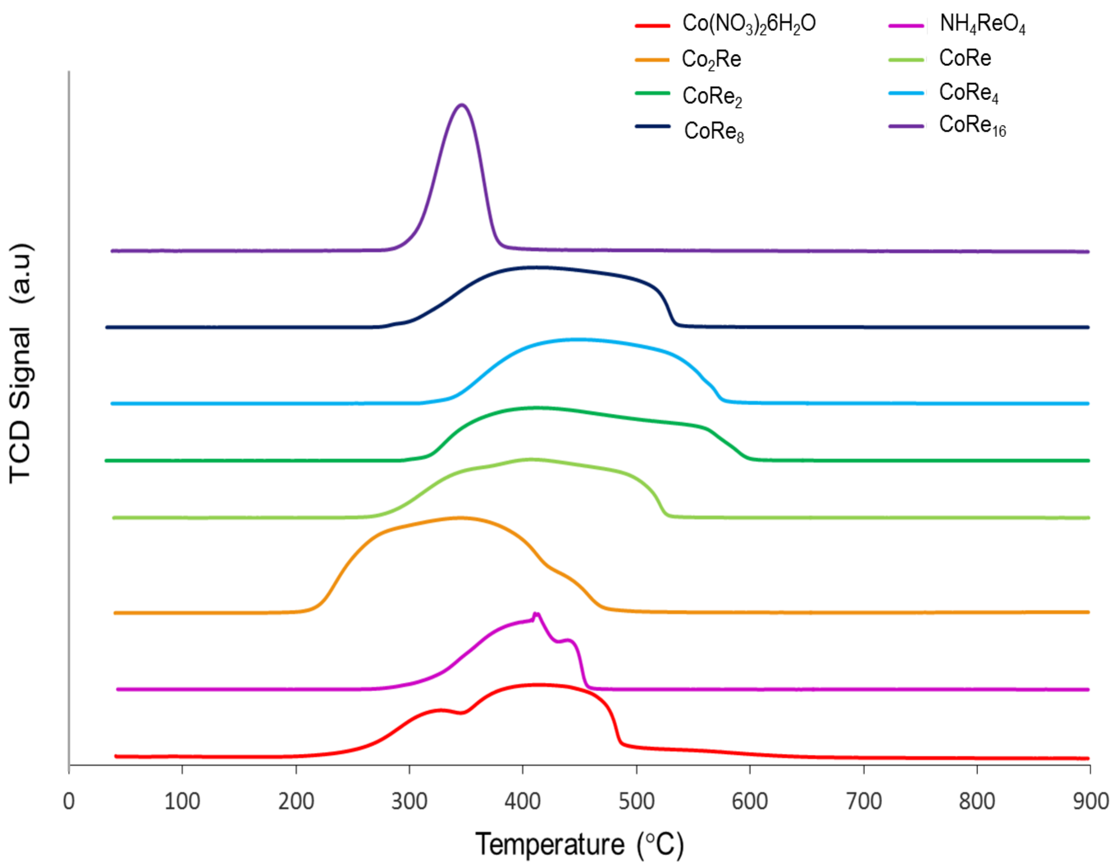

Figure 32: Temperature Programmed Reduction for Cobalt Rhenium Catalysts, pre-treated at 500°C under Ar for 20 minutes prior to TPR using 30 ml min^{-1} of 5% H_2/Ar from 60 to 100°C with a ramp rate of 10°C min^{-1}.

XRD was performed on the post-reaction cobalt rhenium catalysts and the results are presented in Figure 33. XRD analysis was not possible on $CoRe_{16}$ as changes which occurred upon reaction, indicating the loss of a significant portion of its mass, meant post-reaction analysis of the material was not possible.

In the case of Co_2Re, Co_4Re and Co_8Re the activity decreases which correlates with the lack of Re metal reflections only a sharp Co (111) reflection is observed. For CoRe, $CoRe_2$ and $CoRe_4$ an upwards 2θ shift of the Re reflections is observed, possibly due to bimetallic mixing of Re and Co. The XRD pattern for $CoRe_8$ is broad and there is also a Co shoulder present which could possibly suggest the material is partially disintegrating due to the lack of Co. However, it still has high steady state activity of 986 ± 220 µmol g^{-1} h^{-1}.

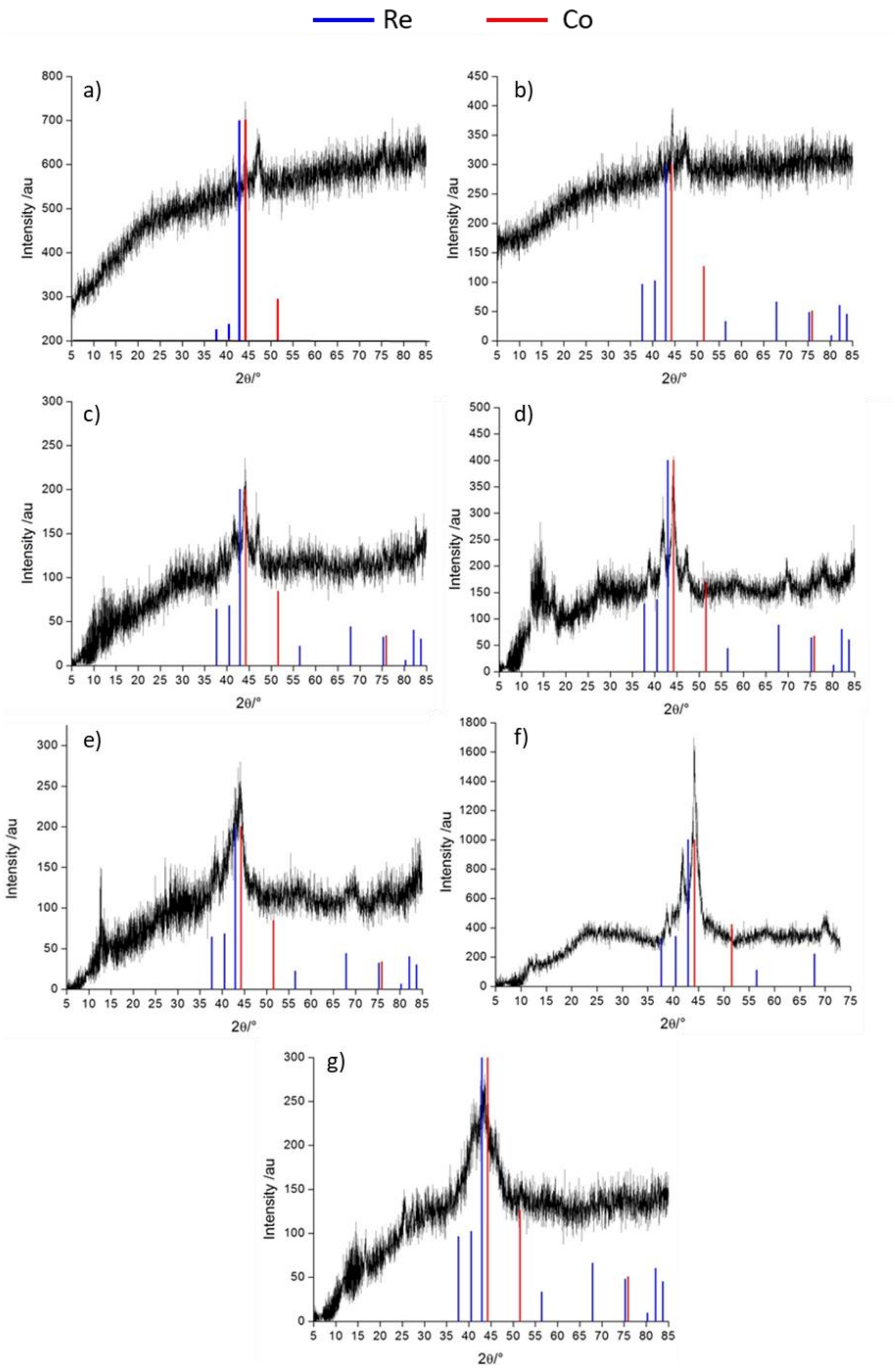

Figure 33: XRD Patterns for Post Reaction Cobalt Rhenium Catalysts a) Co_8Re, b) Co_4Re, c) Co_2Re, d) CoRe, e) $CoRe_2$, f) $CoRe_4$ and g) $CoRe_8$. Blue) Re PDF 00-005-0702 and Red) Co PDF 01-089-4307.

Taking activity, XRD and TPR data into account it can be postulated between the synthesis ratios of Co_2Re and $CoRe_8$ a similar material is forming. To further investigate this hypothesis ICP-MS was performed to elucidate the real Co:Re ratios. The results for pre- and post-reaction materials are displayed in Figures 34 and 35 and Table 8 respectively. ICP-MS was kindly performed by Mr Karsten Kirste at NTNU.

The materials were synthesised using calculations based on the atomic ratio between the Re and Co metals. Therefore, the ratios were consistent regardless of what precursor was used. In the case of all catalysts analysed *via* ICP-MS, NH_4ReO_4 and $Co(NO_3)_2.6H_2O$ were used as the Re and Co precursors.

Figure 34 shows the ICP-MS results for the pre-reaction materials. These materials were synthesised and calcined for 3 hours at 700°C in air. For all the materials tested it can be concluded the original synthesis ratios do not specifically correspond to the resulting materials and differences in composition are observed. For example, the CoRe material was made with a synthesis ratio of 1:1, therefore, this material would be expected to correspond to a pre-reaction percentage of 50 % Co and 50% Re. However, this is not the case and the material appears to have an actual percent ratio of approximately 6 % Co and 37 % Re. Also, it may be assumed the remaining weight percentages are oxygen. This idea can be applied to all of the materials and this theory is reinforced by XAS data presented in Section 3.3.8.2. Where, both Re-O and Co-O shells can be fitted to the pre-reaction material. Also, the pre-reaction patterns (Figure 16) resemble the initial precursor used but there are other reflections present which could correspond to rhenium and cobalt oxides.

Table 8: "Real" Cobalt Rhenium Ratios.

Synthesis Ratio	Actual Ratio	
	Pre-reaction	**Post-reaction**
Co_4Re	$CoRe_{1.8}$	$CoRe_{0.1}$
Co_2Re	$CoRe_2$	$CoRe_{1.5}$
CoRe	$CoRe_{1.9}$	$CoRe_{1.0}$
$CoRe_2$	$CoRe_{1.9}$	$CoRe_{1.7}$
$CoRe_4$	$CoRe_{1.6}$	$CoRe_{1.4}$
$CoRe_8$	$CoRe_{1.8}$	$CoRe_{0.7}$

On the other hand, if it is assumed the only elements present in the pre-reaction materials are Re and Co, the 'real' compositions are presented in Table 8. It can be seen CoRe actually corresponds to a material with a composition of $CoRe_{1.9}$. Moreover, comparison of all the synthesised materials shows the 'actual' ratio to be similar varying only by a standard deviation of 0.137. This proves after synthesis and calcination in air at 700°C for 3 hours the materials are analogous regardless of the initial synthesis ratio.

The post-reaction catalysts are shown in Figure 35. In all cases apart from Co_4Re each material has an increase in percentage of both Co and Re this could be due to the reduction of both Re and Co during the pre-treatment; resulting in a loss of oxygen in the samples. This is a change of approximately 10 % for all samples apart from Co_2Re which has a smaller increase of *ca*. 3 %. The Co_4Re catalyst is the only material in which the Co content is higher in the post-reaction material. It should be noted for the post-reaction materials the sum of both Re and Co does not equal 100% this is possibly due to passivation layers forming on extraction from the reactor and the ICP-MS analysis was performed *ex situ*, but further analysis is required to confirm this.

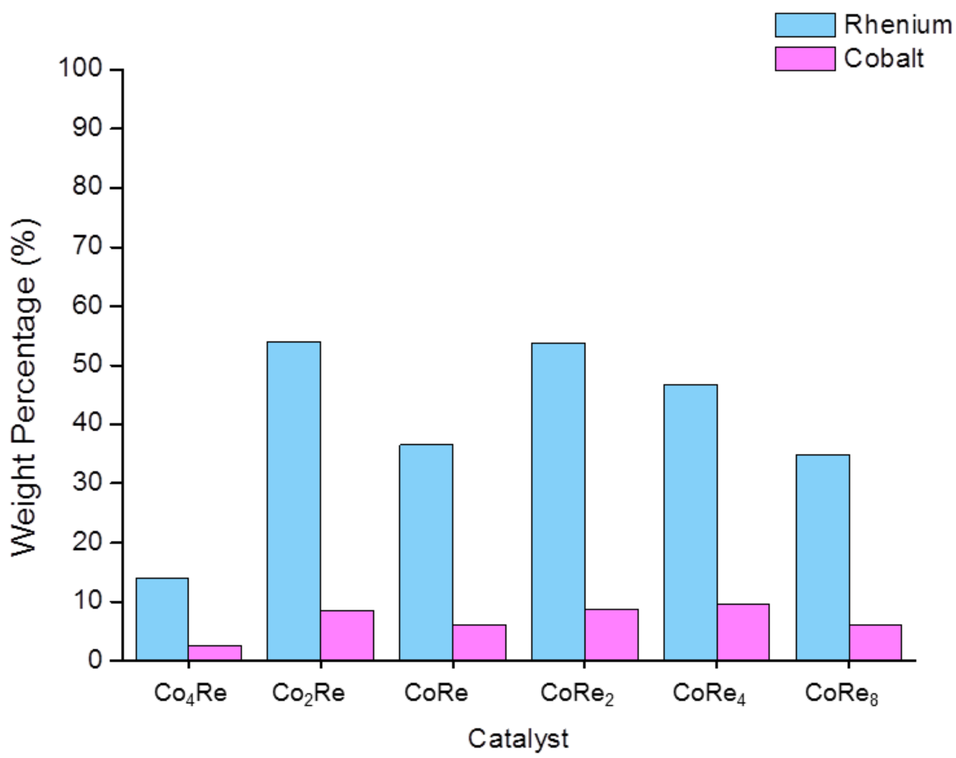

Figure 34: ICP-MS Results for Pre-reaction Cobalt Rhenium Catalysts.

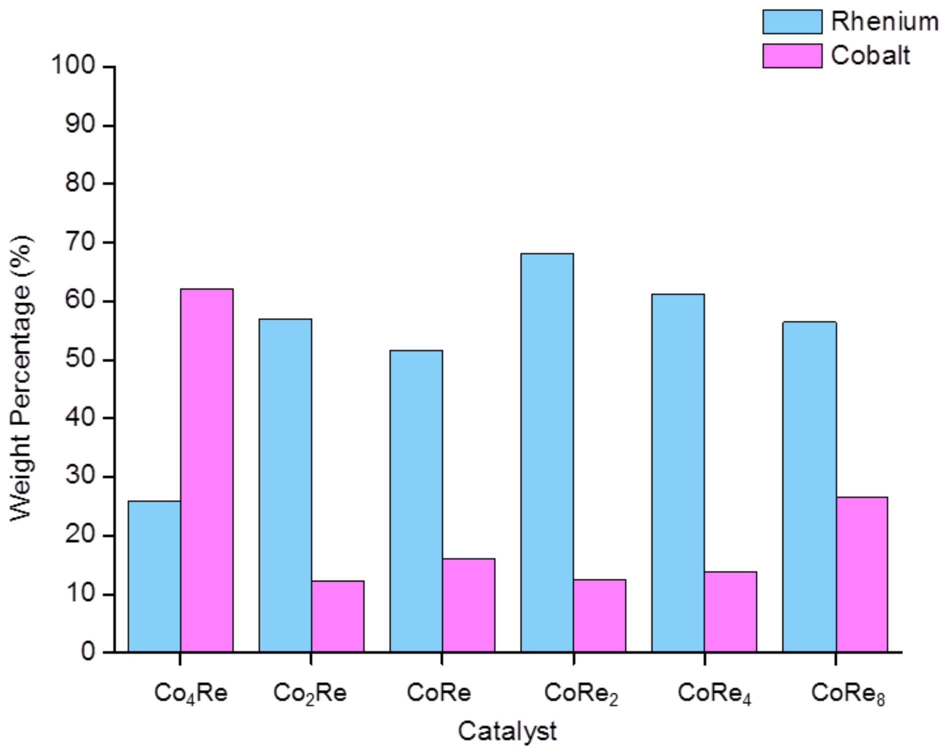

Figure 35: ICP-MS Results for Post-reaction Cobalt Rhenium Catalysts.

Again assuming cobalt and rhenium are the only elements present in the post-reaction materials, the results are presented in Table 8. A greater variation in ratios can be seen for the post-reaction materials, this is of no surprise as the differences in ammonia synthesis activities span a wide range and are outlined in Figure 29.

First, concentrating on Co_2Re to $CoRe_4$, the actual compositions vary from $CoRe_{1.0}$ to $CoRe_{1.7}$. This variation may be considered minor and it is important to note the original synthesis ratio does not correspond to the trend in rhenium concentrations in the materials, for example: $CoRe_2$ ($CoRe_{1.7}$) has a higher Re content compared to $CoRe_4$ ($CoRe_{1.4}$), although more Re was used to synthesize $CoRe_4$. This shows within this range of synthesis ratios the resulting cobalt rhenium catalyst may be considered compositionally similar. This is a significant result as reducing the required amount of rhenium during synthesis is highly desirable.

Kojima and Aika claim Co helps stabilise the Re_3N phase consequentially enhancing the ammonia synthesis activity[43,48]. In the current study, this suggestion may be applicable as significant deactivation and mass loss is noted for the Co-dilute cobalt rhenium system and indeed by the strong deactivation of $CoRe_{16}$ (Figure 31) and the falling Re content of ($CoRe_8$ actual composition $CoRe_{0.7}$). $CoRe_8$ still has high ammonia synthesis activity, however, a drop in the Re content can be seen, falling to half that of $CoRe_4$. The low ammonia synthesis activity of Co_4Re (146 ± 46 µmol g^{-1} h^{-1}) can be explained by the lack of Re in the sample ($CoRe_{0.1}$) which may be attributed to volatilization of Re in the reactor during ammonia synthesis as the volatility of ReO_x is known.

To conclude, this work has demonstrated that the resulting active material forming between molar ratios (Co : Re) of 2 : 1 to 1 : 8 can be considered compositionally similar and there is not a huge discrepancy in the composition of the resulting catalyst. This is in contrast to previous literature that claims $Co\text{-}Re_4$ is the optimum ratio[43, 48].

3.2.7 Effect of Changing the Metals

In order to determine if the enhanced ammonia synthesis activity is specific to a cobalt rhenium based material different mixed metal catalysts were synthesised and tested (as outlined in Section 2.1.2). The ambient pressure ammonia synthesis rates for rhenium based catalysts are presented in Table 9 and cobalt based catalysts presented in Table 11. The highly active $CoRe_4$ catalyst is presented in both tables as a reference to contrast the difference in rates when different metals are used.

Table 9: Reaction Rates for Different Rhenium Based Catalysts. Materials pre-treated with N_2/H_2 (1:3) for 2 hours at 600°C followed by reaction at 400 °C under N_2/H_2 (1:3).

Metals	Formula	Rate (µmol g^{-1} h^{-1})
Nickel Rhenium	$NiRe_4$	30 ± 3
Iron Rhenium	$FeRe_4$	64 ± 15
Cobalt Rhenium	$CoRe_4$	943 ± 44

Comparing the results in this work to those obtained by Kojima and Aika; there is a marked difference in the activity of the mixed metal catalysts ($Ni\text{-}Re_4$ 143 µmol g^{-1} h^{-1} and $Fe\text{-}Re_4$ 275 µmol g^{-1} h^{-1}). It is to be noted the materials prepared by Kojima and Aika have been subjected to ammonolysis. The rates obtained in this work for the $NiRe_4$ and $FeRe_4$ prepared without an ammonolysis stage are lower. This again is perhaps further evidence of the difference applying an ammonolysis stage during synthesis makes to the ammonia synthesis activity of the material. However, it is also evident in Kojima and Aika's work that when both cobalt and rhenium were present an enhanced rate was achieved at 350°C and ambient pressure (492 µmol g^{-1} h^{-1}).

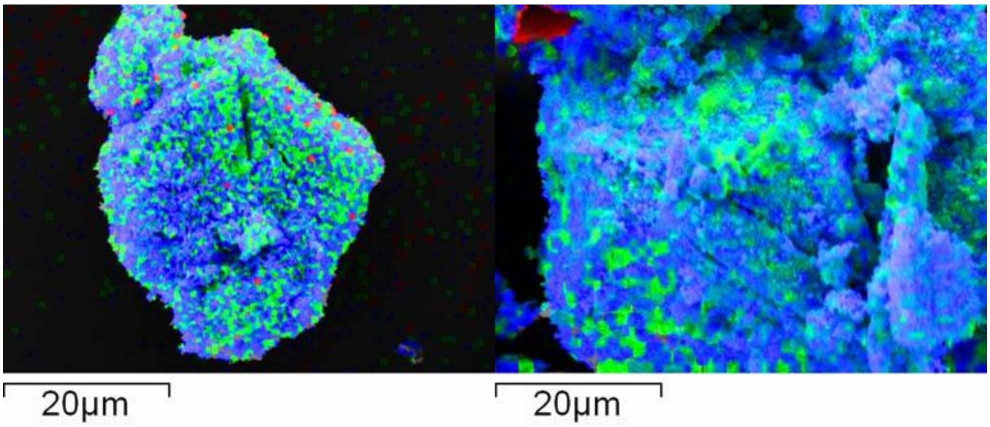

Figure 36: Element Maps for Post Reaction $NiRe_4$, blue) Ni, green) Re and red) O.

Rhenium and manganese are in the same group therefore, it can be suggested similar chemistry might occur, as demonstrated by the high NH_3 synthesis activities of: Fe, Ru and Os. To this end a cobalt manganese catalyst was prepared and tested. As demonstrated in Table 10; Mn and Zn have similar electronegativities and atomic radii. Therefore, a zinc cobalt material was also synthesised and tested for ammonia synthesis activity. The activity data is presented in Table 11 and pre- and post-reaction XRD patterns are shown in Figure 37 ($CoMn_4$) and Figure 38 ($CoZn_4$).

Table 10: Properties of Re, Zn and Mn from the Royal Society of Chemistry[140]

Property	Re	Zn	Mn
Pauling Electronegativity	1.9	1.65	1.5
Melting Point (°C)	3185	419.5	1246
Boiling Point (°C)	5590	907	2061
Electron affinity (kJ mol^{-1})	14.47	Not Stable	Not Stable
Atomic Radius (Å)	2.16	2.01	2.05
Common Oxidation States	7, 6, 4, 2, 0, -1	2, 0	7, 6, 4, 3, 2, 0, -1
Specific Heat Capacity (J kg^{-1} K^{-1})	137	388	479
1^{st} Ionization Energy (kJ mol^{-1})	755.820	906.402	717.274

Table 11: Reaction Rates for Different Cobalt Based Catalysts. Materials were pre-treated for 2 hours at 600°C with N_2/H_2 (1:3) then reacted at 400°C with N_2/H_2 (1:3) at ambient pressure for 8 hours.

Metals	Formula	Rate (μmol g^{-1} h^{-1})
Cobalt Zinc	$CoZn_4$	16 ± 5
Cobalt Manganese	$CoMn_4$	Inactive
Cobalt Rhenium	$CoRe_4$	943 ± 44

From Table 11 it can be seen the $CoMn_4$ catalysts were completely inactive for ammonia synthesis and the $CoZn_4$ had very limited activity (16 ± 5 μmol g^{-1} h^{-1}).

From the XRD pattern in Figure 37 ($CoMn_4$), a mixture of manganese oxides (MnO and Mn_3O_4) are present in the pre-reaction $MnCo_4$. Similarly, ZnO is the main constituent of the $ZnCo_4$ pre-reaction material. In the case of both $CoZn_4$ and $CoMn_4$, Co phases emerge in the post-reaction XRD patterns and also the intensity of the patterns decrease (compared to the pre-reaction patterns).

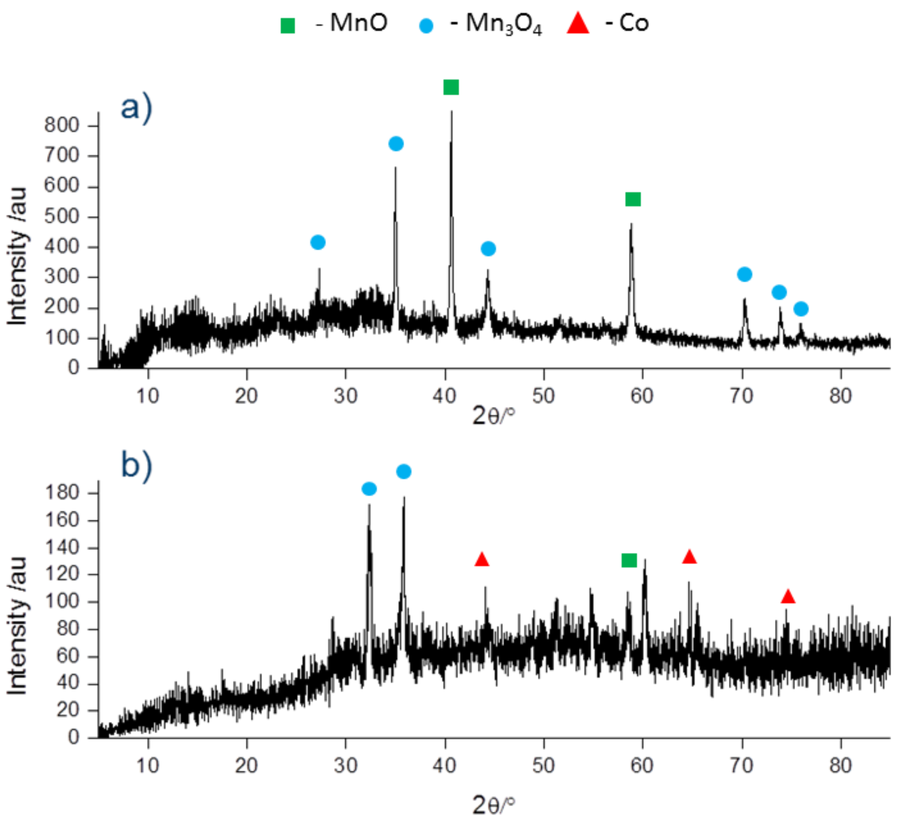

Figure 37: XRD Patterns for $CoMn_4$ (a) Pre- and (b) Post-reaction. Reference PDFs MnO 00-003-1145, Co 01-089-4307 and Mn_3O_4 00-004-0732.

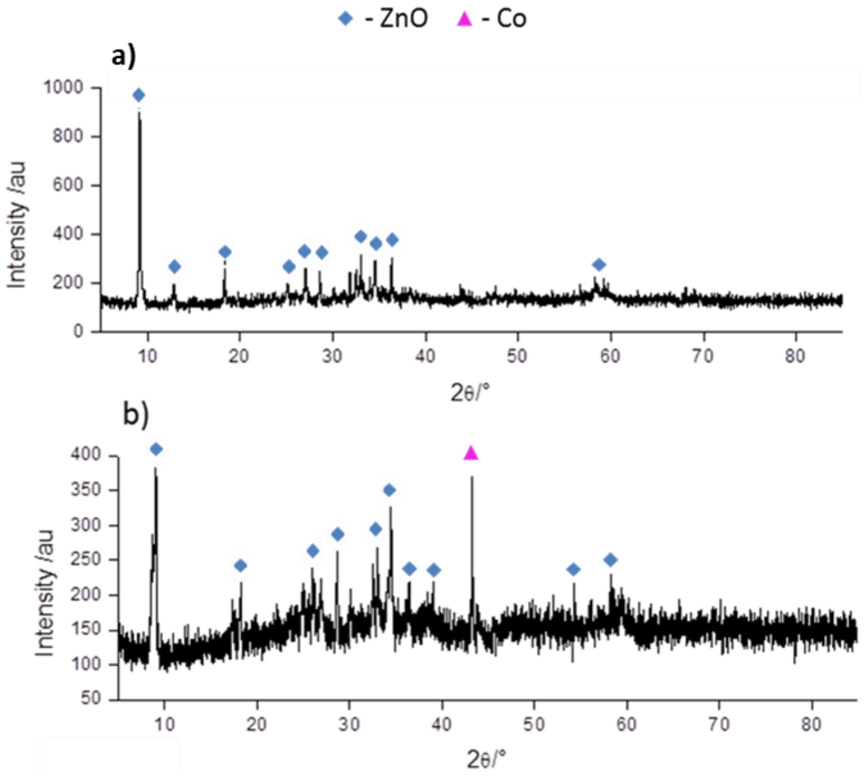

Figure 38: XRD Patterns for $CoZn_4$ (a) Pre- and (b) Post-reaction. Reference PDFs ZnO 01-070-8072 and Co 01-089-4307.

3.2.8 Investigation of Surface Area and Catalyst Mass for $CoRe_4$

Surface area and the ability to scale up in different reactors are important factors in catalysis. Therefore, BET and pelleting measurements were performed on $CoRe_4$. The surface areas and steady state ammonia synthesis rates for various catalysts are presented in Table 12, Figure 39 presents conductivity plots for powder and pelleted forms of $CoRe_4$ and Figure 40 shows mass normalised rates for different masses of $CoRe_4$ tested in the reactor. BET measurements for $CoRe_4$ were performed during a stay at the University of Bath and with the kind help of Ms Tamsin Bell.

Table 12: Surface area, ammonia synthesis and specific activities for various catalysts.

Material	Surface Area ($m^2\,g^{-1}$)	Rate (μmol $g^{-1}\,h^{-1}$)	Specific Activity (μmol $m^{-2}\,h^{-1}$)	Reference
$CoRe_4$	0.2	943	4715	Current Work
$Fe\text{-}K_2O\text{-}Al_2O_3$	14	330	24	[141]
Co_3Mo_3N	21	652	31	[141]

The surface area for $CoRe_4$ was found to be approximately 0.2 $m^2\ g^{-1}$ which is extremely low in comparison to other catalysts and this surface area may be unreliable in terms of the limitations of the measurements applied, therefore, it may be beneficial to perform BET analysis using Kr to give a more accurate result.

The mass normalised ammonia synthesis rate of $CoRe_4$ exceeds those of Co_3Mo_3N and Fe-K_2O-Al_2O_3 despite having a lower surface area. Moreover, the specific activity of $CoRe_4$ is significantly higher than Co_3Mo_3N and Fe-K_2O-Al_2O_3. However, due to limitations of the measurement these specific activities must be taken with caution.

$CoRe_4$ was tested in both the powder and pellet form. Figure 39 presents conductivity plots for powder and pelleted forms of $CoRe_4$. The tested material was from the same batch of $CoRe_4$ in order for direct comparisons to be drawn. It can be clearly seen there is no major difference in activity between the powder and pelleted $CoRe_4$.

The experimental set up involves a packed bed reactor. Figure 40 presents mass normalised rates for different masses of $CoRe_4$ tested in the reactor. There is no distinction when 0.2 g and 0.3 g of material are tested. However, it appears when 0.1 g $CoRe_4$ is tested the mass normalised rate almost doubles. The reason for this apparent change is from the way in which the rate is quoted (see Appendix); the rate is mass normalised. Therefore, as the rate is close to equilibrium the superficial rate difference between different masses of catalyst is only due to the mass normalisation step.

These initial results suggest there are no concerns for pelleting $CoRe_4$ and scale up in a different reactor is possible.

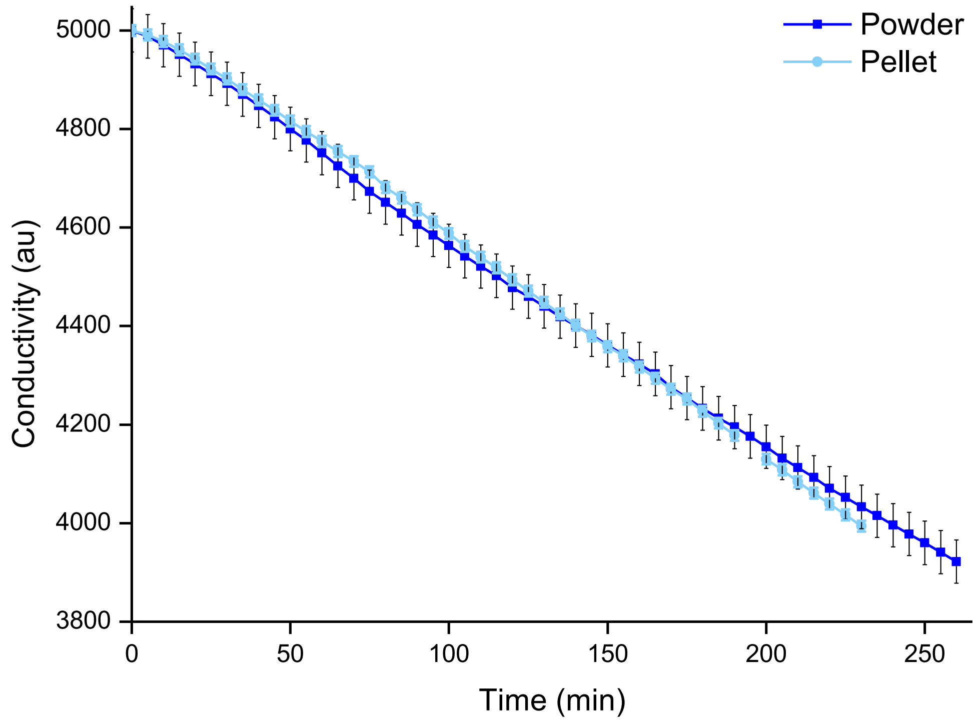

Figure 39: Reaction Conductivity profiles for Powder and Pelleted $CoRe_4$. Pre-treated for 2 hours with N_2/H_2 (1:3) following reaction at 400°C (1:3) at ambient pressure.

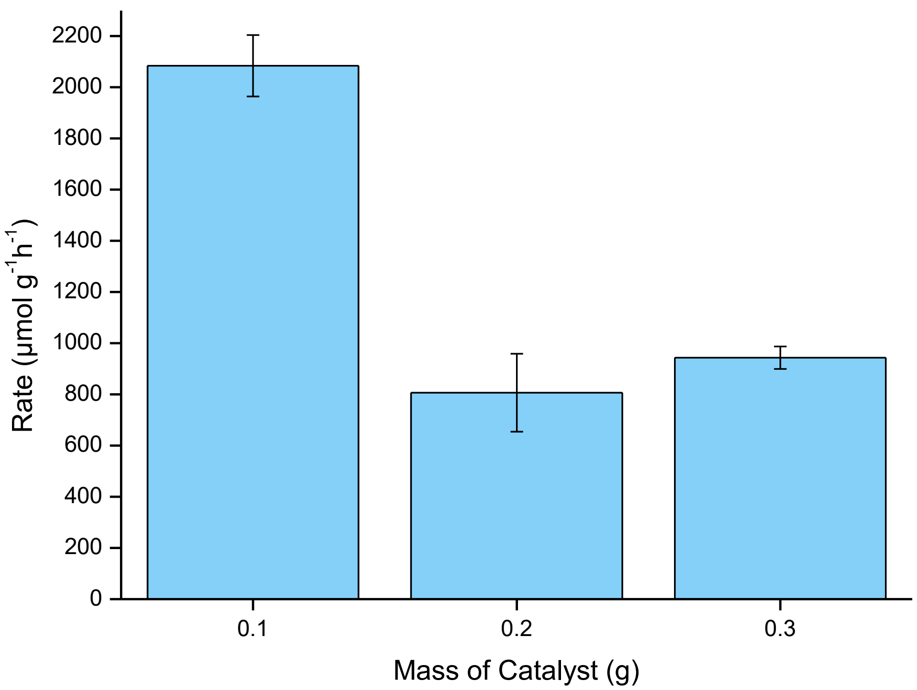

Figure 40: Reaction Rates for Different Masses of $CoRe_4$, pre-treated for 2 hours at 600°C with N_2/H_2 (1:3) then reacted at 400°C with N_2/H_2 (1:3) at ambient pressure.

3.2.9 Supported $CoRe_4$ Materials

In attempt to reduce the Re content of the materials and further enhance the surface area, a set of supported catalysts were prepared. Two different procedures were used to synthesise the supported materials (as detailed in Section 2.1.5). Simultaneous addition of both Re and Co to the support resulted in a material with low ammonia synthesis activity (< 30 μmol g^{-1} h^{-1}). In contrast, the catalysts prepared *via* a two-step synthesis showed good steady state ammonia synthesis activity and the results are presented in Table 13.

Two loadings were investigated: 10 wt% and 20 wt %. The materials are named according to the original synthesis ratio of $CoRe_4$ to support. The ammonia synthesis rates, post-reaction XRD and post-reaction SEM are presented in Figures 41 - 43, respectively. The ammonia synthesis rates are normalised to the total mass of material tested in the reactor.

Table 13: Steady State Ammonia Synthesis Rates for Silica Supported $CoRe_4$, pre-treated for 2 hours at 600°C with N_2/H_2 (1:3) then reacted at 400°C with N_2/H_2 (1:3) at ambient pressure.

Catalyst	Rate (μmol g^{-1} h^{-1})
$CoRe_4$	943 ± 44
10 wt% $CoRe_4$/silica	292 ± 8
20 wt% $CoRe_4$/silica	468 ± 48

The post-reaction XRD patterns are presented in Figure 41. It can be seen both the 10 and 20 wt% $CoRe_4$/silica have broad patterns which comprised of the Re (100), Re (002) and Re (101) reflections however, compared to unsupported $CoRe_4$ no shift in the Re reflections are observed. The Re (110) and (103) reflections are also present. The Re reflections appear sharper in the 20 wt% $CoRe_4$/silica material which might be expected as the loading is higher and the resultant supported particles may be larger.

For both 10 and 20 wt% $CoRe_4$/silica, the SEM images (Figures 42 and 43) reveal a smooth background with crystallites (< 10 μm) attached to the smooth surface. The apparent concentration of these attached crystallites increases with the higher 20 wt% loading. The attached particles have a smooth surface and generally have a rounded shape.

Element maps were used to investigate the surface dispersion of Re and Co. The composition of the surface agglomerates could not be directly determined by element mapping. In both supported materials the dispersion of Co and Re appears to be fairly homogeneous and the attached crystallites cannot be attributed to pure Re or Co.

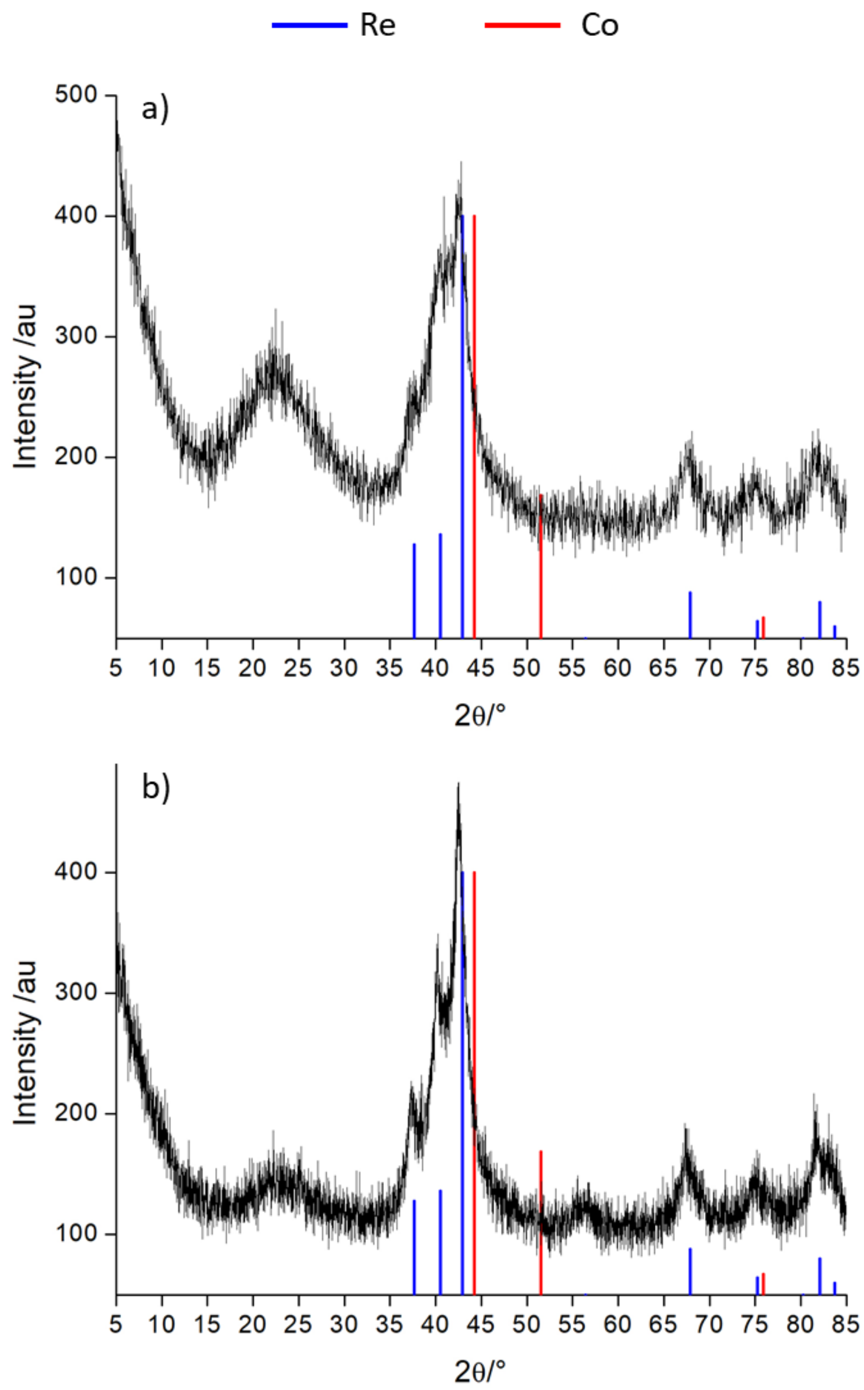

Figure 41: Post-reaction XRD for a) 10 wt% and b) 20 wt% $CoRe_4$/silica and pre-treated for 2 hours at 600°C with N_2/H_2 (1:3) then reacted at 400°C with N_2/H_2 (1:3) at ambient pressure. Reference PDFs Re 00-005-0702 and Co 01-089-4307.

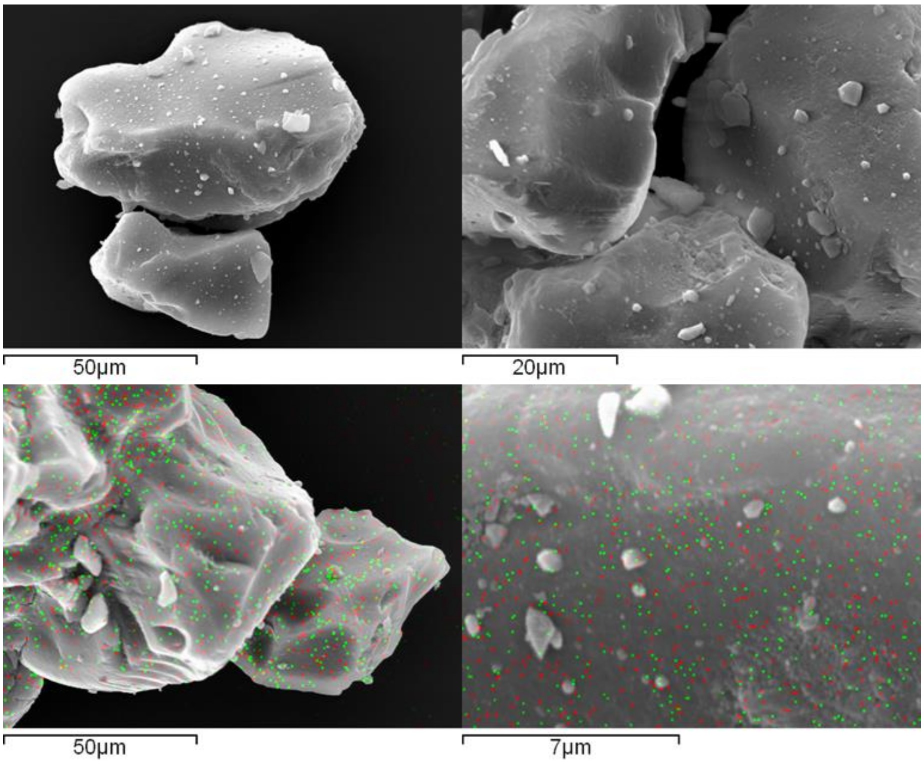

Figure 42: SEM Images and Element Maps for Post Reaction 10 wt% $CoRe_4$/silica, pre-treated for 2 hours at 600°C with N_2/H_2 (1:3) then reacted at 400°C with N_2/H_2 (1:3) at ambient pressure, green) Re and red) Co.

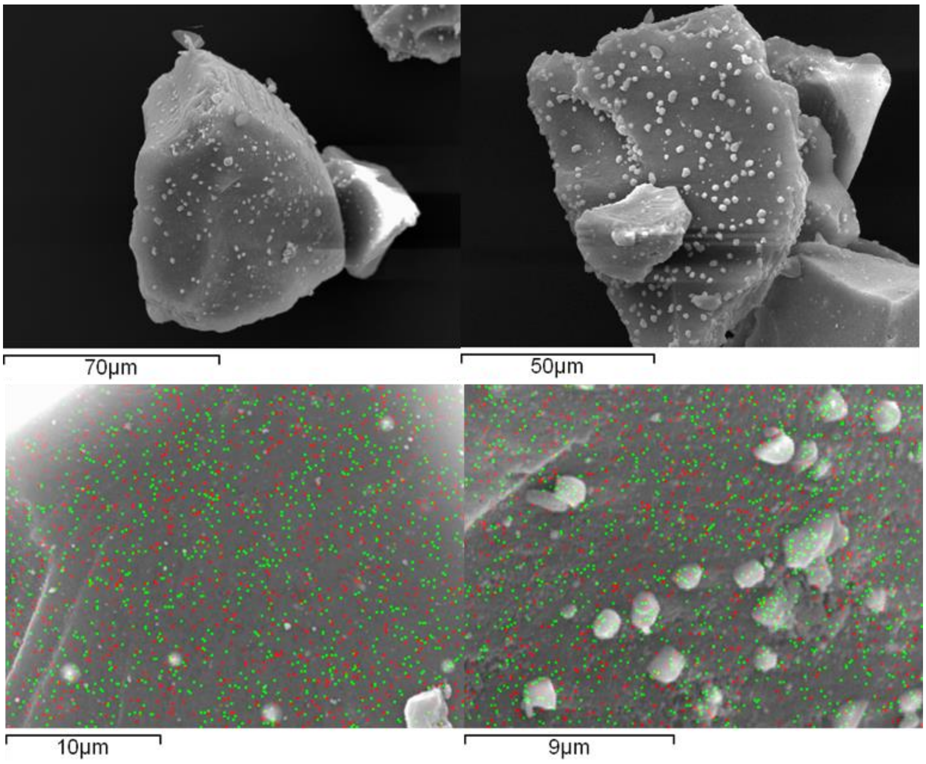

Figure 43: SEM Images and Element Maps for Post Reaction 20 wt% $CoRe_4$/silica, pre-treated for 2 hours at 600°C with N_2/H_2 (1:3) then reacted at 400°C with N_2/H_2 (1:3) at ambient pressure, green) Re and red) Co.

3.2.10 Effect of Reaction Temperature on Ammonia Synthesis Activity

The ammonia synthesis reaction is exothermic ($\Delta H° = -92.44$ kJ mol_{N2}^{-1}) and temperature dependent. Therefore, it is important to evaluate the activity of $CoRe_4$ under a variety of different temperatures. Using $CoRe_4$ and a stoichiometric ammonia synthesis gas feed different temperatures were investigated and the results are presented in Figure 44.

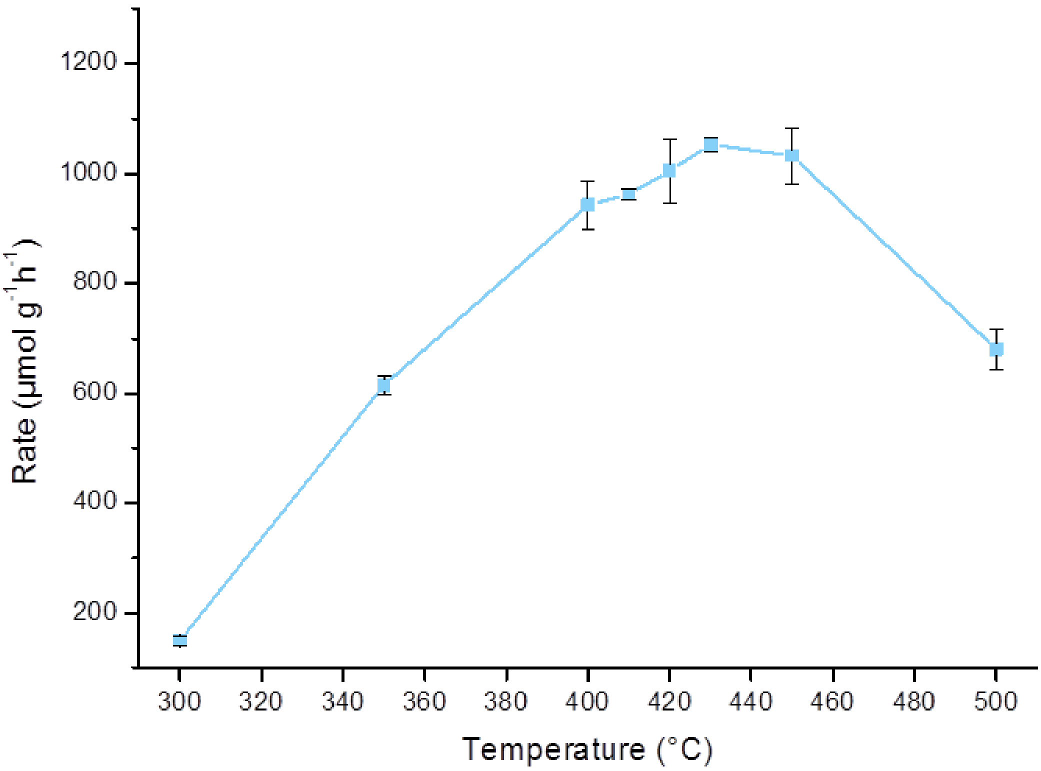

Figure 44: Effect of Temperature on Ammonia Synthesis Activity of $CoRe_4$. Samples pre-treated for 2 hours at 600°C with N_2/H_2 (1:3) then reacted between 300 - 500°C with N_2/H_2 (1:3) at ambient pressure.

Between 300 – 420°C there is an increase in the ammonia synthesis rate with increasing reaction temperature. At 500°C a sharp decline in rate was observed. This might be expected because the reaction is exothermic high temperatures favour the reactant side of the equilibrium therefore reducing the amount of product being produced, given the proximity to equilibrium which the system is apparently exhibiting.

3.2.11 Different Reaction Gas Composition

The behaviour of $CoRe_4$ under different N_2/H_2 reaction gas mixtures was investigated. The N_2/H_2 ratios tested were as follows: 1:3, 1:6, 1:12, 3:1, 6:1 and 12:1. To view the activity trends resulting from changing the gas composition, the results are plotted in Figure 45 and steady state ammonia synthesis rates are displayed in Table 14.

The highest activity (943 ± 44 µmol g^{-1} h^{-1}) is achieved with the stoichiometric N_2/H_2 (1:3) reaction gas is used. As the N_2 content increases (N_2/H_2 3:1, 6:1 and 12:1) the activity steadily falls. This suggests nitrogen is covering the surface and H_2 cannot reach the catalyst surface. Also, it can be seen at higher H_2 concentrations the ammonia synthesis activity increased which is in contrast to the suggestion by Kojima and Aika[43, 48] that hydrogen poisoning causes deactivation of a rhenium catalyst. However, in the case of this $CoRe_4$ material this does not seem to be the case.

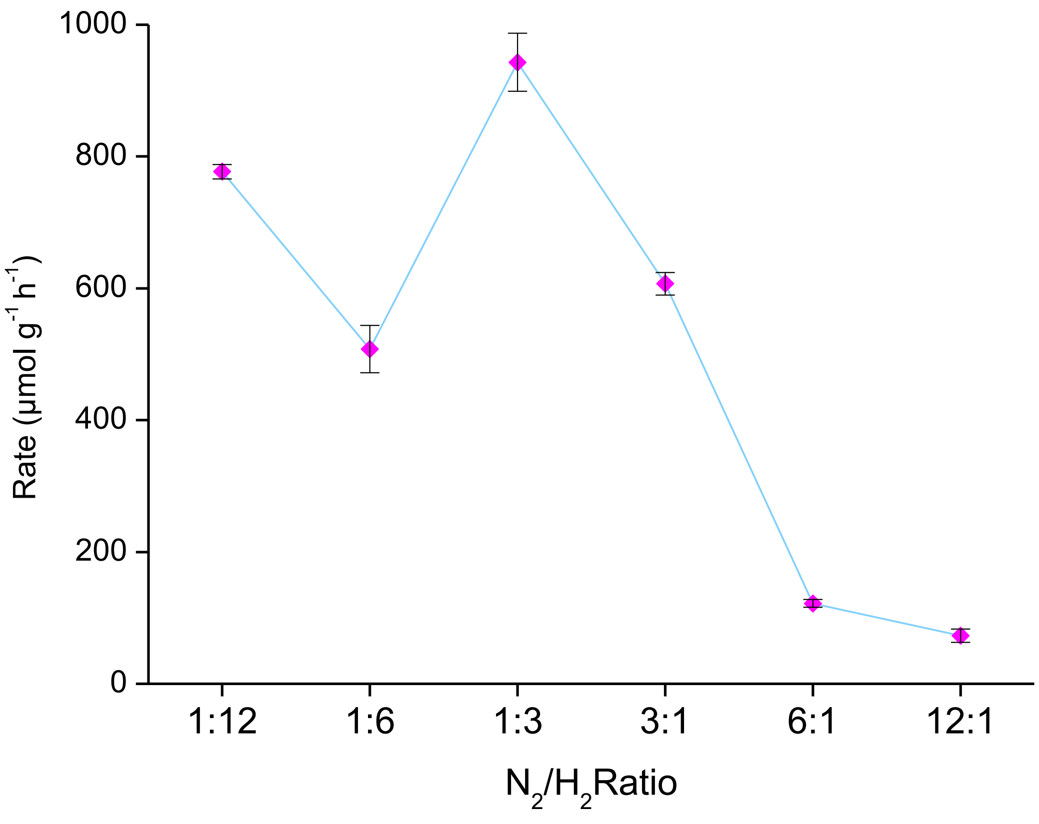

Figure 45: Ammonia Synthesis Rates for $CoRe_4$ under Different N_2/H_2 Gas Compositions. Pre-treated with N_2/H_2 (1:3) at 600°C for 2 hours.

Table 14: Ammonia Synthesis Rates for $CoRe_4$ under Different N_2/H_2 Gas Compositions. Pre-treated with N_2/H_2 (1:3) at 600°C for 2 hours.

	Gas Composition $N_2 : H_2$	**Rate (μmol g^{-1} h^{-1})**
H_2 Rich	1 : 3	943 ± 44
	1 : 6	508 ± 36
	1 : 12	777 ± 11
N_2 Rich	3 : 1	607 ± 17
	6 : 1	122 ± 6
	12 : 1	73 ± 10

3.3 Effect of Pre-treatment on the Ammonia Synthesis Activity of Cobalt Rhenium Catalysts

3.3.1 Ammonia Synthesis Activity of $CoRe_4$

In this study different pre-treatments have been investigated to assess the potential formation of any nitride species and to determine any effect on the ammonia synthesis rate of the resulting catalyst. In this work it has been found the choice of pre-treatment gas mixture influences catalytic performance of the material[127].

Pre-treatments were performed at 600°C for 2 hours then the reactor temperature was lowered to 400°C and the ammonia synthesis feed gas switched in (N_2/H_2 (1:3)) and conductivity of a 0.00108 M H_2SO_4 solution monitored. Pre-treatment was also performed at 700°C, however, no enhancement in rate was achieved therefore, 600°C pre-treatment was used hereon in. Figure 46 presents comparative reaction conductivity profiles for pre-treatments under N_2/H_2 (1:3), Ar/H_2 (1:3) N_2 and Ar. In order to clearly see the activity lag periods the data presented in Figure 46 has been truncated to reaction time of 2 hours. However, the N_2/H_2 pre-treated reaction has been extensively tested and was shown to exhibit steady state behaviour throughout an entire 48 hours testing period. Conductivity data for 48 hour reaction is presented in Figure 12. This is in marked contrasted to the behaviour observed by Kojima and Aika with Re_3N which showed significant deactivation after 2 hours on stream at ambient pressure and 350°C, the deactivation was attributed to hydrogen poisoning[24].

The ammonia synthesis rates were calculated during the steady state period and are displayed in Table 15.

Table 15: Ammonia Synthesis Rates of $CoRe_4$.

Pre-treatment Gas	Ammonia Synthesis Rate ($\mu mol\ g^{-1}\ h^{-1}$)
N_2/H_2 (1:3)	943 ± 44
Ar/H_2 (1:3)	844 ± 58
N_2	634 ± 60
Ar	792 ± 14

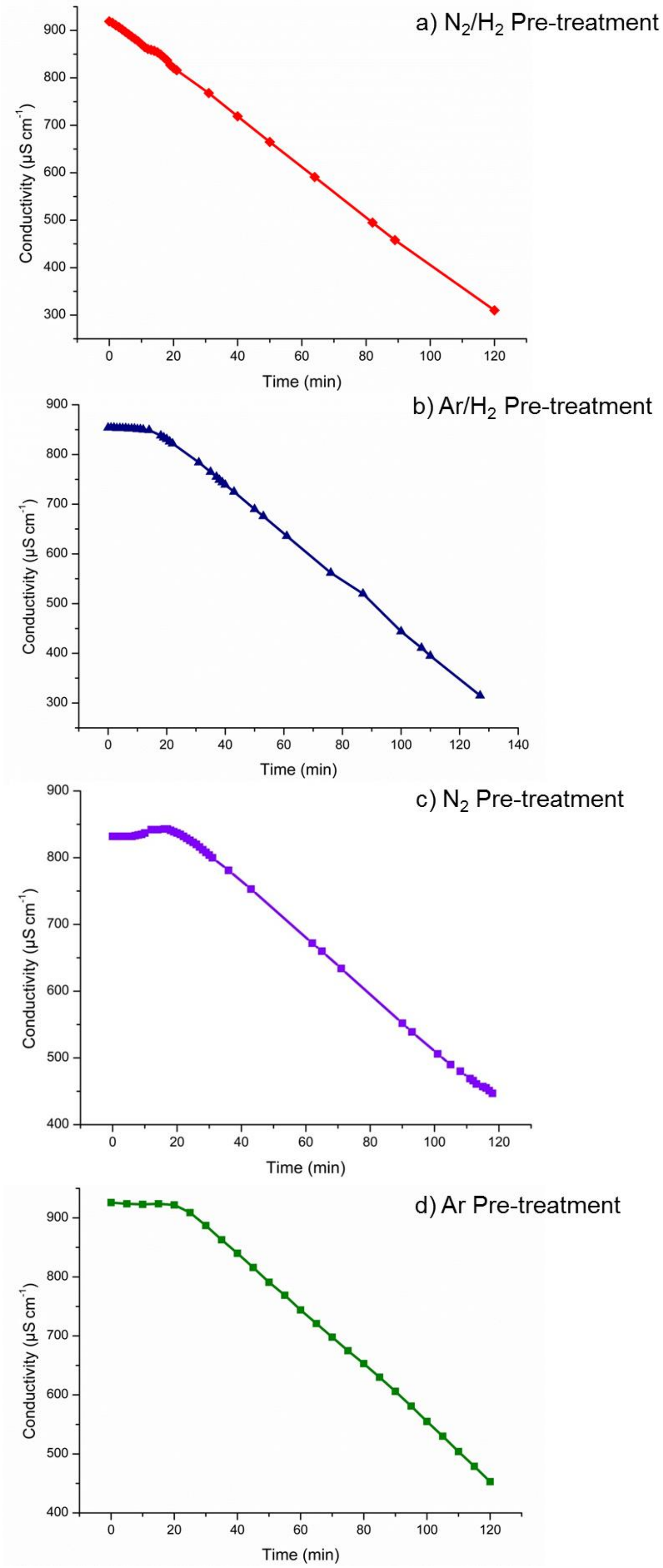

Figure 46: Reaction conductivity profile for N_2/H_2 (1:3) reaction at 400°C. $CoRe_4$ pre-treated for 2 hours at 600°C with: a) N_2/H_2 (1:3), b) Ar/H_2 (1:3), c) N_2 and d) Ar.

From Figure 46 it is evident pre-treatment under N_2/H_2 gives an instantly active material which is represented by an immediate linear decrease in conductivity over time. This is in contrast to pre-treatment under Ar/H_2, Ar and N_2 which lead to an induction period of approximately 20 minutes prior to the catalyst developing ammonia synthesis activity. In the cases of Ar/H_2, Ar, and N_2 pre-treatments it is of interest to note that beyond the induction period, during which the material is apparently inactive, the catalyst exhibits steady state performance.

It was crucial to ensure these lag periods were real and not artefacts caused by temperature discrepancies between the furnace and catalyst or simply a dead volume within the gas lines. Experiments were conducted in which, after the initial 2 hour pre-treatment the reaction was cooled to 400°C under the pre-treatment gas mixture and then the gas was transferred over the bypass essentially trapping the catalyst at 400°C under the pre-treatment gas mixture. Next the ammonia gas feed was switched to N_2/H_2 (1:3) over the bypass and gas lines flushed for 3 hours. This enabled the catalyst to successfully reach 400°C and the gas lines to be fully purged of the pre-treatment gas mixture. This ensured when the ammonia synthesis gas feed was switched over the catalyst and conductivity measurements of a 0.00108 M H_2SO_4 solution preformed the lag period was a real feature. This resulted in the 20 minute lag period proving it is a real feature and not caused by a dead volume effect. An understanding of the structure before and after activation may help elucidate the active material.

In comparison to the active N_2/H_2 pre-treated material in the case of Ar/H_2 and Ar pre-treatments it can be postulated the induction period is due to the material needing an exposure to nitrogen before activating for ammonia synthesis, which could be tentatively associated with the formation of an active nitride phase as proposed by Kojima and Aika[24, 43, 48]. In attempt to assign the role of hydrogen H_2, Ar and N_2 pre-treatments were used to completely eliminate hydrogen from the pre-treatment gas mix. Again, an induction period of 20 minutes is observed. It can be speculated that the metals in the material need to be in their reduced form therefore, exposure to a reducing atmosphere is also required to induce activity. These results suggest two elements are required for activity; reduction of the metals and nitrogen exposure, both of which are confirmed in the active behaviour of the N_2/H_2 pre-treated catalyst. Within the current literature, the experimental procedures use a 30 minute stabilisation step to ensure the catalyst is at 400°C before activity measurements are performed[24,44]. From removing this step in this work it is the first report of these lag periods under different pre-treatment gas mixtures[127].

The highest activities are achieved by pre-treatment with N_2/H_2 (1:3) and Ar/H_2 which gives 943 ± 44 µmol g^{-1} h^{-1} and 844 ± 58 µmol g^{-1} h^{-1} respectively. As stated previously, these are high ammonia synthesis rates when compared to literature values where rates of 600 µmol g^{-1} h^{-1} and *ca.* 470 µmol g^{-1} h^{-1} have been reported[24, 44]. The apparent lower activities may possibly be explained by the variation in surface morphology. Inspection of the N_2/H_2 pre-treated post-reaction SEM images shows a material with agglomerated rounded crystallites. Evaluation of the Ar/H_2 pre-treated post-reaction SEM images show smaller agglomerates with a smoother surface compared to the N_2/H_2 pre-treated $CoRe_4$. Analysis of the N_2 post reaction SEM images (Figure 47) show a smooth fissured surface surrounded by smaller fragmented particles. Elemental mapping of post reaction $CoRe_4$ pre-treated with N_2/H_2, Ar/H_2 or N_2 was unable to detect any specific Re or Co rich areas on the surface of the catalysts.

The biggest contrast in surface morphology is seen in the case of an Ar treated sample also the ammonia synthesis rate is significantly lower compared to pre-treatments under N_2/H_2 or Ar/H_2 (Table 15). The resulting surface morphology appears to differ significantly from the other pre-treatments. Multiple surface ‘needle-like’ growths appear to spawn from nucleation points on the surface of the catalyst and appear throughout the sample. The growths span approximately 10µm in diameter. They are not present in $CoRe_4$ samples pre-treated with other gas mixtures. These growths were further investigated using element mapping. Figure 48 presents post reaction SEM images and element maps for $CoRe_4$ pre-treated with Ar. Using element mapping the growths appear to be ‘needles’ of rhenium metal. The lower activity of 792 ± 14 µmol $g^{-1}h^{-1}$ may be related to the rhenium growths.

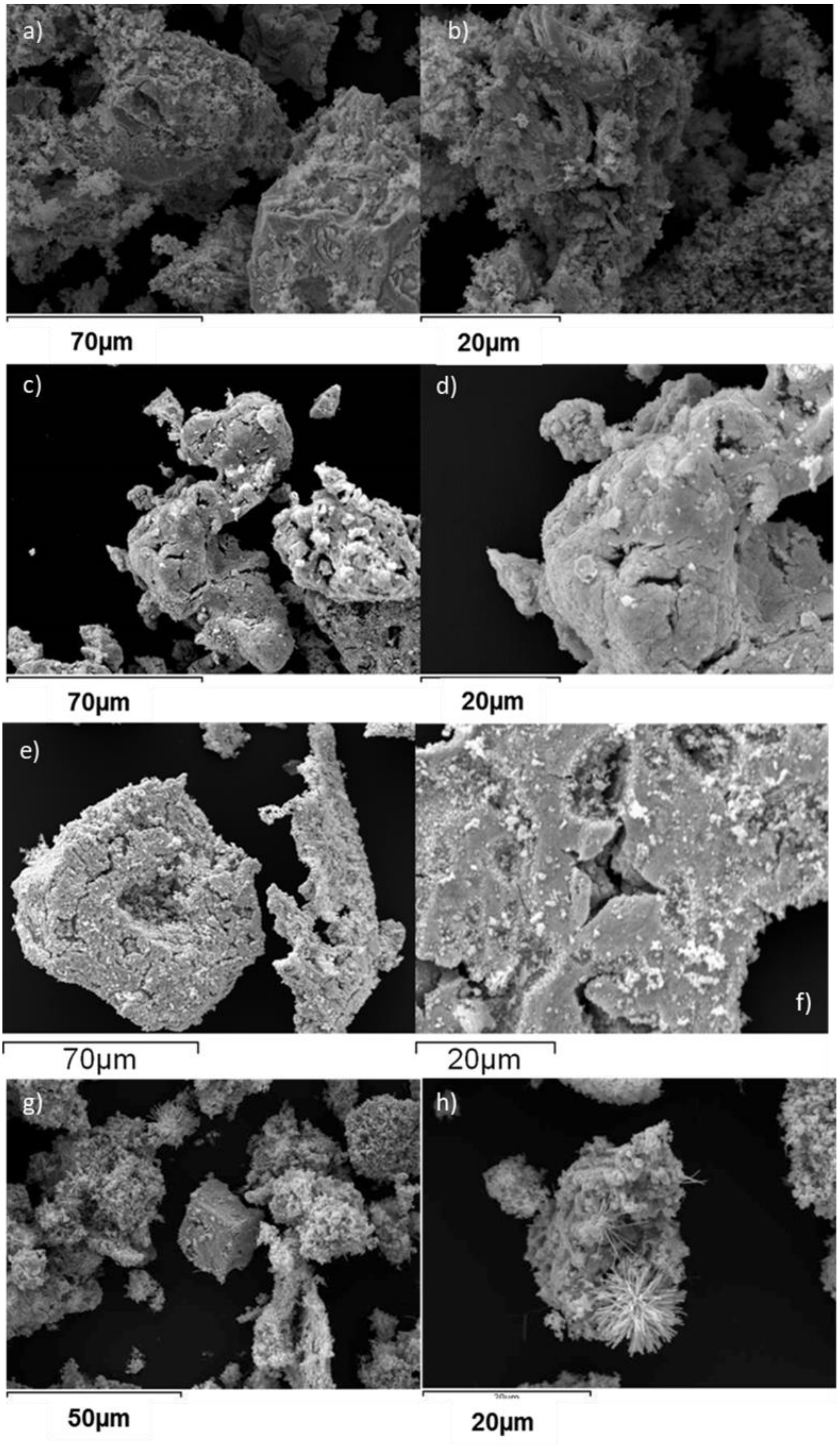

Figure 47: SEM images of post reaction $CoRe_4$ pre-treated at 600°C for 2 hours under: a - b) N_2/H_2 (1:3), c - d) Ar/H_2 (1:3), e - f) N_2 and g - h) Ar then reacted under N_2/H_2 (1:3) at 400°C.

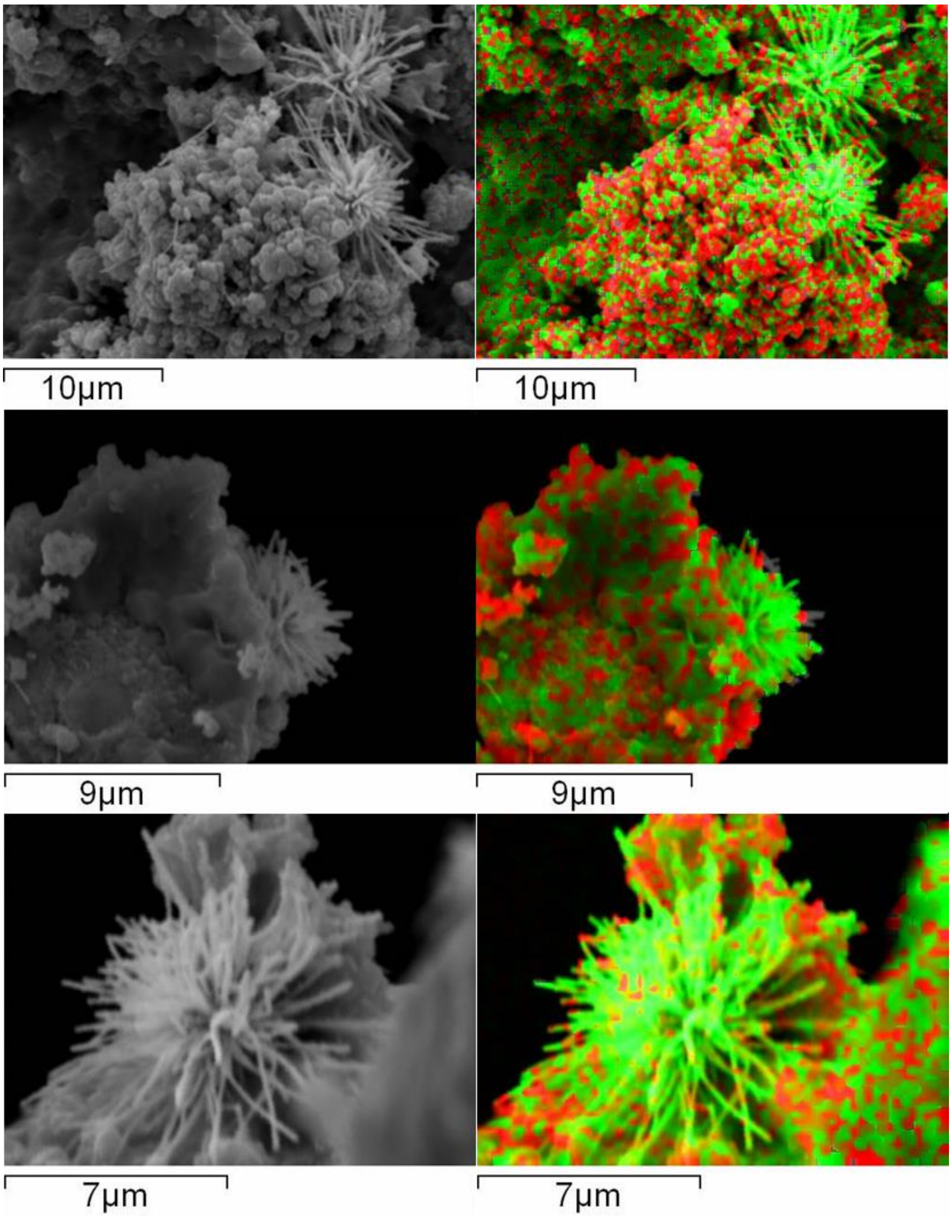

Figure 48: SEM post reaction images of post reaction $CoRe_4$ pre-treated with Ar at 600°C for 2 hours then reacted with N_2/H_2 at 400°C (1:3). With element mapping: Co) red and Re) green.

In conclusion, the N_2/H_2 pre-treatment gives an active material whereas, Ar/H_2, N_2 and Ar pre-treatments result in a lag period of 20 minutes prior to developing activity. The lag periods are real and are due to activation of the material and not artefacts due to temperature differences or dead volumes. It can be postulated that the cobalt rhenium material requires two conditions to give an active material; the metals to be reduced therefore, need to be exposed to a reducing atmosphere (H_2) and the material (in its reduced metal form) must be exposed to nitrogen. The lower activity resulting from the Ar pre-treatment may be connected to the rhenium surface growths.

3.3.2 Thermogravimetric Analysis

It is important to look at the material before the 600°C pre-treatment temperature is reached as this may provide further insight into the $CoRe_4$ material. Thermogravimetric analysis (TGA) was performed, focusing on changes that occur during the initial ramping from ambient temperature to 600°C, the results are presented in Figure 49. The starting material was synthesised using NH_4ReO_4 and $Co(NO_3)_2.6H_2O$ (as outlined in Section 2.1.1) it was then calcined in air at 700°C for 3 hours prior to analysis.

The N_2/H_2 pre-treated $CoRe_4$ has two weight loss peaks at 100°C and a bigger mass loss at 260 - 400°C. There is a slight difference in weight losses when an Ar/H_2 atmosphere is used. The Ar/H_2 pre-treatment appears to result in four mass losses. The second peak has segregated into two mass loss peaks and there is a smaller broad peak at approximately 410 - 480°C. The segregated peaks occur at approximately 300 - 350°C and 380 - 400°C.

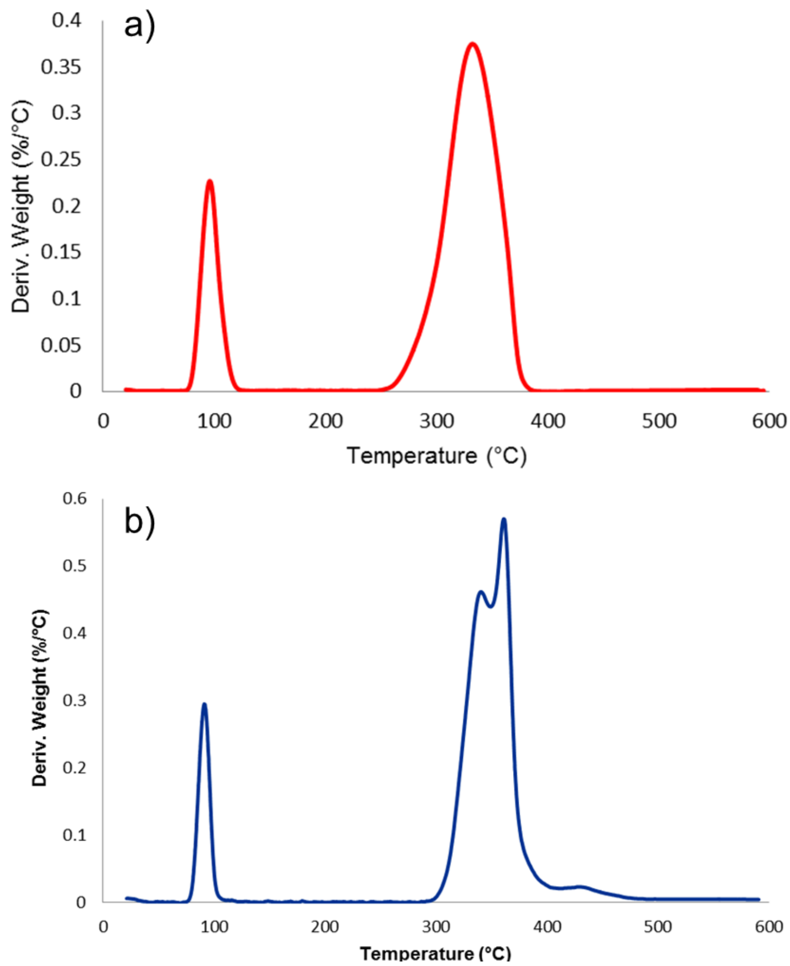

Figure 49: TGA Profiles for $CoRe_4$ Pre-treated with a) N_2/H_2 and b) Ar/H_2.

Slight differences in mass loss are observed in the TGA analysis between pre-treatments, however, the exact compositions of each mass loss were unable to be determined. There are similar overall percentage mass losses for both N_2/H_2 and Ar/H_2 pre-treated $CoRe_4$ which are approximately 26 % and 30 % respectively. It is postulated in both pre-treatment cases, the first mass loss at approximately 100°C is the loss of loosely bound H_2O from the material. The second larger mass losses are believed to originate from the reduction of the oxide precursor.

3.3.3 Heat Flow Profiles

On close inspection of the heat flow profiles a difference is observed between the two different pre-treated $CoRe_4$ materials and the results are presented in Figure 50. These profiles are taken at 400°C under N_2/H_2 after pre-treatment at 600°C under the different pre-treatments. Referring back to Section 3.3.1 pre-treatment with N_2/H_2 gives an instantly active catalyst which retains steady state behaviour whereas the Ar/H_2 requires 20 minute exposure to the N_2/H_2 reaction mix. This is reflected in the heat flow profiles. The profile for the N_2/H_2 pre-treated material shows little to no variation when under ammonia synthesis conditions, which is consistent with a stable material, whereas, for the Ar/H_2 pre-treated material a feature (indicated by the arrow in Figure 50) is detected after 20 minutes under ammonia synthesis conditions, 400°C and N_2/H_2, which suggests a change is occurring within the material in order for it to become active.

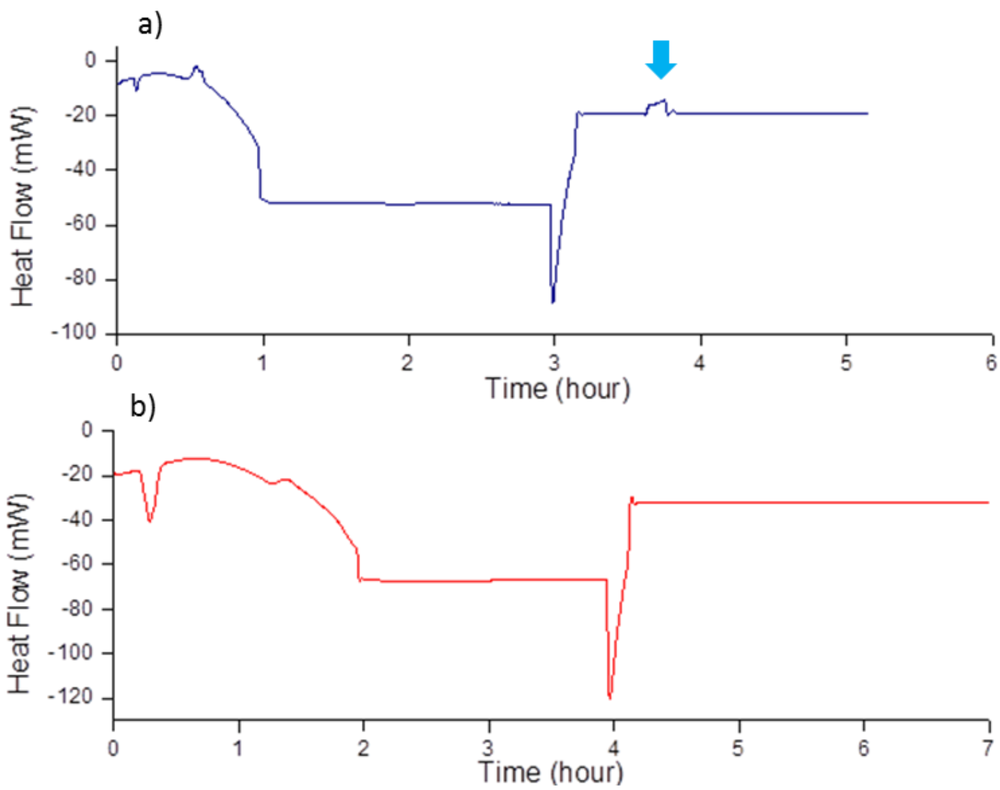

Figure 50: Heat Flow Profiles for $CoRe_4$ in N_2/H_2 at 400°C. a) Pre-treated with Ar/H_2 at 600°C for 2 hours and b) Pre-treated with N_2/H_2 at 600°C for 1 hour.

3.3.4 *Ex Situ* Powder X-ray Diffraction

In order to further understand the effect of pre-treatment on the structure of $CoRe_4$ XRD characterisation was carried out on post-reaction $CoRe_4$ (Figure 51). Each sample has been pre-treated under a different gas mixture at 600°C for 2 hours and then reacted under N_2/H_2 (1:3) at 400°C.

In the cases of the N_2/H_2 and Ar/H_2 pre-treated $CoRe_4$ no Co species can be detected in spite of the high Co concentration in the material; however, the high amorphous background may disguise some features. The intensities of the reflections of the N_2/H_2 treated catalyst are higher than those of the other samples. Regarding the N_2 and Ar pre-treated, catalysts these have been shown to have a lower overall activity towards ammonia. Small metallic Co (200) peaks are present in the lower activity samples.

As previously mentioned in Sections 3.2.2 and 3.2.3, materials with higher ammonia synthesis activities show a higher 2θ value compared to the reference Re XRD pattern. With respect to N_2/H_2 and Ar/H_2 pre-treated $CoRe_4$, a shift of Re reflections is observed which correlates with the higher of activities both the N_2/H_2 and Ar/H_2 pre-treated materials. It is possible the more active materials have a degree of bimetallic Co-Re mixing. In comparison, the lower activity N_2 and Ar pre-treated materials lead to reflections which match up to the Re reference pattern.

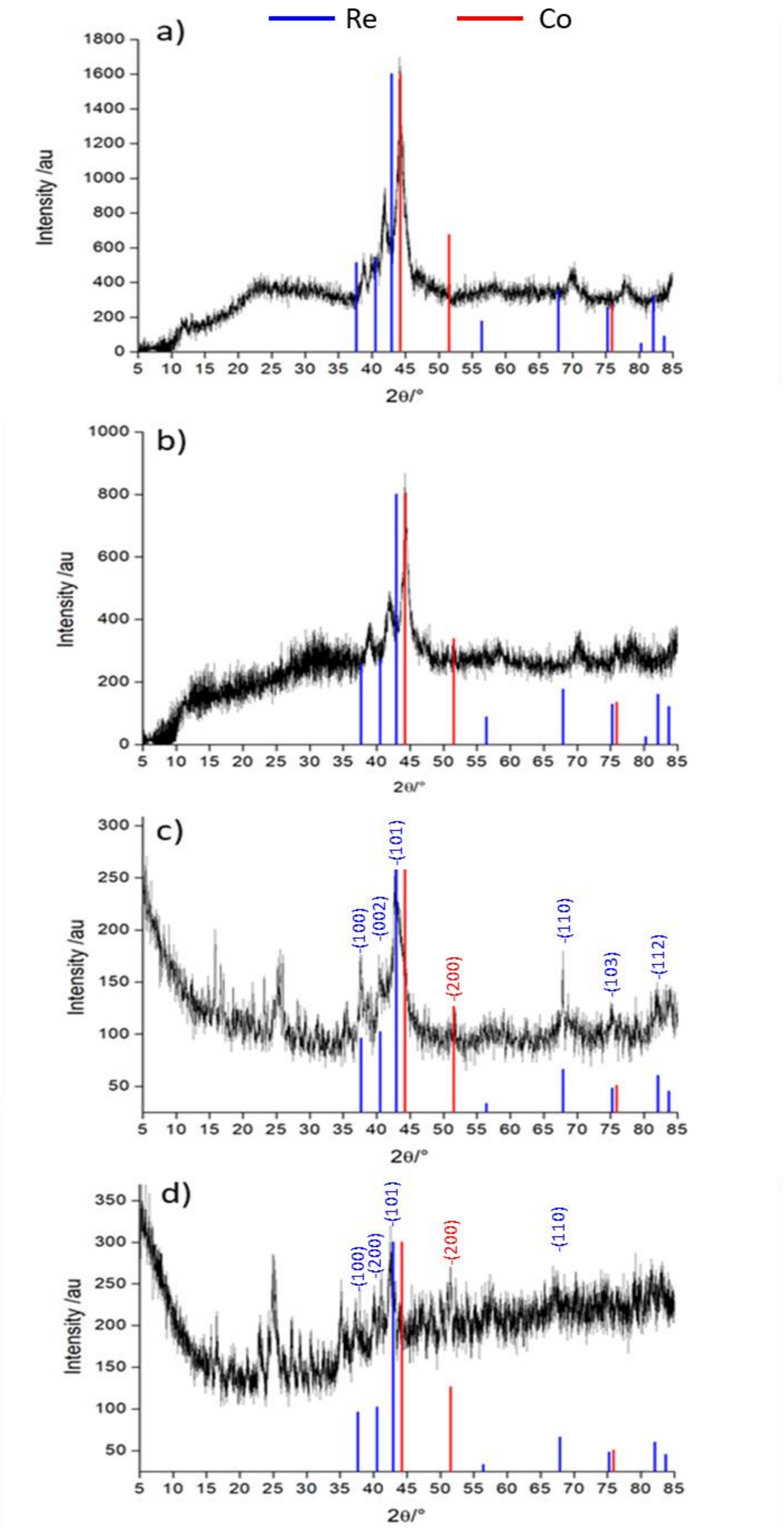

Figure 51: XRD Patterns Reaction for $CoRe_4$, pre-treated for 2 hours at 600°C with: a) N_2/H_2 (1:3), b) Ar/H_2 (1:3), c) N_2 and d) Ar then reacted with N_2/H_2 (1:3) at 400°C at ambient pressure. Reference PDFs Re) 00-005-0702 and Co) 01-089-4307.

3.3.5 *In situ* Powder X-ray Diffraction

In situ XRD data was collected at the ESRF simultaneously with XAS. $CoRe_4$ was diluted with boron nitride. Thee data was collected with the assistance of Dr Wouter van Beek, Dr Karina Mathisen, Dr Said Laassari and Mr Karsten Kirste. Figure 52 presents *in situ* XRD patterns for $CoRe_4$ which were taken after 60 mins in reaction gas (N_2/H_2 1:3) at 400°C. To investigate any phase changes under reaction condtions (N_2/H_2 1:3 at 400°C) multiple *in situ* XRD patterns were collected are plotted over time and are presented in Figure 53.

From Figure 52 it can be seen both patterns are dominated by the BN. No major differences are seen between the two pre-treatments apart from the rhenium reflections being slightly more intense in the N_2/H_2 pre-treated $CoRe_4$. It is suggested the *ex situ* and *in situ* XRD patterns have similar features. Also, no Co phases are detected despite the high concentration of Co in the material and this could be due to the high background disguising features.

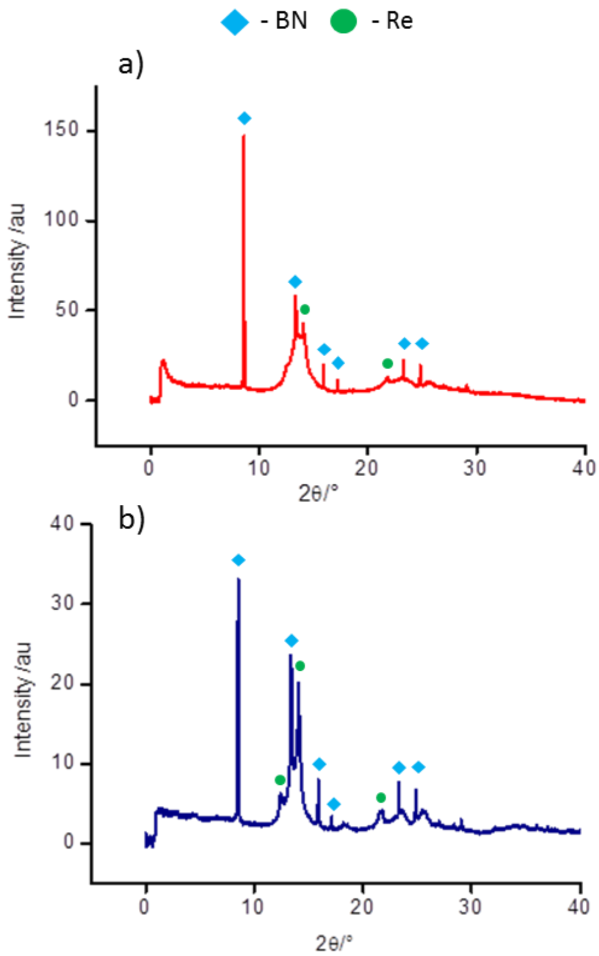

Figure 52: *In situ* XRD Patterns for $CoRe_4$ diluted with BN Pre-treated with a) N_2/H_2 (1:3) and b) Ar/H_2 (1:3). Reference PDFs Re 00-005-0702 and BN 00-015-0500.

From Figure 53 it can be seen regardless of pre-treatment no phase changes occur during reaction conditions. This is interesting for the Ar/H_2 pre-treated material as the catalyst develops activity after 20 minutes in reaction gas. However, no detectable phase changes occur between the 10 minutes (inactive material) and > 20 minutes (active material).

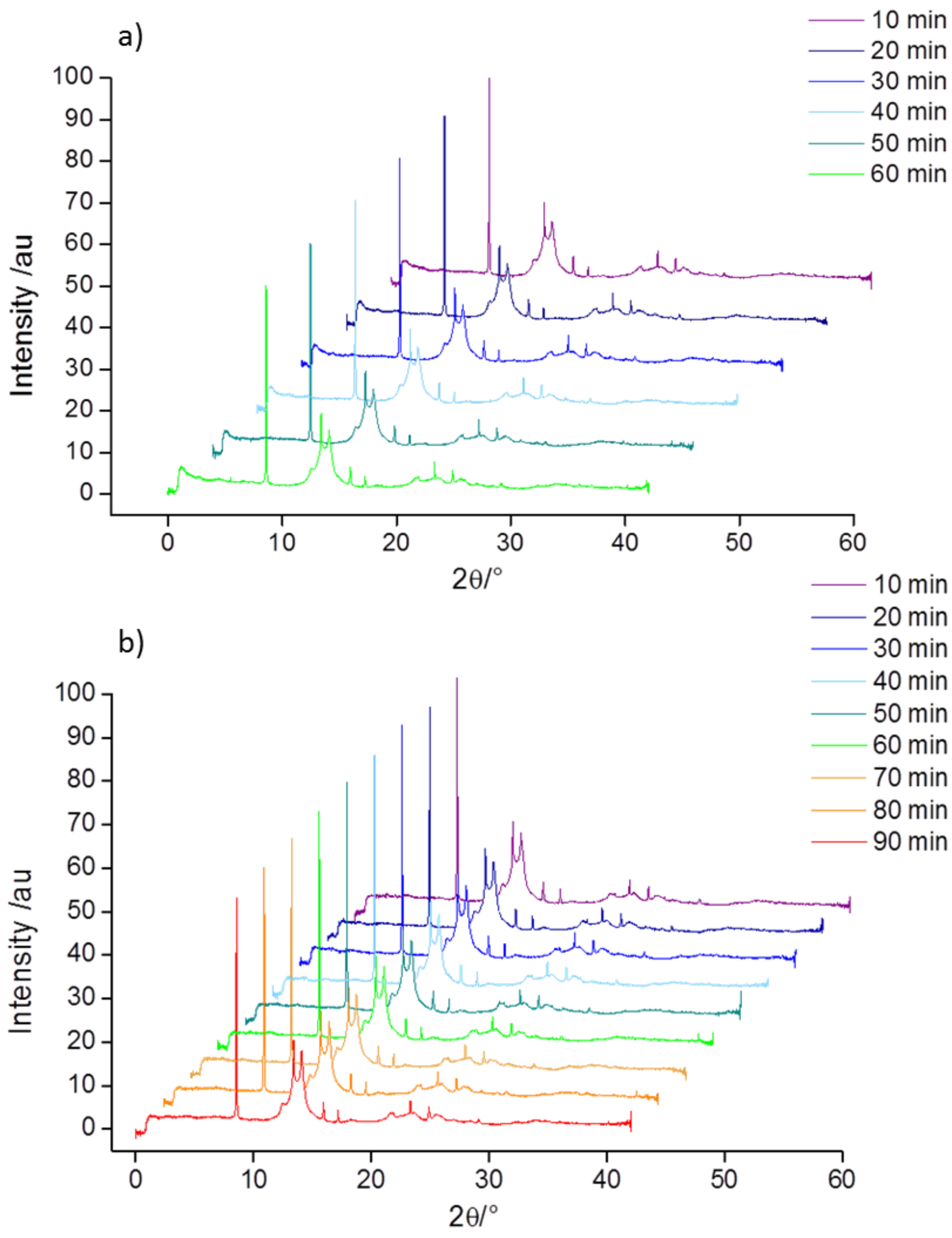

Figure 53: Multiple *In situ* XRD Patterns for $CoRe_4$ diluted with BN Pre-treated with a) N_2/H_2 (1:3) and b) Ar/H_2 (1:3) then reacted in N_2/H_2 (1:3) at 400°C.

3.3.6 Temperature Programmed Homomolecular $^{15}N_2/^{14}N_2$ Isotopic Exchange for $CoRe_4$

To further elucidate the nature of the surface of $CoRe_4$ towards nitrogen activation, temperature programmed homomolecular $^{14}N_2/^{15}N_2$ isotopic exchange was performed. This isotopic exchange can indicate some of the fundamental N_2 activation steps and the results are presented in Figure 54. This technique was performed at the University of Poitiers by Drs Nicholas Bion, Fabien Can and Melissandre Richard.

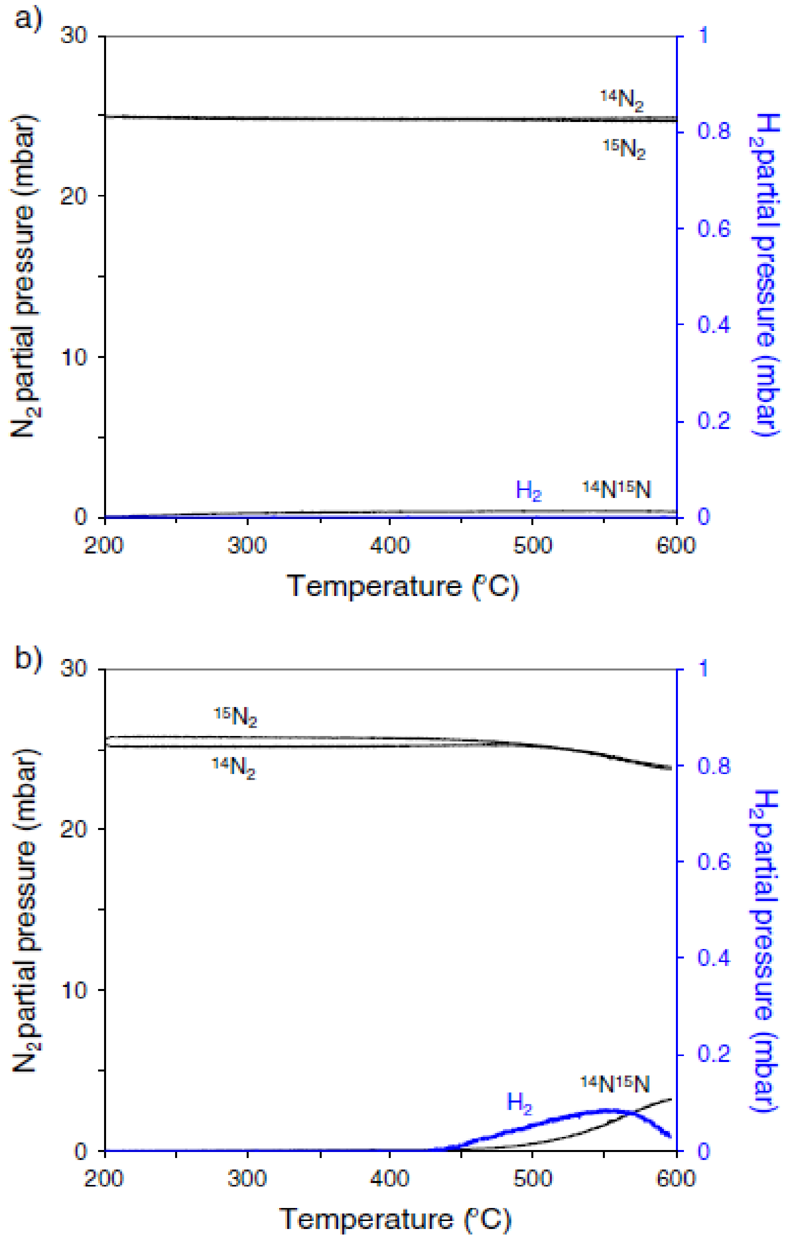

Figure 54: Temperature programmed $^{14}N_2/^{15}N_2$ homomolecular exchange profiles for (a) $CoRe_4$ pre-treated with (1:3) Ar/H_2 at 600°C for 1 hour and application of a secondary vacuum at 200 °C for 1 hour and (b) $CoRe_4$ pre-treated with (1:3) N_2/H_2 at 600°C for 1 hour and application of a secondary vacuum at 200°C for 1 hour[127].

There are significant differences between the exchange profiles for the different pre-treatments. In the applied temperature range the Ar/H_2 pre-treated sample is completely inactive for $^{14}N_2$/$^{15}N_2$ homomolecular exchange, whereas, the N_2/H_2 pre-treated sample is active for exchange after a small amount of H_2 is desorbed from the surface (the maximum pressure recorded at 550 °C is about 0.1 mbar[127]). This reinforces the importance of pre-treatment and the need for exposure to nitrogen to generate and active surface. Moreover, the evolution of H_2 implies the formation of a surface hydride which inhibits N_2 activation.

An interesting feature was noted; application of a vacuum step at 600°C yields $CoRe_4$ materials which are inactive for N_2 exchange and unable to desorb hydrogen. When this step is replaced by a 30 minute 600 °C N_2 pre-treatment, an active $CoRe_4$ material is formed the desorbs a small amount of H_2.

These observations could suggest that there are subtle changes in composition or surface structure which prevent the material from exchanging N_2.

3.3.7 Transmission Electron Microscopy

TEM studies of $CoRe_4$ have been performed to determine any phases not apparent in the XRD studies (Figure 55) and assess any potential differences in morphology. TEM was kindly performed at the University of St. Andrews by Dr Heather Greer and Prof Wuzong. Zhou. Representative micrographs are presented in Figure 55 for $CoRe_4$ activated for 2 hours with (1:3) N_2/H_2, (1:3) Ar/H_2 and post reaction $CoRe_4$.

Images (c) and (f) in Figure 55 have lattice spacings of 2.07Å and 2.09Å. These lattice spacings are consistent with the Re (101) plane and are found in both samples regardless of pre-treatment. The lattice spacing shown in Figure 55 (i) of 4.72Å may correspond to the (111) plane of Co_3O_4. Co_3O_4 could be present in the sample from incomplete reduction of Co during pre-treatment or, more probably, could have been formed by oxidation of reduced Co phases on discharge of the material from the reactor and/or its exposure to air[127]. Comparing the N_2/H_2 (1:3) and Ar/H_2 (1:3) pre-treated $CoRe_4$ it can be noted that the Re plane appears to be at a different orientation close to the termination plane depending on the pre-treatment used. However, given the statistical limitations associated with the number of observations made, this must be treated with caution.

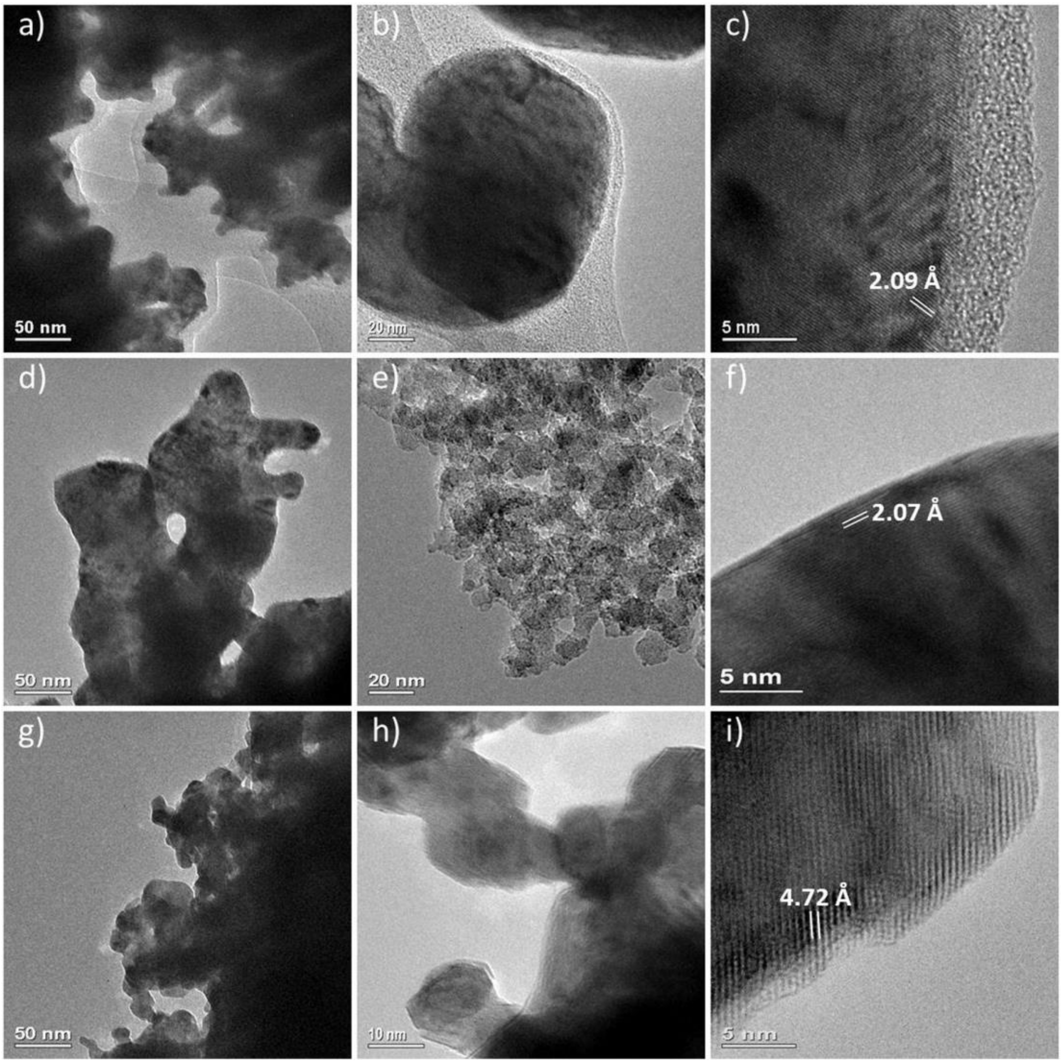

Figure 55: TEM images of $CoRe_4$ samples (a)–(c) following pre-treatment with (1:3) N_2/H_2 at 600 °C for 2 hours, (d)–(f) following pre-treatment with (1:3) Ar/H_2 at 600 °C for 2 hours and (g)–(i) following pre-treatment with (1:3) N_2/H_2 at 600 °C for 2 hours and reaction with (1:3) N_2/H_2 at 400 °C and ambient pressure[127].

On closer inspection of the micrographs, unlike for the case of the Ar/H_2 pre-treated material a pronounced amorphous surface film is observed for the N_2/H_2 pre-treated sample. The image contrast pattern is different from that of amorphous carbon. The amorphous layer may have been formed from surface reaction of the catalyst. It is clear from Section 3.3.1 the pre-treatment greatly affects the material's catalytic ability. However, it is important to note this technique was performed *ex situ* and although there is very apparent differencies between the two different pre-treatments, a degree of caution has to be exercised as exposure to air upon extraction from the reactor could result in varying degrees of surface oxidation[127].

3.3.8 X-ray Absorption Spectroscopy

3.3.8.1 Introduction to X-ray Absorption Spectroscopy

X-ray absorption spectroscopy (XAS) provides information on the chemical composition and local structure of materials[142]. The fundamentals of XAS are based on the absorption of X-rays and the creation of photoelectrons. The photoelectrons are excited to valence level holes or unbound states and scattered by neighbouring atoms in a material[142].

Referring back to Section 3.3.1 it is important to note the initial activity of $CoRe_4$ is dependent on the pre-treatment gas composition. The N_2/H_2 (1:3) pre-treatment results in a material which is instantly active whereas, in comparison when the Ar/H_2 (1:3) pre-treatment is used the material experiences a 20 minute lag period before developing activity. *In situ* EXAFS were performed using 2% H_2/N_2 gas mixtures and N_2/H_2 (1:3) the latter mimicking 'real' reactor conditions. Therefore, it is possible to examine the $CoRe_4$ structure before and after activity has 'switched on'. Any differences between the two structures will allow further insight into elucidating the active material.

Data collection and analysis was performed at the ESRF with the kind help of Dr Karina Mathisen, Mr Karsten Kirste (NTNU), Dr Wouter van Beek (ESRF), Drs Nicholas Spencer, Andrew McFarlane, Said Laassri and Justin Hargreaves (University of Glasgow).

3.3.8.2 $CoRe_4$ Starting Material

In order to examine the oxidation state changes of Re and Co during the reaction, it was important to first establish the initial oxidation states of each metal in the starting material. Using *ex situ* XANES the $CoRe_4$ starting material was compared to Re and Co standards with known oxidation states. XANES was performed on the Re L_3 and Co K edges. The results are presented in Figures 56 and 57 respectively. From Figure 56 the $CoRe_4$ and NH_4ReO_4 and signals are comparable and that $CoRe_4$ exhibits an absorption edge similar to that of the Re (VII) oxide. Therefore, it was concluded Re is in the +7 oxidation state and bares close resemblance to the Re precursor (NH_4ReO_4).

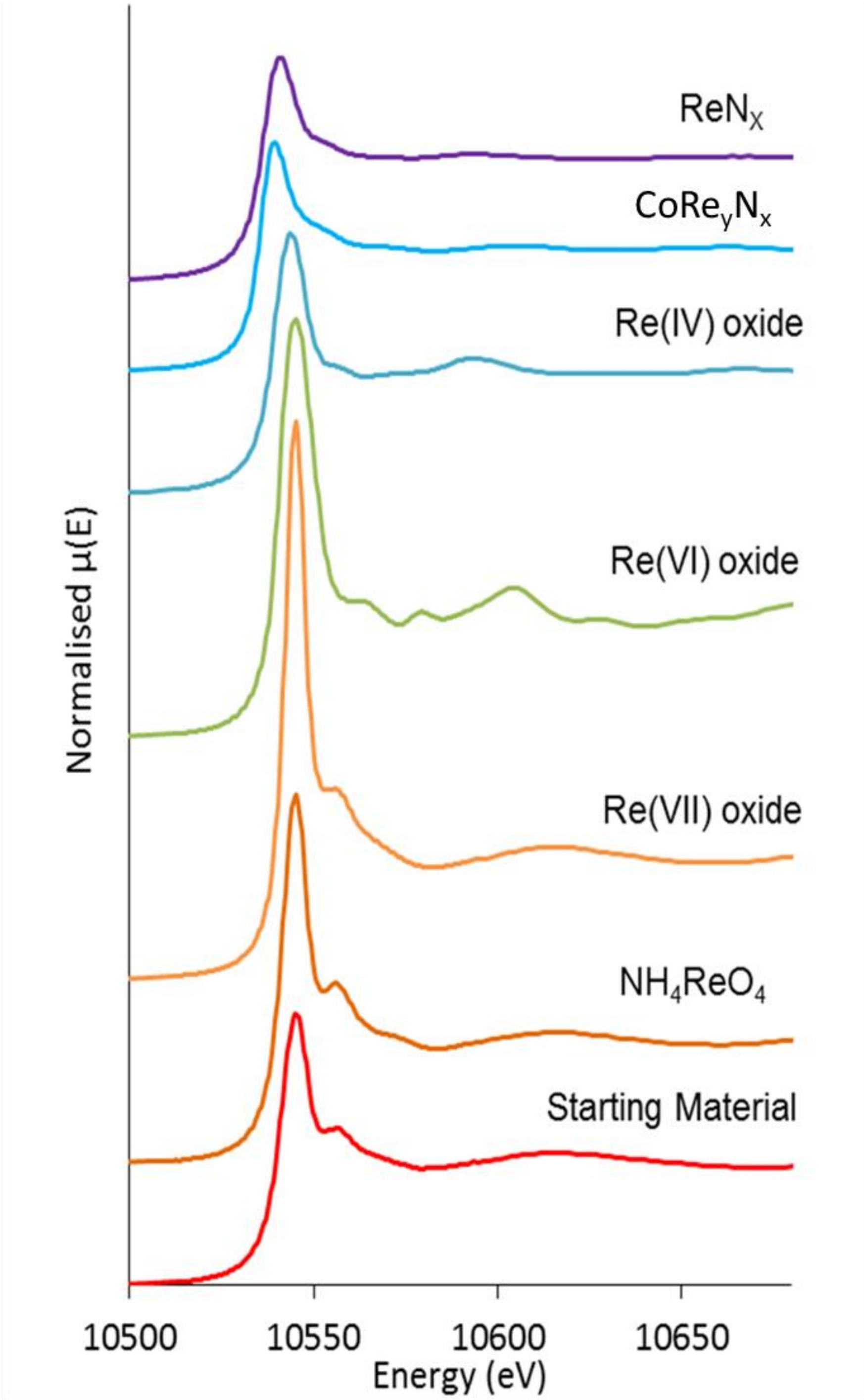

Figure 56: Normalised XANES Spectra for $CoRe_4$ Compared to Reference Compounds at the Re L_3 Edge.

With regard to the Co K edge XANES (Figure 57), the $CoRe_4$ starting material is not similar to any of the cobalt oxide reference compounds and rather the local cobalt environment is comparable to the $Co_3(PO_4)_2$ reference compound. Comparing E_0 values, it is clear there is a mixture of oxidation states of Co (III)/Co (II) in the $CoRe_4$ starting material.

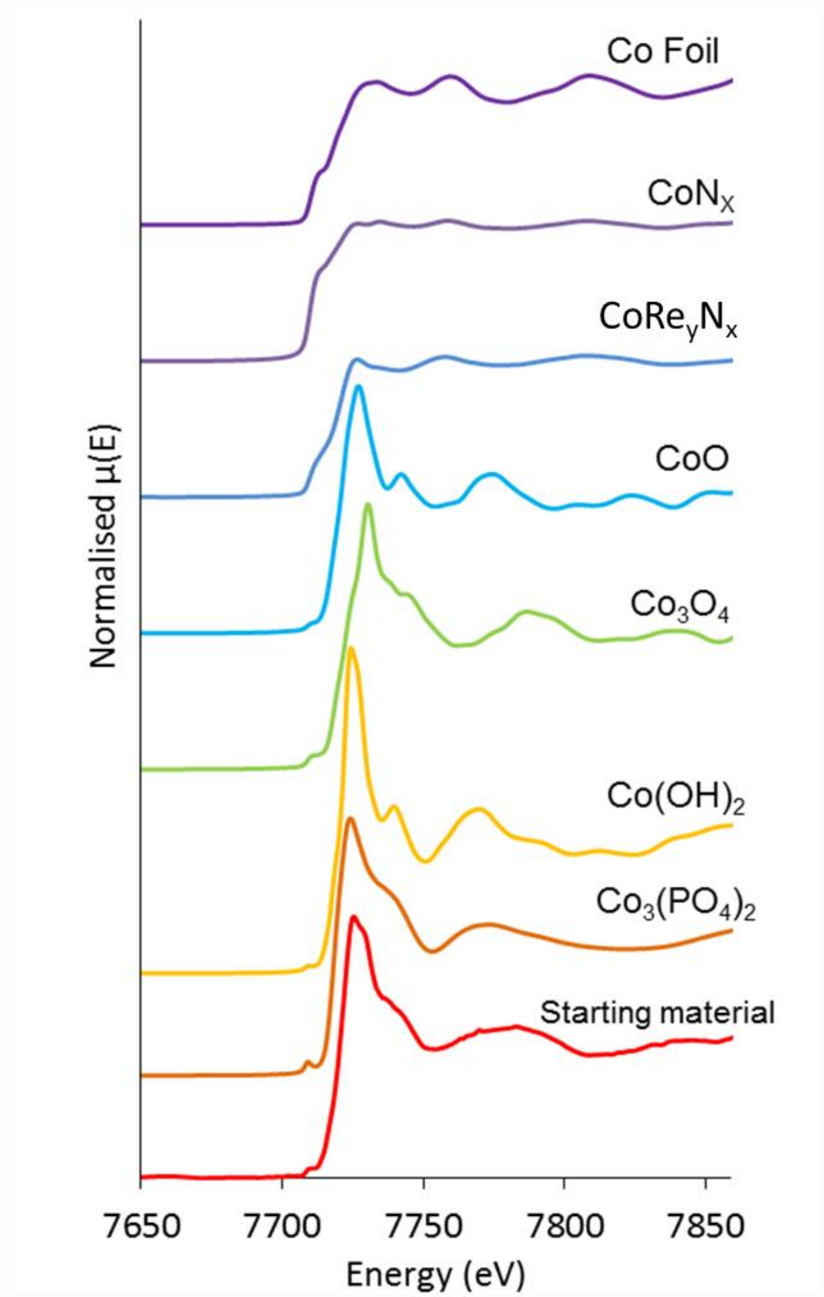

Figure 57: Normalised XANES Spectra for $CoRe_4$ Compared to Reference Compounds at the Co K Edge.

EXAFS refinements for the $CoRe_4$ starting material are presented in Table 16 and the Fourier Transforms are presented in Figure 58. For the Re L_3 edge 3.5 Re-O absorption pairs can be fitted with a bond length of 1.70 Å. This is slightly shorter than 1.74 Å distances reported for tetrahedrally coordinated ReO_4^- in Bi/Re/O materials and longer than longer than Re=O double bonds reported from XRD analysis of organorhenium (+7) oxides (1.67 Å)[143].

An oxygen shell can also be fitted for the Co K edge, with a bond length of 2.01 Å and multiplicity of 2.90. This suggests the starting material is a mixed oxide material comprising of a combination of cobalt and rhenium oxides. In conclusion, from the external standards it was found rhenium begins in the Re^{+VII} oxidation state (as in the Re precursor NH_4ReO_4) and the cobalt begins in a mixture of the +2 and +3 oxidation state. The starting material is a mixed oxide material consisting of a combination of cobalt and rhenium oxides. With respect to octahedral Re-O_{Oh} bonds they generally have a bond length of 1.89 Å[143]. A second Re-O absorption shell is found at 2.15 Å with multiplicity of 3. This bond length is too long to be octahedrally coordinated ReO_6. However, similar Re-O bonds are also reported from EXAFS studies of the oxides of Re/Bi. It can be suggested both rhenium and cobalt are present in the oxidised state in pre-reaction $CoRe_4$.

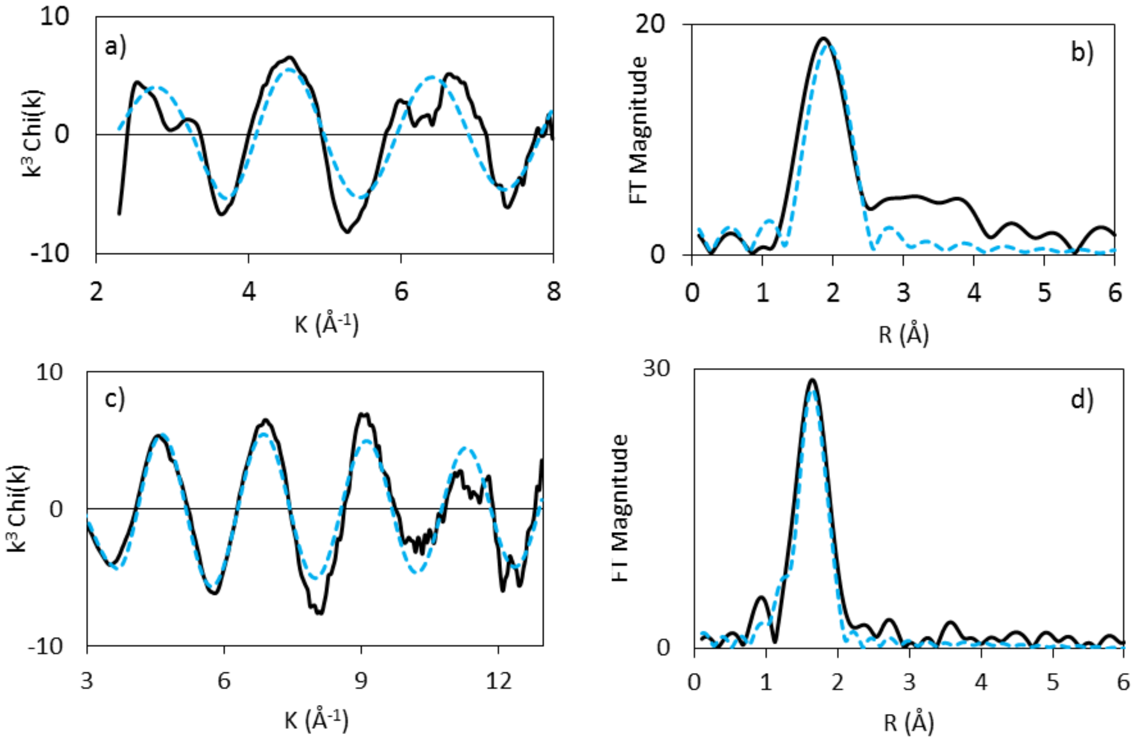

Figure 58: Material Experimental and Calculated k3-weighted EXAFS (left) and its Fourier Transform (right) for the fresh $CoRe_4$ at Co K edge (a-b) and Re L_3 edge (c-d).

Table 16: Results from the least squares EXAFS analysis at Re L_3 edge and Co K edge pre-reaction $CoRe_4$ (AFAC transferred from Co_3O_4 = 0.66, and NH_4ReO_4 = 0.67) and reference compounds $CoRe_yN_x$, Co_xN and Re_xN prepared by ammonolysis (AFAC transferred from Co-foil = 0.79 and Re-foil= 0.8).

Sample	**Shell**	**N**	**R/Å**	**$2\sigma^2$/Å^2**	**EF/eV**	**R/%**	**Δk**
$CoRe_4$	Co-O	4(1)	1.96(2)	0.003(9)	-2(2)	58	2-8
	Re-O	3.4(3)	1.704(7)	0.003(1)	-6(2)	28	2-13
	Re-O	3(1)	2.15(2)	0.02(1)			
$CoRe_yN_x$	Co-Co	4.6(7)	2.468(6)	0.018(3)	-5.0(9)	29	2-10
	Co-Re	2.0(8)	2.66(1)	0.011(7)			
	Re-N	0.4(2)	1.76(3)	0.01(1)	-6(1)	16	3.5-9.5
	Re-Co	3.0(5)	2.57(1)	0.022(3)			
	Re-Re	3.1(8)	2.650(7)	0.018(5)			
Co_xN	Co-Co	4.0(8)	2.50(1)	0.013(3)	-8(2)	43	2-11
Re_xN	Re-N	0.6(5)	1.79(3)	0.014(18)	3(2)	47	3.5-9
	Re-Re	7(2)	2.67(2)	0.032(8)			
Co-foil	Co-Co	12	2.496(7)	0.0132(8)	-16(1)	33	2-12

[a]The EXAFS refinements give information about multiplicity (N), bonding distance (R) and thermal vibration (Debye-Waller factor, $2\sigma^2$). E_F is the refined correction of Fermi energy in vacuum, compared to E_0. The standard deviation in the last significant digit as calculated by DL-excurv is given in parentheses. The deviation for $2\sigma^2$ is ±20%.The Fit index is defined as FI= $\Sigma_i(1/\sigma_i)[\mathrm{Exp}(i) - \mathrm{Theory}\ (i)]^2$. The statistical R-factor is defined as R= $\Sigma_i^N [1/\sigma_i (|\chi_i^{exp}(k) - \chi_i^{th}(k)|)]$ x 100% and gives indication of the quality of fit in k-space.

3.3.8.3 **XAS Results 2% H_2/N_2 Gas Mixtures**

The catalyst was analysed following the 600°C pre-treatement for both gas mixtures (2% H_2/N_2 and 2% H_2/Ar). Table 17 shows the variation between pre-treatments for $CoRe_4$. Figures 59 and 60 compare the multiplicities for each fitted shell for both pre-treatments on the Re L_3 and Co K edge respectively.

Table 17: EXAFS Least Squares Refinements of the $CoRe_4$ in 2% Pre-treatment Gas Mixtures at 600°C at the Re L_3 edge.

Pre-treatment	Shell	Multiplicity (N)	Bond Length (Å)
2% H_2/Ar	Re-Co	3 (1)	2.64 (2)
	Re-Re	4 (1)	2.71 (1)
2% H_2/N_2	Re-N	0.6 (5)	2.20 (7)
	Re-Co	3 (2)	2.66 (3)
	Re-Re	4 (1)	2.715 (9)

The Re-Re bond lengh of 2.71 Å is shorter than the Re–Re distances in bulk rhenium metal (2.74 Å) and are consistant with Re–Re distances obtained by Rønning *et al*[122]. Regarding the Re L_3 edge bimetallic and metallic environmental similarities are observed after pre-treatment in 2% H_2/N_2 and 2% Ar/H_2 at 600°C. Bimetallic Re-Co bonds are present coupled with a slightly higher concentration of metallic Re-Re bonds. A marked difference is found for the Re-N shell. The Re-N shell is present after pre-treatment in 2% H_2/N_2 and not found in the 2% H_2/Ar pre-treated material. Despite the different gas composition (2% H_2/N_2 and 75% H_2/N_2) a similar pattern of results are found in Section 3.3.8.3 for Re-Re and Re-Co species. However, Re-N species is not found in the 75% gas mixtures this could possibly be explained by the difference in N_2 concentration betweent the two gas mixtures (98% versus 25%). The presence of metallic Re-Re bonds are consistent with TEM results (Section 3.3.7) which reveal the presence of Re metal.

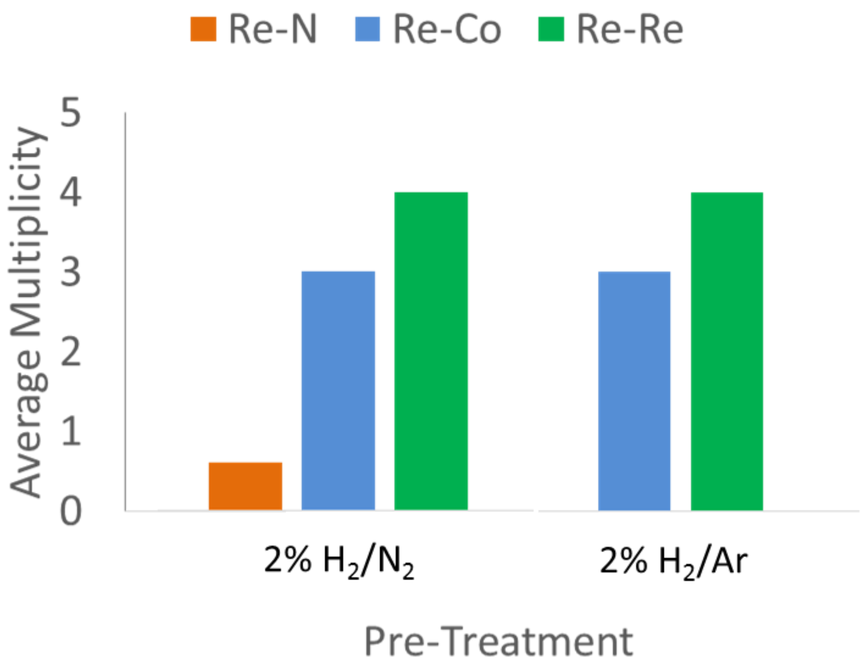

Figure 59: Re L_3 Edge Final Pre-treatment scan at 600°C for $CoRe_4$.

Looking at the Co environment in Figure 60 similar environments are observed for both pre-treatments after pre-treatment at 600°C. Metallic Co-Co bonds and bimetallic Co-Re bonds are observed. Also, no Co-N shell can be fitted to the data.

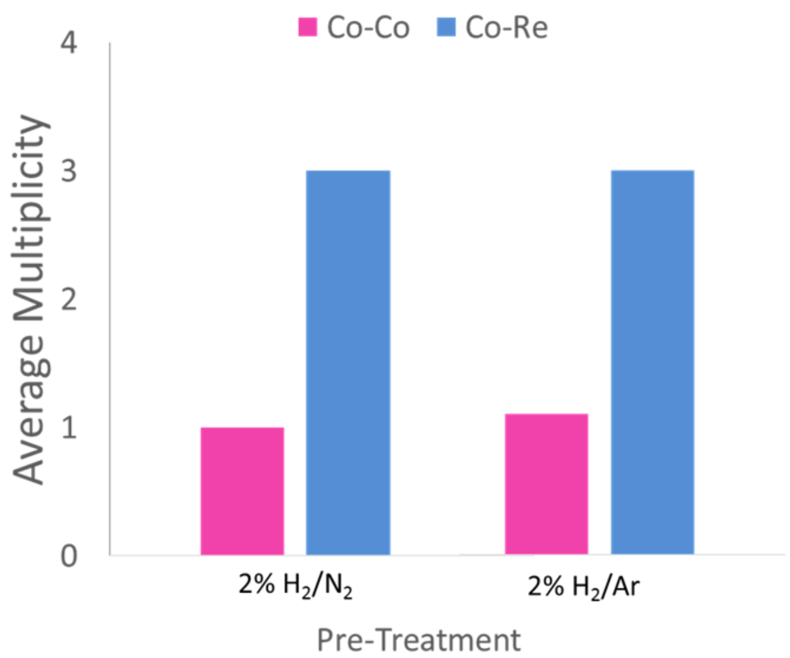

Figure 60: Co K Edge Final Pre-treatment scan at 600°C for $CoRe_4$.

There is no change in the EXAFS signal during the 4 hour testing period. This is shown in Figure 61 with no change in multiple EXAFS signals over 4 hours at 400°C under 2% H_2/N_2 for $CoRe_4$ pre-treated with 2% H_2/N_2 and 2% H_2/Ar. This suggests there are no structural changes occurring. This is surprising because it has been previously shown during the Ar/H_2 (1:3) pre-treatment there is a 'switching on' of activity after 20 minutes in N_2/H_2 (1:3). Analysing the material before and after activity develops may provide more insight into the active material and what changes occur to create the active material. Figure 62 shows the Fourier transforms for both edges for $CoRe_4$ which has been pre-treated with 2% H_2/Ar at 600°C then the temperature was dropped to 400°C and reaction gas mixture of 2% H_2/N_2 switched in.

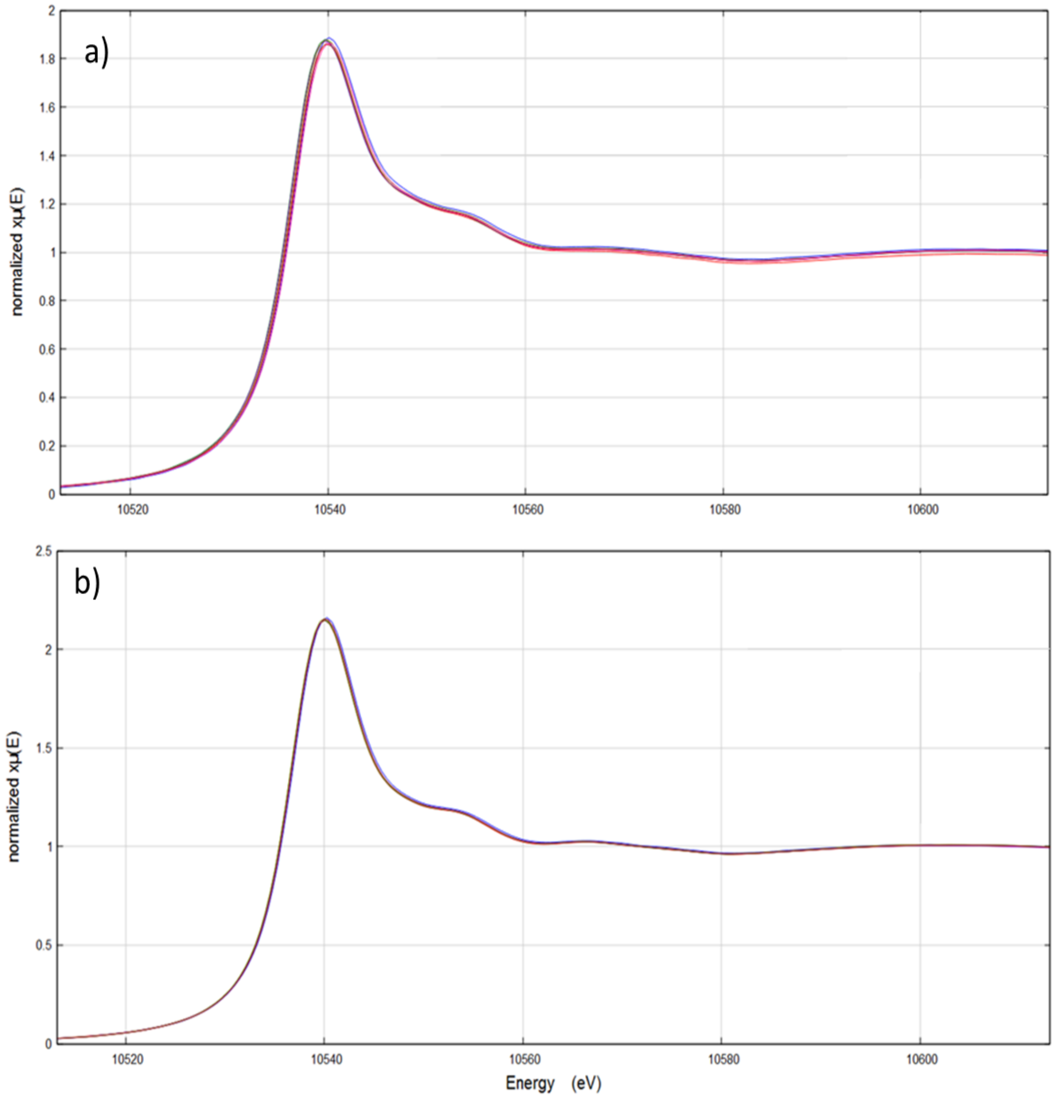

Figure 61: EXAFS scans taken at 400°C over a 4 hours period a) 2% H_2/N_2 and b) 2% H_2/Ar.

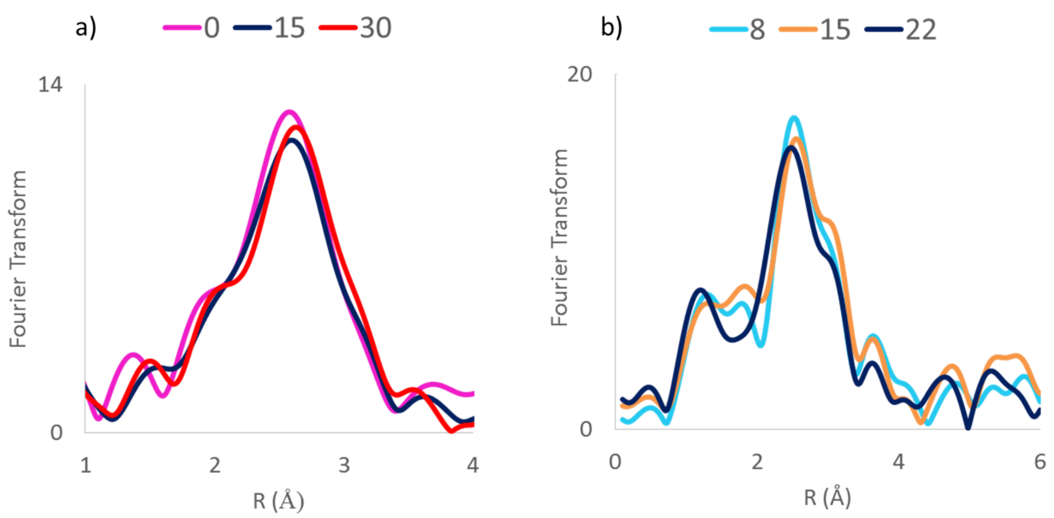

Figure 62: Fourier Transforms for $CoRe_4$ Pre-treated with 2% H_2/Ar. Numbers shown indicate the time (minutes) in Reaction Gas 2% H_2/N_2 at 400°C. a) Re L_3 Edge and b) Co K Edge.

Very little change is observed for either edge which suggests the structure is not changing. However, it must be noted the lack of observed change at the 20 minute point in reaction is postulated to be due to the difference in gas mixtures. The activity data described in Section 3.3.1 uses an Ar/H_2 (1:3) pre-treatment mixture and N_2/H_2 (1:3) reaction gas mixture. The difference in gas compositions may cause the lag period to occur at a different time frame and that is the reason it is not observed in Figure 62.

After 2 hour pre-treatment in either 2% H_2/N_2 or 2% H_2/Ar it can be argued the material has both: bimetallic character from the presence of Re-Co bonds and metallic character from Re-Re and Co-Co bonds. The only marked difference is attributed to the possible Re-N shell that can be fitted in the case of 2% H_2/N_2 pre-treatment.

3.3.8.4 **XAS Using Stoichiometric N_2/H_2 (1:3) Gas Mixtures**

In order to gain a deeper insight into $CoRe_4$ *in situ* XAS was performed using N_2/H_2 (1:3) and Ar/H_2 (1:3). These gas mixtures have the same composition as the ones used for activity testing (Section 3.3.1). This allows for direct structural comparisons to be drawn during lag and steady state periods. It is important to state that these analyses are preliminary and further refinement is ongoing.

3.3.8.4.1 $CoRe_4$ During Pre-treatment

After establishing the oxidation states of Re and Co in the starting material, to investigate any oxidation state changes during the N_2/H_2 (1:3) and Ar/H_2 (1:3) pre-treatments *in situ* XANES were performed on the Re L_3 and Co k edges.

From Figure 63 it can be seen the reduction of Re is a one step process and is fairly consistent regardless of what pre-treatment atmosphere is used. In contrast, a distinction can be seen at the Co k edge. In the Ar/H_2 (1:3) environment a two-step reduction is observed which begins at a lower temperature (approximately 200°C). This is consistent with reports that the reduction of Co is a two stage process: $Co_3O_4 \rightarrow CoO \rightarrow Co$[119]. The $Co^{+3/+2} \rightarrow Co^0$ reduction occurs quite steeply, initiated around 200°C, and occurs before the reduction of $Re^{+VII} \rightarrow Re^0$, which starts at 300°C for both pre-treatments. Considering the Fischer–Tropsch Process; rhenium is sometimes added to catalysts to improve the reduction of Co[116, 117]. Rhenium reduction occurs at roughly the same temperature as the reduction of Co_3O_4 so has little effect on this stage. However, the temperature of the second stage of cobalt oxide reduction is lowered by the presence of Re[118]. During the N_2/H_2 (1:3) pre-treatment Co reduction begins at a higher temperature and more closely resembles a one-step reduction process compared to the two step reduction in the Ar/H_2 (1:3) gas mix. Both elements are reduced to the metallic state between 500 and 600°C. In this study, the cobalt initiates reduction of rhenium during pre-treatments.

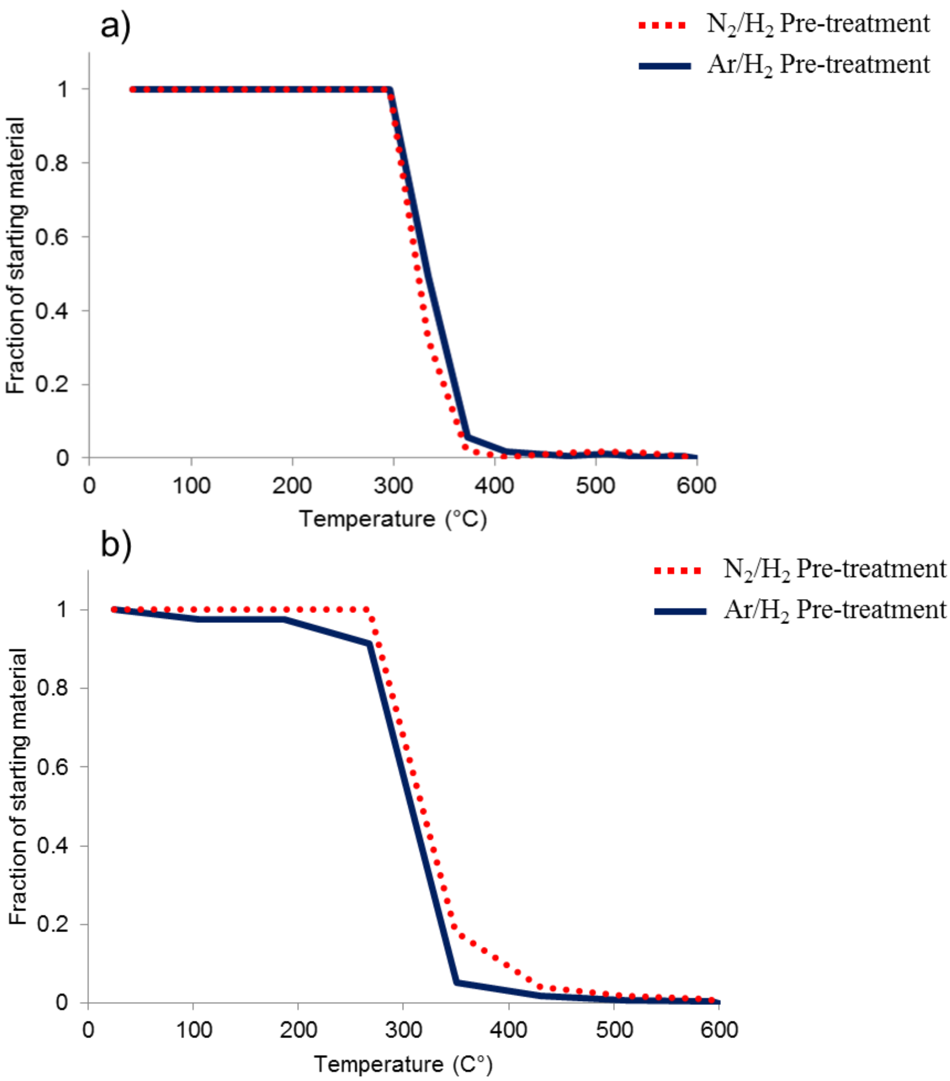

Figure 63: Reduction Profiles for $CoRe_4$ in Stoichiometric (1:3) Gas Mixtures a) Re L_3 edge, b) Co K edge

The normalised XANES are presented for the Re L_3 and Co K edge in for $CoRe_4$ at the end of both the 2 hour pre-treatments at 600°C in are compared to reference compounds and presented in Figures 64 and 65.

For both the Re L_3 and Co K edge and the E_0 values and the shape of the XANES confirm that both the metals are present in the metallic state. Two small features are visible in the Co data in the white line region (Figure 65), whereas the cobalt foil shows one broad feature. Sa *et al*[144] studied $PtCo/Al_2O_3$ and also report these white line features in the cobalt XANES after *in situ* H_2 reduction. Therefore, it can be postulated this feature is indicative of a bimetallic Co-metal interaction.

From Figure 64 it can be seen the Re L_3 edge XANES for all $CoRe_4$ scans occur at a lower E_0 value and have a lower intensity compared to ReN_x and $CoRe_yN_x$. This is due to Re being fully reduced in $CoRe_4$ which is in agreement with the reduction profiles shown in Figure 63. Whereas, the Re in the samples prepared *via* ammonolysis have partially oxidised. This is probably caused on discharge form the reactor as the nitrided cobalt rhenium ($CoRe_yN_x$) data was collected *ex situ*. Independent of pre-treatment for both edges, there are clear similarities between the features observed in the XANES which suggests that there are largely similar local metal environments at this point.

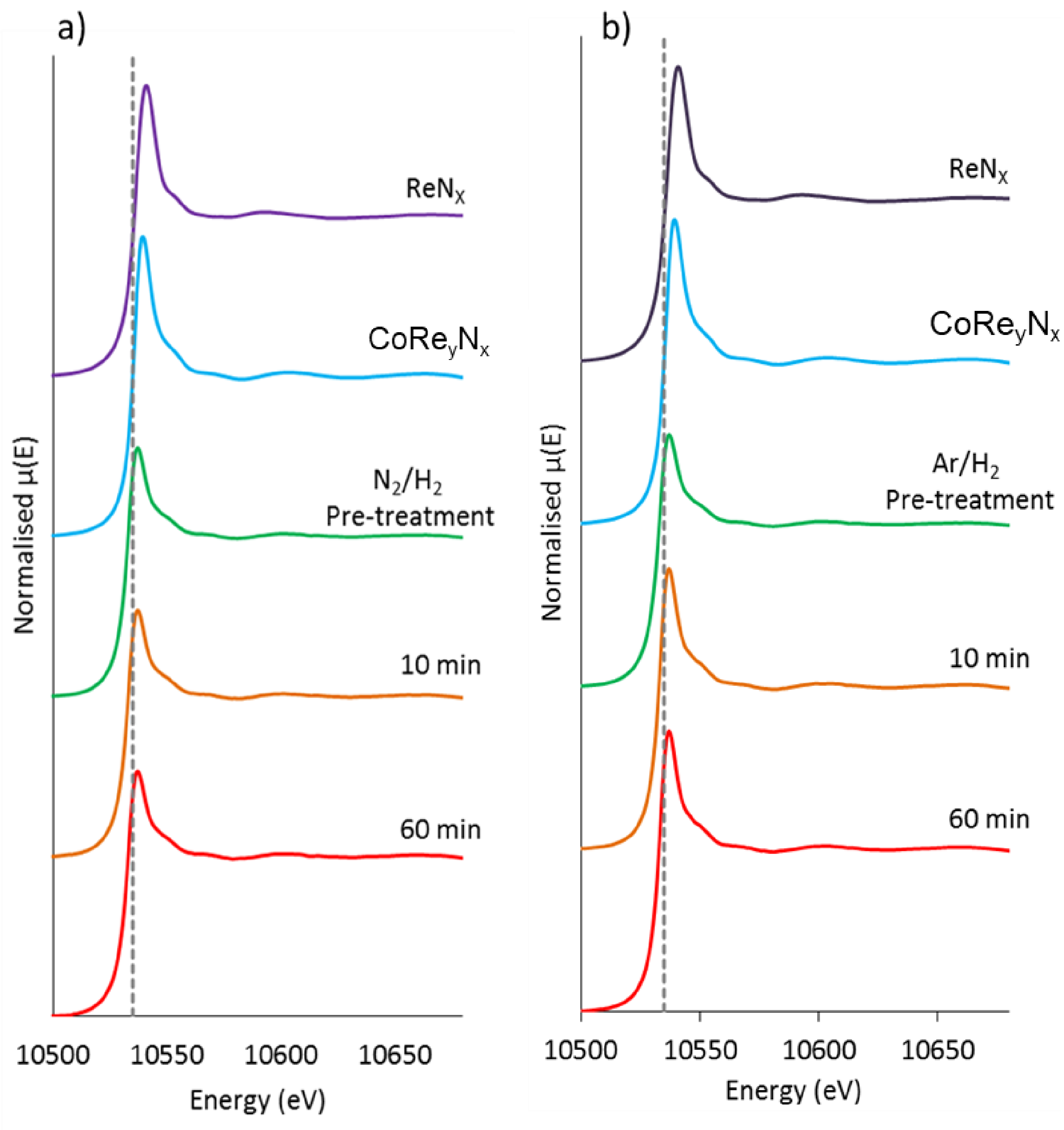

Figure 64: Normalised XANES for $CoRe_4$ pre-treated with (a) N_2/H_2 (1:3) and (b) Ar/H_2 (1:3) during ammonia synthesis compared to reference compounds for Re L_3 Edge.

With respect to the Co K edge (Figure 65) no major discrepancies are observed for the features observed in the XANES between the two pre-treatments. This suggests the Co local metal environment is similar regardless for what pre-treatment gas mixture is used.

The obtained E_0 values and the shape of the XANES confirm at the end of pre-treatment, under both gas mixtures, the Co is in the metallic state. However, comparing the sample to the Co foil slight differences can be seen; there are two small features in the white line region for $CoRe_4$ and these features are not visible from the Co foil as it shows one broad feature this was also reported by Guczi *et al*[145] after *in situ* reduction of Pt-Co/Al_2O_3 catalyst with H_2. Therefore, these features may be associated with bimetallic interactions. The XANES of pre-treated $CoRe_4$ is similar to CoN_x whereas the $CoReN_x$ has a more intense first white line feature which suggests partial re-oxidation has occurred.

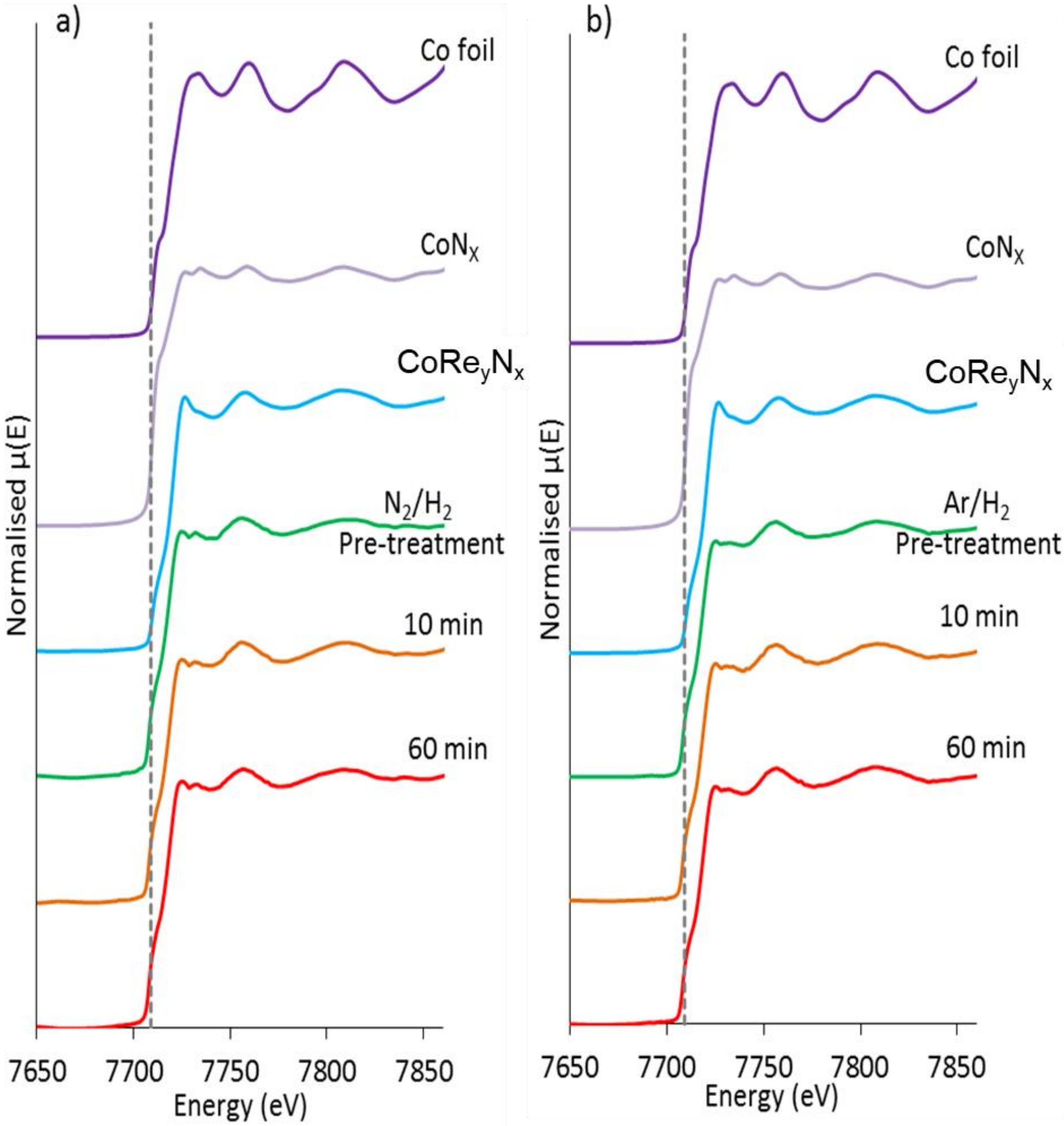

Figure 65: Normalised XANES for $CoRe_4$ pre-treated with (a) N_2/H_2 (1:3) and (b) Ar/H_2 (1:3) during ammonia synthesis compared to reference compounds for Co K Edge.

Table 18 gives the least square refinements for $CoRe_4$ after 2 hour pre-treatment at 600°C. After pre-treatment in N_2/H_2 (1:3) a large degree of Co-Re bimetallic mixing is observed. Comparable results are found for both the Re L_3 and Co K edges; a Re-Co bond length of 2.51 Å and a multiplicity of 3.2 and 3 respectively. $CoRe_4$ also exhibits Co-Co (1.7 at 2.45 Å) and Re-Re (5 at 2.71 Å) backscattering pairs, suggesting pure cobalt and rhenium phases are also present.

EXAFS of $CoRe_4$ after the two different N_2/H_2 (1:3) and Ar/H_2 (1:3) pre-treatments clearly confirms that the presence of nitrogen during pre-treatments is a prerequisite for extensive bimetallic Co-Re mixing. At the rhenium edge (Figure 66) the local environment appears to be very similar. The choice of pre-treatment leads to differing Co environments (Figure 67). Cobalt may be more sensitive to the degree of mixing as there is a lower concentration of Co in the sample.

Comparing the two different pre-treatments it can be concluded the nitrogen containing gas mixture leads to a material with a higher degree of bimetallic mixing. It is postulated this enhanced degree of mixing may be attributed to the enhanced activity achieved with the N_2/H_2 (1:3) pre-treatment. It is important to note this is a preliminary study, attempts to introduce a low multiplicity Re-N shell led to a decrease in the fit factor, therefore, the shell was omitted. It is worth noting there is a lack of second or third metal-metal absorption shell in these samples which indicates a high degree of disordering in the system. Typically a second Re-metal distance is found at 3.56 Å in bulk rhenium, absent in the $CoRe_4$ system[80]. This disorder is also suggested by the XRD analysis as a large amorphous background is present (Figure 53).

Table 18: EXAFS least squares refinements of $CoRe_4$ after 2 hour pre-treatment at 600°C in either N_2/H_2 (1:3) or Ar/H_2 (1:3) for both Co K edge and Re L_3 edge from *in situ* XAS. AFAC transferred from Co-foil = 0.79 and Re-foil= 0.8.

	Sample	Shell	N	R/Å	$2\sigma^2/Å^2$	E_F/eV	R/%	Δk
After 2 hour Pre-treatment at 600°C	N_2/H_2 (1:3)	Co-Co	1.7(6)	2.45(1)	0.011(7)	-6.3(8)	39	2-8.5
		Co-Re	3.2(9)	2.51(1)	0.020(6)			
		Re-Co	3(1)	2.51(2)	0.042(9)	-7(2)	49	3.5-9.5
		Re-Re	5(3)	2.71(3)	0.05(2)			
	Ar/H_2 (1:3)	Co-Co	9(2)	2.46(1)	0.049(5)	-3(1)	36	2-8.5
		Re-Co	1.7(8)	2.51(1)	0.031(9)	-9(1)	47	3.5-9.5
		Re-Re	7(3)	2.73(1)	0.05(1)			

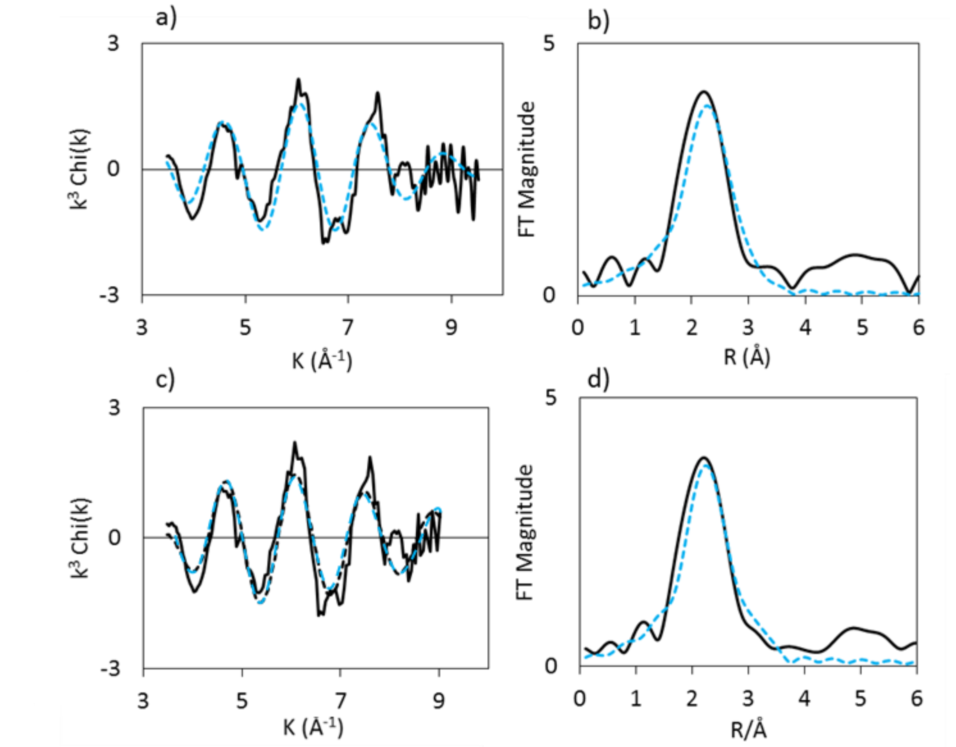

Figure 66: Experimental (-) and calculated (---) k3-weighted EXAFS (left) and its Fourier Transform (right) for $CoRe_4$ after pre-treatment in a - b) N_2/H_2 (1:3) and c - d) Ar/H_2 (1:3) for the Re L_3 edge.

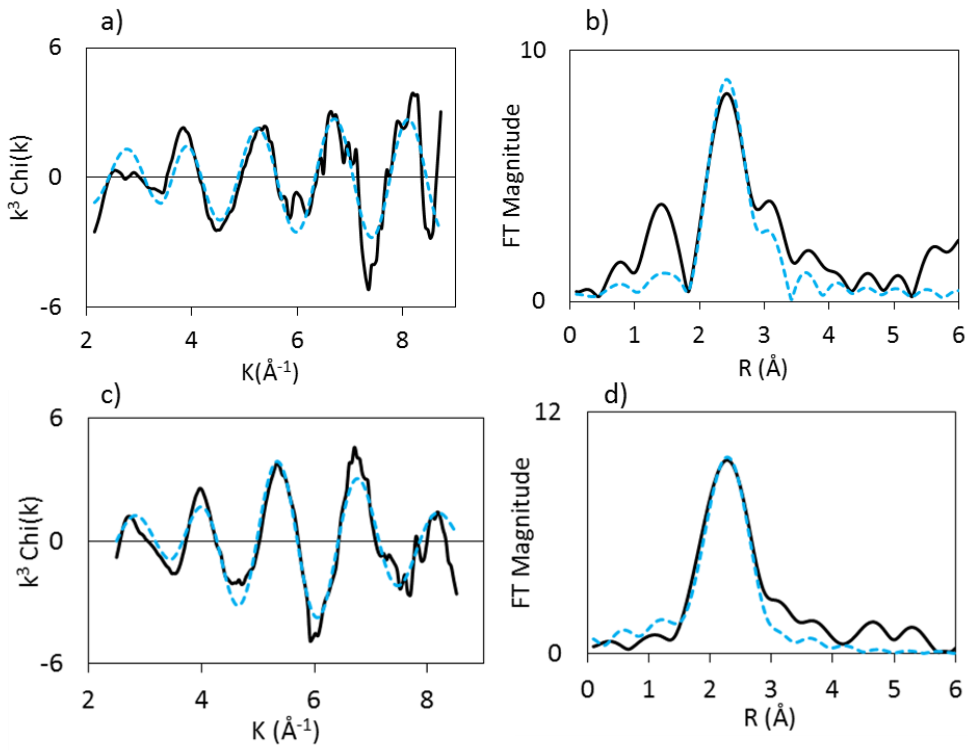

Figure 67: Experimental (-) and calculated (---) k3-weighted EXAFS (left) and its Fourier Transform (right) for $CoRe_4$ after pre-treatment in a - b) N_2/H_2 (1:3) and c - d) Ar/H_2 (1:3) for the Re L_3 edge.

Average coordination numbers for $CoRe_4$ in both pre-treatment gas mixtures are shown in Figure 68. For $CoRe_4$ pre-treated in Ar/H_2 (1:3), attempts to introduce a Co-Re shell were unsuccessful, yielding only a Co-Co shell at 2.46 Å with average coordination of 9[80]. At the rhenium edge, a Re-Co shell could be fitted, with average coordination of 1.7 at 2.51 Å. The major contribution to the signal is the Re-Re shell at 2.71 Å with average coordination of 7. Clearly, the degree of mixing is greatly influenced by the pre-treatment, as the presence of nitrogen ensures bimetallic Co-Re pair formation[80]. It is important to note this is a preliminary analysis and further refinement is required. However, what it proves is that the choice of pre-treatment gas mixture heavily affects the degree of mixing and the presence of nitrogen appears to increase the bimetallic contribution.

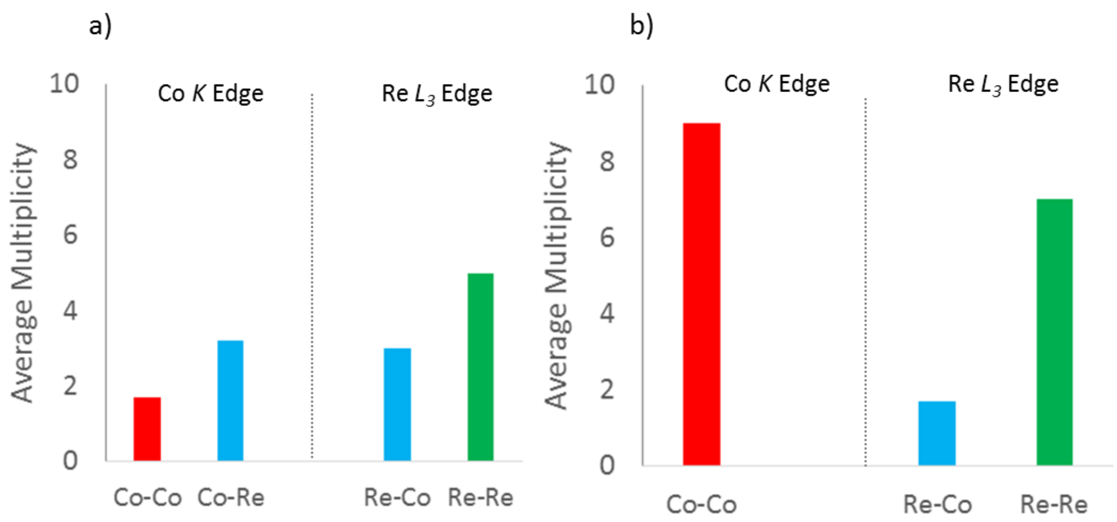

Figure 68: Average coordination numbers from EXAFS analysis for $CoRe_4$ after 120 minutes pre-treatment at 600°C in (a) N_2/H_2 (1:3) and (b) Ar/H_2 (1:3) for Co K edge and Re L_3 edge.

3.3.8.4.2 $CoRe_4$ During Ammonia Synthesis

Analysis in this section will focus on $CoRe_4$ during ammonia synthesis conditions at 400°C under N_2/H_2 (1:3) after pre-treatments. Regarding pre-treatment with Ar/H_2 (1:3) it is of interest to establish whether this observed lag period can be explained by structural changes observed in *in situ* XAS. The normalised XANES for both edges taken after 10 and 60 minutes in reaction gas (75% H_2/N_2) at 400°C after pre-treatment are shown in Figure 65. No apparent changes are observed in the cobalt XANES when compared to the spectra at the end of the 2 hour pre-treatment. This is the same for both pre-treatments and the XANES are similar independent of pre-treatment.

With respect to the XANES on the Re L_3 edge, the white line for $CoRe_4$ pre-treated in Ar/H_2 increases after 10 and 60 minutes in reaction gas. The white line intensity for the Re L_3 edge is caused by a $2p_{3/2}$ to 5d transition and generally the higher the oxidation state, the higher the white line. It is difficult to extract quantitative information from variations in white line intensity for the rhenium L_3 edge. However, it is suggested the observed change in the electronic state of the Re atoms do not correlate with similar changes in the Co atoms. Therefore, it is postulated the change is occurring in a pure rhenium phase which could be connected with the material becoming active for ammonia synthesis. The increase in white line intensity could possibly be an effect of the partial oxidation of rhenium, however attempts to fit a Re-N shell for this sample were not successful.

The results for EXAFS and their corresponding Fourier Transforms for $CoRe_4$ pre-treated with N_2/H_2 and Ar/H_2 are shown in Figures 70 and 71 respectively. The results from the EXAFS refinements are shown in Table 19.

With respect to the N_2/H_2 (1:3) pre-treated material, no distinctive changes are observed in the Fourier Transforms (Figures 70 and 71) between 10 and 60 minutes during NH_3 synthesis. Results from EXAFS refinements, show that during ammonia synthesis at 400°C the Co-Re mixing remains in the sample pre-treated in N_2/H_2 (1:3). After 10 minutes on stream Co-Re distances are found at 2.52 Å on the Co edge and corresponding Re-Co distances are found at 2.54 Å at the Re edge. After 60 minutes, the Co-Re interatomic distances remains at 2.48 Å and a change is observed at the rhenium edge; the coordination number decreased and the interatomic distance remains at 2.48 Å. This may suggest partial nanostructure reorganisation of the material and possible segregation of particles during the ammonia synthesis reaction.

After 60 minutes in N_2/H_2 (1:3) at 400°C at the Co edge; the multiplicity of Co-Re reduces from 5.0 to 2.7 although the bond length elongates to 2.51 Å. Similarly, the Re-Re bond is slightly elongated from 2.66 Å to 2.70 Å, but still has an average coordination between 4 and 5. At the Re edge there is a slight shortening of the Co-Re/Re-Co average bond distance between the 10 and 60 minute periods. During time on stream the Co-Co coordination number reduces.

Considering experimental and refined EXAFS for the Ar/H_2 (1:3) pre-treated material only minor changes are observed in the Co edge, whereas noticeable changes are seen in the local Re environment.

Following pre-treatment in Ar/H_2 (1:3), for the first 10 minutes under ammonia synthesis conditions, when the material is inactive, there is still a lack of Co-Re mixing (Figure 73); Co-Co distances can be fitted at 2.46 Å at the Co K edge. After 60 minutes, the Co-Co coordination slightly reduces to 4.6 and the bond distance remains at 2.45 Å. Adding a second Co-Re contribution at 2.62 Å with average coordination of 2 improves the fit, however the obtained uncertainties and specifically the Debye-Waller factor is questionable suggesting the major contribution is still in fact only Co-Co[80]. At the rhenium edge, the major contribution is the Re-Re interaction with average coordination of 5. However, the bond elongates from 2.68 to 2.73 Å from 10 to 60 minutes on stream. A low coordinated (1.2 and 0.7) Re-Co bond remains at 2.56 - 2.53 Å. Refinements reveal the degree of Co-Re mixing to be irreversible, but as the Re-Co shell is present, some mixing is obtained also after pre-treatment in Ar/H_2 (1:3).

Table 19: EXAFS least squares refinements of $CoRe_4$ after 2 hour pre-treatment at 600°C in either N_2/H_2 or Ar/H_2 and during ammonia synthesis at 400°C for both Co K edge and Re L_3 edge from *in situ* XAS. AFAC transferred from Co-foil = 0.79 and Re-foil= 0.8.

Sample		Shell	N	R/Å	$2\sigma^2$/Å2	E_F/eV	R/%	Δk
N_2/H_2 (1:3) Pre-treated	10 minutes in Reaction Gas at 400°C	Co-Co	5(1)	2.47(1)	0.029(5)	-6.1(8)	29	2-8.5
		Co-Re	2.1(7)	2.52(1)	0.010(7)			
		Re-Co	3(2)	2.54(6)	0.05(2)	-7(2)	45	3.5-9.5
		Re-Re	4(1)	2.66(1)	0.027(7)			
	60 minutes in Reaction Gas at 400°C	Co-Co	2.7(8)	2.509(7)	0.013(7)	-4.0(8)	37	2-8.5
		Co-Re	2.7(7)	2.486(8)	0.005(5)			
		Re-Co	0.9(6)	2.48(1)	0.013(9)	-8(2)	45	3.5-9.5
		Re-Re	5(2)	2.70(1)	0.029(8)			
Ar/H_2 (1:3) Pre-treated	10 minutes in Reaction Gas at 400°C	Co-Co	5.4(9)	2.460(9)	0.026(4)	-1(1)	29	2-8.5
		Re-Co	1.2(5)	2.56(2)	0.013(6)	-9(1)	42	3.5-9.5
		Re-Re	5(2)	2.68(1)	0.030(8)			
	60 minutes in Reaction Gas at 400°C	Co-Co	4.7(8)	2.452(8)	0.024(4)	-1(1)	29	2-8.5
		Co-Re	2(2)	2.62(8)	0.07(5)			
		Re-Co	0.7(3)	2.531(9)	0.002(6)	-11(1)	36	3.5-9.5
		Re-Re	5(2)	2.743(9)	0.026(6)			

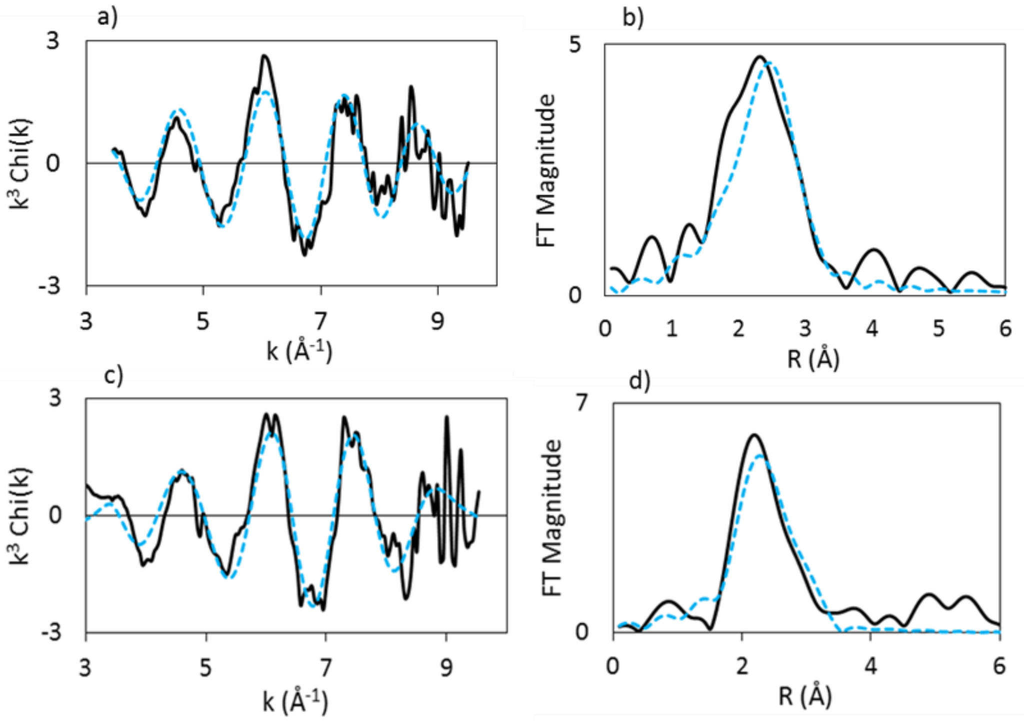

Figure 69: Experimental (-) and calculated (---) k3-weighted EXAFS (left) and its Fourier Transform (right) for $CoRe_4$ after pre-treatment at 600°C in N_2/H_2 (1:3) and after time on stream at 400°C in a - b) N_2/H_2 (1:3) and c - d) Ar/H_2 (1:3) for the Re L_3 edge.

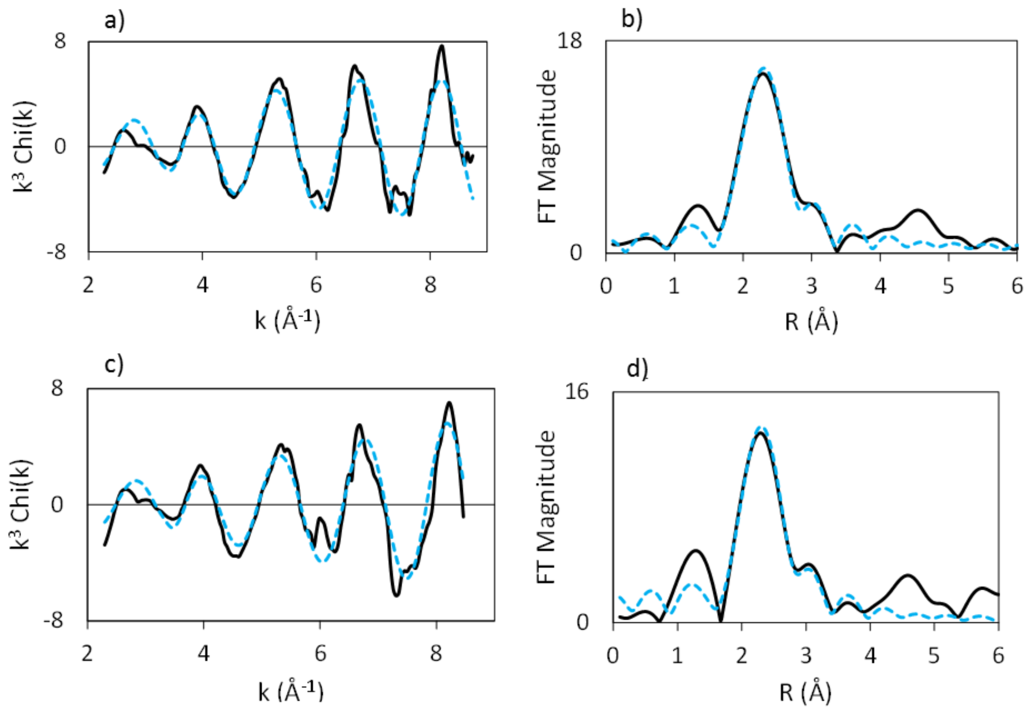

Figure 70: Experimental (-) and calculated (---) k3-weighted (left) and its Fourier Transform (right) for $CoRe_4$ after pre-treatment at 600°C in N_2/H_2 (1:3) and after time on stream at 400°C a - b) N_2/H_2 (1:3) and c - d) Ar/H_2 (1:3) for the Co K edge.

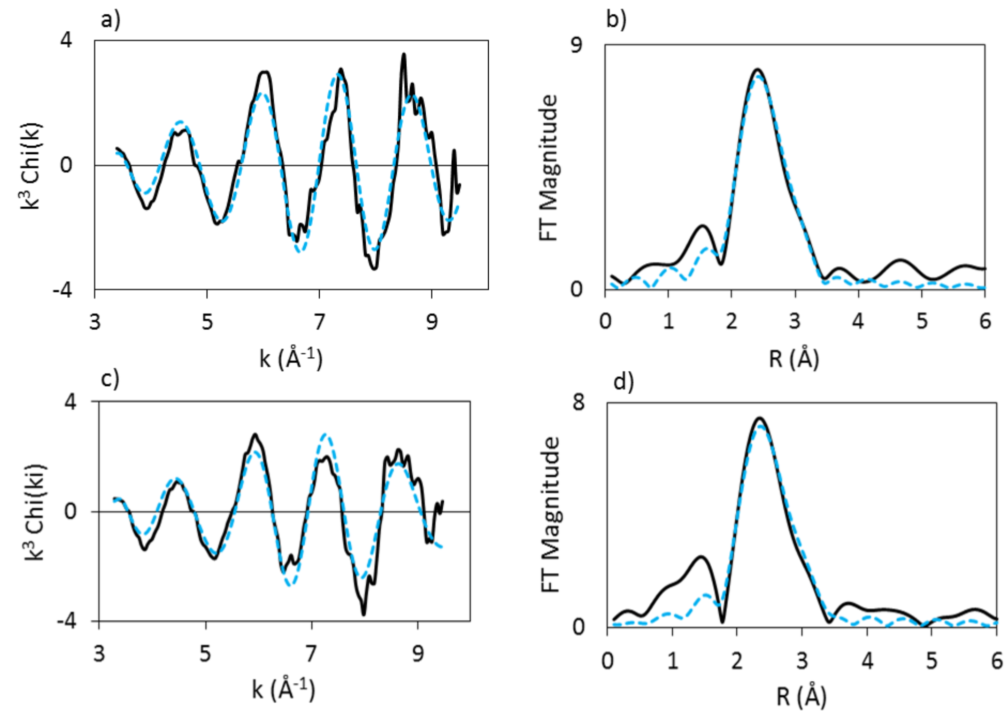

Figure 71: Experimental (-) and calculated (---) k3-weighted EXAFS (left) and its Fourier Transform (right) for $CoRe_4$ after pre-treatment at 600°C in Ar/H_2 (1:3) and after time on stream at 400°C in a - b) N_2/H_2 (1:3) and c - d) Ar/H_2 (1:3) for the Re L_3 edge.

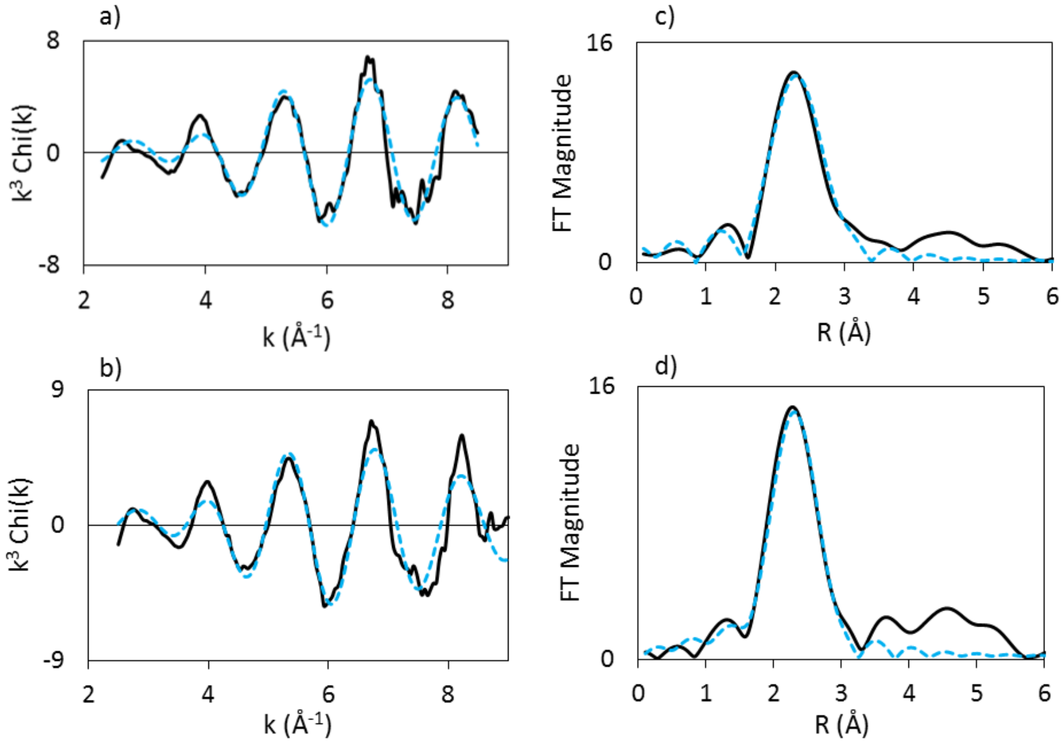

Figure 72: Experimental (-) and calculated (---) k3-weighted EXAFS (left) and its Fourier Transform (right) for $CoRe_4$ after pre-treatment at 600°C in Ar/H_2 (1:3) and after time on stream at 400°C in a - b) N_2/H_2 (1:3) and c - d) Ar/H_2 (1:3) for the Co K edge.

Figure 73 gives the average multiplicities from both the Co K and Re L_3 edges for $CoRe_4$ pre-treated with H_2/N_2 (1:3) and H_2/Ar (1:3). However, a major difference occurs for the bimetallic Co-Re interaction during the first 10 minutes in H_2/N_2 (1:3) after the H_2/Ar (1:3) pre-treatment; at the Co K edge it is not possible to fit this bimetallic shell. Although, the Co-Re shell can be fitted at the Re L_3 edge at the equivalent point it has a lower multiplicity compared to the N_2/H_2 (1:3) pre-treated material.

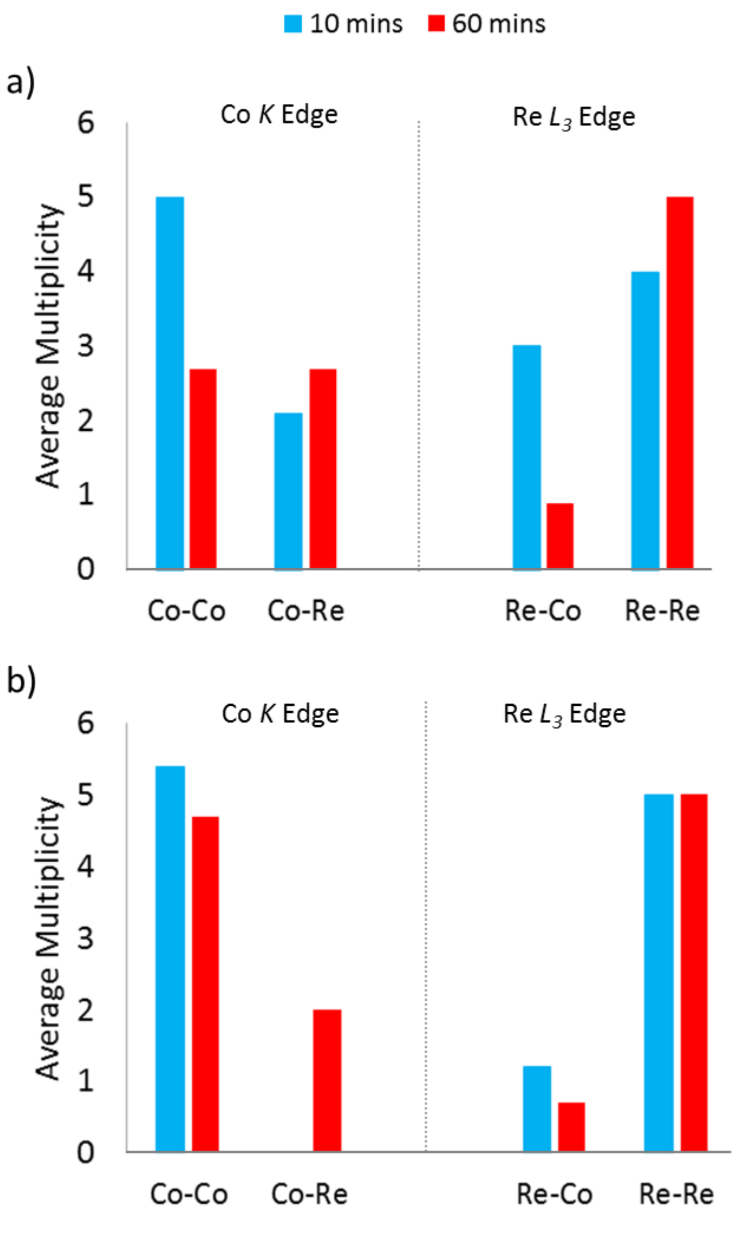

Figure 73: Average coordination numbers from EXAFS analysis for CoRe4 during ammonia synthesis after pre-treatment at 600°C in (a) N_2/H_2 (1:3) and (b) Ar/H_2 (1:3) for the Co K edge and Re L_3 edge.

In conclusion, the initial XAS results for the stoichiometric gas mixtures reveal during ammonia synthesis the active catalyst contains Re-Re, Co-Co and Re-Co interatomic distances. The variety of different bonds demonstrates the complexity of the active system. It can be postulated the presence of bimetallic Re-Co bonds suggest the active catalyst has some alloy-like character. Also, the inclusion of monometallic Re and Co shows there are pure metallic phases present. The confirmation of bimetallic rhenium cobalt interactions may account for the shift in Re reflections observed in the *ex situ* XRD patterns presented in Figure 51. The R factors are fairly large. This is due to high noise in the data at larger K (A^{-1}) values and increasing noise at high temperatures.

After the 600°C pre-treatment in N_2/H_2 (1:3) the major contributions are bimetallic and monometallic Re-Re with a smaller Co-Co contribution. In comparison, following the Ar/H_2 (1:3) pre-treatment the major contribution is monometallic Co and Re and bimetallic Co-Re species are present but in lower quantities. The lack of a second metal-metal absorption shell in the analysis of both Co K edge and Re L_3 edge EXAFS suggests a high degree of disorder in the major phase.

Pre-treatment in Ar/H_2 (1:3) gives a higher refined sum of first shell coordination numbers for $CoRe_4$ which may indicate a larger unit. This is in agreement with previous findings on supported Co/Re systems where the role of rhenium is to prevent cobalt agglomeration and promoting reduction at lower temperatures[146]. The second point is clearly true for this $CoRe_4$ system, as the Co undergoes complete reduction starting as low as 250°C. The pre-treatment atmosphere clearly affects the Co-Re alloying process and is significantly inhibited in Ar/H_2 (1:3). The higher degree of bimetallic mixing for $CoRe_4$ pre-treated in N_2/H_2 (1:3) may account for the higher ammonia activity of this sample. Also, it could be assumed the activity is governed by activation of N_2 by the active phase. From the *in situ* EXAFS analysis it is clear that the sample pre-treated in H_2/N_2 (1:3) has better mixture of the Co-Re pair, or consists of more of the bimetallic phase[80]. The degree mixing remains fairly constant during ammonia synthesis conditions in reaction gas at 400°C for both pre-treatments.

Kojima and Aika[43, 48] suggest the high activity of their Co-Re_4 catalyst is due to a rhenium nitride phase, however that material synthesis involves an ammonolysis stage (as discussed in Section 3.2.2). For the $CoRe_4$ catalyst used in this study, significant bulk nitride formation in N_2/H_2 (1:3) pre-treatment gas mixtures can be excluded, as it was not possible to fit a Re-N shell at any stage during EXAFS refinements. This is further confirmed by

XANES and E_0, which confirms both Re and Co are in the zero oxidation state throughout the ammonia synthesis reaction. It is possible to fit a Re-N pair in 2% H_2/N_2 gas mixtures however these conditions are not comparable to activity measurements due to the difference in gas mixture composition.

3.3.9 Conclusions: Ammonia Synthesis

In this chapter the characteristics and behaviour of cobalt rhenium catalysts were investigated. This work has shown ammonolysis is not required to produce highly active ammonia synthesis catalysts and by bypassing this procedure a more active material is achieved (655 ± 129 μmol g^{-1} h^{-1} versus 943 ± 44 μmol g^{-1} h^{-1}) with a simplified synthesis route.

Both Co and Re components are required for enhanced ammonia synthesis activity as reaction with the individual precursors alone does not give an active steady state material. Also, attempts to replace Re with Ni or Fe while maintaining high activity were unsuccessful. Therefore, it is believed a synergistic effect between Re and Co is required for high activity, which is reflected in the presence of bimetallic Co-Re particles in the active material.

It was previously discussed by Kojima and Aika, Co-Re_4 was the optimum composition for ammonia synthesis[43, 48]. However, in this work activity testing results indicate over a series of synthesis ratios (Co_2Re, CoRe, $CoRe_2$, $CoRe_4$, and $CoRe_8$) within error the activity can be considered the same. This is a promising result as rhenium is expensive and reducing the Re content while maintain high activity is highly desirable. The ammonia synthesis activity decreases at the high Co or high Re containing materials (Co_8Re, Co_4Re and $CoRe_{16}$). For $CoRe_{16}$ this is possibly due to there not being enough Co to stabilise the Re causing volatilization of Re *in situ*. Regarding Co_8Re and Co_4Re, it is postulated the low rhenium content reduced the ammonia synthesis activity. The pre-reaction ICP-MS analysis reveals the combination of both Re and Co only accounts for approximately 40 - 60 % of the composition and the remaining percentage can be attributed to oxygen. This is reinforced by XAS analysis of the starting $CoRe_4$ material, where Re-O and Co-O shells can be fitted to the pre-reaction material, which suggests the pre-reaction material is a mixture of Co oxides and Re oxides. The main focus of this work has been on the material with the synthesis ratio $CoRe_4$ however the actual composition of the active catalyst was revealed to be $CoRe_{1.6}$. The oxidation state of Re in the starting material is +7 and a mixture of +2/+3 for Co.

In all cases of cobalt rhenium catalysts which have high activity (for example: $CoRe_4$ prepared from NH4ReO$_4$ or Re_2O_7 and N_2/H_2 (1:3) or Ar/H_2 (1:3) pre-treated), the post-reaction XRD patterns reveal there is a shift of Re reflections to a slightly higher 2θ angle. It is postulated this is due to bimetallic mixing within the material and this bimetallic interaction is confirmed *via* XAS analysis. The high activity of the $CoRe_4$ catalyst can be obtained *via* a NH_4ReO_4 and Re_2O_7 precursor, but not with $KReO_4$ or $ReCl_5$; this could be due to unfavourable electronic effects of Cl^- and K^+. Also the post-reaction XRD patterns for these low activity materials match the reference pattern for metallic rhenium and show no evidence of bimetallic mixing, which could also contribute to the low activity.

Pre-treatments *via* Ar/H_2, N_2 and Ar result in a 20 minute lag period before the materials become active for ammonia synthesis, whereas, pre-treatment with N_2/H_2 gives an instantly active material. After the initial lag periods all materials exhibit steady state behaviour. $CoRe_4$ and CoRe were tested over a 48 hour period and showed no sign of deactivation. Pre-treatment in Ar results in Re growths on the surface of the material as revealed by SEM analysis. The differences between the N_2/H_2 and Ar/H_2 pre-treatments are reflected in the temperature programmed homomolecular N_2 isotopic exchange studies, where pre-treatment in N_2/H_2 resulted in a material with the ability for N_2 exchange activity following desorption of hydrogen and the Ar/H_2 pre-treatment results in a material inactive for exchange. This lag is also indicated by a feature in the heat flow profiles after 20 minutes under reaction conditions.

During the initial ramping from room temperature to 600°C analysis of the Re XANES reveals a synergistic effect and comparable reduction profiles for both pre-treatment gas mixtures, with Co initiating reduction and Re being completely reduced between 300-375°C. The reducibility of both Co and Re was studied *via* XANES. It was found the Co reduces at a slightly lower temperature in Ar/H_2.

Pre-treatment in N_2/H_2 and Ar/H_2 results in a material with high ammonia synthesis activity. From XAS analysis it was revealed pre-treatment in both N_2/H_2 and Ar/H_2 results in the formation of the following species: Co-Re bimetallic alloys and pure Co and Re monometallic phases. Also, a larger degree of bimetallic mixing is present in the N_2/H pre-treated sample. This higher degree of mixing may be attributed to the higher activity of the N_2/H_2 treated material. Therefore, it is postulated the active material has a combination of:

Re-Re, Co-Co and Re-Co bonds, which suggests the material, has bimetallic and metallic interactions and both Re and Co are in the 0 oxidation state during the ammonia synthesis reaction. The N_2/H_2 (1:3) pre-treatment results in a material where the bimetallic Co-Re phase is the major component, whereas, pre-treatment in Ar/H_2 favours the monometallic Co and Re.

The presence of nitrogen during pre-treatment promotes a high degree of bimetallic Co-Re mixing confirmed by Co-Re/Re-Co absorption shells at both edges. Following pre-treatment in Ar/H_2 (1:3) after 60 minutes in reaction gas restructuring of Re and Co phases is observed and formation of a bimetallic Co-Re phase coincides with the observed lag-time both during catalytic experiments and *in situ* conditions.

In conclusion, a cobalt rhenium catalyst with high ammonia synthesis activity has been prepared despite possessing a very low surface area (< 0.2 m^2g). It is suggested by XAS the active material has both metallic and bimetallic character suggesting the material is closer to an alloy than a nitride as first thought.

3.3.10 **Outlook: Ammonia Synthesis**

In this work experiments were conducted at ambient pressure therefore, reaction testing at elevated pressure would be advised to determine whether the consequentially high efficacy is maintained closer to more realistic process conditions.

Initial results suggest that supporting $CoRe_4$ is possible while maintaining good activity. This should be developed further; investigating different supports and lowering the Re content. Correspondingly, investigation of different Re and Co precursors would be advised to assess if enhanced activity can be achieved.

It would be beneficial to perform depth profiling XPS on the bulk cobalt rhenium system to assess whether surface nitrides are formed or whether surface segregation occurs. This function of pre-treatment as this is not possible by XAS as it is bulk averaging.

The Haber-Bosch iron catalyst is extremely susceptible to poisoning. It is claimed in the literature in general that Re catalysts show a greater resistance to poisons such as S, N and P[88]. A more poison resistant catalyst would be beneficial as this would allow the use of less pure feedstreams. Therefore, experiments involving adding a poison in the reaction gas feed would allow determination of the poison tolerance of the cobalt rhenium system. It is suggested H_2S/Ar, O_2 or steam could be added to the reaction gas feed and activity measurements conducted. It would be advantageous to perform high pressure measurements on the cobalt rhenium catalysts along with benchmarking against current industrial catalysts. Also, it would be beneficial to preform aging cycles to assess the longevity of the material. To gain a clearer idea of how the cobalt rhenium catalysts would operate under industrial conditions it would be of interest to use a recycled gas feed to mimic industrial conditions.

Chapter 4

Ruthenium Based Ammonia Synthesis Catalysts

4.1 Introduction to Ruthenium

Within the periodic table ruthenium and iron are in the same group. Ruthenium has an atomic number of 44 and a relative atomic weight of 101.07 amu. The electronic configurations of iron and ruthenium are [Ar] $3d^6 4s^2$ and [Kr] $4d^7 5s^1$ respectively. It has been established that, ruthenium based catalysts are viable alternatives for next generation ammonia synthesis catalysts because they have high performance under milder conditions than the Haber-Bosch Process[19, 147].

In the 1970's BP started developing a new catalyst for ammonia synthesis, in its ultimate form it comprises of ruthenium, a graphitised carbon support and two promoters[1]. This was the first completely new commercial ammonia synthesis catalyst since the original Haber-Bosch promoted iron catalyst. The Kellogg Advanced Ammonia Process (KAAP) uses this promoted ruthenium/graphite supported material which is reported to be 20 times more active than the traditional promoted iron system. Also, KAAP is operates at lower temperatures and pressures than the Haber-Bosch counterpart[1].

With regard to ruthenium it is believed N_2 dissociation is rate limiting[149]. It is well documented the ammonia synthesis activity of Ru based catalysts are surface sensitive[131]. Dahl *et al*[150] investigated the influence of ruthenium particle size on ammonia synthesis activity using theoretical calculations and experimental. They proposed the dissociation of nitrogen takes place exclusively on the Ru (0001) surface. Further micro-kinetic work by Dahl and co-workers confirm only specific parts of the surface were active[150].

The high activity of Ru catalysts is attributed to the presence of B_5 surface sites, these are step sites which have higher activity than the terrace sites[150, 151]. B_5 sites are an arrangement of three Ru atoms in one layer and two more Ru in the layer directly above this at a monoatomic step on an Ru(0001) terrace[152]. The optimum Ru particle size for a high density of B_5 sites was found to be 1.8 – 3.5 nm[131, 130]. At elevated H_2 partial pressures these highly active B_5 sites and the remaining Ru surface is highly susceptible to hydrogen poisoning. The step size is inversely proportional to the Ru particle size i.e with increasing Ru particle size the step size decreases[131,153,154].

Both Fe and Ru are well known ammonia synthesis catalysts and it is well documented that their activity is drastically enhanced by the addition of alkali and alkaline earth metal promoters (K_2O, BaO, Cs_2O etc)[155,156]. Unpromoted Ru materials have been shown to have limited activity towards ammonia synthesis[147,157,158]. However, their activity drastically increases with the introduction of promoters[141]. Caesium, potassium and barium have been shown to be particularly efficient promoters for ruthenium catalysts[155]. The enhanced activity is explained by the electronic promoting effect where electron transfer from the promoter to the antibonding π-orbitals of N_2 through the metal catalyst occurs. One of the major drawbacks of alkali and alkaline earth metal promoters is they are unstable under ammonia synthesis conditions.

Muhler *et al*[156] tested supported Ru catalysts and characterised them with N_2 physisorption, H_2 chemisorption and XPS. Their activity was found to be: Cs-Ru/MgO > Ru/MgO > Cs-Ru/Al_2O_3 > Ru/Al_2O_3. The activity of Cs-Ru/MgO exceeds that of the multiple promoted Haber-Bosch Fe catalyst. In all cases a negative order in H_2 was obtained and the authors suggest for industrial ammonia production a synthesis gas feed containing a higher ratio of 1:3 N_2/H_2 would be desirable. Addition of Cs^+ was found to decrease the surface areas of all materials.

Larichev and co-workers[159] used $Ru(OH)Cl_3$ to synthesise Ru/MgO and Ru-Cs^+/MgO catalysts. A significant difference in Ru particle size was observed between characterisation techniques. The authors found TEM and XRD data was in agreement whereas the CO chemisorption data was 2-3 times higher. An explanation is presented based on XPS data which suggests the Ru/MgO material comprises of Ru metal and clusters of RuO_2. Due to a strong RuO_2-MgO interaction, RuO_2 clusters are stable and are not detected *via* CO chemisorption. It was reported caesium ruthenates do not form on addition of a Cs^+ promoter to the partially oxidised Ru and instead the promoter causes reduction of the RuO_2 clusters giving ruthenium metal. Larichev[160] analysed Ru/MgO catalysts *via* X-ray photoelectron spectroscopy (XPS), X-ray diffraction (XRD) and transmission electron microscopy (TEM). A significant portion of the supported Ru was reported to have a particle size of <3 nm and exist in an amorphous state. This amorphous ruthenium section exists in different forms depending on the Ru precursor used. These forms consist of; metal, nanoparticles and oxide clusters. In another study by Rosowski *et al*[161] it is suggested the MgO support acts as both a support and an alkaline promoter where promoted sites near the interface are created enhancing activity.

Aika and co-workers[147] found the ammonia synthesis rate over ruthenium supported on active carbon when promoted with Cs^+ gives activity of greater than 10 times the rate of the traditional Haber-Bosch iron catalyst at 250°C and ambient pressure[147]. It was concluded the promoter enables a charge transfer from the alkali metal promoter to the ruthenium; increasing the electron density in the transition metal, which is the favoured state for activation nitrogen. It was also noted the specific rates were higher when active carbon or alumina support was used and it was suggested the support acts as a medium for electron transfer. Rao *et al*[162] note the incorporation of a barium promoter into a caesium promoted Ru/C covered alumina enhances the ammonia synthesis rate and lower the temperature where maximum activity is obtained.

Aika *et al*[163, 164, 165, 166] investigated the effect on Ru precursor on the overall ammonia synthesis activity . In the case of Ru supported on activated carbon, Al_2O_3 and MgO the activity decreased when a $RuCl_3$ precursor was used compared to materials synthesised from Cl-free Ru precursors (for example, $Ru(acac)_3$ $Ru(NO)(NO_3)_3$ and $Ru(CO)_{12}$). The authors suggest Cl^- induces electron withdrawal from the Ru and this is attributed to the lower observed activities. Also, it is suggested the dispersion is increased without the presence of Cl^-[163]. Further work by Aika and Murata[167] compared the efficiency of lanthanide promoters. In comparison to promotion with $CsNO_3$, $Ce(NO_3)_3$, $La(NO_3)_3$, and $Sm(NO_3)_3$ were found to give enhanced activity with regard to Cl^- free Ru/Al_2O_3 catalysts and an 11 – 15 kcal mol^{-1} reduction in the activation energy. It is postulated the lanthanide oxides have a stronger interaction with the Ru than Cs^+ and a lower amount of precursor can be used.

Kitano and co-workers[8,168] synthesised a room temperature stable electride: $12CaO.7Al_2O_3$ ($C12A7:e^-$), which functions as an good electronic promoter for Ru ammonia synthesis catalysts[8]. The crystal structure of $C12A7:e^-$ contains a positively charged framework $[Ca_{24}Al_{28}O_{64}]^{4+}$ and four extra-framework electrons situated in cages as counter ions. A Ru supported on $[Ca_{24}Al_{28}O_{64}]^{4+}(e^-)_4$ catalyst has been developed with reported rates as high as 3550 µmol h^{-1} g^{-1} at 340°C and 0.1 MPa pressure[135].

In order to investigate the relationship between the catalytic ability and electronic properties of Ru supported on $[Ca_{24}Al_{28}O_{64}]^{4+}(O^{2-})_{2-x}(e^-)_{2x}$ (where $0 \leq x \leq 2$), Kanbara and co workers[169] investigated the crystallographic cages of $[Ca_{24}Al_{28}O_{64}]^{4+}$ by substituting electrons for O^{2-} ions. The electron concentration (N_e) was found to play an important role in enhancing the catalytic activity. If N_e was below 1.0×10^{21} cm^3 this led to a material with good performance; where the electrons are localized deep within the material in F^+-

like centres. The rate limiting step for these materials is N_2 dissociation and if N_e is $\geq 1.0 \times 10^{21}$ cm^3 the activity drastically increases and with reduced E_a. The rate limiting step changes to the formation of the N-H bond. The electrons from a more shallow electronic level and are delocalized over C12A7:e^- cages. Moreover, the authors also claim hydrogen poisoning is reduced due to the high density of electrons.

Further work by Kitano *et al*[170] presents the potential of using metal hydrides as efficient promoters for ammonia synthesis. They report ruthenium nanoparticles (Ru/$Ca_2N:e^-$) when combined with a two-dimensional electride ($Ca_2N:e^-$) produces a material with stable catalytic ability as low as approximately 200°C. The authors stated the Ru/$Ca_2N:e^-$ exhibited the highest catalytic activity for low temperature ammonia synthesis presented in the literature. The enhanced activity attributed to a hydrogen deficient Ca_2NH hydride ($[Ca_2N]^+.e_{1-x}{}^-H_x^-$) which is formed during the ammonia synthesis reaction opposed to the $Ca_2N:e^-$ electride. The enhanced activity is due to the ability of the anionic electrons and H^- ions to reversibly exchange (Equation 9). It is also suggested this suppresses hydrogen poisoning of the Ru. The cleavage of the nitrogen triple bond is facilitated by the resultant electrons in the hydride which have a low work function of 2.3 eV.

Equation 9: Proposed Exchange Between Anionic Electrons and H^- ions[170].

$$Ca_2N: e^- + xH \leftrightarrow [Ca_2N]^+.e_{1-x}{}^-H_x^-$$

Recently, Inoue *et al*[171] synthesised a material consisting of Ru nanoparticles supported on $Ca(NH_2)_2$. This material was found to have high activity at ambient pressure and 200°C. During ammonia synthesis Ru is grown across the $Ca(NH_2)_2$ surface and the Ru atoms were found to have a diameter of approximately 2.1 nm. The author attributes this grown to the strong interaction between Ru and N and the epitaxial growth of Ru over $Ca(NH_2)_2$.

As discussed, within the literature Ru based materials are widely accepted as the most active ammonia synthesis catalysts. Therefore, for this work it was imperative to perform a study under the exact same conditions to compare activity and behaviour of both Re and Ru based catalysts. The aim of this section is to provide a preliminary study into Ru/Al_2O_3 materials to allow benchmarking for the cobalt rhenium materials presented in the previous chapter.

4.2 Results and Discussion: 5% Ru/Al_2O_3 Materials

4.2.1 Ammonia Synthesis Activity of 5% Ru/Al_2O_3 Materials

In order to benchmark the ammonia synthesis activity of the cobalt rhenium catalysts, 5% Ru/Al_2O_3 doped with various amounts of $CsNO_3$ were tested for ammonia synthesis activity. The materials were pre-treated with N_2/H_2 (1:3) at 600°C for 2 hours before reaction at 400°C under N_2/H_2 (1:3). The mass normalised steady state ammonia synthesis rates are displayed in Figure 74 and Table 20. The rates are mass normalised to the total mass of catalyst in the reactor (0.3 g).

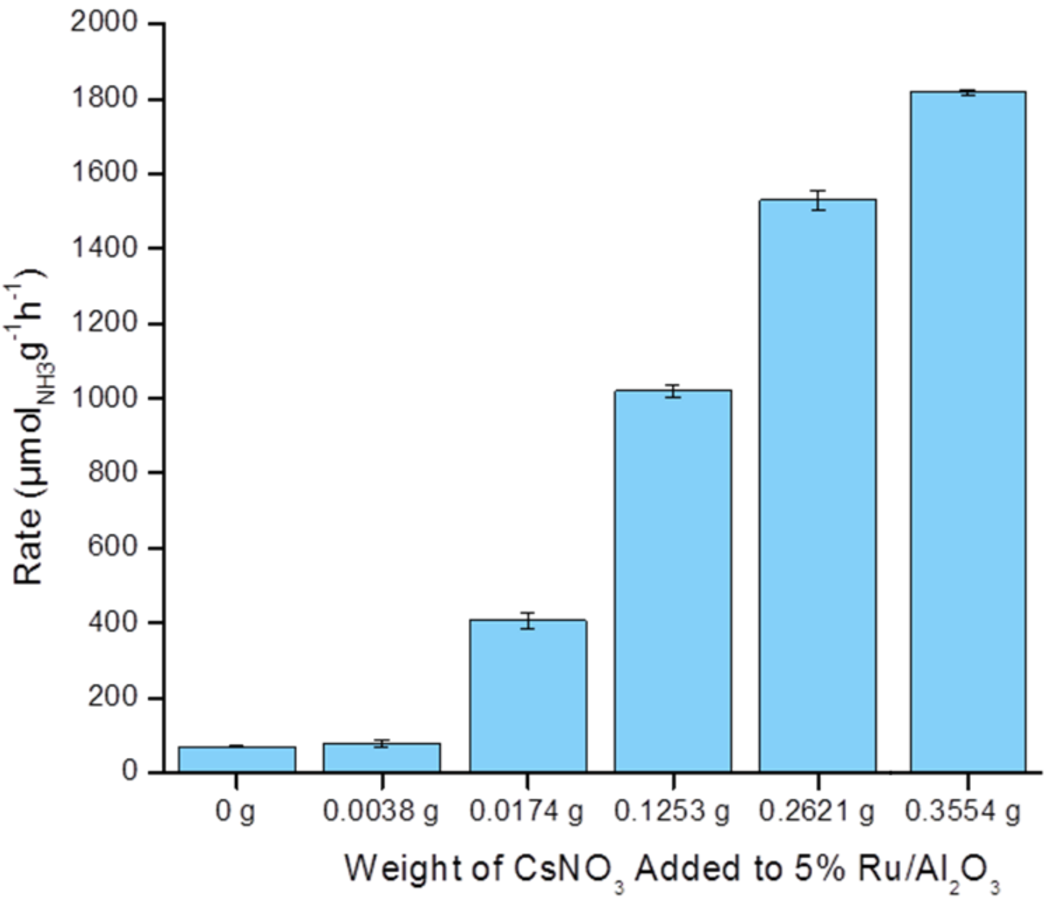

Figure 74: Steady State Ammonia Synthesis Rates of 0.3 g of 5% Ru/Al_2O_3 doped with various amounts of $CsNO_3$, pre-treated for 2 hours at 600°C (1:3) then reacted at 400°C with N_2/H_2 (1:3) at ambient pressure.

The highest activity (1818 ± 6 µmol g^{-1} h^{-1}) was observed for Ru/Al_2O_3 doped with 0.3528g $CsNO_3$. To test for potential deactivation on stream this material was tested for over 40 hours and the conductivity profile is presented in Figure 75.

Table 20: Steady State Ammonia Synthesis Rates of 5% Ru/Al_2O_3 doped with various amounts of $CsNO_3$, pre-treated for 2 hours at 600°C (1:3) then reacted at 400°C with N_2/H_2 (1:3) at ambient pressure.

Mass of $CsNO_3$ Added (g)	Ammonia Synthesis Rate (µmol g^{-1} h^{-1})
0	71 ± 3
0.0038	77 ± 9
0.0174	408 ± 22
0.1253	1020 ± 16
0.2621	1530 ± 25
0.3528	1818 ± 6

From Figure 75 a continuous linear decrease in over time is observed, which relates to steady state behaviour during the entire testing period. Also, this specific reaction results in an ammonia synthesis rate of 1821 µmol g^{-1} h^{-1} which is in accordance with the rates with error bars reported in Table 20.

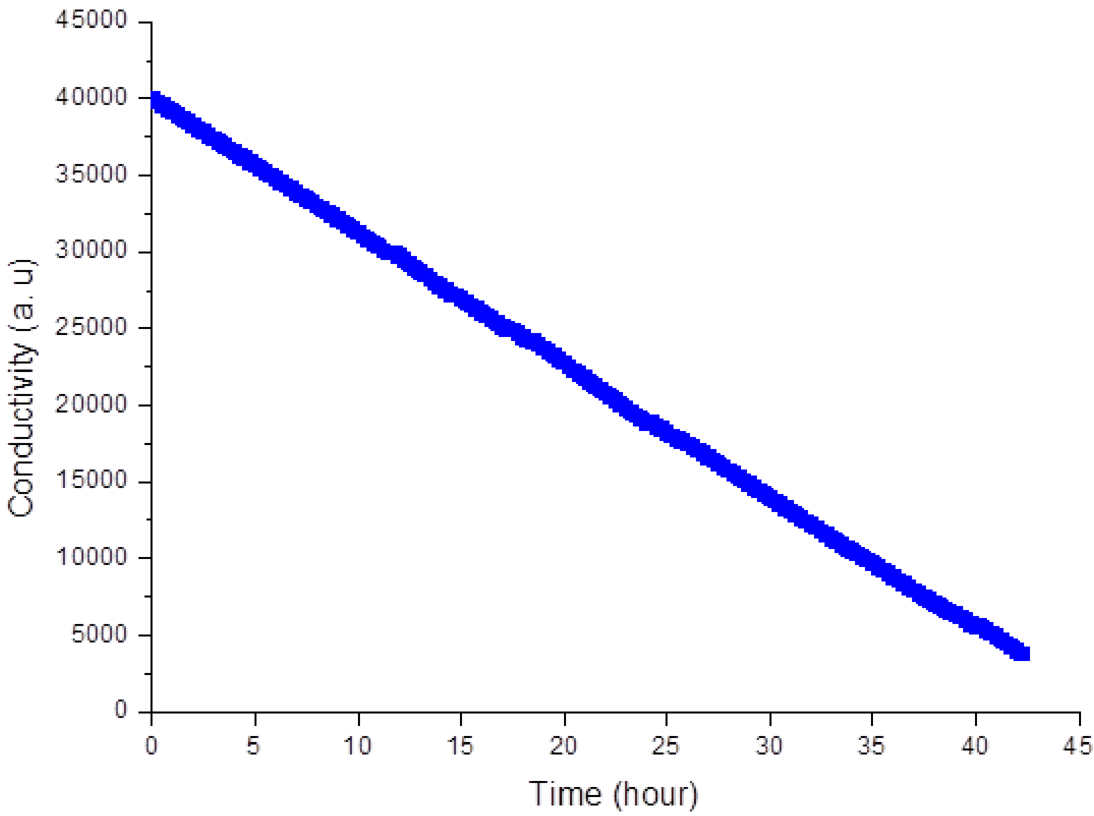

Figure 75: Extended reaction conductivity profile for 5 wt% Ru/Al_2O_3 doped with 0.3528 g $CsNO_3$. Pre-treated for 2 hours with N_2/H_2 (1:3) then reacted at 400°C with N_2/H_2 (1:3) at ambient pressure.

4.2.2 Ammonia Synthesis Activity of Cs^+ Doped $CoRe_4$

From Section 4.2.1 it can be seen, addition of Cs^+ to 5% Ru/Al_2O_3 materials results in an increase in the ammonia synthesis activity. To investigate if this enhanced activity can be achieved *via* Cs^+ promotion for the $CoRe_4$ material discussed in the previous section, Cs^+ was introduced to $CoRe_4$ *via* two methods (outlined in Section 2.1.7): during the original synthesis of $CoRe_4$ and after synthesis/calcination. The results are presented in Table 21.

Table 21: Ammonia Synthesis Rates for Cs^+ Doped $CoRe_4$

Material	Ammonia Synthesis Rates (μmol g^{-1} h^{-1})
5% Ru/Al_2O_3 + 0.3528 g $CsNO_3$	1818 ± 6
$CoRe_4$	943 ± 44
Cs^+ Doped $CoRe_4$ (initial synthesis)	150 ± 6
Cs^+ Doped $CoRe_4$ (after calcination)	388 ± 18

It can be seen from Table 21 regardless of the addition method of Cs^+ to $CoRe_4$, the ammonia synthesis activity actually decreases. A greater decrease in activity is observed when the Cs^+ promoter is introduced during the initial synthesis stage. This decrease in activity is in contrast to the behaviour of Ru/Al_2O_3 based materials which exhibit an increase in activity with the addition of Cs^+.

It was concluded addition of Cs^+ to $CoRe_4$ does not enhance the rate and actually has an adverse effect on the ammonia synthesis activity of the material.

4.2.3 Re-usability Tests of 5% Ru/Al_2O_3 Materials

Preliminary experiments were performed to test the re-usability of the doped Ru catalysts. Similarly to the method employed for $CoRe_4$ (Section 3.2.5) the same 0.3 g sample of Ru material was reacted twice. After the initial reaction the sample was removed (in the quartz reactor tube) from the reactor and stored in air. A 600°C N_2/H_2 (1:3) pre-treatment was only performed on the initial run and the second reaction involved ramping to 400°C at 10°C min^{-1} under N_2/H_2 (1:3) and reaction at 400°C. To gain a clearer picture of the behaviour of the Ru materials both a highly active and lower activity material was tested; 5

wt% Ru/Al_2O_3 doped with 0.1253 g $CsNO_3$ and 5 wt% Ru/Al_2O_3 doped with 0.0174 g. The steady state ammonia synthesis rates of each reaction are displayed in Figure 76.

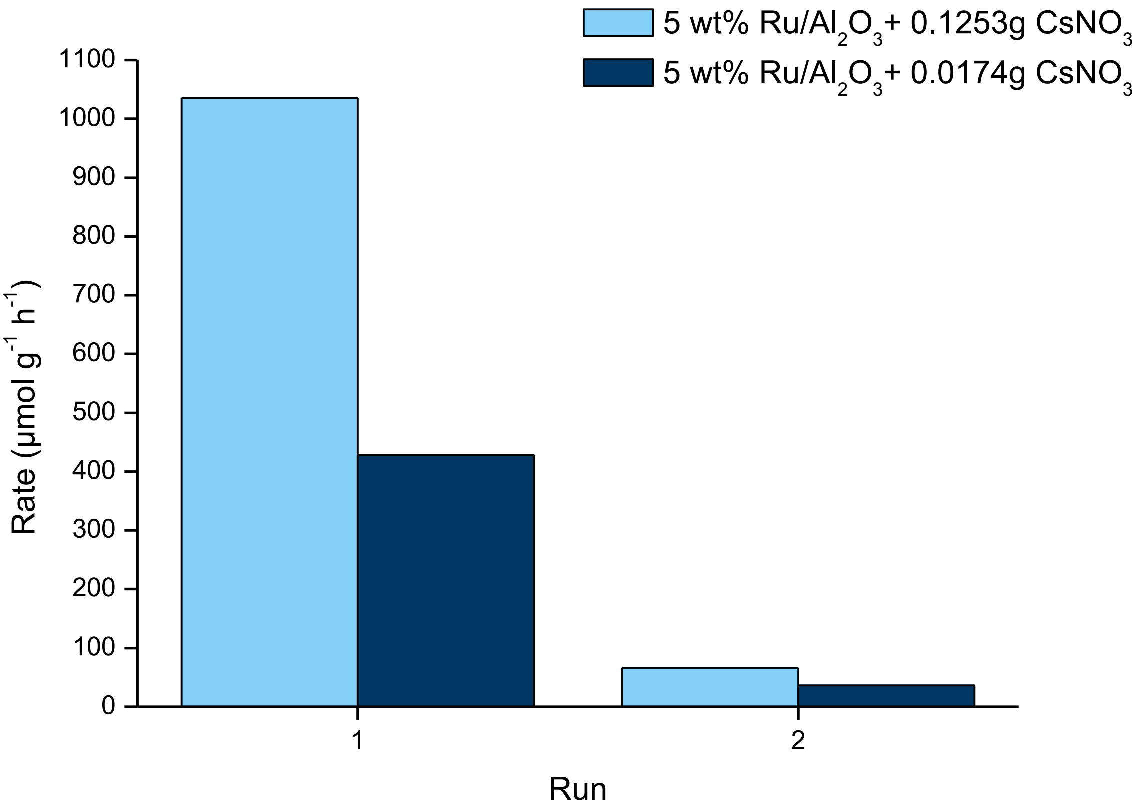

Figure 76: Repeat Reactions on the same Doped Ru/Al_2O_3 Samples.

With regard to the 5 wt% Ru/Al_2O_3 doped with 0.1253 g $CsNO_3$ it can be seen on the initial run the material has high catalytic ability of 1035 μmol g^{-1} h^{-1}, however on the repeat reaction the activity drops to 66 μmol g^{-1} h^{-1}. The same trend is observed for 5 wt% Ru/Al_2O_3 doped with 0.0174 g $CsNO_3$. This material has initial lower steady state activity of 428 μmol g^{-1} h^{-1} but also deactivates on the repeat run to 36 μmol g^{-1} h^{-1}. A major deactivation is found for the repeat run of the each sample and the original sample activity does not seem to affect the extent of deactivation. This could be due to the loss of the Cs^+ promoter in the sample after the initial run. This deactivation is in contrast to the behaviour of $CoRe_4$ which, as discussed in Section 3.2.5, has the ability to maintain high activity over multiple reaction runs.

With consideration of the extended reaction run of 5 wt% Ru/Al_2O_3 doped with 0.3528 g $CsNO_3$ (Figure 75) although the doping level is different, this proves that within the reactor high activity is maintained for over 40 hours. This suggests the deactivation is caused by exposure to air after the initial reaction and does not occur *in situ*.

4.2.4 *Ex Situ* X-ray Diffraction of 5% Ru/Al_2O_3 Based Materials

To further investigate the difference between pre- and post-reaction Ru/Al_2O_3 materials *ex situ* XRD was performed and the results are presented in Figures 78 and 79.

The XRD pattern for un-doped 5 wt% Ru/Al_2O_3 is shown in Figure 77. It can be seen there is a high amorphous background which makes the determination of features difficult and this must be taken into account when assigning $CsNO_3$ reflections to the doped samples. The $CsNO_3$ reflections are not prominent in the lower Cs^+ doped samples (< 0.1253g).

Comparing the pre- and post-reaction materials it can be seen in all cases the $CsNO_3$ reflections are not apparent in the post-reaction materials. This is consistent with the lack of activity achieved on the repeat runs of the 0.1253 g and 0.0174 g doped Ru/Al_2O_3.

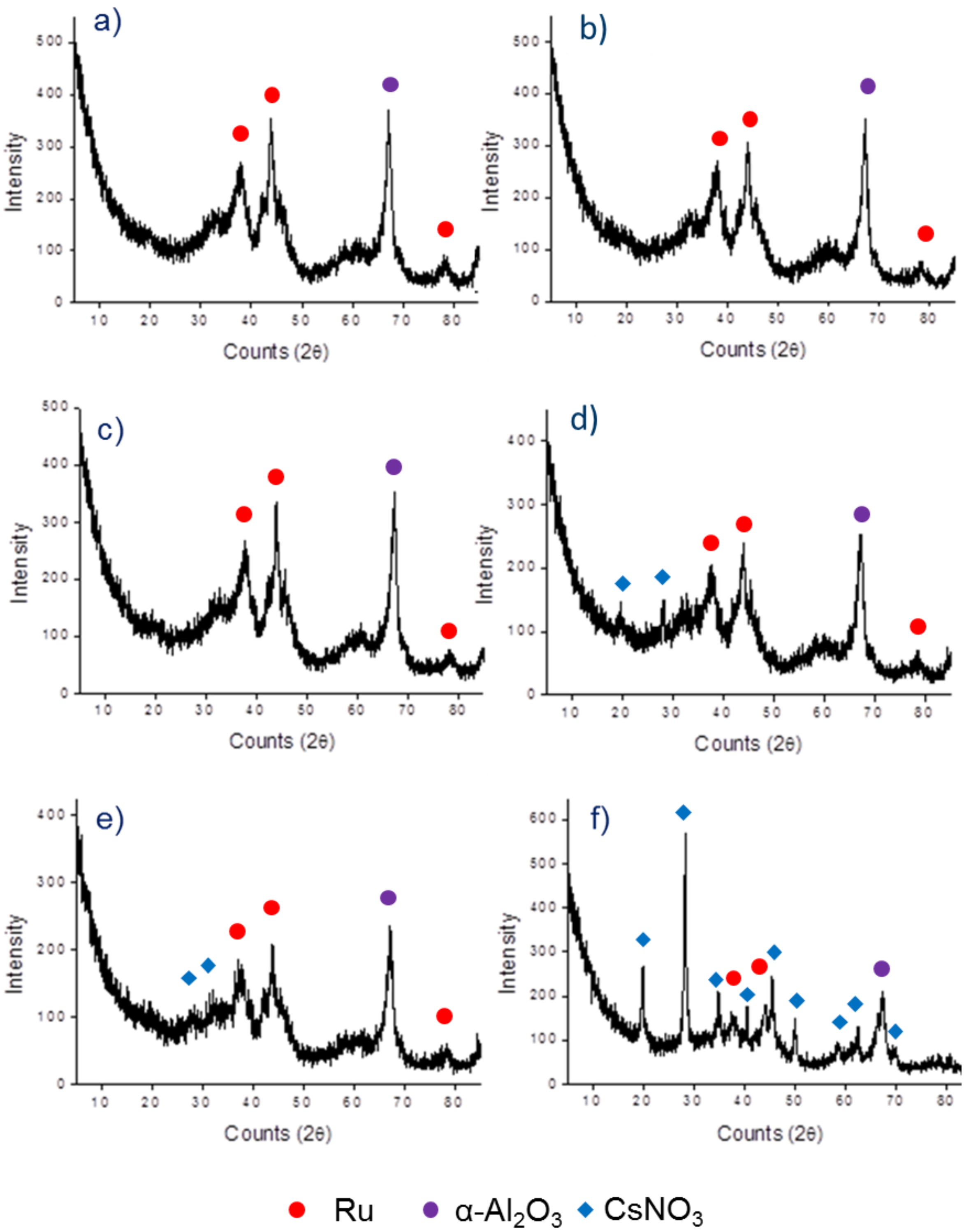

Figure 77: XRD Pre Reaction Patterns for 5 wt% Ru/Al_2O_3 doped with $CsNO_3$, pre-treated for 2 hours with N_2/H_2 (1:3) then reacted at 400°C with N_2/H_2 (1:3) at ambient pressure a) 0 g, b) 0.0038 g, c) 0.0174 g, d) 0.1253 g, e) 0.2621 g, f) 0.3528 g. Reference PDFs Ru 01-0714656, α-Al_2O_3 00-001-1296 and $CsNO_3$ 00-001-0779.

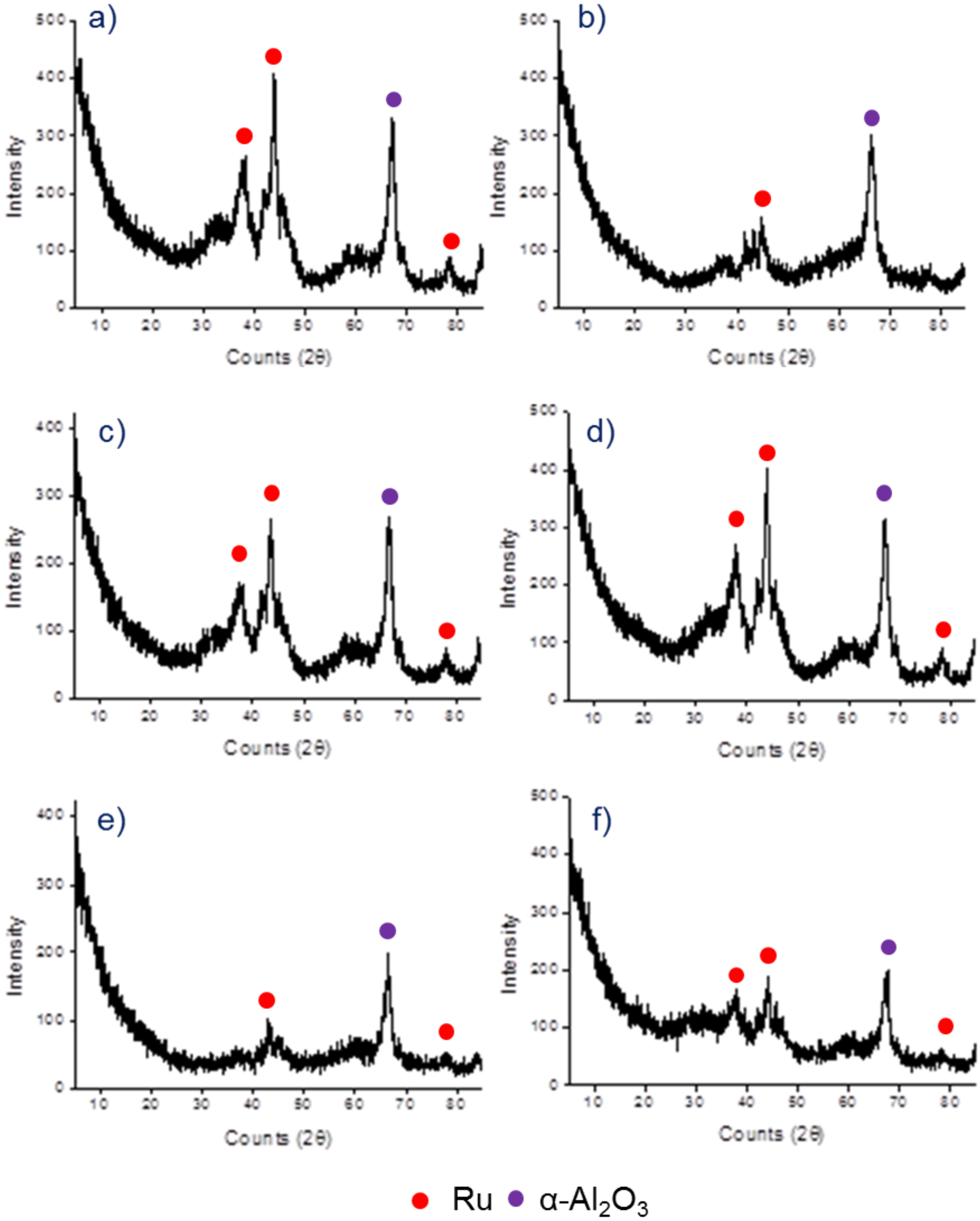

Figure 78: XRD Post-reaction Patterns for 5 wt% Ru/Al_2O_3 doped with $CsNO_3$, pre-treated for 2 hours with N_2/H_2 (1:3) then reacted at 400°C with N_2/H_2 (1:3) at ambient pressure a) 0 g, b) 0.0038 g, c) 0.0174 g, d) 0.1253 g, e) 0.2621 g, f) 0.3528 g. Reference PDFs Ru 01-0714656, and α-Al_2O_3 00-001-1296.

4.2.5 Morphology of 5 wt% Ru/Al_2O_3 Based Materials

The surface of Ru based materials was studies *via* SEM-EDX analysis. Pre- and post-reaction EDX analysis for 5 wt% Ru/Al_2O_3 doped with 0.3528 g $CsNO_3$ are shown in Figure 79. SEM images for the Ru materials are presented in Figures 81 and 82 respectively.

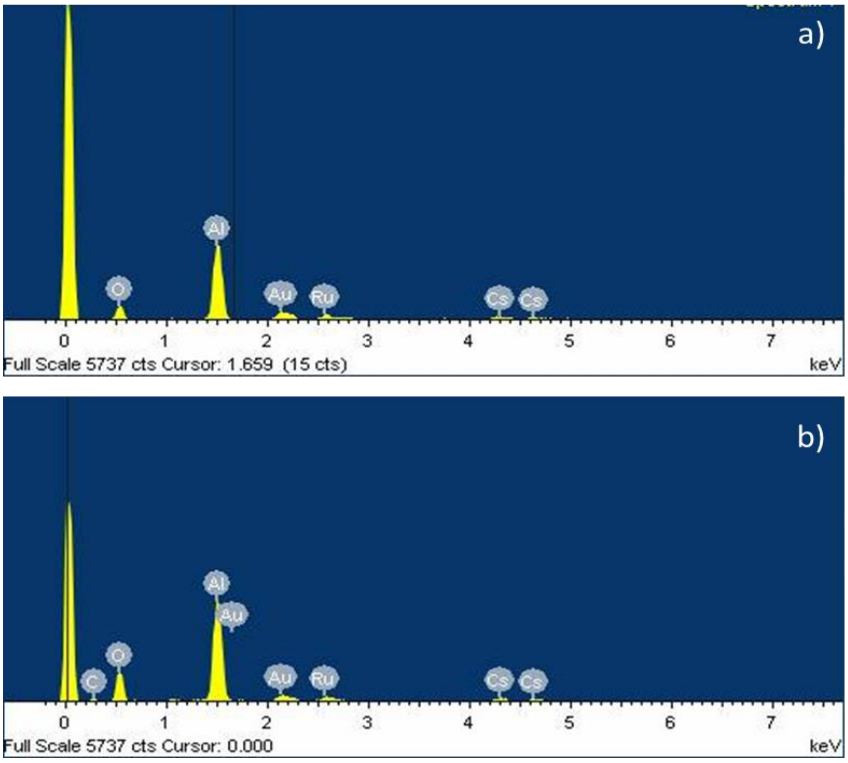

Figure 79: EDX for 5 wt% Ru/Al_2O_3 doped with 0.3528 g $CsNO_3$ a) pre- and b) post-reaction

In contrast to the XRD results, Cs^+ is found in the post-reaction material *via* EDX analysis, which, suggests either: the low level Cs features are hidden in the high background of the XRD patterns or the Cs^+ is present in a dispersed or an amorphous form.

The surface morphology of the pre- and post-reaction materials is very similar. However, a difference can be observed with increasing $CsNO_3$ content. The un-doped Ru/Al_2O_3 has a smooth angular surface with smaller agglomerated crystallites surrounding the particles. As the concentration of $CsNO_3$ increases the smooth surface of the particles decreases and becomes rougher with smaller specs of material on the surface. Results of EDX analysis were unable to detect which elements were specific to smooth or rough regions of the material. The bright areas on the images are due to charging from the beam, it would be beneficial to triple coat the samples in gold to reduce charging.

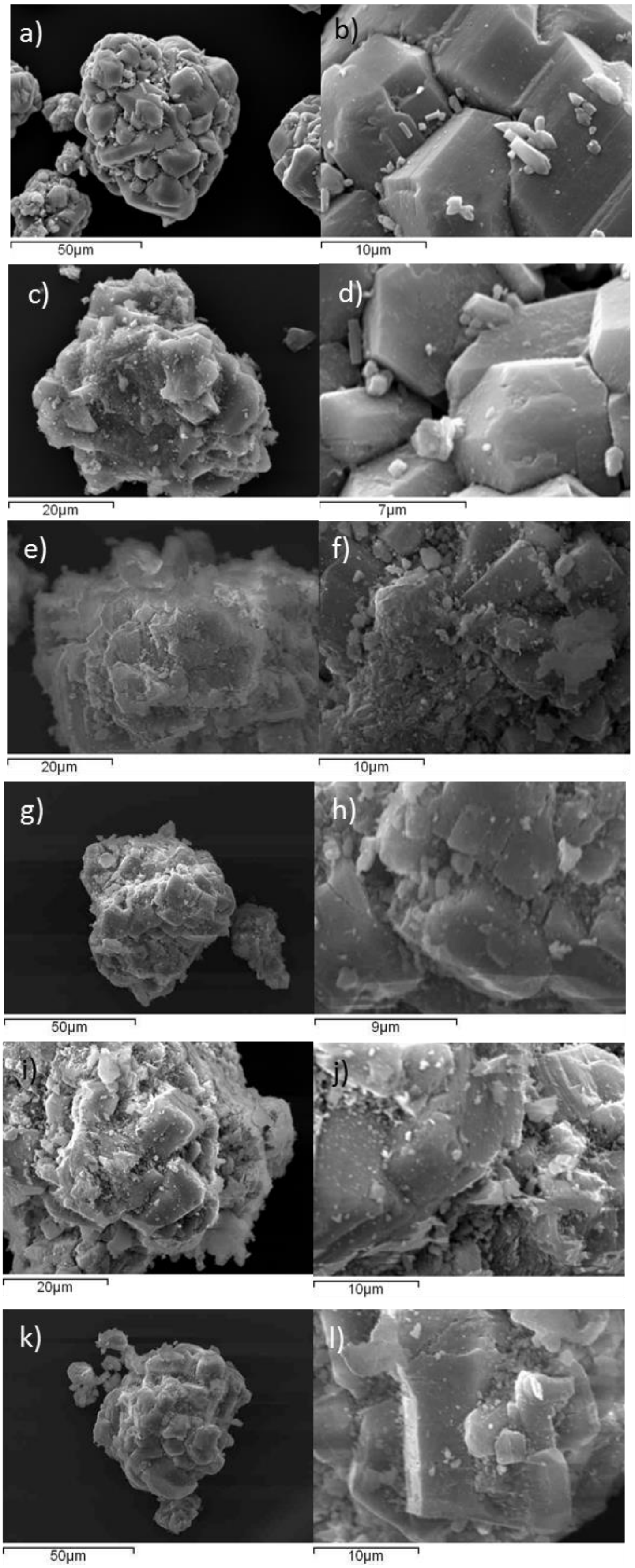

Figure 80: Pre Reaction SEM images for 5 wt% Ru/Al_2O_3 doped with $CsNO_3$ a–b) 0 g, c-d) 0.0038 g, e-f) 0.0174 g, g-h) 0.01253 g, i-j) 0.2621 g, k-l) 0.3528 g.

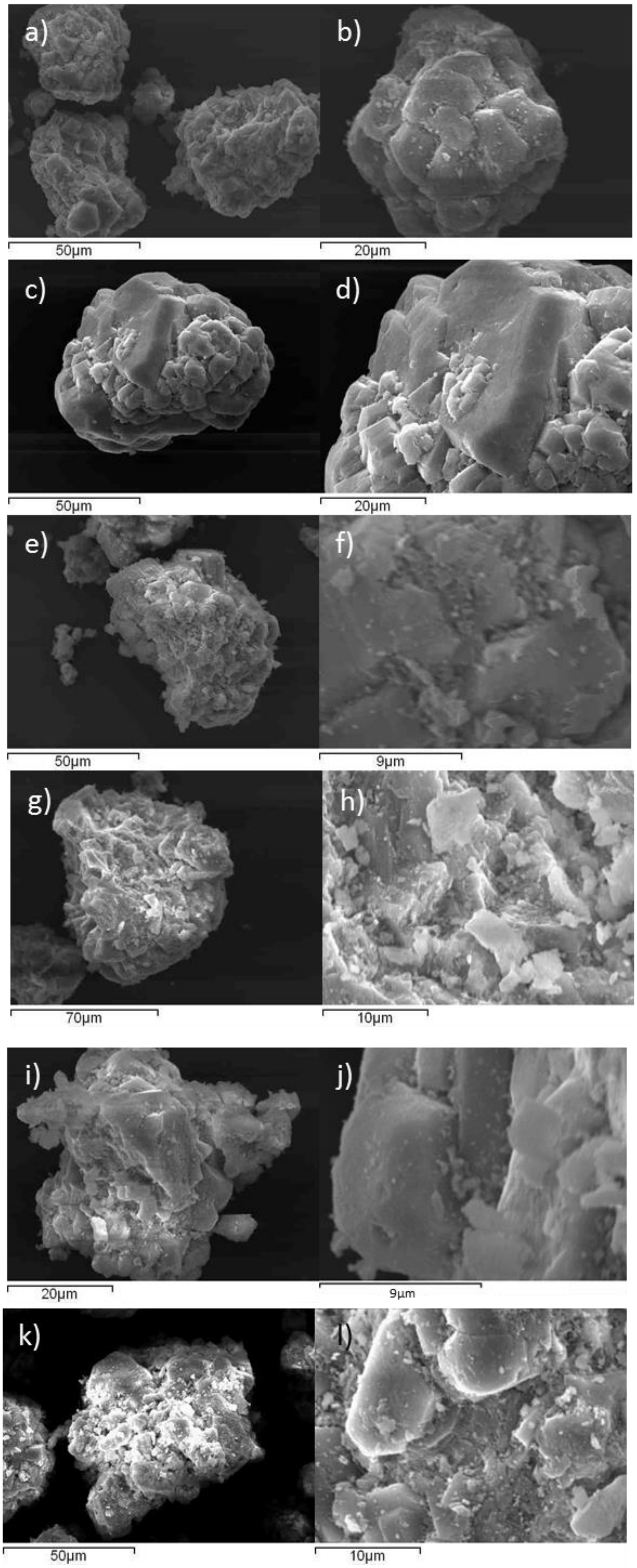

Figure 81: Post Reaction SEM images for 5 wt% Ru/Al_2O_3 doped with $CsNO_3$ a–b) 0 g, c-d) 0.0038 g, e-f) 0.0174 g, g-h) 0.01253 g, i-j) 0.2621 g, k-l) 0.3528 g.

4.2.6 Conclusions: 5 wt% Ru/Al_2O_3 Materials

The ammonia synthesis activity of doped 5 wt% Ru/Al_2O_3 increases with increasing $CsNO_3$ concentration. At low dopant levels (< 0.1 g $CsNO_3$) the activity is extremely low. However, when over 0.1 g of $CsNO_3$ is added very high (> 1000 µmol g^{-1} h^{-1}) ammonia synthesis activity is achieved. Comparing the ammonia synthesis activity of 5 wt% Ru/Al_2O_3 based materials to $CoRe_4$, it can be seen in higher $CsNO_3$ containing materials the rates exceed those of $CoRe_4$. When 0.3528 g of $CsNO_3$ is used the highest rate in this study is obtained (1818 ± 6 µmol g^{-1} h^{-1}) which exceed that of $CoRe_4$ (943 ± 44 µmol g^{-1} h^{-1}). $CsNO_3$ doped 5 wt% Ru/Al_2O_3 materials cannot be removed from the reactor, exposed to air, and re-run with high activity; in both cases the Ru materials deactivated on the second run. This is in contrast to the behaviour of $CoRe_4$ which can maintain high activity on repeated reaction runs. In contrast to the 5 wt% Ru/Al_2O_3 addition of Cs^+ to $CoRe_4$ decreases the ammonia synthesis rate which potentially parallels the observation of decreased efficacy when a K^+ cation precursor is used, as detailed in the previous chapter.

Ex situ XRD patterns reveal the $CsNO_3$ reflections are present in pre-reaction materials but disappear for the post-reaction patterns. However, EDX analysis reveals trace amounts of caesium in the post-reaction material.

4.2.7 Future Work: 5 wt% Ru/Al_2O_3 Materials

It would be beneficial to determine the Ru dispersion on the surface. This could be achieved by CO chemisorption. Also, it would be advised to find the optimal $CsNO_3$ doping amount and attempt doping with K^+ and/or Ba^{2+}. After investigating different dopants attempts should be made to use multiple doping components to enhance the activity.

Chapter 5

Ammonia Decomposition

5.1 Background: Ammonia Decomposition

A 2013 report by the Intergovernmental Panel on Climate Change claims scientific research proves

with 95% certainty the greatest cause of global warming, since the mid-20th Century, is human activity[172]. Environmental concerns regarding anthropogenic CO_2 emissions are the driving force behind new research areas, within the scientific community, to find alternative methods for green energy and sustainable fuels.

There are two main forms of technology competing to combat the clean energy mobile transport industry: electrical and hydrogen fuel cells. Electrical energy is achieved through motors powered though batteries, whereas, polymer exchange membranes (PEM) are powered by hydrogen and generate electricity from the stored hydrogen chemical energy[173]. Hydrogen fuel cells are clean alternative to fossil fuels[174, 175]. Modern fuel cell technology has been known for the last century however, the cost of turning this technology into reality and being made available on the consumer market, is now a reality[176]. In 2006 the US Department of Energy set hydrogen storage targets for 2015, these specifications include[175, 177]:

1. High hydrogen storage capacity (81 $L^{-1}g$ volumetric capacity and 9 wt% hydrogen content)
2. Operating temperature of < 60°C
3. Low cost
4. The ability to fill the system quickly
5. Non-toxic and inert materials

Research has focused on developing new materials with a high hydrogen storage capacity. This has led to the synthesis and characterization of new materials, some of which are detailed in Table 22. Hydrogen can be physically stored in the pores of materials such as zeolites or metal organic frameworks (MOFs). However, the carbon footprint of ammonia production is large and this must be considered in relation to environmental benefits.

Table 22: Examples of Hydrogen Storage Materials.

Class of Material	Examples
Metal Nitrides	VN[31], Mo_2N, Co_3Mo_3N, Ni_2Mo_3N, and Fe_3Mo_3N[32]
Metal Hydrides	AlH_3[178], $LiAlH_4$[179], MgH_2[180] and $NaAlH_4$[181, 182]
MOFs	MOF-177[183], IRMOF–1 and Cu–BTC[184]
Borohydrides	$LiBH_4$[185] and $Mg(BH_4)_2$[186]
Amide/Imide Systems	Li_3N[187], $NaNH_2$[188]
Alloys	CaMg-based[189], Mg_2Ni[190]

Regarding hydrogen storage there are many drawbacks of using pure hydrogen. When in liquid or compressed form hydrogen has a low volumetric energy density[191]. Also, with respect to hydrogen powered cars and on board storage, hydrogen is extremely flammable so there is the high risk of explosion in the event of a collision. Chemical storage is an attractive alternative. Molecules such as methanol, ammonia and methane have a high hydrogen content and comply with the desired US Department of Energy Regulations.

There are many advantages of using ammonia as a hydrogen storage fuel. The Kyoto Protocol[192] strives to reduce greenhouse gas emissions and ammonia is not classed a greenhouse gas. In comparison to conventional hydrocarbon fuels and alcohols the end product has zero CO_2 emissions[193, 194], however the original process of making ammonia has a large carbon footprint. The main advantage is the high capacity for hydrogen storage; the molecular formula of ammonia is NH_3 which corresponds to a hydrogen weight percentage of 17.65 w% per molecule of ammonia[191]. Ammonia can also be liquefied using mild conditions; therefore, it can be stored in a non-pressurised simple vessel with a volumetric hydrogen density of approximately 45% higher than pure liquid H_2. Moreover, ammonia can be easily catalytically decomposed[193].

In 1813, Louis Jacques Thénard first discovered that ammonia can be catalytically decomposed over a variety of metals to give nitrogen and hydrogen[195]. Ammonia decomposition generates CO_x free hydrogen and the equation for is presented in Equation 10 (ΔH^0 = + 46 kJ mol_{NH3}^{-1}). Ammonia decomposition is a reversible reaction and is thermodynamically limited at low temperatures. However, due to this there will always be a small quantity of residual NH_3 which may cause concern as ammonia is toxic and can potentially damage membranes, fuel cells etc.

Equation 10: Ammonia Decomposition.

$$2NH_{3(g)} \rightleftharpoons 3N_{2(g)} + H_{2(g)}$$

Traditionally ammonia decomposition has been studied to gain insight into ammonia synthesis, however, as the potential for ammonia as hydrogen storage increases so has the interest in decomposition catalysts[196]. Microscopic reversibility suggests similar materials to be both: a good ammonia synthesis and decomposition catalyst[197, 198]. In contrast, Boisen and co-workers[72] argue although ammonia decomposition is the opposite of ammonia synthesis; this does not necessarily mean the optimal catalyst for both processes is the same material. For their argument they implement a model proposed by Logadottir *et al*[199]. The model calculates the overall ammonia synthesis turnover frequency over transition metals, with regard to the dissociative nitrogen adsorption energy on the active sites. This model can be used to calculate the activity trends for ammonia decomposition. The top section of Figure 82 shows the calculated volcano relationships for NH_3 decomposition and synthesis. To support these theoretical calculations several materials were prepared and tested: Co, Cu, Fe, Ni and Ru supported on $MgAl_2O_4$ and Co_3Mo_3N. The bottom section shows the experimental results. There is excellent correlation between the predicted and experimental values. Boisen *et al*[72] also present Figure 83 where it shows the optimal binding energy differs for the two different processes when dealing with different concentrations of ammonia. Therefore suggesting the optimal ammonia synthesis catalyst will be different from the optimum ammonia decomposition material.

At a given set of conditions the rate of ammonia decomposition can be written:

$$r_{decomp} = r_{syn} \frac{p_{NH3}^2}{p_{N2}\, p_{H2}^3\, K_{eq}} = r_{syn}\beta$$

Where:

- r_{decomp} = rate of ammonia decomposition
- r_{syn} = rate of ammonia synthesis
- K_{eq} = equilibrium constant
- p_x = partial pressure of specified gas
- β = the approach to equilibrium

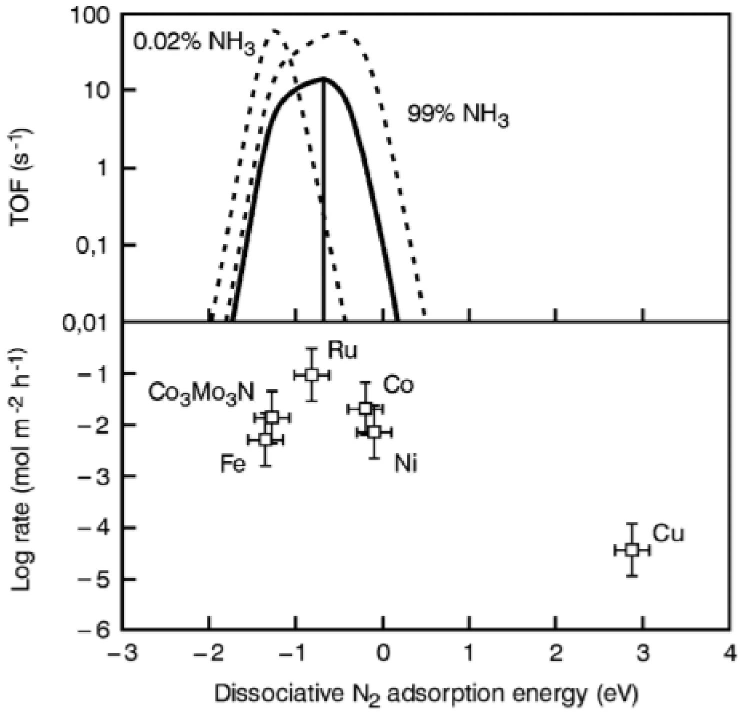

Figure 82: Calculated turnover frequencies of ammonia synthesis/decomposition at 773 K, 1 bar, 3:1 H_2/N_2, and 0.02, 20 (solid line), and 99% NH_3 as a function of the reaction energy of dissociative N_2 adsorption. The vertical line gives the dissociative nitrogen binding energy of the optimal ammonia decomposition catalyst when the ammonia concentration is 20%. At these conditions the gas phase equilibrium NH_3 concentration is 0.13% (top). Experimental rates of ammonia decomposition over various catalysts at 773 K, 1 bar, 3:1 H_2/N_2, and 20% NH_3 (bottom)[72].

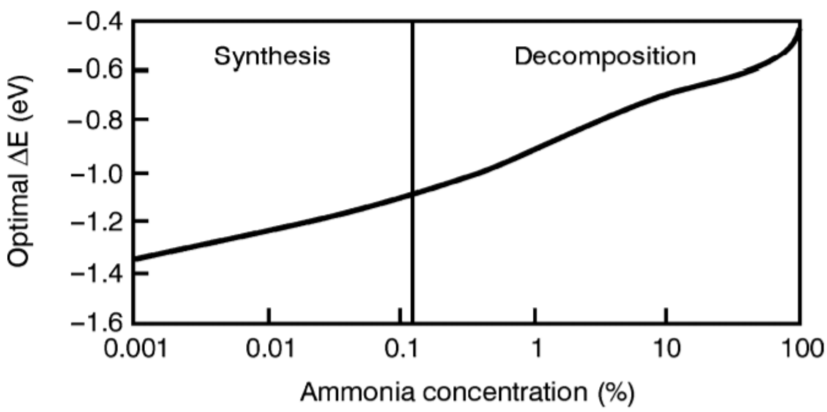

Figure 83: Dissociative N_2 adsorption energy of optimal catalyst for ammonia synthesis/decomposition at 773 K, 1 bar and 3:1 H_2/N_2. Equilibrium corresponds to *ca.* 0.13% ammonia[72].

A method of using ammonia decomposition to produce CO_x free hydrogen in proton membranes was first proposed in 1982 by Green[200]. Hansgen *et al*[201] devised a twelve step mechanism for ammonia decomposition is presented in Figure 84. The authors did not suggest a rate determining step. The process begins with the adsorption of ammonia on an active site, followed by cleavage of the N-H bonds. Then recombination of nitrogen and hydrogen and finishing with desorption of molecular nitrogen and hydrogen.

$$
\begin{aligned}
NH_3 + * &\rightarrow NH_3 * \\
NH_3 * &\rightarrow NH_3 + * \\
NH_3 * + * &\rightarrow NH_2 * + H * \\
NH_2 * + H * &\rightarrow NH_3 * + * \\
NH_2 * + * &\rightarrow NH * + H * \\
NH * + H * &\rightarrow NH_2 * + * \\
NH * + * &\rightarrow N * + H * \\
N * + H * &\rightarrow NH * + * \\
N * + N * &\rightarrow N_2 + 2 * \\
N_2 + 2 * &\rightarrow N * + N * \\
H * + H * &\rightarrow H_2 + 2 * \\
H_2 + 2 * &\rightarrow H * + H *
\end{aligned}
$$

Figure 84: Elementary Reaction Steps for Ammonia Decomposition[201].

There are contrasting reports in the literature over the rate limiting step. Ganley and co-workers[202] report that at 580°C the rate limiting step is dependent on the metal catalyst used. They claim breakage of the N-H bond is rate limiting for Cu, Ir, Pd, Pt and Rh, whereas nitrogen desorption is the rate limiting step in the case of Co and Fe. Contrary to these findings Wang *et al*[203] used tracking experiments and propose irrespective of the metal catalyst nitrogen desorption is rate limiting. Currently desorption of nitrogen is widely accepted as the rate-limiting step and the active sites are B_5 sites[204]. B_5 sites are 3D structures that consist of 5 Ru atoms arranged on two distinct planes. Three atoms are on the lower plane forming a terrace like area and two atoms are on the upper plane forming a step to the lower plane[205, 206].

Sørensen and co-workers[204] studied un-promoted Co, Fe, Pd and Ru catalysts for ammonia decomposition at 575°C and 650°C using a NH_3/Ar (1:1) gas mixture. It was established Co was the most active metal for ammonia decomposition and its activity was five times higher than the rate for Fe when comparable masses of material was tested under the same conditions. Lendzion-Bielun *et al*[207] produced a cobalt oxide material (64 m^2g^{-1}) it was found promotion with Mn and Cr was found to increases the specific surface area but decreased catalytic activity. Cobalt sintering was observed on reduction at 600°C.

Equation 11 presents the activity tends according to Ganley *el al*[202] for monometallic metals supported on activated alumina. Activity is not solely dependent on the metal; catalyst structure, active site and promoters heavily influence catalytic activity[208].

Equation 11: Activity Trend for Metals Supported on Activated Alumina[202].

$$Ru > Ni > Rh > Co > Ir > Fe \gg Pt > Cr > Pd > Cu \gg Te, Se, Pb$$

Zhang *et al*[209] tested two commercial carbon nanotubes (CNTs); Co- and Fe-containing. Elemental combustion analysis of the CNTs revealed they contained 4.1 wt% Fe and 2.8 wt% Co respectively. The Fe containing CNTs had a long activation period of 1200 minutes where the activity slowly increased over time and reached a maximum conversion of 76%. The active species was attributed to iron nitride. The Co containing CNTs were found to have good stability for 1500 minutes on stream. The authors conclude Co containing CNTs showed a superior to the Fe containing CNTs and that their activity exceeds that of commercial catalysts.

Ruthenium catalysts have been widely studied with regard to ammonia decomposition[76, 158, 173, 210, 211]. There is a general consensus that Cs^+ promoted Ru/graphite are the most active catalysts[76, 173, 210, 212, 213]. Zhang *et al*[212] developed a new method of producing highly dispersed Ru/MgO catalysts with lower Ru content. The group investigated MgO supported Ru catalysts prepared by a polyol reduction method. The Ru salt and Mg precursor were dissolved in ethylene glycol at 110°C. Next flowing nitrogen was passed over the material and after cooling stoichiometric amounts of KOH were added to the solution and washed with deionized water then calcined at 450°C. These materials were doped *via* the conventional wetness impregnation method. TEM revealed the Ru particle size was in the range of 1.2 – 2.3 nm. The unprompted catalysts were shown to have a mesoporous structure with a surface area of 151 $m^2\ g^{-1}$. Promotion *via* $CsNO_3$ showed the highest ammonia decomposition activity and exceeded that of promotion with potassium. The authors suggest this difference is due to the higher electronegativity of Cs^+.

Another unusual method of preparation was carried out by Yin and co-workers[214]. A ZrO_2-KOH super-basic support was prepared by a reflux digestion of $ZrO(OH)_2$ gel in KOH aqueous solution. This produced a super-basic support with high surface area. Ruthenium nanoparticles were then added to this support by impregnation and had a resulting Ru particle size of 2 – 7 nm. This material was found to have high activity for ammonia decomposition and the activity is enhanced when the Cl^- free Ru precursor is used. The variations in activity depending on the precursor used are in agreement with work by Aika *et al*[164, 165] regarding ammonia synthesis Ru materials.

Graphene nanosheets were investigated as a support for Ru based catalysts[211]. Ethylene glycol was used to simultaneously reduce Ru ions and graphene oxide. Improvements in the nano-structure and hydrogen evolution rate were observed when water was used as the co-solvent. Catalytic activity was consistent for 80 hours at 450°C but at 500°C sintering of the Ru particles was observed.

Ru/CNTs are highly active for the decomposition of ammonia (6353 mol_{H2} mol_{Ru}^{-1} h^{-1} at 430°C)[76, 213]. CNTs have high conductivity and this is believed to contribute to the high activity[211, 213]. This is due to their ability to facilitate the transfer of electrons to the Ru, which enhanced the recombination desorption of N atoms from the Ru surface[213].

The activity can be further enhanced by the addition of a Cs^+ promoter (7870 mol_{H2} mol_{Ru}^{-1} h^{-1} at 370°C)[76, 210]. Hill and Torrente-Murciano[210] achieved low temperature ammonia decomposition below 320°C, using multi-walled CNTs to support Ru nanoparticles and promoted the resulting materials with Cs^+. Increasing the Cs^+ content increased the rate of hydrogen production at low temperatures, however, exceeding a Cs^+:Ru molar ratio of 3 appeared to lower activity and this was attributed to the Cs^+ blocking active sites on the Ru. The activation energy was measured at 96.7 kJ mol^{-1} for the Ru/CNTs and decreased to 59.3 kJ mol^{-1} when a Cs^+:Ru molar ratio of 3 was utilised. The elevated rate is accredited to the location of the electron donating Cs^+ near the CNT surface and the Cs^+ causing electronic modifications of the Ru. Currently, the most effective ammonia decomposition catalyst comprises of ruthenium dispersed on carbon nanotubes (CNTs) giving an activity of 6353 mol_{H2} mol_{Ru}^{-1} h^{-1} at 430°C[76, 213]. It is well documented promotion with Ba^{2+} or Cs^+ greatly enhances the catalytic ability. Raróg-Pilecka *et al* report Cs^+ is a more efficient promoter than Ba in regard to Ru/C and the difference is attributed to a greater dispersion of Cs^+.

For Ru materials the low temperature enhancing effect of Cs^+ promotion and graphitized CNTs compared to Ru/CNTs is shown in Figure 85.

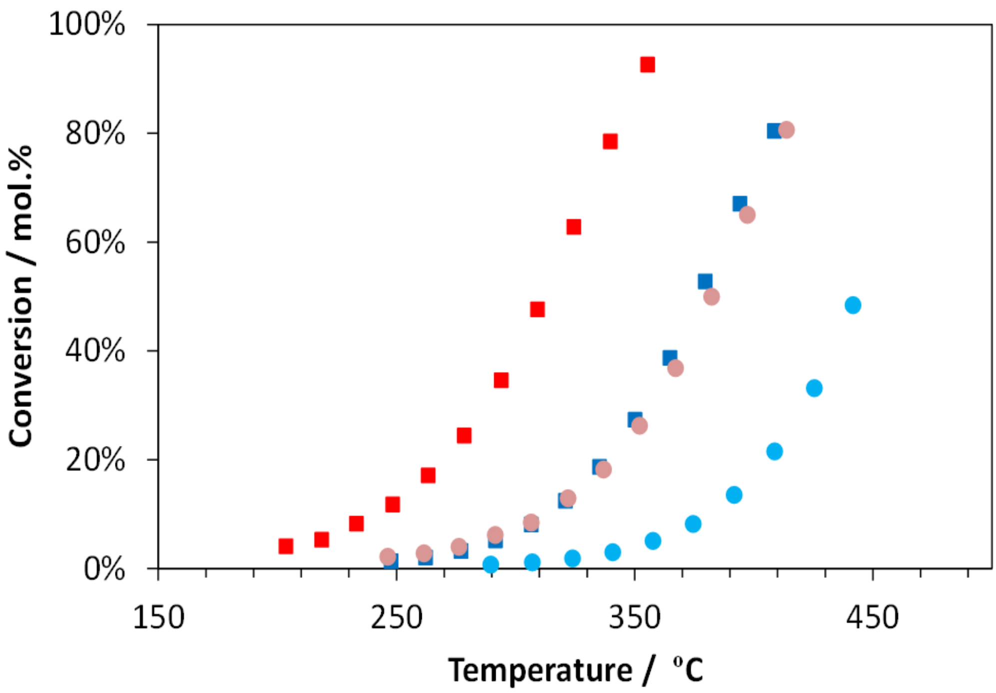

Figure 85: Ammonia decomposition plots supplied by Torrente-Murciano and Bell[76]. Red) Ru-Cs/graphitised CNTs, pink) Ru/graphitised CNTs, dark blue) Ru-Cs/CNTs and light blue) Ru/CNTs.

In comparison to Co and Ru, there is limited literature on rhenium systems for ammonia decomposition. Cholach *et al*[215] studied hydrogen adsorption on a polycrystalline rhenium wire and a monocrystal rhenium tip using field emission microscopy (FEM) and thermal desorption studies. At 350°C H_2 adsorption on rhenium was found to be dissociative. In 1951 McGeer and Taylor[216] reported metallic rhenium powder for ammonia decomposition. The activity increased when rhenium was more thoroughly reduced and the activity at 500°C was found to be promising. The activation energy and rate equation are given as 32 ± 3 kcal and $[NH_3]^{0.53}[H_2]^{-0.89}$ respectively. It was concluded, rhenium has many similar properties to iron and the surface is non-uniform and heterogeneous.

Rhenium filaments have been investigated by Gasser and Green[217]. Different pressures (1.3, 1.7 and 2.1 Torr) and temperatures 25 – 630°C were examined and steady state behaviour was observed. Cholach *et al*[218] present a brief investigation the adsorption and decomposition of ammonia on rhenium. Analysis was performed on a rhenium monocrystal tip. The authors propose a mechanism which first involves dissociation of NH_3 on the rhenium surface giving the formation of hydrogen and Re_2N_2. Next this Re_2N_2 reacts with another NH_3 molecule and this forms an imide species and liberates H_2 forming a proposed species of $(Re_2N_2)NH$. Two of these species combine giving N_2 and H_2 forming two moles of Re_2N_2. This then decomposed giving first Re_2N and N_2 then Re metal and N_2.

With respect to the highly active ruthenium supported electride catalyst for ammonia synthesis[8, 133, 135, 219] Hayashi and co-workers[220] tested Ru/C12A7:e^- for ammonia decomposition. The authors state that at 400°C the Ru/C12A7:e^- give ammonia decomposition rates 4 – 10x higher than previously reported elsewhere (66.1 kg_{NH3} kg_{cat}^{-1} h^{-1}).

With regard to this chapter, it is of interest to explore the possibility of using cobalt rhenium catalysts for ammonia decomposition. As discussed, Co has well documented activity whereas; there is limited mention in the literature of rhenium based materials for ammonia decomposition and indeed no previous literature on bimetallic cobalt rhenium systems. Also, it is widely accepted finely dispersed particles are required for high ammonia decomposition activity. However, the cobalt rhenium catalysts prepared in this work have an extremely low surface area (< 0.2 m^2 g^{-1}). This section is a preliminary study with the aim to investigate the activity of cobalt rhenium catalysts for ammonia decomposition.

5.2 Results and Discussion Ammonia Decomposition

5.2.1 Ammonia Decomposition Activity Data for Cobalt Rhenium Catalysts

Cobalt rhenium catalysts were investigated for ammonia decomposition. Ammonia decomposition experiments were performed by the author on a visit to the University of Bath and in collaboration with Dr Laura Torrente-Murcanio and Ms Tamsin Bell. Figure 86 shows the catalytic performance of various cobalt rhenium catalysts for ammonia decomposition.

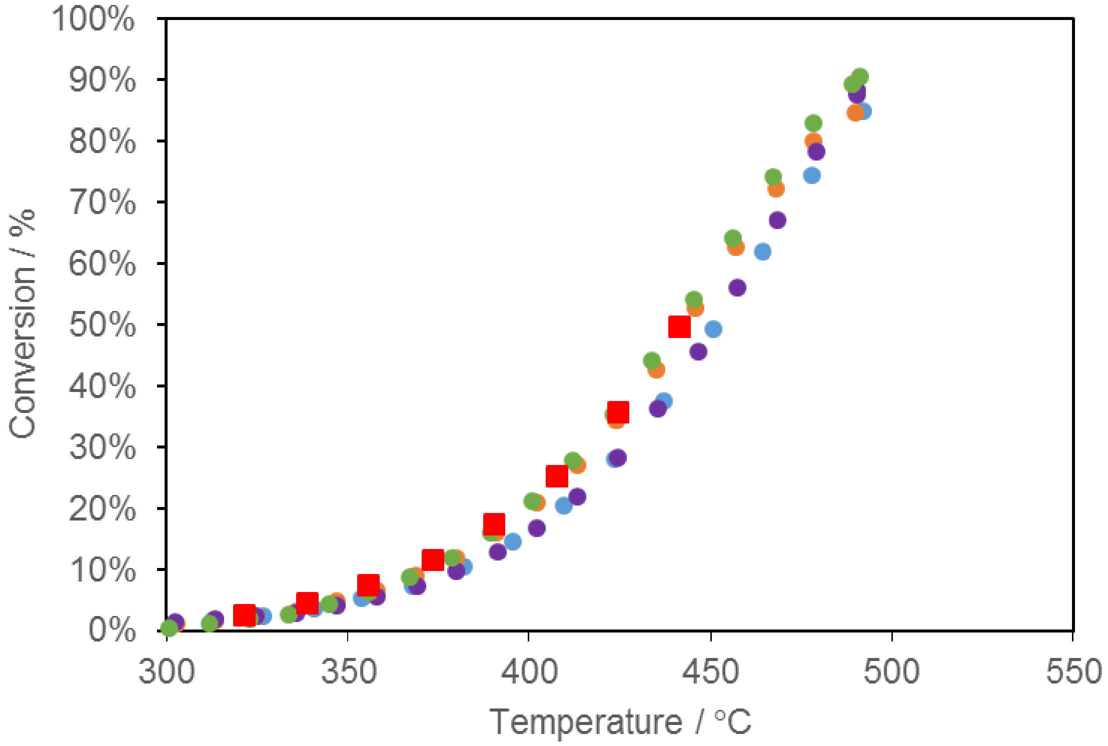

Figure 86: Ammonia decomposition conversion as a function of reaction temperature of 7 wt% Ru/CNTs (red), CoRe (blue), $CoRe_4$ (purple) and $CoRe_{16}$ (green).

From Figure 86 it can been suggested all materials showed improving ammonia conversion at increasing temperatures over the temperature range studied. Also, that the initial synthesis ratio does not seem to affect the overall ammonia decomposition ability of the materials. As previously discussed in Section 3.2.6 the initial ICP-MS results indicate the resulting cobalt rhenium composition is not dependent on the initial synthesis ratio and indeed similar materials are forming. This result can be attributed to why the materials exhibit the same ammonia decomposition activity. Regarding $CoRe_{16}$, in contrast to the ammonia synthesis results, (Section 3.2.6) where deactivation is observed, in the case of ammonia decomposition; the catalyst has comparable activity to the higher Re containing catalysts (CoRe and $CoRe_4$) and still maintains high activity.

It is desirable to lower the Re content of the catalysts. The initial results for the higher Co containing materials (Co_2Re and Co_4Re) show high promising results and are comparable to the catalysts synthesised with higher Re contents. It can be seen the cobalt rhenium materials are highly competitive with the 7 wt% Ru/CNTs and indeed appear to have very similar activity. This is a very promising result because in all previous cases within the literature it is assumed highly dispersed nanoparticles are required for high activity. In contrast the cobalt rhenium materials have high activity despite a very low surface area (< 0.2 $m^2\ g^{-1}$). This gives precedent to developing these materials to maximise the surface area to enhance the activity. However, it has not been possible to perform anything other than a comparative study since there was a problem which was subsequently discovered with the microreactor. This does not interfere with comparative measurements, but means that absolute performance cannot be stated at the present stage. Due to the time constraints of this work it has not been possible to re-run the cobalt rhenium materials on the modified equipment since the collaborators have recently moved institution and then building within their new institution.

5.2.2 *In Situ* and *Ex Situ* X-ray Diffraction

In order the assess the structure of the active catalyst *in situ* XRD experiments were performed on $CoRe_4$ at the ESRF with the help of Dr Karina Mathisen, Mr Karsten Kirste (NTNU), Drs Wouter van Beek (ESRF) and Said Laassri (University of Glasgow).

Ex situ and *in situ* XRD patterns are presented in Figures 88 and 89 respectively. Also, multiple XRD patterns were obtained *in situ* throughout the reaction and these are presented in Figure 89. Reference patterns were taken from PDFs: Re 00-005-0702, SiC 00-003-0880 and BN 00-015-0500.

Activity testing involved diluting $CoRe_4$ with SiC and this dominates the ex situ XRD pattern. However, a low intensity Re reflection can be found (Figure 87). For the *in situ* XRD pattern (Figure 88) this was taken simultaneously with XAS at the ESRF and BN was a required component for XAS to avoid over saturation.

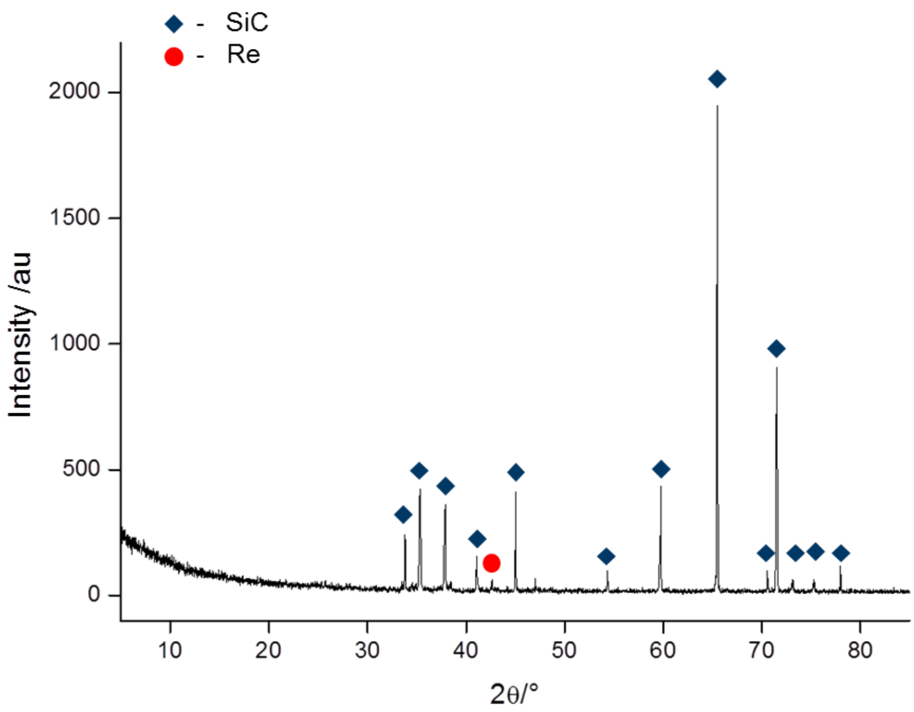

Figure 87: *Ex situ* XRD Pattern for Post Reaction $CoRe_4$ pre-treated with H_2 for 1 hour then reacted under 6 ml min^{-1} He with 2.4 ml min^{-1} NH_3 from room temperature to 500°C.

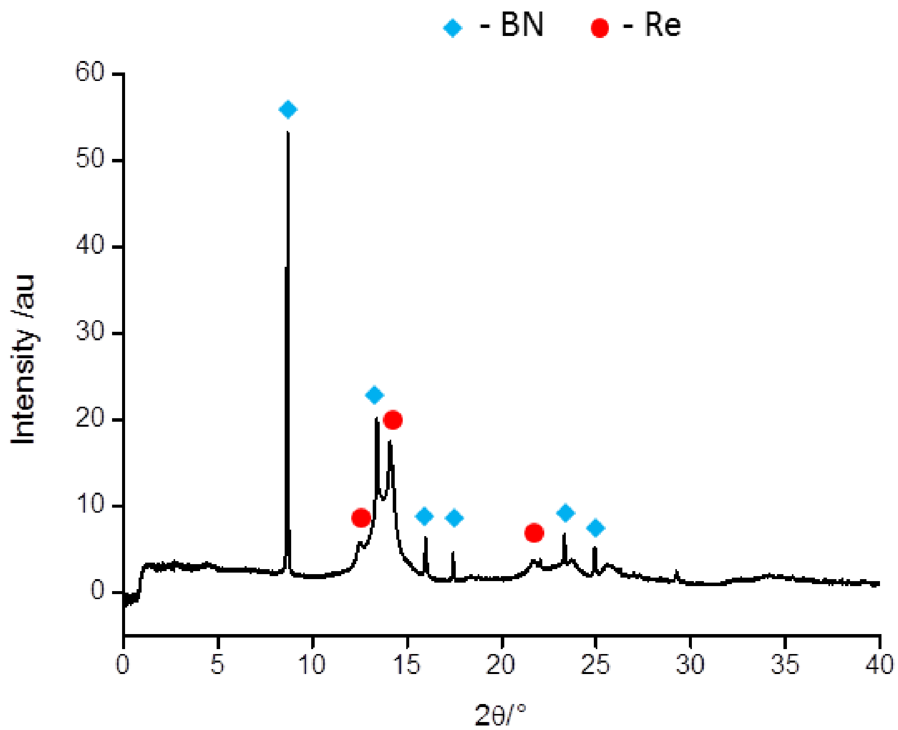

Figure 88: *In situ* XRD Pattern for $CoRe_4$ pre-treated with 75% Ar/H_2 (1:3) for 1 hour then reacted under 4% NH_3/He at 500°C.

Figure 89 presents multiple XRD patterns taken over 100 minutes during the ammonia decomposition reaction. Comparison of the XRD patterns over 100 min, reveals the catalyst does not change during the entire reaction. It is interesting to note, the *in situ* XRD patterns for both ammonia synthesis and ammonia decomposition are equivalent, suggesting the same active material is involved in both reactions.

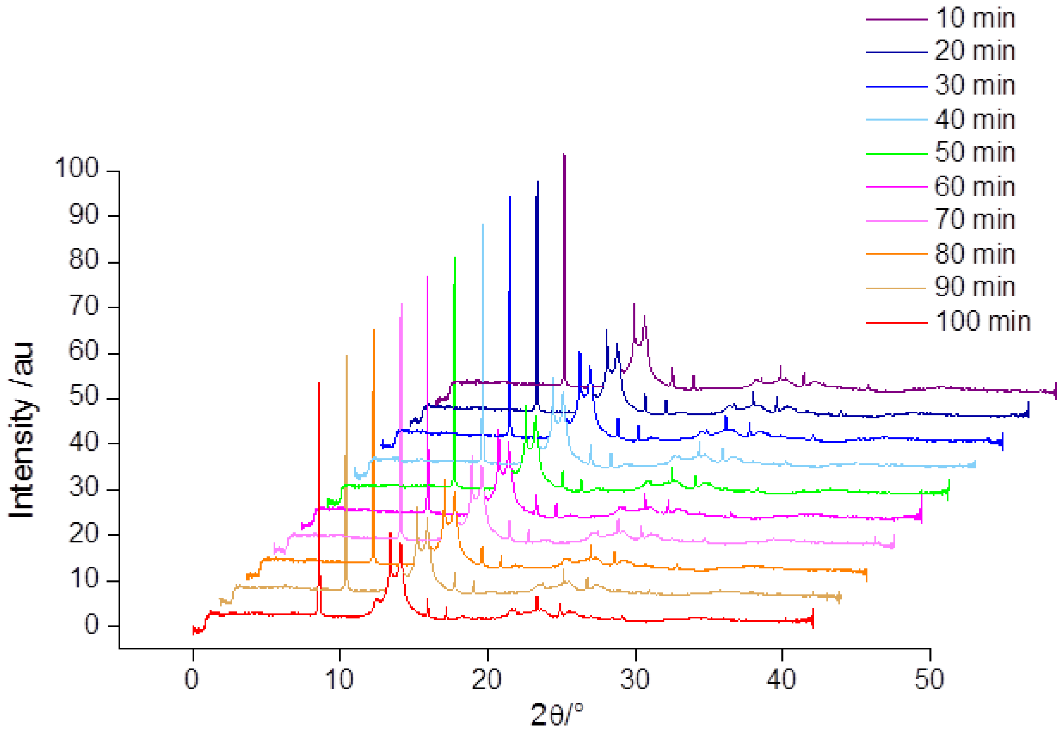

Figure 89: Multiple *In situ* XRD Patterns for $CoRe_4$ During Ammonia Decomposition over the temperature range 300 – 500°C under 4% NH_3/He.

5.3 Conclusions: Ammonia Decomposition

Hydrogen production from ammonia decomposition occurs at temperatures below 500°C using cobalt rhenium catalysts. This is the first report of bimetallic cobalt rhenium catalysts for ammonia decomposition. This work has shown, in contrast to the current literature, that low surface area materials can provide high ammonia decomposition activity and finely dispersed particles per se are not necessarily required.

It is important to note the cobalt rhenium catalysts are essentially crude materials that have not been optimised and despite this their rates are equivalent to the highly studied 7% Ru/CNTs catalyst. This high activity provides prominence for a more in-depth study to be performed to exploit these cobalt rhenium materials.

5.4 Outlook: Ammonia Decomposition

These cobalt rhenium materials will be re-tested in order for absolute ammonia decomposition rates to be determined. Similarly, to the ammonia synthesis outlook, it would be beneficial to support these materials to try and maximise the surface area.

Chapter 6

Conclusions

Cobalt rhenium catalysts have been shown to be active for ammonia synthesis and decomposition. This is the first report of un-supported, low surface area materials which exhibit promising activity for ammonia decomposition. In contrast to previous literature related to ammonia synthesis, cobalt rhenium materials were prepared without an ammonolysis step and it was found bypassing this stage gives a more active ammonia synthesis material (943 ± 44 μmol g^{-1} h^{-1} versus 655 ± 129 μmol g^{-1} h^{-1}) with a simplified synthesis route.

It was previously claimed the optimal cobalt rhenium synthesis ratio for ammonia synthesis catalysts, was 1:4 (Co:Re) to investigate this claim the cobalt rhenium synthesis ratio was varied and the materials tested for ammonia synthesis and decomposition. Results *via* ICP-MS revealed the original synthesis ratio does not directly correspond with the resulting active material and between Co_2Re to $CoRe_8$ can be considered compositionally similar. With respect to ammonia synthesis the higher Re or Co containing materials ($CoRe_{16}$, Co_4Re, Co_8Re) showed low activity, whereas, for ammonia decomposition these more extreme ratios did not appear to affect the activity. For ammonia decomposition this is a great result as the very low rhenium containing materials, (Co_4Re was found to have an actual ratio of $CoRe_{0.1}$) still have very good activity, suggesting future studies could involve lowering the rhenium content even more and hence reducing the cost of the catalyst.

Pre-treatment for 2 hours with N_2/H_2 (1:3) at 600°C gives an instantly active material under ammonia synthesis conditions (60 ml min^{-1}, 400°C, N_2/H_2 (1:3) and ambient pressure). Pre-treatment with Ar, Ar/H_2 (1:3) or N_2 leads to a 20 minute lag period before becoming active. Beyond these lag periods, the materials exhibit steady state ammonia synthesis activity however, the activity is slightly lower in comparison to the N_2/H_2 (1:3) pre-treated material. CoRe and $CoRe_4$ were tested for over 48 hours and retained steady state behaviour over the entire testing period. Regarding the active material it can be postulated that both Co and Re need to be in the reduced form and have a prolonged exposure to N_2. Attempts to introduce a Re-N shell during XAS analysis was unsuccessful suggesting the material is not a nitride as first thought. Pre-treatment seems to affect the degree of bimetallic mixing; N_2/H_2 has a better degree of Co-Re mixing which may be the reason for the enhanced activity. The preliminary XAS analysis suggests the cobalt rhenium catalyst is bimetallic in nature.

The Cs^+ promoted 5 wt % Ru/Al_2O_3 were studied and the highest activity (1818 ± 6 µmol g^{-1} h^{-1}) was observed for Ru/Al_2O_3 doped with 0.3528 g $CsNO_3$. These rates exceed that of the cobalt rhenium materials however, $CoRe_4$ has a low surface area of < 0.2 m^2 g^{-1}. Also, $CoRe_4$ has been shown to maintain high activity on repeated reactions and after exposure to air and ambient moisture. The Cs^+ promoted Ru/Al_2O_3 catalyst deactivated after exposure to air. It is important to note, 5 wt % Ru/Al_2O_3 doped with 0.3528 g $CsNO_3$ was tested for over 48 hours and maintained steady state ammonia synthesis activity. In contrast to the enhanced activity observed for the 5 wt % Ru/Al_2O_3 materials, Cs^+ promotion on $CoRe_4$ has a negative effect on the ammonia synthesis rate.

This work has shown the potential of cobalt rhenium catalysts for ammonia synthesis and decomposition synthesised a novel way without an ammonolysis stage. Initial XRD results suggest it is the same material active for both processes. XAS analysis suggests the active material has bimetallic Co-Re and monometallic Re and Co phases.

An accepted limitation of the current work was that testing was conducted at ambient pressure using pure feeds. This was undertaken to facilitate enhanced understanding of the cobalt rhenium system. To further advance the knowledge of these materials it would be beneficial to test them under realistic ammonia synthesis industrial conditions and use a recycled gas feed containing residual ammonia.

References

1. D. E. Brown, T. Edmonds, R. W. Joyner, J. J. McCarroll and S. R. Tennison, *Letters in Catalysis*, 2014, **144**, 545-552.

2. V. Smil, *Scientific American*, 1997, **277**, 76-81.

3. RSC, Feed the World - General Briefing Sheet, (accessed 23rd May, 2016).

4. V. Smil, *Nature (London)*, 1999, **400**, 415.

5. W. M. Stewart, D. W. Dibb, A. E. Johnston and T. J. Smyth, *Agronomy*, 2004, **97**, 1-6.

6. J. G. Reuvers, J. R. Brightling and D. T. Sheldon, *Ammonia Technology Development from Harber-Bosch to Current Times*, International Fertiliser Society, 2014.

7. J. M. Erisman, M. A. Sutton, J. Galloway, Z. Kilmont and W. Winiwarter, *Nature Geoscience*, 2008, **1**, 636-639.

8. M. Kitano, Y. Inoue, Y. Yamazaki, F. Hayashi, S. Kanbara, S. Matsuishi, T. Yokoyama, S. Kim, M. Hara and H. Hosono, *Nature Chemistry*, 2012, **4**, 934-940.

9. Y. Tanabe and Y. Nishibayashi, *Coordination Chemistry Reviews*, 2013, **257**, 2551-2564.

10. S. Zhang, We Need a New, Sustainable Way to Make Fertilizer, (accessed 8th June, 2017).

11. G. J. Leigh, *The World's Greatest Fix: A History of Nitrogen and Agriculture*, Oxford University Press, New York, 2004.

12. F. Haber, *Nobel Lecture*, 1920.

13. J. R. Jennings, *Catalytic ammonia synthesis : fundamentals and practice*, Plenum, New York, 1991.

14. G. Ertl, M. Weiss and S. B. Lee, *Chemical Physics Letters*, **60**, 391-394.

15. T. Rayment, R. Schlogl, J. M. Thomas and G. Ertl, *Nature*, 1985, **315**, 311-313.

16. A. Mittasch and W. Frankenburger, *Journal of Chemical Education*, 1929, **6**, 2097.

17. A. Mittasch, *Catalytic Agents and Process of Making Them*, 1916.

18. K. Aika and A. Ozaki, *Journal of Catalysis*, 1970, **16**, 97-101.

19. A. Ozaki, *Accounts of Chemical Research*, 1981, **14**, 16-21.

20. A. K. Rhodes, *Oil and Gas Journal*, 1996.

21. D. McKay, PhD, University of Glasgow, 2008.

22. R. Kojima and K. Aika, *Applied Catalysis A: General*, 2001, **215**, 149-160.

23. R. Kojima and K. Aika, *Applied Catalysis A: General*, 2001, **218**, 121-128.

24. R. Kojima and K. Aika, *Applied Catalysis A: General*, 2001, **209**, 317-325.

25. A. M. Alexander and J. S. J. Hargreaves, *Chemistry Society Reviews*, 2010, **39**, 4388-4401.

26. D. A. King and F. Sebba, *Journal of Catalysis*, 1965, **4**, 253-259.

27. C. J. H. Jacobsen, *Chemical Communications*, 2000, 1057-1058.

28. N. Segal and F. Sebba, *Journal of Catalysis*, 1967, **8**, 105-112.

29. N. Segal and F. Sebba, *Journal of Catalysis*, 1967, **8**, 113-119.

30. G. I. Panov and A. S. Kharitonov, *Reaction Kinetics and Catalysis Letters*, 1985, **29**, 267-274.

31. W. J. McGill and F. Sebba, *Journal of Catalysis*, 1963, **2**, 104-108.

32. A. Srifa, K. Okura, T. Okanishi, H. Muroyama, T. Matsui and K. Eguchi, *Catalysis Science & Technology*, 2016, **6**, 7495-7504.

33. C. J. H. Jacobsen, S. Dahl, B. S. Clausen, S. Bahn, A. Logadottir and J. K. Nørskov, *Journal of the American Chemical Society*, 2001, **123**, 8404-8405.

34. A. Mittasch and W. Frankenburg, in *Advances in Catalysis*, eds. W. G. Frankenburg, V. I. Komarewsky and E. K. Rideal, Academic Press, 1950, vol. 2, pp. 81-104.

35. J. S. J. Hargreaves, *Coordination Chemistry Reviews*, 2013, **257**, 2015-2031.

36. D. R. Strongin, J. Carrazza, S. R. Bare and G. A. Somorjai, *Journal of Catalysis*, 1987, **103**, 213-215.

37. M. R. Hillis, C. Kemball and M. W. Roberts, *Transactions of the Farady Society*, 1966, **62**, 3570-3585.

38. C. D. Zeinalipour-Yazdi, J. S. J. Hargreaves and C. R. A. Catlow, *Journal of Physical Chemistry: C*, 2015, **119**, 28368-28376.

39. J. S. J. Hargreaves and D. McKay, *Journal of Molecular Catalysis A: Chemical*, 2009, **305**, 125-129.

40. R. Schlögl, *Angewandte Chemistry International Edition*, 2003, **42**, 2004-2008.

41. K. Aika and A. Ozaki, *Journal of Catalysis*, 1969, **14**, 311-321.

42. A. Friedrich, B. Winkler, L. Bayarjargal, W. Morgenroth, E. A. Juarez-Arellano, V. Milman, K. Refson, M. Kunz and K. Chen, *Physical Review Letters*, 2010, **105**, 085504.

43. R. Kojima, H. Enomoto, M. Muhler and K. Aika, *Applied Catalysis A: General*, 2003, **246**, 311-322.

44. A. M. Alexander, J. S. J. Hargreaves and C. Mitchell, *Topics in Catalysis*, 2013, **56**, 1963-1969.

45. F. Kawamura, H. Yusa and T. Taniguchi, *Applied Physics Letters*, 2012, **100**.

46. G. Soto, H. Tiznado, W. de la Cruz and A. Reyes, *Journal of Materials*, 2014.

47. M. Asscher, J. Carrazza, M. M. Khan, K. B. Lewis and G. A. Somorjai, *Journal of Catalysis*, 1986, **98**, 277-287.

48. R. Kojima and K. Aika, *Chemistry Letters*, 2000, 912-913.

49. S. Giddey, S. P. S. Badwal and A. Kulkarni, *International Journal of Hydrogen Energy*, 2013, **38**, 14576-14594.

50. T. Murakami, T. Nohira, T. Goto, Y. H. Ogata and Y. Ito, *Electrochimica Acta*, 2005, **50**, 5423-5426.

51. T. Murakami, T. Nishikiori, T. Nohira and Y. Ito, *Journal of the American Chemical Society*, 2003, **125**, 334-335.

52. A. Milward and S. B. Saul, in *The Economic Development of Continental Europe 1780-1870*, George Allen & Unwin Ltd, Great Britain, 1979, ch. 8.

53. *Catalysts for Nirtogen Fixation*, Springer Science & Business Media, 2004.

54. G. J. Leigh, *Nitrogen Fixation at the Millennium*, Elsevier, 2002.

55. G. Ertl, in *Encyclopedia of Catalysis*, John Wiley & Sons, 2002.

56. R. L. Zimdahl, *Six Chemicals That Changed Agriculture*, Elsevier Science, 2015.

57. A. S. Travis, in *The Synthetic Nitrogen Industry in World War I: Its Emergence and Expansion*, Springer International Publishing, 2015, pp. 17-72.

58. F. Aftalion, *A History of the International Chemical Industry*, Chemical Heritage Press, 2001.

59. R. C. Burns and R. W. F. Hardy, *Nitrogen Fixation in Bacteria and Higher Plants*, Springer-Verlag Berlin Heidelberg, 1st edn., 1975.

60. T. M. Paschkewitz, PhD, University of Iowa, 2012.

61. B. K. Burgess and D. J. Lowe, *Chemical Reviews*, 1996, **96**, 2983-3012.

62. P. C. Dos Santos, R. Y. Igarashi, H. I. Lee, B. M. Hoffman, L. C. Seefeldt and D. R. Dean, *Accounts of Chemical Research*, 2005, **38**, 208-214.

63. B. J. Hales, D. Langosch, J and E. E. Case, *The Journal of Biological Chemistry*, 1986, **8**, 15301-15306.

64. A. Müller, K. Schneider, K. Knüttel and W. R. Hagen, *FEBS Letters*, 1992, **303**, 36-40.

65. B. Hinnemann and J. K. Nørskov, *Topics in Catalysis*, 2006, **37**, 55-70.

66. M. do Vale Barreto Figueiredo, A. C. do Espírito Santo Mergulhão, J. K. Sobral, M. de Andrade Lira Junior and A. S. F. de Araújo, in *Plant Microbe Symbiosis: Fundamentals and Advances*, ed. N. K. Arora Spinger India, 2013, ch. 10.

67. J. Postgate, *The Fundementals of Nitrogen Fixation*, Cambridge University Press, 1982.

68. B. E. Smith, *Science*, 2002, **297**, 1654-1655.

69. C. M. Halbleib and P. W. Ludden, *The Journal of Nutrition*, 2000, **5**, 1081-1084.

70. R. D. Milton, R. Cai, S. Abdellaoui, D. Leech, A. L. DeLacey, M. Pita and S. D. Minteer, *Angewandte Chemie*, 2017, **56**, 2680-2683.

71. A. Banerjee, B. D. Yuhas, E. A. Margulies, Y. Zhang, Y. Shim, M. R. Wasielewski and M. G. Kanatzidis, *Journal of the American Chemical Society*, 2015, **137**, 2030-2034.

72. A. Boisen, S. Dahl, J. K. Nørskov and C. H. Christensen, *Journal of Catalysis*, 2005, **230**, 309-312.

73. G. Svehla, *Vogel's Textbook of Macro and Semimicro Qualitative Inorganic Analysis. 5th Ed*, Longman Group Ltd., 1979.

74. D. Duprez, J. S. J. Hargreaves, S. D. Jackson and G. Webb, *Isotopes in Heterogeneous Catalysis*, Imperial College Press, London, 2006.

75. D. Martin and D. Duprez, *Journal of Physical Chemistry*, 1996, **100**, 9429-2438.

76. A. K. Hill and L. Torrente-Murciano, *Applied Catalysis B: Environmental*, 2015, **172–173**, 129-135.

77. J. E. Penner-Hahn, 2007.

78. B. K. Teo, *EXAFS: Basic Principles and Data Analysis*, Springer-Verlag Berlin Heidelberg, 1986.

79. T. Shibata, B. A. Bunker, Z. Zhang, D. Meisel, C. F. Vardeman and J. D. Gezelter, *Journal of the American Chemical Society*, 2002, **124**, 11989-11996.

80. K. Mathisen, K. Kirste, J. S. J. Hargreaves, S. Laassiri, K. McAulay, A. R. McFarlane and N. A. Spencer, *Topics in Catalysis*, 2017.

81. B. Ravel and M. Newville, *Journal of Synchrotron Radiation*, 2005, **12**, 537-541.

82. RSC, http://www.rsc.org/periodic-table/element/75/rhenium, (accessed 15th January, 2016).

83. R. D. Peacock, in *The Chemistry of Manganese, Technetium and Rhenium*, Pergamon, 1973, pp. 905-978.

84. U.S. Geological Survey, *Mineral Commodity Summaries*, Virginia, Jan 2016.

85. A. I. Grabezhev, *Geology of Ore Deposits*, 2013, **55**, 13-26.

86. V. I. Spetsyn, I. E. Mikhailenko and O. V. Pokrovskaya, *Doklady Physical Chemistry*, 1982, **14**, 225-228.

87. V. I. Spetsyn, I. E. Mikhailenko and O. V. Pokrovskaya, *Doklady Akademii Nauk SSSR*, 1982, **263**, 656-660.

88. W. H. Davenport, V. Kollonitsch and C. H. Klein, *Industrial & Engineering Chemistry*, 1968, **60**, 10-19.

89. D. Mukherji and J. Rösler, *Journal of Physics: Conference Series*, 2010, **240**.

90. J. Rösler, D. Mukherji and T. Baranski, *Advanced Engineering Materials*, 2007, **9**.

91. B. Gorr, V. Trindade, S. Burk, H.-J. Christ, M. Klauke, D. Mukherji and J. Rösler, *Oxidation of Metals*, 2009, **71**, 157-172.

92. P. G. Greco, *Rhenium Alloys Iron Group Metals (Electrodeposition and Properties)*, U. S. Army, Rensselaer Polytechnic Institute, 1971.

93. M. Huang and J. Zhu, *Rare Metals*, 2016, **35**, 127-139.

94. W. S. Walston, J. C. Schaeffer and W. H. Murphy, *Superalloys*, 1996, 9-18.

95. M. Koch, W. Kock, D. F. Lupton and F. Scholz, *Journal*, 2000.

96. D. H. Buckley and R. L. Johnson, *Wear*, 1968, **11**, 405-419.

97. D. H. Buckley and R. L. Johnson, *Friction and Wear of Hexagonal Metals and Alloys as Related to Crystal Structure and Lattice Parameters in Vacuum*, 1966.

98. W. A. Brainard and D. H. Buckley, *Preliminary Friction and Wear Studies of Cobalt-Rhenium Solid Solution Alloy in Air and Vacuum*, NASA, 1971.

99. T. B. Massalski, J. L. Murray, L. H. Bennett and H. Baker, *Binary alloy phase diagrams*, American Society for Metals, Metals Park, Ohio, 1986.

100. E. N. Kablov, N. V. Petrushin, M. B. Bronfin and A. A. Alekseev, *Russian Metallurgy* 2006, **2006**, 406-414.

101. V. Raghavan, *Journal of Phase Equilibria and Diffusion*, 2004, **25**, 282-284.

102. S. Karup-Møller and E. Makovicky, *Neues Jahrbuch für Mineralogie Monatshefte*, 1999, 265-280.

103. R. Toreki and R. R. Schrock, *Journal of the American Chemical Society*, 1990, **112**, 2448-2449.

104. K. R. Rovik, A. Hagen, I. Schmidt, S. Dahl, I. Chorkendorff and C. H. Christensen, *Catalysis Letters*, 2006, **109**, 153-156.

105. C. G. Michel, W. E. Bambrick, R. H. Ebel, G. Larsen and G. L. Haller, *Journal of Catalysis*, 1995, **154**, 222-229.

106. C. G. Michel, W. E. Bambrick and R. H. Ebel, *Fuel Processing Technology*, 1993, **35**, 159-182.

107. R. Burch, *Platinum Metals Review*, 1978, **22**, 57-60.

108. R. Prestvik, B. Tøtdal, C. E. Lyman and A. Holmen, *Journal of Catalysis*, 1998, **176**, 246-252.

109. A. S. Fung, M. J. Kelley, D. C. Koningsberger and B. C. Gates, *Journal of the American Chemical Society*, 1997, **119**, 5877-5887.

110. R. Prestvik, K. Moljord, K. Grande and A. Holmen, *Journal of Catalysis*, 1998, **174**, 119-129.

111. A. Moen, D. G. Nicholson, M. Rønning and H. Emerich, *Journal of Materials Chemistry*, 1998, **8**.

112. M. E. Dry, *Catalysis Today*, 2002, **71**, 227-241.

113. L. Spadaro, F. Arena, M. L. Granados, M. Ojeda, J. L. G. Fierro and F. Frusteri, *Journal of Catalysis*, 2005, **234**, 451-462.

114. J. Li, G. Jacobs, Y. Zhang, T. Das and B. H. Davis, *Applied Catalysis A: General*, 2002, **223**, 195-203.

115. A. Voronov, N. E. Tsakoumis, N. Hammer, W. van Beek, H. Emerich and M. Rønning, *Catalysis Today*, 2014, **229**, 23-33.

116. F. Morales and B. Weckhuysen, *Catalysis*, 2006, **19**, 1-40.

117. A. M. Hilmen, D. Schanke and A. Holmen, *Catalysis Letters*, 1996, **38**, 143-147.

118. G. Jacobs, J. A. Chaney, P. M. Patterson, T. K. Das and B. H. Davis, *Applied Catalysis A: General*, 2004, **264**, 203-212.

119. C. Tang, T. Leu, W. Yu, C. Wang and S. Chien, *Thermochimica Acta*, **473**, 18-26.

120. V. Bakken, E. Bergene, E. Rytter and O. Swang, *Catalysis Letters*, 2010, **135**, 21-25.

121. N. E. Tsakoumis, A. Voronov, M. Rønning, W. v. Beek, Ø. Borg, E. Rytter and A. Holmen, *Journal of Catalysis*, 2012, **291**, 138-148.

122. M. Rønning, D. G. Nicholson and A. Holmen, *Catalysis Letters*, 2001, **72**, 141-146.

123. A. S. Fung, P. A. Tooley, M. J. Kelley, D. C. Koningsberger and B. C. Gates, *The Journal of Physical Chemistry*, 1991, **95**, 225-234.

124. H. C. Yao and M. Shelef, *Journal of Catalysis*, 1976, **44**, 392-403.

125. Z. Zhao, K. Bao, D. Li, D. Duan, F. Tian, X. Jin, C. Chen, X. Huang, B. Liu and T. Cui, *Scientific Reports*, 2014, **4**, 4797.

126. P. Clark, B. Dhandapani and S. Ted Oyama, *Applied Catalysis A: General*, 1999, **184**, 175-180.

127. K. McAulay, J. S. J. Hargreaves, A. R. McFarlane, D. J. Price, N. A. Spencer, N. Bion, F. Can, M. Richard, H. F. Greer and W. Z. Zhou, *Catalysis Communications*, 2015, **68**, 53-57.

128. M. Boudart, A. Delbouille, J. A. Dumesic, S. Khammouma and H. Topsøe, *Journal of Catalysis*, 1975, **37**, 486-502.

129. D. Szmigiel, W. Raróg-Pilecka, E. Miśkiewicz, M. Gliński, M. Kielak, Z. Kaszkur and Z. Kowalczyk, *Applied Catalysis A: General*, 2004, **273**, 105-112.

130. W. Raróg-Pilecka, E. Miśkiewicz, D. Szmigiel and Z. Kowalczyk, *Journal of Catalysis*, 2005, **231**, 11-19.

131. C. J. H. Jacobsen, S. Dahl, P. L. Hansen, E. Törnqvist, L. Jensen, H. Topsøe, D. V. Prip, P. B. Møenshaug and I. Chorkendorff, *Journal of Molecular Catalysis A: Chemical*, 2000, **163**, 19-26.

132. R. S. Wise and E. J. Markel, *Journal of Catalysis*, 1994, **145**, 344-355.

133. F. Hayashi and M. Iwamoto, *Microporous and Mesoporous Materials*, 2011, **146**, 184-189.

134. N. Bion, F. Can, J. Cook, J. S. J. Hargreaves, A. L. Hector, W. Levason, A. R. McFarlane, M. Richard and K. Sardar, *Applied Catalysis A: General*, 2015, **504**, 44-50.

135. F. Hayashi, M. Kitano, T. Yokoyama, M. Hara and H. Hosono, *ChemCatChem*, 2014, **6**, 1317-1323.

136. Atomic Radius of the Elements, (accessed June 26th, 2017).

137. A. Tougerti, S. Cristol, E. Berrier, V. Briois, C. La Fontaine, F. Villain and Y. Joly, *Physical Review B*, 2012, **85**, 125136.

138. B. Krebs, A. Muller and H. Beyer, *Chemical Communications*, 1968, 263-265.

139. K. F. Mucker, G. S. Smith and Q. Johnson, *Acta Crystallographica: B*, 1967, **24**, 874-879.

140. RSC, Periodic Table, (accessed 10th April, 2017).

141. D. McKay, D. H. Gregory, J. S. J. Hargreaves, S. M. Hunter and X. Sun, *Chemical Communications*, 2007, 3051-3053.

142. D. C. Koningsberger and R. Prins, *X-ray absorption : principles, applications, techniques of EXAFS, SEXAFS, and XANES*, Wiley, New York, 1988.

143. C. C. Romão, F. E. Kühn and W. A. Herrmann, *Chemical Reviews*, 1997, **97**, 3197-3246.

144. J. Sa, C. Kartusch, M. Makosch, C. Paun, J. A. van Bokhoven, E. Kleymenov, J. Szlachetko, M. Nachtegaal, H. G. Manyar and C. Hardacre, *Chemical Communications*, 2011, **47**, 6590-6592.

145. L. Guczi, D. Bazin, I. Kovács, L. Borkó, Z. Schay, J. Lynch, P. Parent, C. Lafon, G. Stefler, Z. Koppány and I. Sajó, *Topics in Catalysis*, 2002, **20**, 129-139.

146. D. Bazin, L. Borkó, Z. Koppány, I. Kovács, G. Stefler, L. I. Sajó, Z. Schay and L. Guczi, *Catalysis Letters*, 2002, **84**, 169-182.

147. K. Aika, H. Hori and A. Ozaki, *Journal of Catalysis*, 1972, **27**, 424-431.

148. D. E. Brown, T. Edmonds, R. W. Joyner, J. J. McCarroll and S. R. Tennison, *Catal. Lett.*, 2014, **144**, 545-552.

149. S. Dahl, A. Logadottir, R. C. Egeberg, J. H. Larsen, I. Chorkendorff, E. Tornqvist and J. K. Norskov, *Physical Review Letters*, 1999, **83**, 1814-1817.

150. S. Dahl, E. Tornqvist and I. Chorkendorff, *Journal of Catalysis*, 2000, **192**, 381-390.

151. T. W. Hansen, P. L. Hansen, S. Dahl and C. J. H. Jacobsen, *Catalysis Letters*, 2002, **84**, 7-12.

152. H. Bielawa, O. Hinrichsen, A. Birkner and M. Muhler, *Angewandte Chemie International Edition*, 2001, **40**, 1061-1063.

153. K. Honkala, A. Hellman, I. N. Remediakis, A. Logadottir, A. Carlsson, S. Dahl, C. H. Christensen and J. K. Nørskov, *Science*, 2005, **307**, 555.

154. J. Gavnholt and J. Schiøtz, *Physical Review B*, 2008, **77**, 035404.

155. Z. Kowalczyk, M. Krukowski, W. Raróg-Pilecka, D. Szmigiel and J. Zielinski, *Applied Catalysis A: General*, 2003, **248**, 67-73.

156. M. Muhler, F. Rosowski, O. Hinrichsen, A. Hornung and G. Ertl, in *Studies in Surface Science and Catalysis*, Elsevier, 1996, vol. Volume 101, pp. 317-326.

157. L. Forni, D. Molinari, I. Rossetti and N. Pernicone, *Applied Catalysis A: General*, 1999, **185**, 269-275.

158. W. Raróg-Pilecka, D. Szmigiel, Z. Kowalczyk, S. Jodzis and J. Zielinski, *Journal of Catalysis*, 2003, **218**, 465-469.

159. Y. V. Larichev, *The Journal of Physical Chemistry C*, 2011, **115**, 631-635.

160. Y. V. Larichev, *The Journal of Physical Chemistry C*, 2008, **112**, 14776-14780.

161. F. Rosowski, O. Hinrichsen, M. Muhler and G. Ertl, *Catalysis Letters*, 1996, **36**, 229-235.

162. K. S. R. Rao, S. K. Masthan, P. S. S. Prasad and P. K. Rao, *Applied Catalysis*, 1991, **73**, 1-5.

163. S. Murata and K. Aika, *Journal of Catalysis*, 1992, **136**, 110-117.

164. S. Murata and K. Aika, *Applied Catalysis A: General*, 1992, **82**, 1-12.

165. H. S. Zeng, K. Inazu and K. Aika, *Journal of Catalysis*, 2002, **211**, 33-41.

166. K. Aika, T. Takano and S. Murata, *Journal of Catalysis*, 1992, **136**, 126-140.

167. S. Murata and K. Aika, *Journal of Catalysis*, 1992, **136**, 118-125.

168. Y. Inoue, M. Kitano, S. Kim, T. Yokoyama, M. Hara and H. Hosono, *ACS Catalysis*, 2014, **4**, 674-680.

169. S. Kanbara, M. Kitano, Y. Inoue, T. Yokoyama, M. Hara and H. Hosono, *Journal of the American Chemical Society*, 2015, **137**, 14517-14524.

170. M. Kitano, Y. Inoue, H. Ishikawa, K. Yamagata, T. Nakao, T. Tada, S. Matsuishi, T. Yokoyama, M. Hara and H. Hosono, *Chemical Science*, 2016, **7**, 4036-4043.

171. Y. Inoue, M. Kitano, K. Kishida, H. Abe, Y. Niwa, M. Sasase, Y. Fujita, H. Ishikawa, T. Yokoyama, M. Hara and H. Hosono, *ACS Catalysis*, 2016, **6**, 7577-7584.

172. Intergovernmental Panel on Climate Change, *Climate Change 2013 The Physical Science Basis*, 2013.

173. A. Hill, PhD, University of Bath, 2014.

174. *The Hydrogen Economy: Oppertunities and Challenges*, Cambridge University Press, New York, 2009.

175. S. Satyapal, J. Petrovic, C. Read, G. Thomas and G. Ordaz, *Catalysis Today*, 2007, **120**, 246-256.

176. Concurrent Technologies Corporation, *Annual Report*, Concurrent Technologies Corporation, 2009.

177. S. Satyapal, C. Read, G. Ordaz and G. Thomas, *Journal*, 2006.

178. K. Ikeda, H. Ohshita, N. Kaneko, J. Zhang, M. Yonemura, T. Otomo, K. Suzuya, H. Yukawa, M. Morinaga, H. Li, S. Semboshi and S. Orimo, *Materials Transactions*, 2011, **52**, 598-601.

179. R. T. Walters and J. H. Scogin, *Journal of Alloys and Compounds*, 2006, **421**, 54-56.

180. R. Checchetto, N. Bazzanella, A. Miotello and P. Mengucci, *Journal of Alloys and Compounds*, 2007, **446–447**, 58-62.

181. R. Xiong, G. Sang, X. Yan, G. Zhang and X. Ye, *Journal of Materials Chemistry*, 2012, **22**, 17183-17189.

182. T. Vegge, *Physical Chemistry Chemical Physics*, 2006, **8**, 4853-4861.

183. F. Hiroyasu, M. A. Miller and O. M. Yaghi, *Journal of Materials Chemistry*, 2007, **17**, 3197-3204.

184. S. Tedds, A. Walton, D. P. Broom and D. Book, *Faraday Discussions*, 2011, **151**, 75-94.

185. Z. Łodziana and T. Vegge, *Physical Review Letters*, 2006, **97**, 119602.

186. C. J. Sahle, S. Kujawski, A. Remhof, Y. Yan, N. P. Stadie, A. Al-Zein, M. Tolan, S. Huotari, M. Krischa and C. Sternemannc, *Journal of Physical Chemistry*, 2016, **18**, 5397-5403.

187. M. Gupta and R. P. Gupta, *Journal of Alloys and Compounds*, 2007, **446–447**, 319-322.

188. W. I. F. David, J. W. Makepeace, S. K. Callear, H. M. A. Hunter, J. D. Taylor, T. J. Wood and M. O. Jones, *Journal of the American Chemical Society*, 2014, **136**, 13082−13085.

189. T. Nobuki, M. Chiba and T. Kuji, *Journal of Alloys and Compounds*, 2007, **446–447**, 152-156.

190. Y. Kodera, N. Yamasaki, T. Yamamoto, T. Kawasaki, M. Ohyanagi and Z. A. Munir, *Journal of Alloys and Compounds*, 2007, **446–447**, 138-141.

191. G. Thomas and G. Parks, *Potential Roles of Ammonia in a Hydrogen Economy*, U.S. Department of Energy, 2006.

192. United Nations Framework Convention on Climate Change, *Kyoto Protocol to the United Nations Framework Convention on Climate Change*, 1998.

193. A. Klerke, C. H. Christensen, J. K. Nørskov and T. Vegge, *Journal of Materials Chemistry* 2008, **18**, 2304–2310.

194. F. Schuth, R. Palkovits, R. Schlogl and D. S. Su, *Energy & Environmental Science*, 2012, **5**, 6278-6289.

195. A. J. B. Robertson, *Platinum Metals Review*, 1975, **2**.

196. B. J. Hansen, in *Ammonia Catalysis and Manufacture*, ed. A. Nielsen, Springer-Verlag Berlin Heidelberg, 1 edn., 1995, ch. 4, pp. 149-190.

197. K. Aika and K. Tamaru, in *Ammonia* ed. A. Nielsen, Springer-Verlag Berlin Heidelberg, 1 edn., 1995, ch. 3, pp. 103-148.

198. Z. Knor, *Applied Catalysis A: General*, 2003, **245**, 185-189.

199. A. Logadottir, T. H. Rod, J. K. Nørskov, B. Hammer, S. Dahl and C. J. H. Jacobsen, *Journal of Catalysis*, 2001, **197**, 229-231.

200. L. Green, *International Journal of Hydrogen Energy*, 1982, **7**, 355-359.

201. D. A. Hansgen, D. G. Vlachos and J. G. Chen, *Nature Chemistry*, 2010, **2**, 484-489.

202. J. C. Ganley, F. S. Thomas, E. G. Seebauer and R. I. Masel, *Catalysis Letters*, 2004, **96**, 117-122.

203. L. Wang, Y. Zhao, C. Liu, W. Gong and H. Guo, *Chemical Communications*, 2013, **49**, 3787-3789.

204. R. Z. Sørensen, L. J. E. Nielsen, S. Jensen, O. Hansen, T. Johannessen, U. Quaade and C. H. Christensen, *Catalysis Communications*, 2005, **6**, 229-232.

205. L. Leiva, Sharper image of a catalyst – warts and all, https://www.psi.ch/media/sharper-image-of-a-catalyst-warts-and-all, (accessed 4th May, 2017).

206. F. R. García-García, A. Guerrero-Ruiz and I. Rodríguez-Ramos, *Topics in Catalysis*, 2009, **52**, 758-764.

207. L. Lendzion-Bielun, U. Narkiewicz and W. Arabczyk, *Materials*, 2013, **6**, 2400-2409.

208. T. E. Bell and L. Torrente-Murciano, *Topics in Catalysis*, 2016, **59**, 1438-1457.

209. J. Zhang, M. Comotti, F. Schuth, R. Schlogl and D. S. Su, *Chemical Communications*, 2007, 1916-1918.

210. A. K. Hill and L. Torrente-Murciano, *International Journal of Hydrogen Energy*, 2014, **39**, 7646-7654.

211. G. Li, M. Kanezashi and T. Tsuru, *Catalysts*, 2017, **7**.

212. J. Zhang, H. Xu, Q. Ge and W. Li, *Catalysis Communications*, 2006, **7**, 148-152.

213. S. F. Yin, B. Q. Xu, X. P. Zhou and C. T. Au, *Applied Catalysis A: General*, 2004, **277**, 1-9.

214. S. F. Yin, B. Q. Xu, S. J. Wang and C. T. Au, *Applied Catalysis A: General*, 2006, **301**, 202-210.

215. A. R. Cholach, V. A. Sobyanin and V. V. Gorodetskii, *Reaction Kinetics and Catalysis Letters*, 1981, **18**, 371-375.

216. J. P. McGeer and H. S. Taylor, *Journal of the American Chemical Society*, 1951, **73**, 2743-2751.

217. R. P. H. Gasser and D. P. Green, *Surface Science*, 1979, **82**, 582-584.

218. A. R. Cholach, V. A. Sobyanin and V. V. Gorodetskii, *Reaction Kinetics and Catalysis Letters*, 1981, **18**, 391-396.

219. S. Matsuishi, Y. Toda, M. Miyakawa, K. Hayashi, T. Kamiya, M. Hirano, I. Tanaka and H. Hosono, *Science*, 2003, **301**, 626.

220. F. Hayashi, Y. Toda, Y. Kanie, M. Kitano, Y. Inoue, T. Yokoyama, M. Hara and H. Hosono, *Chemical Science*, 2013, **4**, 3124-3130.

Appendix

i How to Calculate the Rate of Ammonia Production from Conductivity Measurements

The mean conductivity of six different H_2SO_4 (0.00108 mol L^{-1}) and $(NH_4)_2SO_4$ solutions were determined. Results are presented in Table 23.

Table 23: Mean Conductivities of H_2SO_4 and $(NH_4)_2SO_4$.

Conductivity of H_2SO_4 (μScm^{-1})	**Conductivity of $(NH_4)_2SO_4$ (μScm^{-1})**
836	320
828	319
830	320
844	321
836	315
832	325
Mean *ca.* 834	Mean *ca.* 320

This calculation demonstrates how to calculate the ammonia synthesis rates with respect to the conductivity versus time plot for each ammonia synthesis experiment. For each reaction 200 ml of 0.00108 molL^{-1} of H_2SO_4 was used.

Calculate number of moles of H_2SO_4 in conductivity flask:

$$n\ H_2SO_4 = concentration\ \times volume$$

$$n\ H_2SO_4 = 0.00108\ \times 0.2$$

$$n\ H_2SO_4 = 2.16 \times 10^{-4}\ mol$$

Multiply by 2 to account for mole ratio for equivalent H^+ in NH_3:

$$\mathbf{2NH_3 + H_2SO_4 \rightarrow (NH_4)_2SO_4}$$

$$2.16 \times 10^{-4} \times 2 = \ 4.32 \times 10^{-4}\ mol\ ammonia$$

$$\mathbf{4.32 \times 10^{-4}\ \textit{moles ammonia}}$$ **required to completely react with** $\mathbf{H_2SO_4}$

The change in conductivity for reaction:

$$\Delta\ Conductivity = [Cond. at\ t0] - [Cond. at\ Exhaustion\ of\ H_2SO_4\ (320)]$$

$$\Delta\ Conductivity = 834 - 320$$

$$\boldsymbol{\Delta\ Conductivity = 514\ \mu Scm^{-1}}$$

No moles required / change in conductivity:

$$Moles\ H_2SO_4\ Consumed = \frac{4.32 \times 10^{-4}\ moles}{\Delta\ Conductivity}$$

$$Moles\ H_2SO_4\ Consumed = \frac{4.32 \times 10^{-4}\ moles}{514\ \mu Scm^{-1}}$$

$$\boldsymbol{Moles\ H_2SO_4\ Consumed = 8.41 \times 10^{-7} \mathrm{mol/\mu Scm}^{-1}}$$

ii Standard Error Calculation

First the mean rate was calculated from repeated runs of the same reaction:

$$y = \frac{r1 + r2 + \ldots}{n}$$

Where:

- y is the mean of the data set
- $r1, r2$ is the individual rates of reaction
- n is the total number of data points

Next, the standard deviation was calculated using:

$$SD = \sqrt{\sum \frac{|x-y|^2}{n}}$$

Where:

- SD is the standard deviation
- x a value in the data set
- y is the mean of the data set

- $n$is the total number of data points

Lastly the standard error was calculated using:

$$SE = \frac{SD}{\sqrt{n}}$$

Where:

- SE is the standard error
- SD is the standard deviation
- $n$is the total number of data points

To give: $mean\ experiemtal\ rate\ (y) \pm\ standard\ error(SE)$